

UNIVERSITY OF OXFORD

Understanding the Anti-tumour Immune Response to Radionuclide Therapy using PSMA targeting Radiopharmaceuticals in a Prostate Cancer Model

Rachel Anderson

St Cross College

Oxford Institute for Radiation Oncology

Department of Oncology

University of Oxford

Word count: 36,710

A thesis submitted to the Medical Sciences Division of the University of Oxford in partial fulfilment of the requirements for the degree of Doctor of Philosophy

Abstract

The ability of external beam radiation (EBRT) to modulate the tumour immune microenvironment is becoming increasingly well understood, leading to the development of combinatorial EBRT and immunotherapeutic combinations to improve patient responses. Despite this, there is very limited understanding of if, and how, the related modality of targeted radionuclide therapy (TRT) can interact with the immune system. Given its similarities with EBRT it seems likely that immune factors may play a role in the response to TRT. However, differences between the two radiotherapeutic modalities may result in some interesting differences that may be exploitable in combination therapies. As such, I sought to assess the impact of TRT on the tumour immune microenvironment, with the ultimate aim of identifying synergistic TRT and immunotherapy combinations.

Here, I have established a TRT targetable, immunocompetent prostate cancer model in our lab, namely PGLS allografts. This enabled evaluation of the immune response to the clinically relevant radiopharmaceutical [177Lu]-PSMA-I&T. Using this model, I was able to show for the first time that [177Lu]PSMA-I&T is capable of inducing changes to the TIME, with a notable reduction in immune cells 72 hours post treatment followed by a return to no-treatment levels by day 12 with a trend towards an increase. Strikingly this initial decline was not observed for EBRT treatment, though a similar increase in immune cells was seen by day 12. I went on to investigate the potential mechanisms involved in this interaction with the immune system, demonstrating that both TRT and EBRT can induce immunogenic cell death in this model. Interestingly, this ability to eliminate tumour growth in a vaccination study was absent in the treatment of established tumours, suggesting other factors in the TIME are limiting the capacity of TRT to induce a functional immune response. Finally, I investigated potential combinations with immunotherapies to eliminate possible barriers. Transcriptional analysis of a large prostate cancer patient cohort demonstrated a strong correlation of TGFβ expression with worse outcomes highlighting this protein as a potential target for combination therapeutics. However, no synergistic effect was observed in *in vivo* studies. Strikingly, I demonstrate that TRT can cause a remarkable increase in PDL1 expression suggesting that this may be an important mechanism of radioresistance, thus I suggest that combination of TRT with anti-PDL1 and potentially TGFβ could be a valuable avenue to explore. Ultimately, this work provides evidence that the immune response to TRT is a field worthy of persuing and highlights several key areas of interest for further exploration.

Acknowledgements

First and foremost, I would like to thank Professor Katherine Vallis for giving me the opportunity to carry out this work. Without her encouragement and support, this thesis would not have been possible.

I would also like to thank all past and present members of the Vallis group. My biggest thanks go to Sarah; for answering my constant battery of questions, for putting up with bins full of seemingly never decaying lutetium waste, and for lending a hand with mouse studies. My thanks also go to Ole, for helping me find my feet in the lab and helping me to embark on this project. And to Irini, for taking on the mantle of this work after I've posed so many open questions! To Elliot, Martin, Eloise, Edyta, Bas, Abirami, Javian, and the many other Vallis group members for your help and encouragement that got me to this point. And of course, a huge thanks also goes to the BMS team, Karla and Magda, for many pieces of helpful advice, and many, many expertly placed cannulas.

Of course, this work would not have been possible without the MRC and the Department of Oncology for funding this project, so thank-you.

It would be amiss to not mention the many people outside of the lab, without whom I would never have survived 8 years at Oxford. To the coach and members of Wadham College Boat Club, for giving me a sport to fall in love with. To OUWLRC and OUWBC for giving me the privilege to train and race alongside some of the most courageous, strong, loyal and kind women I have ever had the pleasure to meet. And to the lifelong friendships I have built there - most importantly to Livia Dewaele, Jade Bogart and Moyo Tian, for spending one year starving ourselves to 59 kg and every year since binging on cake and cocktails – long may it continue. And to Laura Depner, Anna Murgatroyd, Juliette Perry, Tilly Edwards and of course, Liv Weatherhead, for time spent in boats and at balls, repeatedly watching the greatest showman and making sure Laura never controls the minibus playlist, and for being some of the greatest friends anyone could ask for. And to the members of OUTriC for giving me a home when rowing no longer fit around looking after radioactive mice. Finally, to everyone else who has made this journey so enjoyable, thank-you.

Finishing this DPhil in such unprecedented times in the midst of a global pandemic has not been easy. So an extra thanks to my amazing housemates Laura Clark and Rob Dixon for the pub quizzes, movie nights, homemade pizza nights and homemade pasta nights, and of course, the defeating of the meatball monster, that made lockdown bearable.

And to my parents, who have given me every opportunity to find my own path in life. I would never have gotten here without your support.

Finally, my sincerest thanks go to my partner Joe who has been there through it all. For putting up with endless 5am starts, weekend lab shifts and 'my-experiment-isn't-working' bad moods, and for entertaining my constant drive to do slightly insane things like cycling up Everest - and only sometimes complaining. For being my partner and my best friend. Thank-you.
We (almost) have 5 Oxford degrees between us now, I think it's time to stop.

Specific Acknowledgements

Figure 3.7: Contrast ultrasound was performed with the help of Sheena Wallington. DCE-MRI and tumour contouring were performed by Sheena Wallington. The DCE-MRI parameters were calculated by Danny Allen.

For all animal studies involving TRT, cannulas were placed by Karla Watson or Magda Hutchins

Abbreviations:

131I	Iodine-131
153Sm	Samarium
177Lu	Lutetium-177
213Bi	Bismuth-213
223Ra	Radium-223
32P	Phosphorus-32
90Y	Yttrium-90
ADCC	Antibody-dependent Cellular Cytotoxicity
ADT	Androgen Deprivation Therapy
APC	Antigen Presenting Cell
ATP	Adenosine Triphosphate
BCR	Biochemical Recurrence
cGAMP	cyclic GMP-AMP
cGAS	cyclic GMP-AMP synthase
CI	Confidence Intervals
CRT	Calreticulin
CTL	Cytotoxic T lymphocyte
CXCL	C-X-C Motif Chemokine Ligand
CXCR	C-X-C Motif Chemokine receptor
DAMP	Damage Associated Molecular Pattern
DC	Dendritic Cell
EBRT	External Beam Radiotherapy
EDTMP	ethylene diamine tetramethylene phosphonate
ER	Endoplasmic Reticulum
GM-CSF	granulocyte–macrophage colony-stimulating factor
HMGB1	High Mobility Group Box 1
HR	Hazard Ratio
i.p.	Intraperitoneal
ICAM-1	Intercellular Adhesion Molecule 1
ICD	Immunogenic Cell Death
ID	Injected Dose
IDO1	Indoleamine-2,3 dioxygenase 1
IFN	Interferon
IHC	Immunohistochemistry
IL	Interleukin
LRP1	LDL receptor related protein 1
mCRPC	Metastatic Castration Resistant Prostate Cancer
MHC	Major Histocompatibility Complex
MIBG	Meta-idobenzylguanidine
NET	Norepinephrine Transporter
NKG2D	Natural Killer Group 2 Member D

NKT cells	Natural Killer T Cells
ORR	Overall response rate
p.i.	Post Injection
PCa	Prostate Cancer
PD-1	programmed cell death 1 receptor 1
PD-L1	programmed cell death receptor ligand 1
PGLS	PSMA-positive, Green fluorescent protein–positive, and LuciferaSe-positive
PSA	Prostate-specific antigen
PSMA	Prostate specific membrane antigen
RE	Radioembolization
STING	stimulator of interferon genes
TA	Tumour Antigen
TIL	Tumour infiltrating lymphocyte
TIME	Tumour Immune Microenvironment
TLR	Toll Like Receptor
TME	Tumour Microenvironment
TNF-α	Tumour Necrosis Factor α
TRT	Targeted Radionuclide Therapy
TSP1	Thrombospondin-1

Contents:

Abstract 2
Acknowledgements 3
Specific Acknowledgements 4
Abbreviations 5
List of Figures 10
List of Tables 11

CHAPTER 1: **Introduction**
1.1. Radiotherapy in Oncology 13
1.2. Discovery of Immune Activation by Radiotherapy 15
1.3. Immunomodulation by EBRT can Contribute to Therapeutic Efficacy 17
1.4. Molecular Understanding of Immunomodulation by EBRT
1.4.1 Lymphocyte Activation 19
1.4.2 Lymphocyte Recruitment 22
1.4.3 Increasing Sensitivity of Tumour Cells to Cytotoxic Immune Cells 22
1.4.4 Concurrent Immune-Suppressive Effects 23
1.5. Targeted Radionuclide Therapy and the Immune System
1.5.1 Targeted Radionuclide Therapy 27
1.5.2 Factors Affecting the Immune Response to TRT 29
1.6. Understanding the Mechanisms of Immune Activation by TRT
1.6.1 Lymphocyte Activation 33
1.6.2 Lymphocyte Recruitment 34
1.6.3 Increasing Sensitivity of Tumour Cells to Cytotoxic Immune Cells 34
1.7. Clinical Evidence of Immune Activation by TRT 35
1.8. TRT Immunotherapy Combinations 36
1.9. Research Objectives 39

CHAPTER 2: **Materials and Methods**
2.1. Cell lines and cell culture 40
2.2. In vitro irradiations 41
2.3. Western blotting 41
2.4. Radiochemistry 43
2.5. Radionuclide stability 43
2.6. Binding and internalisation 43
2.7. Retention 44
2.8. HMGB1 ELISA 44
2.9. TGFb ELISA 45
2.10. Assessment of Calreticulin exposure or PD-L1 by Flow cytometry 46

2.11. Assessment of Calreticulin exposure by Immunocytochemistry 47
2.12. Animal work and associated experiments
2.12.1. *Animals and husbandry* 47
2.12.2. *Tumour inoculation* 48
2.12.3. *Vaccination / rechallenge study* 48
2.12.4. *Treatment* 49
2.12.5. *Ultrasound* 49
2.12.6. *DCE-MRI* 50
2.12.7. *SPECT/CT* 50
2.12.8. *Ex vivo Biodistribution* 51
2.13. Tumour sectioning 51
2.14. Autoradiography 51
2.15. Nanostring 51
2.16. Transcriptomics 52
2.17. Statistical Analysis 53

CHAPTER 3: **Establishing a model to assess the immune response to TRT**
3.1. Introduction
3.1.1 Targeted Radiotherapy (TRT) 54
3.1.2 Iodine-131 MIBG 55
3.1.3 Lutetium-177 PSMA 56
3.2. Aims 58
3.3. Results
3.3.1 *Murine Neuroblastoma Cell Lines 9464D and 975A2 Demonstrate Significant [131I]MIBG uptake in vitro, whilst Murine Prostate Cancer Cell Line PGLS Demonstrates significant [177Lu]PSMA-I&T uptake* 59
3.3.2 *9464D and 975A2 Tumour Uptake of 131I-MIBG is Poor* 65
3.3.3 *PGLS Cells Form Fast Growing, Well Perfused Tumours in Immunocompetent Mice* 69
3.3.4 *PGLS tumours show high, tumour selective, PSMA dependent uptake of [177Lu]PSMA-I&T* 72
3.3.5 *Both EBRT and TRT induce growth delay of PGLS tumours* 74
3.4. Discussion 76
3.4.1 *Despite in vitro uptake, no [123I]MIBG tumour accumulation is observed in vivo for 9464D or 975A2 allografts* 76
3.4.2 *PGLS allografts provide one of the first models suitable for the study of the immune response to TRT* 77
3.4.3 *PSMA dependent uptake and retention is consistent with clathrin mediated endocytosis* 78
3.4.4 *Endogenous PSMA expression varies between mice and humans but biodistribution is comparable* 80
3.4.5 *60MBq of [177Lu]PSMA-I&T produces an observable effect in PGLS allografts* 83

CHAPTER 4: **Treatment with TRT can induce changes to the TIME**

4.1. Introduction 85

4.2. Aims 90

4.3. Results

4.3.1 *The immune response to [177Lu]PSMA-I&T is characterised by an initial reduction in immune cells, followed by immune stimulation* 91

4.3.2 *EBRT treatment of PGLS tumours results in TIME stimulation at both early and late timepoints* 104

4.3.3 *[177Lu]PSMA-I&T induces the molecular markers of immunogenic cell death in vitro* 111

4.3.4 *[177Lu]PSMA-I&T induces immunogenic cell death in vivo* 117

4.4. Discussion

4.4.1 *[177Lu]PSMA-I&T, but not EBRT, triggers an initial reduction of immune cells in the TIME* 119

4.4.2 *The frequency of immune cells in the TRT treated TME is equal to or greater than untreated tumours by day 12* 120

4.4.3 *The ultimate impact of the immune cell depletion will depend on the phenotype and functionality of the depleted cells* 121

4.4.4 *The phenotype and functionality of the immune cells populating the TIME 12 days post treatment is another important factor* 123

4.4.5 *[177Lu]PSMA-I&T induced changes to the TIME differ from EBRT induced changes at day 12* 126

4.4.6 *Induction of immunogenic cell death may contribute to TIME changes* 128

4.4.7 *Despite preventing tumour growth by vaccination, [177Lu]PSMA-I&T treatment fails to cure established tumours* 130

CHAPTER 5: **Combining Targeted Radionuclide Therapy with Immunotherapy**

5.1 Introduction 132

5.2 Aims 138

5.3 Results

5.3.1 *CD47 expression is a positive prognostic marker for PCa, whilst TGFβ1 is a negative prognostic marker* 139

5.3.2 *TGFβ1 is not induced by [177Lu]PSMA-I&T and TGFβ inhibition does not work synergistically with a single dose of [177Lu]PSMA-I&T or EBRT in the PGLS model* 145

5.3.3 *PDL1 is elevated in response to [177Lu]PSMA-I&T and may represent a good target for combination therapy* 149

5.4 Discussion

5.4.1 *CD47 levels predict favorable outcomes in PCa* 151

5.4.2 *Combination of [177Lu]PSMA-I&T with anti-TGFβ* 153

5.4.3 *PD-L1 and other alternatives* 155

CHAPTER 6: **Concluding Remarks**
6.1 Synopsis 160
6.2 Limitations
6.2.1 *Limitations of mouse models* 161
6.2.2 *Human data* 163
6.2.3 *Timing and dose considerations* 163
6.2.4 *Immune cell enumeration* 164
6.2.5 *Immunotherapy targets and combination therapies* 165
6.3 Future Directions
6.3.1 *Immune cell phenotype and mechanistic insights* 166
6.3.2 *Metastatic disease* 167
6.3.3 *Dose and timing* 167
6.3.4 *Immune targets in PCa* 168
6.3.5 *Patient stratification* 168
6.3.6 *Immune cell sensitivity to [177Lu]PSMA-I&T* 169
6.3.7 *Different radioisotopes, targeting moieties and indications* 169
6.4 Conclusions 170

References 171
Appendix 192

List of Figures:

Figure 1.1: The efficacy of radiotherapy is dependent on the immune response in B16 tumours
Figure 1.2: Tumoural Immunosuppression and the Immune Response to EBRT
Figure 1.3: Possible Factors Affecting Immune Response to TRT

Figure 3.1: Structure of NET and PSMA targeting small molecules
Figure 3.2: Radiopharmaceutical uptake can be achieved in murine cell lines and is dependent on receptor expression
Figure 3.3: PSMA labelling
Figure 3.4: [177Lu]PSMA-I&T stability
Figure 3.5: 9464D growth and biodistribution
Figure 3.6: [123]MIBG Biodistribution in Smaller 9464D and 975A2 Tumours
Figure 3.7: PGLS growth and vascularization
Figure 3.8: PGLS Biodistribution
Figure 3.9: PGLS Response to radiotherapy
Figure 3.10: Human vs. Mouse PSMA homology

Figure 4.1: NanoString Technology
Figure 4.2: Immunogenic cell death
Figure 4.3: NanoString quality control
Figure 4.4: NanoString normalization
Figure 4.5: Marker gene concordance plots
Figure 4.6: Marker gene concordance heatmap
Figure 4.7: Cell type measurements for [177Lu]PSMA-I&T treated vs untreated tumours 72 hours post treatment
Figure 4.8: Immune cell populations in PGLS tumours 72 hours post [177Lu]PSMA-I&T treatment
Figure 4.9: Cell type measurements for [177Lu]PSMA-I&T treated vs untreated tumours 12 days post treatment
Figure 4.10: Immune cell populations in PGLS tumours 12 days post [177Lu]PSMA-I&T treatment
Figure 4.11: Cell type measurements for EBRT treated vs untreated tumours 72 hours post treatment
Figure 4.12: Immune cell populations in PGLS tumours 72 hours post EBRT treatment
Figure 4.13: Cell type measurements for EBRT treated vs untreated tumours 12 days post treatment
Figure 4.14: Immune cell populations in PGLS tumours 12 days post EBRT treatment
Figure 4.15: Differential gene expression in PGLS tumours 12 days post EBRT vs TRT treatment
Figure 4.16: Cell surface CRT staining
Figure 4.17: [177Lu]PSMA-I&T induces cell surface exposure of ER chaperone proteins CRT and ERp57
Figure 4.18: [177Lu]PSMA-I&T induces release of HMGB1

Figure 4.19: [177Lu]PSMA-I&T induces immunogenic cell death in vivo
Figure 4.20: [177Lu]PSMA-I&T causes initial reduction in immune cells, followed by repopulation

Figure 5.1: Prognostic value of potential immunological targets in prostate cancer
Figure 5.2: Assessment of the validity of T cell marker genes in the PRAD dataset
Figure 5.3: Assessment of the validity of neutrophil marker genes in the PRAD dataset
Figure 5.4: CD47 and TGFB1 correlation with immune cell infiltration in prostate cancer
Figure 5.5: Neither EBRT nor [177Lu]PSMA-I&T increase TGFb expression in PGLS cells
Figure 5.6: Combination of anti-TGFb with radiotherapy does not improve therapeutic efficacy
Figure 5.7: Both EBRT and [177Lu]PSMA-I&T induce expression of PDL1 in PGLS cells

Figure A1: Pilot study to assess the efficacy of EBRT in PGLS tumours
Figure A2: Expression of PSMA in murine prostate cancer cell lines
Figure A3: Pilot biodistribution study to assess biodistribution of [177Lu]PSMA-I&T in PGLS allografts

List of Tables:

Table 1.1: List of Antibodies
Table 1.2: Radioisotope characteristics
Table 4.1: Summary of changes in immune cells in PGLS tumours following irradiation
Table 5.1: Potential immunological targets for combination with [177Lu]PSMA-I&T in prostate cancer

Chapter I:
Introduction

1.1 Radiotherapy in Oncology

Since its discovery in the late 19th century, external beam radiation therapy (EBRT) has become a cornerstone of oncology treatment and is used around the world[1]. Today, as many as 60% of cancer patients receive EBRT for both curative and palliative treatment. This therapy delivers high doses of radiation to defined tumour or at-risk volumes but is limited by side effects caused by exposure of surrounding normal tissue.

Historically, the prevailing explanation for the antitumour effects of EBRT has been the induction of complex DNA damage leading to cell death and abrogated clonogenic survival, ultimately providing local disease control[2]. This damage results from both direct action whereby the atoms of the DNA itself are ionized or excited resulting in direct damage, or indirect action where the radiation first interacts with other atoms or molecules (eg. water) in the cell producing free radicals that go on to damage the DNA.

Normal tissue will inevitably be irradiated alongside tumour tissue, resulting in normal tissue damage by the same mechanisms. The effectiveness of irradiation is thus limited by the exposure of normal tissue leading to toxicity. This led to the concept of a therapeutic ratio. This is the ratio of tumour response for a fixed level of normal tissue damage. Due to differences in the characteristics of normal tissue and tumour tissue this ratio can be increased by fractionating the radiation dose. The '5Rs' of radiotherapy are thought to describe how tumour cells and normal cells will respond to fractionated EBRT. These Rs are repair, reassortment, repopulation, reoxgenation and radiosensitivity.

Because some of the inflicted damage is sub-lethal, fractionation provides time for the cell to repair the damage before more accumulates becoming potentially lethal. Malignant cells often suppress pathways involved in DNA damage recognition and repair, and cell cycle arrest and thus fractionation can increase the therapeutic ratio.

Reassortment impacts the biological effect of irradiation due to the differing radiosensitivity of different phases of the cell cycle, with cells in S phase being typically radioresistant whilst those in late G2 and M phase are relatively radiosensitive. Reassortment between fractions thus redistributes surviving cells over cell-cycle phases and so avoids repeated irradiation in resistant phases.

Repopulation occurs following cell killing by irradiation. This can limit normal tissue toxicity, but can also allow tumour cells to start to repopulate.

Reoxygenation is important due to the often acute or chronic hypoxia observed in tumours. The presence of oxygen is key to the formation of radical oxygen species (ROS) causing indirect damage. In the case of acute hypoxia which results from transient closure of capillaries or arterioles serving parts of the tumour, fractionation raises the likelihood that the capillaries will be open at one irradiation time. Meanwhile where chronic hypoxia occurs due to poor tumour vasculature, irradiation is more effective for cells close to capillaries where oxygen can diffuse in. Fractionated doses thus removes these cells enabling chronically hypoxic cells to move closer to the oxygen source, and thus become more sensitive to subsequent doses of irradiation.

Finally, radiosensitivity of cells is also key. Different cells have different radiosensitivity, for example cells like stem cells, intestinal cells and blood cells are radio-sensitive, whilst neurons, brain cells, and various tumour cells are relatively radioresistant. The radiosensitivity of tumour cells to varying single doses determines the biological effect when the fraction size is increased, whilst the radiosensitivity of surrounding normal tissue determines the corresponding toxicity of increased fraction size.

Importantly, the concept of a 6th 'R' of radiotherapy - reactivation of the anti-tumor immune response – has now been proposed, but this is a relatively new addition [3]. Indeed, avoiding immune recognition is also a more recent addition to the hallmarks of cancer as described by Hanahan and Weinberg [4]. Targeting these hallmarks through combination therapies to increase the therapeutic ratio of radiotherapy has become a key aim for improving radiotherapy outcomes. For example, using anti-angiogenic agents, anti-invasives, or inhibition of growth factor signal transduction [5]. As

understanding of the role of immune activation by radiotherapy evolves, the potential for combination of radiotherapy with immunotherapeutics is an increasingly exciting prospect.

Interestingly, for some time EBRT was considered to be immunosuppressive. This line of thought arose predominantly from observations of lymphopenia following EBRT[6, 7] and the widespread use of total body irradiation as an immune suppressant to prevent immunologic rejection during bone marrow transplantation[8, 9]. However, in recent years it has become increasingly clear that the immune system can be key to EBRT efficacy, with a plethora of mechanisms that can contribute to triggering a functional antitumor immune response alongside direct tumor cell killing[10].

Despite its widespread use the potency of EBRT as a stimulus of the immune response may be limited by a number of factors, such as the inability to target all sites of disseminated disease. This may be addressed using an alternative form of radiotherapy known as targeted radionuclide therapy (TRT). This increasingly common modality employs therapeutic radioisotopes conjugated to targeting moieties[11]. These small molecules, antibodies or other ligands specifically recognise and bind to tumour antigens and thus enable specific accumulation within all tumour sites following systemic administration. As the isotope decays it provides a protracted, low dose rate radiation dose to the tumour site. Analogous to EBRT, this may stimulate an anti-tumour immune response, however evidence for this is thus far lacking. Importantly, differences between the modalities may result in differing immune stimulation. For example, the use of systemic radiotherapy enables treatment of all sites of metastatic disease which could promote induction of a functional immune response at all disease sites. Other differences such as dose, dose rate and radiation quality are also likely to impact the landscape of the immune response in various ways, as discussed below.

1.2 Discovery of Immune Activation by Radiotherapy

In the early years of radiotherapy, consideration of the immune response was limited. In 1917, shortly after the introduction of radiotherapy, Ewing noted the accumulation of lymphocytes and polymorphonuclear leukocytes within days of administering of radium. However, more direct

assessment of the effects of irradiation on immunity was lacking until much later [12]. Almost 40 years after this initial observation, Cohen and Cohen conducted a number of studies demonstrating that inoculation of murine hosts bearing pre-established xenografts with *ex vivo* irradiated tumour samples improved the efficacy of irradiation [13, 14]. They went on to suggest such a response *'could be explained only on the basis of a subliminal systemic resistance mechanism, possibly in the nature of a circulating iso-antibody arising in the host'*. Again, there was a long wait before further studies provided conclusive evidence for this hypothesis, but in the 1970s Suit *et al.* and Slone *et al.* both observed that the radiosensitivity of murine xenografts was significantly affected by the immune status of the mouse host, with additional effects on the likelihood of developing metastasis [15, 16]. Unfortunately, this aspect of EBRT then received little attention for decades, perhaps due to the critique of Hewitt *et al.* who assessed the ability of lethally irradiated murine tumour cells to vaccinate isogenic mice [17]. Importantly, Hewitt used murine tumour cells of spontaneous origin for these experiments and thus suggested that opposing literature showing any vaccination effect was an artefact of immunity associated with the virally or chemically induced tumours used in those studies[17]. In hindsight, whilst this appreciation of the importance of tumour immunogenicity is undoubtedly important, this erroneous dismissal of the immune effects of irradiation likely impeded advancement of the field for decades.

Slowly, belief that EBRT may induce an anti-tumour immune response was reignited by observations of therapeutic responses outside the irradiated field across a range malignancies [18–20]. Such a response was first described in 1953[21], though observations remained scarce with two further cases in papillary adenocarcinoma of unknown origin and melanoma described in 1973 and 1975, respectively [19, 20]. Due to the local nature of treatment, these systemic responses were unexpected and could not be explained by established theories which suggested that cell death could only be achieved by direct induction of cytotoxic DNA and cellular damage. This phenomena, coined the abscopal effect [21], has since been shown to be a function of the immune response induced by EBRT [22–24]. Whilst such cases are rare and anecdotal, it is becoming increasingly clear that radiation

commonly induces an immune response, however concurrent immune-suppressive effects – particularly in tumours outside the radiation field - may have thus far limited the effectiveness of this response in the clinic [25]. Indeed, despite the millions of patients treated with EBRT between 1969 and 2014, only 46 cases of abscopal effects have been reported [26]. Whilst observation of abscopal effects are rare, more widespread clinical evidence for the importance of immune activation by EBRT includes the observed effect of immunosuppressants, genetic mutations and low lymphocyte count on EBRT efficacy[27].

Importantly, the induction of an immune response provides the possibility of systemic, long-lasting protection, highlighting the potential for synergistic responses to combined radiotherapy-immunotherapy combinations. Consistently, since the introduction of immune checkpoint inhibitors into the clinic reports of abscopal responses have been increasing. One key case report from Memorial Sloan Kettering Cancer Centre in 2012 described a metastatic melanoma patient progressing on the immune checkpoint inhibitor ipilimumab, and subsequently treated with palliative EBRT[28]. Following RT there was significant regression of both the treated lesion and non-targeted lesions, with stable disease 10 months later, marking a resurgence of interest in the field of radio-immunology. In a similar case study, another patient with metastatic melanoma who had been treated with ipilimumab and stereotactic body radiotherapy to two of seven liver metastases was recently reported to be in complete remission, with no evidence of disease or recurrence 6.5 years after treatment [29].

1.3 Immunomodulation by EBRT can Contribute to Therapeutic Efficacy

Given this new understanding that in rare cases EBRT can induce a functional systemic immune response, it became of interest to see how widespread this immune induction is and indeed if it more generally contributes to the locoregional tumour control of EBRT.

Striking evidence that, at least in some cases, immune activation is not only a contributing factor but is essential to therapeutic efficacy for local tumour control arose from a standout study by Lee *et al.* Here, the authors demonstrated the loss of B16 tumour radiosensitivity in immunocompromised

(nude) mice, compared to wildtype (WT) mice [30]. These investigators went on to show that this loss of response is due to the need for an intact immune system and not a result of the differing strains using antibody mediated CD8+ T cell depletion to dramatically reduce tumour response in WT mice (Figure 1.1) [30]. A similar trend was demonstrated in both EG7 and LLC-OVA tumour bearing mice [31], as well as in EL4 tumour bearing mice where the loss of response in immunosuppressed mice was accompanied by loss of cytokine and antibody production [32]. These studies highlight the potential importance of the EBRT induced immune response to locoregional tumour control alongside its role in mediating abscopal effects.

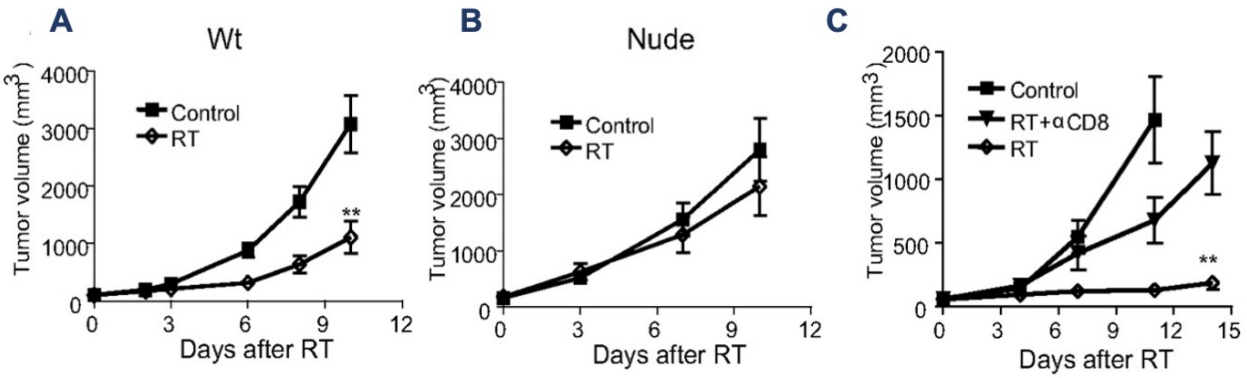

Figure 1.1: The efficacy of radiotherapy is dependent on the immune response in B16 tumours
Lee et al., 2009 demonstrate radiosensitivity of B16 tumours observed in wildtype (WT) mice (A) is lost in mice lacking a thymus and thus immunodeficient (B). To show this is not due to the different mice strains, this is then repeated in WT mice using anti-CD8 antibodies to deplete CD8 T cells, demonstrating a significant reduction in therapeutic efficacy (C). *Figure reproduced from Lee et al., 2009 [27].*

1.4 Molecular Understanding of Immunomodulation by EBRT

Having established the importance of the immune response to EBRT efficacy, there is now accumulating literature exploring the mechanisms underlying these effects. Such work has revealed a plethora of changes induced by EBRT that act at various stages of the cancer immunity cycle [33],

including; promoting dendritic cell (DC) activation and subsequent T cell priming, further stimulation of T cell activation and recruitment of lymphocytes to the tumour site, and promoting changes to the tumour cells to increase their susceptibility to T cell killing (Figure 1.2).

1.4.1 Lymphocyte Activation:

During tumorigenesis aberrant protein expression occurs, for example through expression of mutated genes resulting from non-synonymous point mutations or frameshift mutations[34, 35], expression of genes of endogenous retroviruses [36], changes in post-translational modifications generating new epitopes [37], or expression of genes not covered by self-tolerance such as those endogenous to immune privileged sites [38]. This leads to generation of tumour antigens (TAs) that can be recognised by cognate TCRs leading to targeted elimination of cancer cells. This destruction requires an antigen presenting cell (APC), typically a DC, to first engulf tumour cells or tumour cell debris, and process the antigens for exposure on their surface in association with a major histocompatibility complex (MHC) class II molecule. These activated DCs travel to the lymph nodes where they interact with and activate cognate T cells. Typically, these processes are limited or stopped by a developing tumour in order to escape the immune response [39], however various mechanism have now been identified by which EBRT can promote activation of lymphocytes within the tumour microenvironment (TME).

Perhaps the best understood of these mechanisms, is immunogenic cell death (ICD) [40, 41]. This highly immunogenic form of programmed cell death results in the release of a number of immunostimulatory compounds that go on to activate and prime an anti-tumour immune response, particularly via activation of DCs that go on to induce effector T cell activation. Three key molecular determinants of ICD have been defined: Exposure of Calreticulin (CRT) on the cell surface, release of high mobility group box 1 (HMGB1), and release of adenosine triphosphate (ATP)[42].

Relocation of the endoplasmic reticulum protein, CRT, to the cell surface allows it interaction with the TME. In this context it acts as a potent ‘eat-me’ signal, promoting uptake of the tumour cell by

macrophages and DCs, and thus subsequent processing and presentation of tumour TAs [43, 44]. HMGB1 released from the cell further stimulates this process via action on several APC receptors, including toll-like receptor 4 (TLR-4)[45, 46]. This results in a number of downstream effects, for example inhibition of lysosome-dependent degradation of phagosomes thus enabling antigen processing and degradation rather than breakdown, and ultimately driving DC activation [47]. Meanwhile, released ATP acts as a key cell-cell signalling factor via activation of P2X7 purinergic receptors on DCs. This interaction triggers inflammasome activation and thus Interleukin-1β (IL-1β) production [48, 49]. IL-1β subsequently primes CD8+ T cells which act as key mediators of the antitumour immune response. The importance of these processes has been highlighted by work demonstrating that for various ICD inducers loss of these key mediators prevents induction of an immune response and thus limits efficacy. For instance Apetoh *et al.* demonstrated that loss of the HMGB1/TLR4 axis in $Tlr4^{-/-}$ mice could significantly diminish the efficacy of EBRT [45].

In conjunction with ICD mediated DC stimulation, activation of complement with local production of pro-inflammatory anaphylatoxins C3a and C5a has also been shown to stimulate DC maturation following irradiation[50]. These anaphylatoxins bind directly to their receptors on DCs thereby supporting their maturation[51–53]. Moreover, T cells also express complement components and anaphylatoxin receptors that are critical to T cell co-stimulation[54]. Importantly, signalling via the anaphylatoxin receptors C3aR1 and C5aR1 during DC cognate interaction with CD4 T cells counteracts the development of FoxP3+ regulatory T cells which may be critical in preventing further immune suppression that could limit therapeutic responses[55]. Consistent with this, Surace et al. observed an increase in Fox3P+ T cells in C3ar1-/-C5ar1-/- mice, along with reduced CD8+ T cell activation[50]. Correspondingly, they also demonstrated that the therapeutic efficacy of radiotherapy was lost in both C3 knockout mice and C3 or C5 receptor knockout mice, suggesting complement activation may be critical for tumour responses.

Alongside the key mediators of ICD and complement, a number of other immunostimulatory factors are released by the stressed and dying tumour cells following irradiation that are capable of

stimulating DCs as well as T cells and other immune cells in the TME. These include a range of cytokines such as granulocyte–macrophage colony-stimulating factor (GM-CSF), IL-6, IL-8, and tumour necrosis factor-α (TNF-α) which can all contribute to activation of immune cells [56–58]. Natural killer group 2 member D (NKG2D) ligands are also induced in tumour cells treated with radiation, enabling interaction with NKG2D on various lymphocytes including natural killer T cells (NKT cells), macrophages and a proportion of CD4+ and CD8+ T cells [59]. This interaction can again promote lymphocyte activation prompting an immune response against the tumour cells.

Another key family of cytokines stimulated by RT are interferons (IFNs), which can be induced via the cGAS/STING pathway. This mechanism has been receiving much attention recently following a number of studies highlighting how beneficial this activation may be, and leading to the development of STING agonists [60, 61]. DNA damage induced by radiation causes the generation of micronuclei and/or accumulation of DNA in the cytoplasm [62–64]. This activates the cytoplasmic DNA-binding protein cyclic GMP-AMP synthase (cGAS). Activated cGAS produces the secondary messenger cyclic GMP-AMP (cGAMP) from ATP and GTP, which in turn activates stimulator of interferon genes (STING) [65–67]. Downstream pathways then result in the expression and secretion of interferons I, II and III, which may be key to RT efficacy [62, 68–70]. For example, in B16 melanoma the antitumor effects of RT were abolished in type I IFN nonresponsive murine hosts [62, 69]. Despite this apparent benefit, there is also accumulating evidence that cGAS/STING activation and interferon responses may also be immunosuppressive in certain circumstances [71–73]. Indeed, activation of interferon stimulated genes (ISGs) may be associated with resistance to RT through both PDL1-dependent and PDL1-independent mechanisms [71]. There is also evidence that STING activation by RT can cause infiltration of myeloid derived suppressor cells (MDSCs) which contribute to the generation of an immune-suppressive environment[72].

Alongside its effects on DCs and subsequent T cell activation, there is also some evidence that radiation can reduce the presence of immune-supressing cells such as T_{reg} cells and M2 macrophages, which commonly populate the TME to generate an immunosuppressive environment [74, 75].

Reducing the number of these cells thus alleviates their immunosuppressive effects enabling a functional immune environment to develop within the tumour. Notably though, the converse effects have also been observed (see section 1.4.5).

1.4.2 Lymphocyte Recruitment

Following their activation by APCs in the lymph node, the activated T cells return to the circulation and infiltrate the tumour through a process promoted by chemokines and adhesion molecules produced by local inflammation. Again, this process is typically reduced in tumorigenesis, however in conjunction with increased lymphocyte activation EBRT additionally promotes recruitment of lymphocytes to the tumour site, which can enable access to otherwise poorly infiltrated tumours.

Various mechanisms have been shown to mediate this response including increased expression of chemokines and adhesion molecule along with other physical changes to the TME. For example *in vitro* irradiation of human and mouse breast tissue has been observed to elevate C-X-C Motif Chemokine Ligand 16 (CXCL16) secretion [76]. As a ligand for C-X-C Motif Chemokine receptor 6 (CXCR6) on T-helper and CD8+ effector T cells, this chemokine participates in the recruitment of these immune cells to sites of inflammation. Similarly, CXCL10, a ligand for the CXCR3 receptor on monocytes, natural killer (NK) cells, and T cells, was significantly elevated following RT treatment in mice. Moreover, prevention of CXCL10 upregulation correlated with loss of RT-induced T cell infiltration in a B16 melanoma model [77]. Alongside these transcriptional changes, radiation-induced normalisation of aberrant tumour vasculature can further trigger efficient recruitment of otherwise excluded immune cells [74].

1.4.3 Increasing Sensitivity of Tumour Cells to Cytotoxic Immune Cells

Having reached the tumour site, activated T lymphocytes must locate and kill target cells expressing their cognate TA. Tumour cells avoid this by downregulation of key molecules involved in T cell mediated killing as well as producing factors that directly or indirectly inhibit T cells [78–83]. Again,

there have been a number of observations suggesting that treatment with EBRT can increase sensitivity of tumour cells to immune-mediated killing. This increased sensitivity is a result of a number of factors including upregulation of various cell surface proteins involved in cytotoxic T lymphocyte (CTL):target cell interactions. One such protein, Fas, is increased in a dose-dependent fashion in response to EBRT [84]. This protein binds Fas-ligand expressed on CTLs inducing death of the tumour cell.

RT can also increase the expression of MHC class I complexes [85]. It is these complexes that expose antigens from within the cell, including TAs, to the surveying immune cells in the TME. Only when expressed in this way are T cells able to recognise their cognate antigens and exert their cytolytic activity on the host cell. Perhaps unsurprisingly then, tumour cells often downregulate these molecules during the process of tumourigenesis, masking themselves from immune surveillance [78–81]. Consequently, radiation-induced upregulation enables recognition and destruction of TA-expressing cells. Upregulation of DNA damage response and cell cycle regulation genes by radiotherapy may also help this process. These newly transcribed proteins are more likely to be processed for MHC-loading, and as these proteins are often mutated in cancer their increased presentation on the cell surface provides neoantigens for recognition by T cells [85, 86].

As well as enabling recognition of existing TAs, it is also possible that radiation can induce neoantigen generation via its DNA damaging effects, increasing the number of tumour specific antigens available for recognition.

1.4.4 Concurrent Immune-Suppressive Effects

Whilst the mechanisms described above have the potential to produce a curative systemic immune response, this is rarely the case with RT alone. This is likely due to the existing immunosuppressive processes active in the TME, however activation of further immune-suppressive mechanisms that limit the immune response may also contribute to this.

Alongside pro-immunogenic changes, EBRT is also known to induce a wound repair response at the site of irradiation. This response, primarily mediated by macrophages, is predominantly immunosuppressive. Macrophages of the suppressive M2 phenotype accumulate in the tumour following RT [87], though it is worth noting that this accumulation may be dose-dependent, with observations that low dose RT can cause M1 polarisation as mentioned above (Section 1.4.1 – Lymphocyte Activation) [74]. The immune-stimulatory M1 phenotype produce high levels of proinflammatory cytokines and nitric oxide, and present antigens leading to the death of unhealthy cells. Meanwhile, M2 cells are characterised by low production of proinflammatory cytokines and do not produce nitric oxide. Instead, M2 cells express arginase I and IL-10 which promotes the building of extracellular matrix that enhances rather than prevents tumour growth.

RT may also drive development of various other immune suppressive cells, including T_{regs}, MDSCs, tolerogenic DCs and tumour-associated neutrophils [88–95]. Here, the treatment regimen appears key, for example ablative hypofractionated RT has been shown to reduce rather than increase MDSCs [96].

Another major immune-suppressive mechanism employed by tumours is the expression of immune-checkpoint molecules that bind receptors on T cells to inhibit T cell function [97]. There is evidence that RT may promote expression of such checkpoints, for example in a murine carcinoma model fractionated EBRT caused an increase in tumour cell PD-L1 expression [98]. Similar observations were made in a number of cell lines following chemoradiation [99].

Ultimately, the balance must be tipped to create an immune-promoting environment within the tumour to overcome the limiting factors. This provides a strong rationale for developing combination therapeutics with EBRT to provide a multi-pronged approach that can overcome the abundant immune-suppressive mechanisms present in a tumour. Another possibility is modulation of the radiotherapy regimen to promote the immune-activating mechanisms and simultaneously avoid immune-suppression. Tipping the scales may be possible with alteration of dose and fractionation, or through the use of other forms of radiotherapy such as TRT.

Following page - ***Figure 1.2: Tumoural Immunosuppression and the Immune Response to EBRT – (1) Suppressive tumour microenvironment*** *– Tumourigenesis requires the formation of an immune-suppressive microenvironment to enable tumour growth unhindered by the immune system. The major mechanisms employed by the tumour to generate this environment produce three key changes (A) Reducing sensitivity to cytotoxic immune cells including CD8+ T cells and NKT cells. This is achieved via a number of mechanisms, including (i) reduced expression of MHC class I complexes, which are required to present peptides derived from intracellular proteins on the cell surface in a format recognisable by cognate T cell receptor of cytotoxic T cells that activates them to kill the target cell. (ii) Tumour cells also down regulate other cell surface proteins involved in these cytotoxic interactions, including Fas-L. (B) Tumours create either 'immune desert' or 'immune excluded' microenvironments, characterised by poor infiltration of T cells with high MSDC counts, or high tumour infiltrating lymphocytes in the surrounding stroma but no infiltration into the tumour parenchyma, respectively. (C) For those cells that do enter the tumour, there is a plethora of mechanisms awaiting to inhibit lymphocyte activation. This includes (i) the production of immune suppressive molecules by both tumour cells and immune cells. (ii) High expression of immune checkpoint molecules such as PDL-1, which inhibits PD-1 positive T cells. (iii) Presence of various immune-suppressive subtypes, including regulatory T cells, M2 macrophages and MDSCs, which can facilitate angiogenesis, immunosuppression, and inflammation.* ***(2) Immune activation by EBRT*** *– is achieved via abrogation of these immune-suppressive effects in various ways. (A) Increasing sensitivity to cytotoxic immune cells by restoring/increasing (i) MHC-1 and (ii) other immune cell interacting molecules. (iii) Release of tumour associated antigens leads to increased T cell priming and recruitment of cognate T cells. (B) Lymphocyte recruitment converts 'immune desert' or 'immune excluded' tumours into 'immune inflamed' tumours with high numbers of tumour infiltrating T cells. This is achieved by (i) secretion of chemokines that are recognised by chemokine receptors on immune cells recruiting them to the tumour site, and (ii) normalisation of aberrant vasculature, enabling access to previously excluded tumour sites. (iii) These lymphocytes are then activated by (i) immune-stimulatory cytokines release by the tumour and immune cells. (ii) Reduced immune checkpoint expression may also help to 'release the brakes' on the anti-tumour immune response. (iii) Changes in the ratios of immune subtypes e.g., Treg:CD8 T cells, M2:M1 macrophages, Toloregenic:Mature DCs, shifts to the immune activating cells. Alongside activation and various immune promoting mechanisms such as (iv) immunogenic cell death, and (v) the cGAS STING pathway to produce further immune-stimulating molecules.* ***(3) Immune Suppression by EBRT*** *unfortunately occurs alongside the immune activating mechanisms and may limit response. These inhibitory changes predominantly act to inhibit lymphocyte activation and may compete with immune-activating mechanisms in a dose-dependent manner. Major changes that have been observed under certain settings include (i) increases in MDSCs and M2 macrophages, and (ii) immune-suppressive effects of cGas/STING activation.*

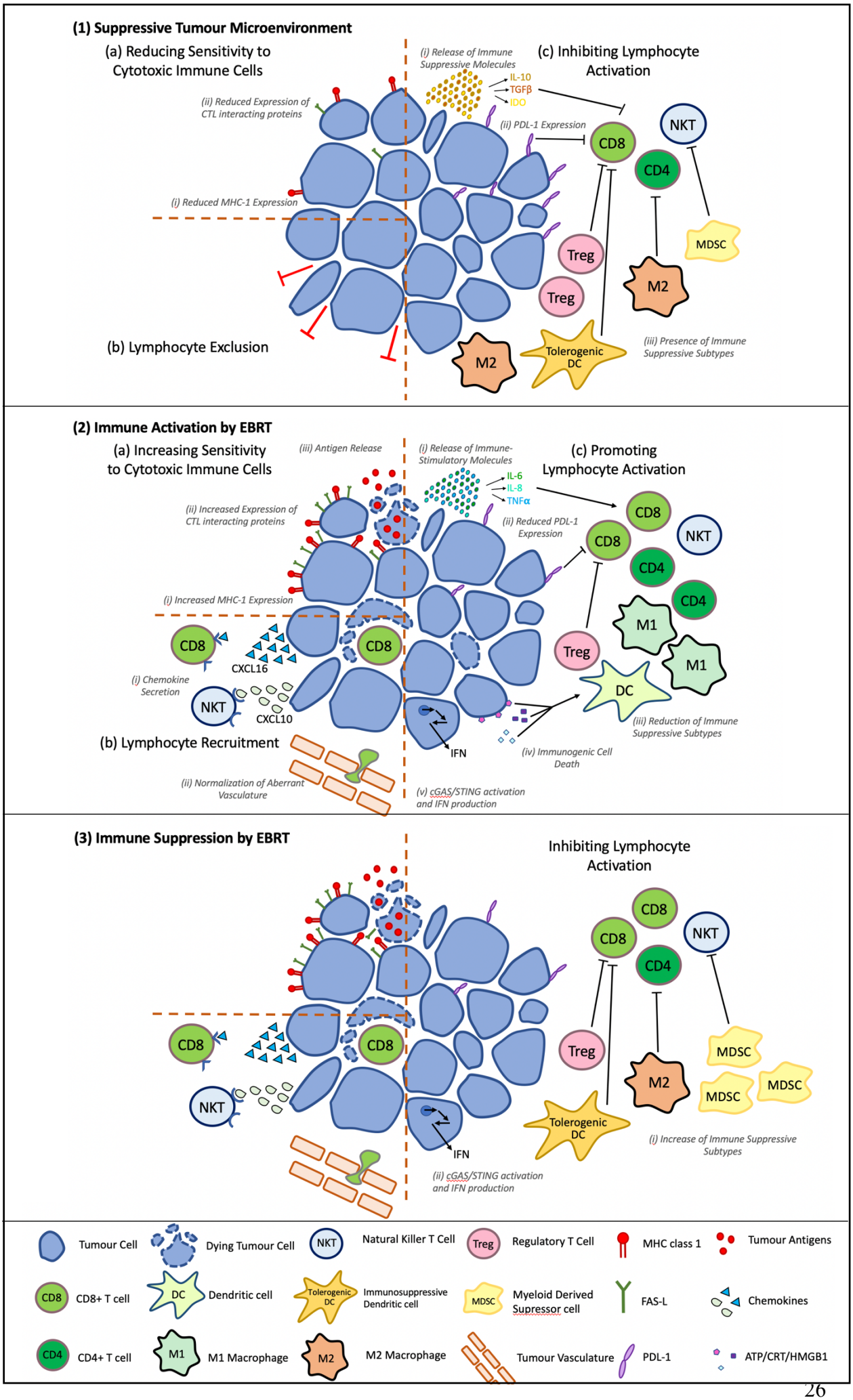
(1) Suppressive Tumour Microenvironment
(a) Reducing Sensitivity to Cytotoxic Immune Cells
(i) Release of Immune Suppressive Molecules
IL-10
TGFβ
IDO
(c) Inhibiting Lymphocyte Activation
(ii) Reduced Expression of CTL interacting proteins
(ii) PDL-1 Expression
CD8
NKT
CD4
(i) Reduced MHC-1 Expression
MDSC
Treg
M2
Treg
(b) Lymphocyte Exclusion
M2
Tolerogenic DC
(iii) Presence of Immune Suppressive Subtypes
(2) Immune Activation by EBRT
(a) Increasing Sensitivity to Cytotoxic Immune Cells
(iii) Antigen Release
(i) Release of Immune-Stimulatory Molecules
IL-6
IL-8
TNFα
(c) Promoting Lymphocyte Activation
(ii) Increased Expression of CTL interacting proteins
(ii) Reduced PDL-1 Expression
CD8
CD8
NKT
CD4
CD4
(i) Increased MHC-1 Expression
M1
CD8
CD8
CXCL16
Treg
M1
(i) Chemokine Secretion
DC
NKT
CXCL10
(iii) Reduction of Immune Suppressive Subtypes
IFN
(iv) Immunogenic Cell Death
(b) Lymphocyte Recruitment
(ii) Normalization of Aberrant Vasculature
(v) cGAS/STING activation and IFN production
(3) Immune Suppression by EBRT
Inhibiting Lymphocyte Activation
CD8
CD8
NKT
CD4
CD8
CD8
Treg
MDSC
M2
MDSC
MDSC
NKT
Tolerogenic DC
(i) Increase of Immune Suppressive Subtypes
IFN
(ii) cGAS/STING activation and IFN production
Tumour Cell
Dying Tumour Cell
NKT
Natural Killer T Cell
Treg
Regulatory T Cell
MHC class 1
Tumour Antigens
CD8
CD8+ T cell
DC
Dendritic cell
Tolerogenic DC
Immunosuppressive Dendritic cell
MDSC
Myeloid Derived Supressor cell
FAS-L
Chemokines
CD4
CD4+ T cell
M1
M1 Macrophage
M2
M2 Macrophage
Tumour Vasculature
PDL-1
ATP/CRT/HMGB1

1.5 Targeted Radionuclide Therapy and the Immune System

1.5.1 Targeted Radionuclide Therapy

TRT represents a distinct form of radiotherapy, which unlike EBRT provides systemic treatment enabling targeting of multiple tumour sites. Imaging and/or therapeutic radioisotopes may naturally accumulate in cells (for example iodine in the thyroid via a sodium iodide symporter), or can be conjugated to targeting moieties such as small molecules, antibodies or other ligands to promote specific accumulation within the tumour site following systemic administration. These isotopes then provide protracted, low dose rate irradiation to the tumour as the isotope decays.

This radiation can be of several different types, ie. alpha, beta or gamma, or a combination of multiple types. X Rays/ gamma rays are indirectly ionising and deposit energy to electrons producing fast moving electrons and ionised atoms. This can cause direct or indirect DNA damage as described in section 1.1. Beta emitters emit a negatively charged electron (beta particle) from their nucleus as the atom decays. Beta particles cause ionisations by collision with, or coming into close proximity to, an orbital electron causing it to be ejected. Alpha emitters release an alpha particle upon radioactive decay, which consists of two protons and two neutrons. Due to their double positive charge and large mass, these alpha particles rip electrons off nearby atoms thus causing multiple ionisations.

Alongside these differences in mechanisms of ionisation, different radiation emissions have different spatial distribution of the ionising events. This is described by linear energy transfer (LET), which is defined the energy transferred per unit length of track which the individual charged particles travel along. This has a significant impact on the biological activity of different radioisotopes. X Rays/ gamma rays are sparsely ionising (low LET), and have a long track length. Beta electrons also have a very low LET except for the few nanometers at the end of their range. For both of these radiation types the long range means that cross-fire occurs between cells. This means that it is not necessary to target every cell within a tumour, as long as all cells are within the range of decaying radionuclides.

Conversely, alpha particles have very high LET along their short path length of up-to-100-µm, with a peak near the end of this path.

The unit of radioactivity for radioisotopes is the Bequerel (Bq), where one Bq is defined as quantity of radioactive material in which there is one decay event per second. In order to have a comparison with EBRT, the absorbed dose in Gray (Gy) must be determined. The absorbed dose is defined as the energy absorbed per unit mass of tissue, and thus depends on both the activity per unit mass of tissue, and the amount of energy emitted per nuclear transition (discussed in section 3.4.5).

A range of radiotherapeutics have entered clinical use over the last century, with many more being explored pre-clinically. These pharmaceuticals employ various targeting approaches and radioisotopes, and these differences may impact the immune changes they induce.

The history of TRT began with the discovery of radium by Marie and Pierre Curie in 1898. Observations that exposure of living tissue to radium cause tissue damage led to the use of naturally occurring radioisotopes (primarily radium) in treating a variety of skin conditions and tumours. In the 1930s, the discovery that radioactive versions of other elements could be produced by exposure of these stable elements to radioactive emissions, led to the production of radioactive iodine and the observation of natural thyroid accumulation [100]. This resulted in the use of radioiodine for the treatment of thyroid disorders due to its natural accumulation in the thyroid [101]. Since then, the field has grown to include other naturally accumulating small molecules such as Radium-223 [223Ra] dichloride (Xofigo, Bayer HealthCare) approved by the FDA in 2013. As a calcium mimetic, [223Ra] dichloride naturally seeks the hydroxyapatite matrix in the bone making it ideal for treating bone metastasis. Similarly, strontium and rhenium isotopes also accumulate in bone and have been used in the treatment of bone metastasis [102–104]. Phosphorus-32 [32P] has also been used as a radiopharmaceutical, for the treatment of haematological malignancies such as thrombocytopenia [105]. Alongside these simple molecules, more molecularly advanced radiopharmaceuticals have been developed employing targeting moieties such as antibodies, nanobodies, or small molecules, conjugated to a therapeutic

isotope. Currently, Leutitium-177 [177Lu] Dotatate (Luthera, Novartis) a somatostatin analogue used for treatment of somatostatin receptor positive neuroendocrine tumours, Yttrium-90 [90Y] ibritumomab tiuxetan (Zevalin) a monoclonal antibody used for therapy of recurrent and resistant forms of low-grade follicular B-cell non-Hodgkin's lymphoma, and Iodine-131 [131I] Meta-idobenzylguanidine (MIBG), a norepinephrine analogue used for treatment of MIBG avid pheochromocytoma or paraganglioma, are all used clinically. Others are progressing through clinical trials, including various derivatives of [177Lu] Prostate specific membrane antigen (PSMA) which are currently undergoing extensive clinical testing and expected to enter routine clinical practice in the near future.

1.5.2 Factors Affecting the Immune Response to TRT

Despite growing understanding of the role of immune engagement by EBRT, little is known about how these mechanisms may contribute to TRT. Given its similarity to EBRT, it follows that TRT is likely to also be capable of promoting an anti-tumour immune response, with the potential for this activation to contribute to the observed efficacy. Indeed, there is accumulating evidence that the closely related modality, brachytherapy where a sealed radiation source is placed in or beside the treatment site, also acts via modulation of the immune response [106–109]. However, differences in various factors such as dose rate and treatment duration are likely to differently shape this immune response (Figure 1.3).

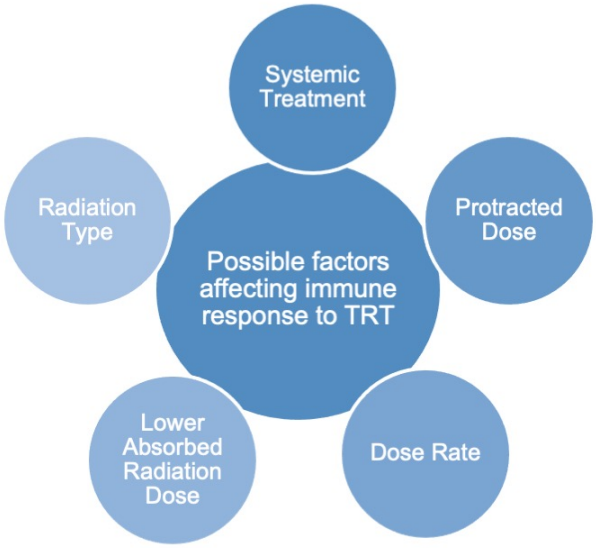

Figure 1.3: Possible factors affecting the immune response to TRT

One potential benefit comes from the systemic nature of treatment. There is mounting evidence that treatment of multiple tumour sites is an important factor for generating a systemic immune response with EBRT [25]. The reasons for this are multi-fold and are predominantly due to effects on the TME.

Firstly, the immune suppressive effects of the TME may only be alleviated by RT locally and thus whilst activated anti-tumour T cells may be in circulation their action at non-irradiated lesions may be limited - for example because of the continued presence of M2 macrophages and T_{reg}, along with expression of immune checkpoints. Secondly, the TME may continue to exclude immune cells from non-irradiated sites. Whilst irradiation can cause changes in the tumour vasculature and expression of immune cell-recruiting chemokines locally, non-targeted tumours may remain poorly infiltrated by anti-tumour immune cells. A third consideration is that heterogeneity of the tumour cells themselves may also pose an issue for single site irradiation. The activated immune response will be directed against the subset of tumour antigens (TAs) released form the irradiated lesion, should the TAs at other sites differ they will not be targeted. It has also been shown that the microenvironment of disseminated tumours can continue to modulate the immune response in the primary tumour affecting response to immunotherapies [110]. This again points to reduced efficacy when only treating a single site. All of

these problems associated with single site irradiation may be overcome when systemically administered TRT is used, enabling simultaneous irradiation of all lesions.

The protracted irradiation associated with TRT may also impact the antitumour immune response, though this is somewhat difficult to predict and may well be impacted by the half-life and tumour retention of any given radiopharmaceutical. For example, lymphocytes are highly radiosensitive, and thus immunosuppressive TILs present in the tumour may be killed by any form of radiotherapy (EBRT or TRT)[111]. This may be beneficial, enabling repopulation with activated lymphocytes; however the prolonged irradiation by TRT may limit this repopulation due to retention of radioactivity and ongoing irradiation of the tumour. Notably though, the relative radiosensitivity of different immune cells to EBRT is still under exploration, and the radiosensitivity to TRT is yet to be explored.

Another consideration is dose rate. EBRT provides high dose rate irradiation, whilst radiopharmaceuticals provide comparatively lower dose rate. It has been suggested that high dose rates are more biologically effective, however the impact on immune-activation remains to be seen.

In general TRT results in a lower total radiation absorbed dose compared with EBRT, which is another interesting factor to consider, with conflicting evidence as to the benefits of high versus low dose irradiation for immune activation [112].

Radiation type is also likely to impact the effect on the immune response. As described above, alpha, beta and gamma emission produce irradiations through different mechanisms resulting in differing linear energy transfer. For alpha particles, the high density of ionisations within a cell may stimulate different immune-modulating mechanisms for example impacting the induction of ICD. Moreover, the short path length will result in non-homogenous distribution of ionisations throughout the tumour. This means that not all tumour cells will be impacted by irradiation due to the inability of radiopharmaceuticals to uniformly penetrate the tumour, the high interstitial pressure, and any differences in receptor/transporter expression throughout the tumour. This may mean that localised

areas of immune-stimulation arise whilst other areas remain immune supressed. Conversely, immune cells wouldn't be targeted by cross fire and thus will avoid irradiation.

Questions arise over the extent to which TRT, like EBRT, will be capable of inducing pro-immunogenic changes such as ICD, cGAS/STING, and vascular changes. Equally important will be consideration of how TRT may impact immunosuppressive mechanisms such as macrophage polarisation and MDSC recruitment, with the ultimate balance between these pro- and anti-immunogenic processes defining the resulting immune response. Understanding the immune landscape of the tumour following TRT may ultimately inform decisions on TRT-immunotherapy combinations.

Whilst study of this response remains limited, a small body of emerging pre-clinical and clinical research addresses the immune response to TRT and is beginning to illuminate the details of this response. However, this work is further complicated by the plethora of targeting agents and radioisotopes available that will likely result in variations in the immune responses they evoke.

1.6 Understanding the Mechanisms of Immune Activation by TRT

Accumulating pre-clinical data is beginning to investigate the role of the immune system in the response to TRT. Unfortunately, the fragmented nature of much of the work in this area makes it hard to form a cohesive account of the immunological effects of a single radionuclide. Instead, small insights from various different radioisotopes and targeting moieties, with differing pharmacokinetics, half-lives and dose rates, studied in different models, and used for different indications provide a somewhat disjointed depiction of the immune response to TRT. Nonetheless, this does provide an indication that immunostimulatory effects can be initiated by some radioisotopes in certain settings. In keeping with studies evaluating EBRT, there are indications in the literature that suggest that T cells may be central to this response. There is now evidence that a range of radiopharmaceuticals are capable of inducing changes that can ultimately promote T cell killing of tumour cells. Analogous to

EBRT, this can occur either by promoting DC activation, T cell recruitment, T cell activation, or increasing the susceptibility of the cancer cell to cytotoxic T cells [113–126].

1.6.1 Lymphocyte Activation

As with EBRT, radiopharmaceuticals have also been shown to promote mechanisms that can stimulate T cell priming. As described above (section 1.4.1), one key mechanism for immune stimulation by EBRT is via activation of ICD. Whilst comprehensive analysis of ICD activation by TRT is so far lacking, various studies have hinted at activation of this process by a number of radiopharmaceuticals. [223Ra] was shown to promote calreticulin upregulation and exposure on the cell surface [114], whilst Gorin et al. demonstrated that another alpha emitter, Bismuth-213 [213Bi], is capable of inducing HMGB1 release in a murine model of adenocarcinoma [127]. Moreover this work, along with work by Hernandez *et al.* using a tumour-targeting alkylphosphocholine (NM600) radiolabelled with [90Y] in EL4 tumours [120], demonstrated induction of ICD *in vivo* via the gold standard rechallenge experiment. Here, cells are treated *in vitro* to induce cell death before injection into one flank of a syngeneic murine host. Subsequently, healthy non-irradiated cells are injected into the contralateral flank. The treated cells, if undergoing ICD, will produce a vaccination effect preventing growth of the contralateral tumour. Gorin *et al.* also tested the animals at later time points to assess the longevity of the immune response, demonstrating a long-lived immune response had been induced. Using a similar experimental setup, the authors went on to show that, again analogous to EBRT, this immune response is T cell dependent, being absent in athymic nude mice. Hernandez *et al.* similarly verified the necessity of T cells for the response to [90Y]NM600 using immuno-compromised Rag2 KO mice which lack mature T and B lymphocytes of the same syngeneic C57BL/6 genetic background. The authors went one step further, transplanting the mice with T cells from either naïve WT mice, or from WT mice previously cured of EL4 tumours by [90Y]NM600 TRT. Both showed significant initial tumour regression following a single 9.25 MBq [90Y]NM600 dose. However, 80% of the naïve T cell transplanted mice experienced tumour recurrence, compared with only 20% of those mice that had received adoptive T cell transfer from complete responders. These percentages were similar to durable response rates in

immunocompetent mice confirming the crucial role of T cells in producing a systemic anti-tumour immune response.

1.6.2 Lymphocyte Recruitment

Alongside these effects on T cell activation, there is some evidence that TRT can promote tumour infiltrating lymphocyte (TIL) recruitment. Wu *et al.* addressed this question in a study investigating [177Lu]DOTATATE in a mouse model of human neuroendocrine tumours [121]. However, as the tumours were human, nude mice were used that are athymic and thus lack T cells and mature B cells of the adaptive immune response, restricting this study to assessment of the innate compartment including dendritic cells (DCs). Whilst this prevented assessment of the complete immune response, the authors were able to show an increase in CD86 expression and increased infiltration of $CD86^+$ APCs into the tumour. Given expression of this co-stimulatory molecule has been shown to be both necessary for and correlated to the efficacy APC-mediated CD8+ T cell activation [122, 123], this suggests [177Lu]Lu-DOTATATE has the potential to induce a $CD8^+$ mediated anti-tumour immune response as has been observed for EBRT.

An increase in CD8+ T cells following TRT has also been directly observed using a syngeneic model of T-cell Non-Hodgkin's Lymphoma treated with [90Y]NM600 [120]. Alongside the increase CD8+ T cell presence, a reduction of tumour associated immunosuppressive T_{reg} cells was observed, suggesting TRT may be able to further promote an anti-tumour immune response by removing this suppressive barrier.

1.6.3 Increasing Sensitivity of Tumour Cells to Cytotoxic Immune Cells

As has been seen with EBRT, increasing the sensitivity of tumour cells to cytotoxic immune cells can be achieved via upregulation of various cell surface molecules on the tumour cells that promote T cell activity in various ways (section 1.4.3). For example, a key surface molecule, MHC class I, has been shown to be upregulated by β- and γ-emitting Samariam-153 [153Sm] chelated to bone-seeking

ethylene diamine tetramethylene phosphonate (EDTMP) and α-emitting [223Ra] dichloride [113, 114].

[153Sm]EDTMP has also been shown to cause upregulation of Intercellular Adhesion Molecule 1 (ICAM-1), an adhesion molecule thought to increase T cell binding and thus enhance cytolytic activity, along with Fas which binds Fas ligand on CTLs mediating direct tumour cell killing [113]. Along with these changes in expression of surface receptors, [153Sm]EDTMP can also increase expression of TAs and thus increase tumour immunogenicity. Ultimately, these changes were shown to produce an increase in susceptibility to killing by TA specific CTLs, demonstrating a functional response. Similar effects on promoting TA specific T cell mediated lysis have also been observed for α-emitting, bone seeking [223Ra] dichloride in human prostate, breast, and lung carcinoma cells [114].

1.7 Clinical Evidence of Immune Activation by TRT

Along with the preclinical studies described above, a small number of clinical observations suggest immune activation by TRT. In particular, observations of abscopal effects - whilst generally prohibited by the systemic nature of most TRTs – have been described for a small number of related therapies. For example, [90Y]radio-embolization (RE), a treatment that is delivered directly to tumours in the liver via injection into the hepatic artery, was noted to cause complete regression of a nontargeted, left hepatic lobe lesion in a patient following targeted [90Y]RE of a right lobar lesion [115].

There is also evidence of possible abscopal effects with the α-emitter [223Ra]. The highly bone-seeking nature of ^{223}Ra combined with the short range of the emitted α-particles mean it is not expected to act on carcinomas in soft tissue. However, there have been multiple observations of regression of tumours at distant sites indicative of an abscopal effect [116, 117].

Recent work has also directly probed the immune effects of various TRTs, also supporting the hypothesis of immune activation. Again looking at [90Y]RE, Chew *et al.* employed a noteworthy combination of time-of-flight mass cytometry and next generation sequencing to demonstrate local

immune activation in [90Y]RE-treated tumours [118]. Using this combination these investigators not only observed an enrichment of $CD8^+$ and $CD4^+$ T cells and NKT cells alongside a reduction in immunosuppressive T_{reg} cells, but also probed the immune activation pathways stimulated by [90Y]RE. This analysis demonstrated a number of mechanisms including MHC upregulation, CD28-dependent T cell activation pathways and upregulation of the adhesion molecule ICAM-1 which is important for lymphocyte recruitment. The authors went on to show that upregulation of chemokines CXCL16 and CCL5 correlated with the increased $CD8^+$ T cell infiltration. Furthermore, response to [90Y]RE could be effectively predicted based on peripheral blood immune status highlighting the potential importance of immune activation for TRT response.

There is also evidence that the related modality, brachytherapy, can trigger an antitumour immune response. For example, proteomic analysis of the response to high dose rate brachytherapy of prostate cancer demonstrated protein activation cascades of three immunological pathways: humoral immune response, leukocyte mediated immunity and complement activation [128]. Transcriptomics analysis in a similar clinical setting also identified changes in immunological regulation [107]. Induction of CD4 and CD8 T cells has also been observed following low dose rate brachytherapy in PCa, although this is limited to analysis of peripheral blood and not tumour samples [129].

1.8 TRT Immunotherapy Combinations

Following this early work demonstrating the ability of various radiopharmaceuticals to induce an immune response, there is now increasing interest in developing combination therapies with immunotherapeutics. As with EBRT, immune checkpoint inhibitors (ICIs) have been tested as possible combination therapeutics. Combination of a checkpoint inhibitor (anti-CTLA4 antibody) has been tested *in vivo* with a novel radioisotope-based therapy. Here, [131I] labelled catalase enzyme was injected intratumourally with sodium alginatem which then produces a homogenously distributed hydrogel at the physiological concentration of Ca^{2+} within the tumour. The addition of this treatment

to anti-CTLA4 demonstrated that this combination could effectively induce abscopal effects accompanied by a significant increase in tumour infiltrating $CD8^+$ T cells, and a reduction in T_{regs} [130]. This radionuclide treatment was also tested in combination with the immune adjuvant CpG, an oligodeoxynucleotide that can activate the TLR9 receptor of innate immune cells, demonstrating that local treatment with the [131I]Cat/CpG/ALG mixture could generate a strong systemic anti-tumour immune response with robust resistance to tumour rechallenge. Combination with CpG was also effective with diffusing α-emitter radiation therapy (DaRT) [125].

DaRT has also demonstrated initial success preclinically in combination with various other TLR agonists (TLR3, TLR1,2) in the CT26 colon cancer mouse model [131]. This combination is further enhanced by concurrent treatment with MDSC inhibitor sildenafil. Importantly this treatment regimen provided long term immunologic memory, protecting from tumour rechallenge. Similarly, DaRT synergises with pattern recognition receptor activators causing tumour rejection, metastasis clearance and antitumour immune memory [132]. Though DaRT is a form of brachytherapy rather than TRT - utilizing implantable seeds embedded with low activity [224Ra] - it still indicates the ability of radioisotopes to induce an anti-tumour immune response.

Traditional TRTs have also been employed in combination studies. Choi *et al.* first combined immune checkpoint inhibitors with [177Lu] TRT in 2018, making use of VLA-4 targeting with [177Lu]LLP2 [133]. This demonstrated a significant enhancement of overall survival compared with TRT or checkpoint inhibition alone in B16F10 murine melanoma models. However, it is worth noting that this study was impacted by significant immune cell targeting by the radiopharmaceutical which resulted in binding of the TRT to immune cells in the TME due to immune cell expression of the VLA-4 target. Using a different targeting moiety to target cell surface receptor integrin $\alpha v\beta 3$ of murine MC38 carcinoma, Chen *et al.* showed a similar synergistic response with a [177Lu] radiopharmaceutical ([177Lu]EB-RGD) combined with anti-PDL1 treatment. These investigators went on to show the importance of scheduling with an improved response achieved using concurrent, rather than sequential treatment

[134]. Indeed, this treatment schedule resulted in immunologic memory that protected mice from tumour re-challenge.

Alpha emitting-TRT has also been shown to combine successfully with immunotherapy in the form of adoptive T cell therapy in preclinical assessment [126]. Here, a multiple myeloma murine model expressing the tumour antigen CD138 and ovalbumin (OVA) was treated with α-emitting [213Bi] conjugated anti-CD138 antibody, followed by adoptive transfer of OVA-specific CD8+ T cells producing significant tumour growth control and improved survival.

Evidence thus far has been sufficient to provoke the initiation of clinical trials combining TRT with immunotherapeutics. Following on from the promising data for [90Y]RE, multiple studies are investigating combination of [90Y]RE with immunotherapeutics (NCT03802747 and NCT03033446). Beyond this, studies are also commencing investigating other systemically delivered radiopharmaceuticals; one phase 1 study is looking into combining [177Lu]PSMA, a small molecule targeting the prostate cancer antigen PSMA, with the anti-PD1 immunotherapeutic Pembrolizumab (NCT03805594). In another trial, a phase I/II study is investigating combination of another anti-PD1 immunotherapeutic Nivolumab, with [177Lu]DOTATATE in treating patients with relapsed or refractory extensive-stage small cell lung cancer or grade I-II lung neuroendocrine tumours (NCT03325816). Although pre-clinical data for either combination is thus far lacking.

Whilst these studies have begun to reveal the potential of combined TRT- Immunotherapy (TRT-IT) combinations, it will be important to expand our understanding of the immune landscape following TRT to inform rational selection of combinations and dosing regimens to achieve the best possible responses.

1.9 Research Objectives

For decades the immune-modulating properties of radiotherapy were largely ignored, but now the essential nature of immune activation by EBRT is finally being acknowledged. Changes in the immune landscape following EBRT are increasingly well understood, leading to combination therapies with immunotherapeutics. However, the role of immune activation by TRT remains largely unexplored. Here, I have summarised the early work in this area which has already demonstrated the potential for TRT to instigate immune-activating mechanisms, including increasing sensitivity to cytotoxic immune cells, promoting lymphocyte recruitment, and promoting lymphocyte activation, much the same as EBRT (Figure 1.2). However, as has been highlighted this body of work is sparse, and moreover is scattered across a range of different radiotherapeutics, lacking in-depth analysis of any given radiopharmaceutical.

I hypothesise that due to similarities with EBRT, TRT will similarly be able to modulate the tumour immune microenvironment. However, due to difference between the two modalities I hypothesise that there will be differences in the landscape of this immune response. Based on this I further hypothesise that combination of TRT with immunotherapeutics will result in synergistic responses.

Consequently, here I aim to do the following:

1. Establish a model for the assessment of the immune response to a clinically relevant radiopharmaceutical.
2. Assess the impact of TRT on the tumour immune microenvironment and the mechanisms underlying these changes.
3. Evaluate potential immunotherapy-TRT combinations.

Chapter II:
Materials and Methods

2.1 Cell lines and cell culture

The 9464D and 975A2 murine neuroblastoma cells lines were a kind gift from Dr Rimas Orentas (NIH Bethesda). The murine prostate cancer cell lines PGLS, RM1-PSMA$_{high}$, RM1-PSMA$_{mid}$ and RM1-PSMA$_{low}$ were a kind gift from Dr Johannes Czernin (UCLA). These cell lines had been produced from parental RM1 cells stably transduced with human PSMA and SFG-Egfp/Luc (RM1-PGLS). A pMIY II-hPSMA plasmid was generated by the insertion of the human PSMA coding sequence into the multiple cloning site of the pMIY II (pMSCV-IRES-YFP II, Addgene 52108) plasmid. Amphotropic retroviruses were generated as previously described [135]. The RM1-PSMA low, med and high cell line had also been produced from RM1 parental cells transduced with the respective amphotropic retroviruses and were then sorted by flow cytometry to isolate pure populations of transduced cells.

The murine prostate cancer cell line RM1 and the human prostate cancer cell line LnCAP were purchased from ATCC. 9464D, 975A2, RM1, PGLS, RM1-PSMA$_{high}$, RM1-PSMA$_{mid}$ and RM1-PSMA$_{low}$ cells were maintained in Dulbecco Modified Eagle medium (DMEM, Sigma-Aldrich, UK) supplemented with 10% (v/v) fetal bovine serum (Invitrogen, UK) and 1% (v/v) penicillin/streptomycin/glutamine (Invitrogen, UK), and were grown at 37°C in 5% CO_2. LnCAP cells were maintained in Roswell Park Memorial Institute medium 1640 (RPMI, Sigma-Aldrich, UK) supplemented with 10% (v/v) FBS (InvitrogenTM, UK) and 1% (v/v) penicillin/streptomycin/glutamine InvitrogenTM, UK), and were grown at 37°C in 5% CO_2.

When cells reached approximately 90% confluency, they were washed in phosphate buffer saline (PBS) (37 mM NaCl; 2.7 mM KCl; 4.3 mM Na2HPO4; 1.47 mM KH2PO4; pH 7.4) and detached from the flask using trypsin-ethylenediaminetetraacetic acid (Trypsin-EDTA) (Sigma-Aldrich, UK). Detached cells were transferred to a falcon tube and spun at 100 x g for 5 minutes in a HeraeusTM MegafugeTM 40 centrifuge (Thermo Fisher Scientific, UK). Following removal of the supernatant,

cells were resuspended in fresh culture media and transferred to a fresh flask. Cells were kept for no more than 15 passages, and tested regularly for mycoplasma sing a MycoAlert testing kit (Lonza, UK), according to the manufacturer's instructions.

2.2 In vitro irradiations

Cells were seeded 20-24 hours prior to irradiation and left to adhere at 37°C in 5% CO_2. Media was then refreshed 30 minutes prior to irradiation. For external irradiations, cells were then transferred to the irradiator in a sterile polystyrene box. Irradiation was delivered using a [137Cs] laboratory irradiator (IBL 637, CISbio International, France), producing 0.662 MeV gamma rays at a dose rate of 0.81 Gy min^{-1}. Following irradiation, cells were returned to incubate at 37°C in 5% CO_2.

For radionuclide treatments, cells were seeded and left to adhere as above. Media was refreshed 30 minutes prior to radionuclide addition. The radionuclide was then added to the cell media under sterile conditions and cells were returned to incubate at 37°C in 5% CO_2.

2.3 Western blotting

Cells were lysed using RIPA buffer (Sigma) containing cOmplete™ Mini protease inhibitors cocktail (Roche) for 30 minutes on ice. Cell lysates were transferred to eppendorfs and centrifuged at 14,000 x g for 5 minutes at 4°C. The supernatants were harvested, and protein concentration of each sample determined using a bicinchoninic acid (BCA) Protein Assay Kit (Thermo Fisher Scientific, UK) according to manufacturer's instructions. Absorbance was measured using an Infinite 200 Pro plate reader (Tecan, Germany). 40 μg protein was mixed with 4μl LDS loading buffer (Invitrogen) and 2 μl NuPAGE™ reducing agent (Thermo Fisher Scientific, UK), then heated at 70°C for 10 minutes. Samples were then separated on 4-12% Bis Tris gel (10 well, NuPAGETM Novex™, Thermo Fisher Scientific, UK) in an XCell SureLock™ Mini-cell system (Thermo Fisher Scientific, UK) using NUPAGE® MES SDS Running Buffer diluted 1:20 in deionised water. Gels were run for up to 1 hour using a PowerPacTM High- Current power supply (Bio-Rad Laboratories Ltd., UK). SeeBlue™ Plus2 Pre-stained Protein Standard (Thermo Fisher Scientific,

UK) was used as a standard marker. Protein transfer on to a nitrocellulose membrane was carried out using NUPAGE® Transfer Buffer diluted 1:20 in deionised water and 20% (v/v) methanol at 100V for 1 hour. Membranes were blocked using 5% (w/v) milk in 1x PBS-T (PBS with 0.1% (v/v) Tween-20) for 1 hour on Boekel Scientific Orbital Platform Shaker (Boekel Scientific, USA). Following blocking, membranes were incubated with primary antibodies (table 1.1) diluted in blocking buffer, then washed 3 x 5 minutes with PBS-T. Membranes were then incubated with secondary horseradish peroxidase (HRP) conjugated antibody for 1 hour and again washed for 3 x 5 minutes with PBST. Membranes were then coated in enhanced luminescence western blotting substrate (Thermo Fisher scientific, UK) for 3 minutes. Excess reagent was blotted onto tissue and the membrane was wrapped in Saran wrap and placed protein side up into an X-ray cassette. X-ray film (Fuji Super RX-N, Fujifil, Japan) was placed on top of the membrane under red safe light for up to 5 minutes. The film was then processed using a Compact X4 film processor (Xograph, UK) or the membrane imaged directly using a LI-COR C-DiGit blot scanner (LI-COR, USA).

ANTIBODY	SPECIES	CLONE	MANUFACTURER	DILUTION
anti-NET	Rabbit	78190	Abcam	1:800 (WB)
Anti-bactin	Rabbit	ab8227	Abcam	1:2000
Anti-PSMA	Mouse	GCP-0404	Novusbio	1:1000 (WB)
Anti-CRT	Rabbit	Ab2907	AbCam	1:100 (ICC, FC)
Anti-PDL1	Rat	10F.9G2	Biolegend	1:60 (FC)
Anti-pdl2	Rat	TY25	Biolegend	1:60 (FC)
Goat anti-rabbit Alexa Fluor 488	Goat	*(RRID AB_143165)*	Invitrogen	1:250 (ICC, FC)
Goat anti-rat Alexa Fluor 488	Goat	*(RRID AB_2534074)*	Invitrogen	1:250 (ICC, FC)
Goat anti-rabbit IgG (H+L), HRP	Goat	*(RRID AB_2533967)*	Invitrogen	1:1000 (WB)
Rabbit anti-mouse IgG (H+L), HRP	Rabbit	*(RRID AB_2533933)*	Invitrogen	1:1000 (WB)

TABLE 1.1: *WB = Western blot; ICC = Immunocytochemistry; FC = Flow cytometry*

2.4 Radiochemistry

Pre-labelled [123I]-MIBG and [131I]-MIBG were purchased from GE healthcare. Characteristics of these radioisotopes are shown in table 1.2.

PSMA-I&T was purchased from Diagnostic Imaging Ltd. [177Lu] was also purchased from Diagnostic Imaging Ltd (isotope characteristics shown in table 1.2). For labelling, 25MBq no carrier added [177Lu] was added to 1 μl of 1 mM PSMA-I&T in 9 μl 0.5 M MES buffer (0.5M MES free acid in dH_2O, adjusted with 10N NaOH to pH 5.5). This reaction mix was incubated for 25 minutes at 95°C. Radio-labelling efficiency was then assessed by HPLC (1260 Infinity II, Aligent Technologies; FlowRAM Radio HPLC Detector, LabLagoic; xBridge® C18 3.5um 3.0x150mm column PN:186003028) and thin layer chromatography.

Isotope	Half life	Decay products	Beta energies	Gamma energies
Iodine-123	13.2 hrs	Tellurium-123	n/a	159 keV (83%); 27 keV (70%); 31 keV (16%); others (< 10%)
Iodine-131	8.1 days	Xenon-131	Primary 606 keV (89% abundance); others 248 – 807 keV	Primary 364 keV (81% abundance); others – 723 keV
Lutetium-177	6.6 days	Hafnium-177	490 keV	113 keV (3%), 210 keV (11%)

Table 1.2 – Radioisotope characteristics (source: hpschapters.org)

2.5 Radionuclide stability

5 MBq freshly labelled [177Lu]PSMA-I&T was diluted in 1.5 ml complete DMEM in an Eppendorf, and incubated at 37°C with 5% CO_2. At various timepoints, 0.5 MBq was removed and assessed by HPLC.

2.6 Binding and internalisation

Cells were seeded in a 6 well plate and left overnight to adhere at 37°C in 5% CO_2. The following day, media was refreshed and left to equilibrate at 37°C for 30 minutes. 3 MBq of [177Lu]PSMA-I&T or [131I]MIBG diluted in 100 μl media was added, and cells incubated for 15, 30, 60 and 180

minutes at 37°C in 5% CO_2. Following incubation, the supernatant was removed and cells thoroughly rinsed in PBS. Cells were then incubated in ice cold glycine acid wash (0.1 M glycine, 0.02 M hydrochloric acid) at for 6 minutes 4°C to remove receptor surface bound radioactivity and removed to a counting tube. Cells were rinsed thoroughly in 1 ml ice cold PBS and this fraction combined with the glycine acid wash fraction. To release internalised activity, cells were incubated in 1 ml 1 N NaOH for 15 minutes at room temperature and removed to a counting tube, followed by a second rinse in 1 ml NaOH added to the same tube. PBS was added to counting tubes to make volumes in all tubes equal to ensure equivalent counting efficiency across samples. Tubes were counted using a Wizard γ counter (Perkin Elmer, MA, USA).

2.7 Retention

Cells were seeded in a 6 well plate and left overnight to adhere at 37°C in 5% CO_2. The following day, media was refreshed, and left to equilibrate at 37°C for a minimum of 30 minutes. 3 MBq of [177Lu]PSMA-I&T or [131I]MIBG diluted in 100 μl media was added, and cells incubated for 120 minutes at 37°C in 5% CO_2. Following incubation, the supernatant was removed, and cells thoroughly rinsed in PBS. Cells were then incubated in fresh media for 0.5, 1, 2, 4 or 24 hours. Following incubation, bound and internalised radioactivity was assessed as in section 2.6.

2.8 HMGB1 ELISA

Cells were seeded in a 6 well plate and left overnight to adhere at 37°C in 5% CO_2. The following day, media was replaced with serum free media and left to equilibrate at 37°C for 30 minutes. Cells were treated by addition of 5 MBq, 10 MBq or 50 MBq of [177Lu]PSMA-I&T diluted in 100 μl media, or subjected to 5 Gy, 10 Gy or 50 Gy delivered using a [137Cs] laboratory irradiator (section 2.2). Cells were then incubated for 24 hr, 96 hr or 144 hr at 37°C in 5% CO_2. Following incubation, 500 μl supernatant was removed to an Eppendorf and centrifuged at 800 x g for 5 minutes to clear cellular debris. HMGB1 concentration was then assessed using HMGB1 ELISA kit II (TECAN IBL, ST51011) according to manufacturer's instructions. Briefly, 100 μl sample dilutant

was added to each well of the ELISA plate, followed by 10 μl sample diluted 1:2 in dilutant, or 10 μl standard. The plate was placed briefly on a plate mixer, then sealed using a plate seal and incubated for 20 hours at 37°C. Following incubation, the supernatant was removed, and wells washed 5 times with wash solution using a multi-channel pipette. 100 μl POD-conjugate was then added to each well, before the plate was sealed with Plate Seal, and incubated for 2 hours at room temperature. Again, wells were washed 5 times with wash solution. 100 μl substrate solution was then added to each well using a multi-channel pipette. The plate was sealed and incubated for 30 minutes at room temperature. 100 μl Stop solution was then added in the same sequence as the substrate solution using a multi-channel pipette. Absorbance of each well was measured at 450 nm using a Magellan Infinite M200Pro plate reader (TECAN).

2.9 TGFb ELISA

Cells were seeded in a 6 well plate and left overnight to adhere at 37°C in 5% CO_2. The following day, media was replaced with serum free media and left to equilibrate at 37°C for a minimum of 30 minutes. Cells were treated with various doses of [177Lu]PSMA-I&T or EBRT. Cells were then incubated for 24 hr, 96 hr or 144 hr at 37°C in 5% CO_2. Following incubation, 500 μl supernatant was removed to an Eppendorf and centrifuged at 800 x g for 5 minutes to clear cellular debris. TGFb concentration was then assessed using Mouse/Rat/Porcine/Canine TGF-beta 1 Quantikine ELISA Kit (R&D systems) according to manufacturers instructions. Briefly, samples were first activated by addition of freshly prepared activation reagent followed by neutralisation. 50 μl assay dilutant RD173was added to each well of the ELISA plate, followed by 50 μl sample, control or standard. The plate was briefly tapped to mix, then sealed using a plate seal and incubated for 2 hours at room temperature. Following incubation, the supernatant was removed, and wells washed four times with wash solution using a multi-channel pipette. 100 μl TGFb1-conjugate was then added to each well, before the plate was sealed and incubated for 2 hours at room temperature. Again, wells were washed four times with wash solution. 100 μl substrate solution

was then added to each well using a multi-channel pipette. The plate was sealed and incubated for 30 minutes at room temperature. 100 µl Stop solution was then added in the same sequence as the substrate solution using a multi-channel pipette. Absorbance of each well was measured at 450 nm using a Magellan Infinite M200Pro plate reader (TECAN).

Activated TGFb concentration was assessed as above but excluding the activation step.

2.10 Assessment of Calreticulin exposure or PD-L1 by Flow cytometry

Exposure of calreticulin was assessed by flow cytometry. Cells were seeded in 6 well plates and left to adhere overnight at 37°C in 5% CO_2. Following media refresh, cells were treated by addition of [177Lu]PSMA-I&T or external irradiation using the Cs irradiator and left to incubate at 37°C in 5% CO_2. Following treatment, supernatant was removed, and cells washed gently in PBS. Cells were detached using trypsin-ethylenediaminetetraacetic acid (Trypsin-EDTA) (Sigma-Aldrich, UK) and removed to labelled tubes to be centrifuged at 200 x g for 5 minutes. The supernatant was discarded, and the pellet washed in 2 ml PBS, then again centrifuged at 250 x g for 5 minutes. The supernatant was discarded, and the pellet blocked in 1 ml 2 % FBS/PBS then centrifuged at 250 x g for 5 minutes. The supernatant was discarded, and the pellet resuspended in 100µl primary antibody diluted in 2% FBS/PBS. Cells were incubated for 30 minutes, and vortexed halfway through to resuspend the cells. 1 ml of 2% FBS/PBS was then added, and the samples centrifuged at 250 x g for 5 minutes. The supernatant was discarded, and the pellet resuspended in 100 µl secondary antibody diluted in 2% FBS/PBS. Samples were incubated for 30 minutes in the dark, and vortexed halfway through to resuspend the cells. 1 ml of 2% FBS/PBS was then added, and the samples centrifuged at 250 x g for 5 minutes. The supernatant was discarded, and the pellet resuspended in 500 µl 2% FBS/PBS containing 10 µl of 1mg ml-1 PI (Thermo Fisher Scientific, UK) and 100 µg ml^{-1} RNase A (Thermo Fisher Scientific, UK) and incubated for 10 minutes in the dark. Cells were then assessed in the FACSort flow cytometer (BD Bioscience). The FACS data was analysed using BD CellQuest Pro, using gating to exclude dead cells. The staining procedure was carried out at 4°C for CRT staining, and room temperature for PDL1 staining.

2.11 Assessment of Calreticulin exposure by Immunocytochemistry

PGLS cells were seeded in Thermo Scientific Nunc Chamber slides (Thermo Scientific, 154453) and left to adhere overnight at 37°C in 5% CO_2. Cells were then treated by addition of 1 uM mitoxantrone (Sigma-Aldrich, UK), and left to incubate at 37°C in 5% CO_2. Following treatment, supernatant was removed, and cells washed gently in PBS. Cells were blocked in 200 μl 2% BSA (Sigma-Aldrich, UK) for 20 minutes on ice. Blocking buffer was carefully removed and replaced with 100 μl primary antibody [Abcam, Anti-Calreticulin antibody: ab2907] diluted 1:100 in cold blocking buffer. Cells were incubated for 30 minutes on ice, before washing 3 x 5 minutes in cold PBS. 200 μl secondary antibody [Goat anti-rabbit Alexa Fluor 488, Life technologies A11008] diluted 1:250 in cold blocking buffer was added for 30 minutes on ice. Cells were washed 3 x 5 minutes in cold PBS, then fixed and stained with 1:2,000 Hoercst in 4% paraformaldehyde (Fisher Scientific, UK) for 10 minutes. The chamber and gasket were removed and a small drop of Vectashield (Vector laboratories Inc, CA) and covered with a coverslip and sealed with nail varnish. Slides were imaged using a Leica SP8 inverted scanning confocal microscope (Leica Biosystems).

2.12 Animal work and associated experiments

2.12.1 Animals and husbandry

Animal procedures were carried out in accordance with UK Animal law (Scientific Procedures Act 1986), and local ethics reviews. Experiments were conducted within the limits of the Home Office issued project licence (Project licence number 30/3115). C57BL/6 mice were purchased from Charles River Laboratories (Kent, UK). Animals were housed in specific pathogen-free facilities with temperature control (24±1°C) and humidity control (55%±10%), and 12 hour light/dark cycles. Mice were fed *ad libitum and* had unlimited access to water. Weight was checked twice weekly, and were only entered into studies if weight exceeded 17.0 g. If > 10% weight loss was

observed then mice were culled. Mouse health was monitored daily, including monitoring for ulceration. Mice culled if wet ulceration was detected, or tumour size approached 1000 mm^3.

Mouse numbers for efficacy experiments were determined using power calculation for an unpaired t-test in the Experimental Design Assistant (EDA, nc3rs, https://eda.nc3rs.org.uk/) per ARRIVE guidelines (https://arriveguidelines.org/arrive-guidelines). Variability was estimated using standard deviation of data collected on tumour growth from initial tumour growth analysis (figure 3.7A). The power of the experiment was set to 80%.

2.12.2 Tumour inoculation

Cells were harvested in log-growth phase (approximately 70% confluency) and diluted in PBS. For the 9464D and 975A2 models, 2 x 10^6 cells were injected subcutaneously into the flank of anaesthetised mice using a 23G needle. For the PGLS model, 5 x 10^5 cells were injected subcutaneously into the flank of anaesthetised mice using a 23 G needle. Tumour size was measured twice weekly using callipers, and tumour volume calculated using the formula: Tumour volume = (length x width x height)/2. Mice were culled when tumour volume approached 1,000 mm^3.

2.12.3 Vaccination / rechallenge study

PGLS cells were seeded in T25 flasks and left to adhere overnight at 37°C in 5% CO_2. Cells were then treated by addition of 60 MBq [177Lu]PSMA-I&T or 50 Gy external irradiation using the Cs irradiator and left to incubate for 144 hours at 37°C in 5% CO_2. Following treatment, supernatant was removed, and cells washed gently in PBS. Cells were detached using trypsin-ethylenediaminetetraacetic acid (Trypsin-EDTA) (Sigma-Aldrich, UK) and removed to labelled tubes to be centrifuged at 200 x g for 5 minutes. The supernatant was discarded, and the pellet washed in 5 ml ice cold PBS, then again centrifuged at 250 x g for 5 minutes. This wash step was repeated. Cells were counted using a haemocytometer (Hawksley, UK). 5 x 10^5 cells were injected subcutaneously into the right flank of anaesthetised mice using a 23 G needle. Mice were

monitored for tumour growth. 7 days later, 5 x 10^5 viable PGLS cells were injected as described in section 1.10.2. Mice were monitored for tumour growth for 80 days post rechallenge.

2.12.4 Treatment

Mice were subjected to treatment when their tumour sizes reached 80 mm^3. EBRT was delivered using a GulmayRS320 X-ray irradiation system (Gulmay Medical Ltd, UK) at 300 KV, dose rate 2.25 Gy per minute under anaesthesia. Mice were shielded using lead so only the tumour was exposed.

TRT was delivered via tail vein cannula under anaesthesia. The radiopharmaceutical was diluted in PBS to a volume of 100 µl prior to injection.

For biodistribution analysis [123I]-MIBG and [177Lu]-PSMA-I&T were used in the neuroblastoma and prostate cancer models, respectively. [123I]-MIBG was used rather than [131I]-MIBG in biodistribution studies for radiation safety reasons as no therapeutic effect was needed and biodistribution is not thought to be impacted. For treatment studies, [177Lu]-PSMA-I&T was used in the prostate cancer model.

For combination treatment, 200 µg anti-TGFb clone 1D11 (#BP0057; 2BScientific, UK) was administered via intra-peritoneal injection twice weekly for 5 weeks. 24 hours following the first treatment, mice were given 100 MBq [177Lu]PSMA-I&T via tail vein cannula or 10Gy EBRT.

Tumour volume was measured two to three times weekly. When mice reached the study endpoint (1,000 mm^3 tumour or severe ulceration), they were sacrificed via schedule 1 methods. Cannulations were performed by Karla Watson or Magda Hutchins.

2.12.5 Ultrasound

Contrast enhanced US was performed on anaesthetised mice using a Vevo3100 scanner (FUJIFILM Visualsonics, Netherlands) with a MX250 probe (Centre Transmit 267 Frequency: 20 MHz, Axial Resolution: 75 µm). 50 µl SonoVue (SV) (Bracco Imaging) was administered intravenously. Non-Linear Contrast mode was used for imaging acquisition. Vevo LAB software

(FUJIFILM Visualsonics) was used to quantify contrast intensity over time for both the tumour core and outer edge.

Contrast ultrasound was performed with the help of Sheena Wallington.

2.12.6 DCE-MRI

DCE-MRI was performed on anaesthetised mice using a 4.7T MRI system (Varian Inova) with a 25 mm quadrature birdcage radiofrequency coil. Mice were cannulated and placed in the scanner with respiratory and temperature monitoring. Gadodiamide (30 µL of 0.5 mmol/mL; Omniscan, GE Healthcare) was injected via tail vein cannula 2 min from the start of acquisition. The scan was acquired using a 3D gradient echo (GE) sequence. Images were segmented in ITK-SNAP. The images were then processed to determine the parameters of initial area under the curve (IAUC) and pixel enhancement ratio. These were performed on a voxel by voxel basis within tumour regions. The whole tumour average was calculated.

DCE-MRI and tumour contouring was performed by Sheena Wallington. The DCE-MRI parameters were calculated by Danny Allen.

2.12.7 SPECT/CT

At specified timepoints post radionuclide treatment, animals were anaesthetised and placed in a purpose-built cradle with a pressure balloon to monitor respiratory rate and temperature probe. Data was acquired in list mode (gamma spectrum collection from 0-1200 keV) with a single gantry SPECT/PET/CT scanner (VECTor4CT, MILabs, Netherlands) equipped with the HE-UHR-RM collimator containing pinhole apertures of 1.8 mm diameter, using MILabs acquisition software v7.39. Triple-energy-window based scatter correction was applied for lutetium-177 peaks (103-126 and 197-221 keV) and background peaks (98.4-103, 126-130.6, 192.2-197 and 221-225 keV). All images were reconstructed with MILabs reconstruction software. Following reconstruction, SPECT and CT data were co-registered followed by CT based attenuation correction. Image slice displays and maximum intensity projections were generated using pMOD v3.36.

2.12.8 Ex vivo Biodistribution

At a specified timepoint following radionuclide treatment and any SPECT/CT imaging sessions, animals were euthanised and selected organs, tissues and blood were removed and placed in pre-weighed counting tubes. The activity in each tube was counted using a Wizard γ counter (Perkin Elmer, MA, USA), alongside a tube containing the injected dose prepared at the time of treatment (to account for decay) to enable calculation of the % injected dose. Tubes were reweighed to determine tissue weight to enable calculation of % injected dose per gram.

2.13 Tumour sectioning

Immediately following sacrifice tumours were excised. Tumours were flash frozen in liquid nitrogen and stored at -80°C until required for sectioning. Frozen tumours were embedded in optimal cutting temperature (OCT) compound (25608-930 TissueTek) mounted on a specimen holder using the specimen quickfreezer of a Leica CM1950 Cryostat (Leica Biosystems). 10 μm sections were prepared and mounted on SuperFrost plus microscope slides (ThermoFisher). Slides were either used immediately or stored at -80°C.

2.14 Autoradiography

Autoradiography was performed on sequential tumour sections within 24 hours of excision. Tumour sections mounted on microscope slides were exposed to a Super Resolution Phosphor screen in an autoradiography cassette. A Cyclone Plus Storage Phosphor system (PerkinElmer) was then used to scan the film to generate autoradiographs of the tumour sections.

2.15 NanoString

Prior to RNA work, an RNAse free workspace was cleared in the laboratory. Surfaces and equipment were regularly cleaned with ethanol and RNase zap (ThermoFisher). Immediately following sacrifice, tumours were excised, and subcutaneous fat and any lymph nodes removed. Tumours were flash frozen in liquid nitrogen and powdered using a pestle and mortar. Powdered

samples were transferred to falcon tubes in dry ice. Samples were then diluted in Buffer RLT containing β-mercaptoethanol (Qiagen), and passed through a 20 G needle 20 times to ensure complete homogenisation. RNA was extracted from the lysate using RNeasy Mini Kit (Qiagen) according to manufacturer's instructions. All RNA were dissolved in RNase-free water and stored at -80°C. RNA quality and quantity were assessed using a NanoDrop 2000 microvolume spectrophotometer (Thermo Fisher). RNA samples with the ratio of absorbance at 260 and 280 nm (A260/280) > 1.8 and A260/230 > 2.0 were used for subsequent analysis.

The NanoString hybridisation reaction was then set up using the PanCancer Immune Profiling Panel Reporter CodeSet and Capture ProbeSet according to manufacturer's instructions (NanoString). The following day, samples were analysed using a SprintProfiler (Nanostring). Results were analysed using nSolver software with nSolver Advanced Analysis Module (Nanostring) with further analysis in R (v4.0.1, Institute for Statistics and Mathematics, Vienna, Austria).

2.16 Transcriptomics

The RNA-sequencing data and corresponding clinical information of patients with prostate cancer were downloaded from The Cancer Genome Atlas (TCGA) (https://cancergenome.nih.gov/) and $\log_2$ transformed. In order to assess the impact of various immune markers on BCR, patients with a follow up time of less than 36 months were excluded, leaving 204 patients with sufficient follow up time. The cut-off value of immune target mRNA expression was determined based on its median value. Survival curves were determined by Kaplan-Meier method and log-rank test. Univariate Cox analyses were used to evaluate the role of expression of each immune target on BCR. Immune cell numbers were determined using the Danaher et al. method [136]. In order to confirm the validity of the marker genes, the pairwise similarity statistic was determined between all marker gene pairs as set out in the original paper using the formula:

$$similarity\,(x, y) = \frac{\sum (x - \overline{x})\,(y - \overline{y})}{\frac{(n-1)}{2}(var(x) + var(y))},$$

All marker genes had a PSS of > 0.6 and thus were included in analysis. The spearman method was used to assess correlation between immune cell infiltration and specified immune targets. TCGA data were analysed using R (v4.0.1, Institute for Statistics and Mathematics, Vienna, Austria).

2.17 Statistical Analysis

Statistical analyses were performed using Graphpad Prism, version 9.0.0 (GraphPad Software, USA). The number of repeats or number of mice per group is indicated in figure legends. Statistical significance was determined by unpaired *t* test or one-way ANOVA performed with Dunnett's or Tukey's post hoc adjustment for multiple comparisons. Survival curves were generated using the Kaplan-Meier method. Log-rank tests were used to compare median survival time. For transcriptomics, Univariate Cox analyses were also used to evaluate the role of expression of each immune target on BCR. Results are given as Hazard Ratio (HR), confidence intervals (CI), and p value (p). Graphs show mean with standard error of the mean (SEM) to indicate the uncertainty in the estimate of the mean. Asterisk symbols are used to denote statistical (p) significance values: *p<0.05 **p<0.01 ***p<0.001 ****p<0.0001.

Chapter III:

Establishing a Model to Study the Immune Response to TRT

3.1 Introduction:

3.1.1 Targeted Radiotherapy (TRT)

With increasing understanding of the importance of immune activation for therapeutic efficacy of external beam radiotherapy (EBRT)[19, 21, 23–25, 27, 31, 32, 84, 85, 137], along with promising results from EBRT-immunotherapy (IT) combinations [28, 138–140], it seems likely that similar factors may play a role in the response to targeted radiotherapy (TRT). Differences between the two radiotherapeutic modalities may result in some interesting differences that may be exploitable in combination therapies (see Chapter 1, sections 1.5-1.8).

Pre-clinical examination of the immune response to TRT requires the use of an immune-competent, TRT-targetable model. Given the limited existing literature assessing immune responses to TRT, it is perhaps unsurprising that very few models have been developed for such purposes. Rather, a majority of pre-clinical assessment of TRTs has been conducted in human xenograft models using immune-compromised mice, making it impossible to conduct in depth immunological analysis. Establishing a suitable model for this programme of research was thus necessary. For the sake of simplicity, and for more direct clinical relevance, I chose to limit my search to a radiopharmaceutical that is already in use in the clinic.

As described in chapter 1.5, a range of radiotherapeutics have entered clinical use over the last century, with many more being explored pre-clinically. For proof of concept that radionuclides can indeed induce changes to the immune landscape, I have limited my choice of molecules for this work to the clinically relevant radiopharmaceuticals, [131I]MIBG and [177Lu]PSMA.

3.1.2 Iodine-131 MIBG

As an analogue of norepinephrine, MIBG can enter cells via the norepinephrine transporter (NET) (Figure 3.1(A)). This transporter - typically present at sympathetic neuronal synapses - provides sodium-facilitated uptake of norepinephrine and dopamine from the synapse, but is also expressed at high levels by various neuronal crest tumours. This prompted the development of MIBG over 40 years ago as an imaging agent [141], however the tumour avidity of MIBG has also led to its use as a therapeutic via conjugation to therapeutic radioisotope [131I] to provide a localised dose of radiation. Whilst widespread clinical use is currently limited to pheochromocytoma and paraganglioma, it is also established for neuroblastoma. Neuroblastoma is a cancer that most commonly effects children under 5. It develops from immature nerve cells most commonly in and around the adrenal gland, however it can also develop in other areas including the abdomen, chest, neck and spine. [131I]MIBG is proving to be effective in both newly diagnosed and relapsed patients with good responses in both groups, and MIBG uptake in >90% of neuroblastomas including both primary tumours and sites of metastatic disease [142–144]. As a disease with high biological heterogeneity, patients with low and intermediate risk neuroblastoma have favourable prognosis with a five year survival rate of >90%, however for high risk neuroblastoma patients - approximately 60% of cases - prognosis remains unfavourable. Standard treatments have major side effects, demonstrate particularly poor efficacy in late stage disease, and often fail to prevent subsequent relapse due to their inability to control minimal residual disease. As such, there is much hope that immunotherapeutics will be able to overcome these problems for high-risk neuroblastoma patients. So far the greatest therapeutic strides have been made by targeting tumour associated antigens such as GD2 with monoclonal antibodies or chimeric antibody receptor T cells. Unfortunately, use of 'classic' immunotherapeutics such as checkpoint inhibitors are yet to show significant efficacy for neuroblastoma. Here I aim to use [131I]MIBG for proof of principle studies to show whether TRT is able to induce an immune response that may subsequently enable [131I]MIBG to enhance the efficacy of immunotherapeutics in neuroblastoma through RT-IT combinations.

3.1.3 Lutetium-177 PSMA

A second clinically relevant radiopharmaceutical is [177Lu] prostate specific membrane antigen ([177Lu]PSMA). In recent years, various derivatives of [177Lu]PSMA have been developed and are demonstrating promising results in clinical trials for the treatment of prostate cancer (PCa). This confusingly named radiopharmaceutical binds its namesake prostate specific membrane antigen (PSMA), a type II transmembrane enzymatic protein that is weakly expressed in normal prostate tissue, but highly upregulated in 90-100% of PCa cases [145–147]. Importantly, the complex is internalised following ligand binding, thus trapping the radiopharmaceutical in the cell.

Various molecules have been developed based on the same PSMA binding domain with a linker region connecting to a chelator, typically 1,4,7,10-tetraazacyclododecane-1,4,7,10-tetraacetic acid (DOTA) or 1,4,7,10-tetraazacyclododececane,1-(glutaric acid)-4,7,10-triacetic acid (DOTAGA), enabling labelling with various radionuclides including the beta and gamma emitting therapeutic isotope 177-lutetium [177Lu] (Figure 3.1(B)). Such radiopharmaceuticals have now been used in thousands of patients worldwide[148–152], with the major agents being PSMA-617 and PSMA-I&T (Figure 3.1(C)). Whilst both PSMA-617 and PSMA-I&T have the same PSMA binding motif and chelator, the linker regions differ resulting in slightly differing pharmacokineticsc[153].

This therapeutic is particularly promising for treatment of metastatic castration resistant prostate cancer (mCRPC) which has a poor prognosis, with a median survival of approximately 3 years yielding an acute need for improved therapeutics. mCRPC is an advanced disease state that can develop following treatment with androgen deprivation therapy (ADT) which is used as a first line treatment for patients with refractory disease. Unfortunately, despite causing remission with a prostate-specific antigen (PSA) decline in 90% of patients, the disease progresses after a median time of 2-3 years [154]. Through this progression, the cancer becomes resistant to androgen deprivation leading to mCRPC with very limited treatment options. It is hoped that development of [177Lu]PSMA will improve this, enabling irradiation of multiple sites, and furthermore is potentially helped by previous ADT which may promote further PSMA upregulation [155–157].

Whilst this new approach is not curative in the mCRPC setting (and is yet to be trialled in less advanced disease), data thus far is promising and offers the possibility to identify synergistic combinatorial approaches– for example employing immunotherapeutics. Indeed, pioneering immunotherapies met with success in PCa. Sipuleucel-T – a cell based immunotherapy – improved overall survival in the IMPACT trial resulting in FDA approval [158]. However, other immunotherapeutics - notably immune checkpoint inhibitors - have thus far not met success [159]. This is perhaps due to the relatively poor immune infiltration and activation observed in PCa tumours, with low TIL numbers and elevated regulatory phenotype immune cells [160, 161]. This may imply a potential benefit of radiotherapy, which has been shown to increase immune cell infiltration and shift the ratio of regulatory: anti-tumour immune cells [68, 75, 121]. Here the aim was to develop a murine model to enable us to identify whether [177Lu]PSMA-I&T is capable of inducing such changes.

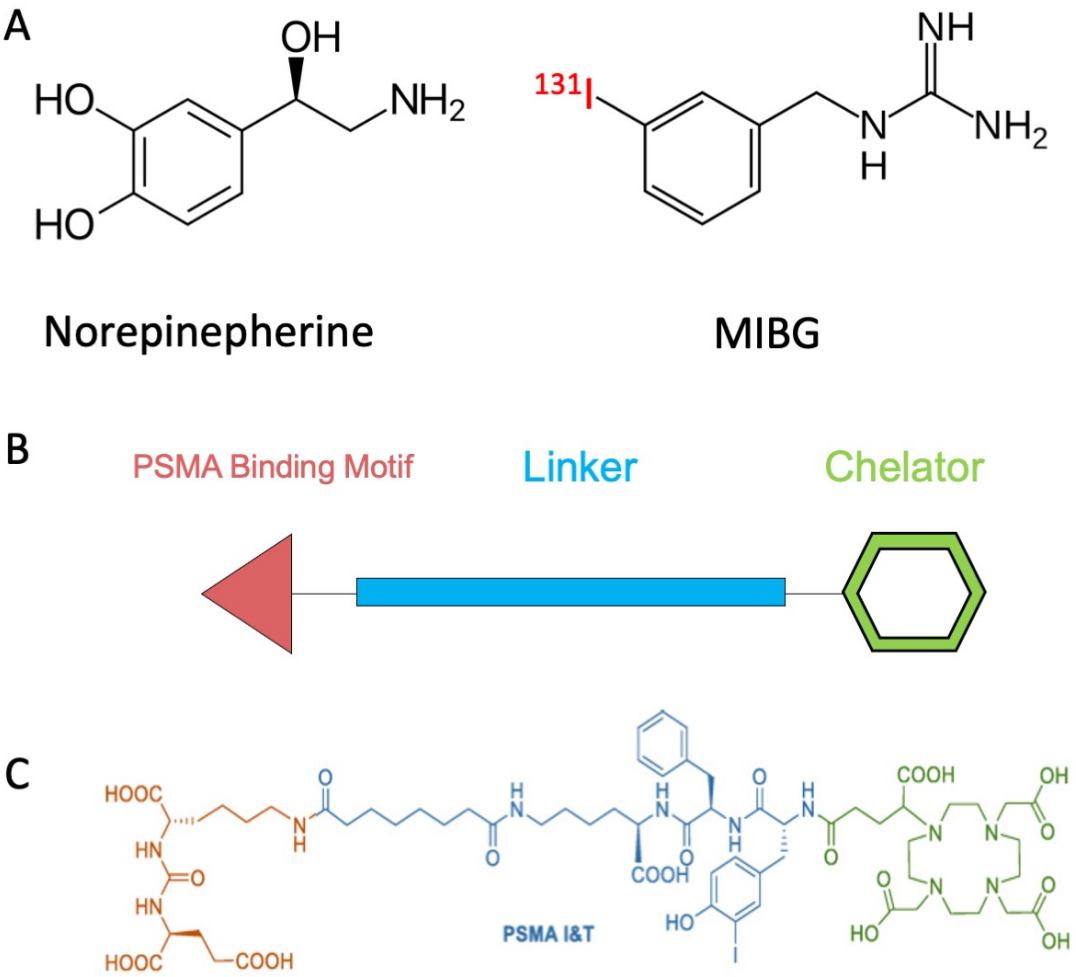

Figure 3.1: Structure of NET and PSMA targeting small molecules
(A) The structure of MIBG (right) is an analogue of norepinephrine (left) (B) Schematic of the basic construct of a PSMA targeting small molecule, consisting of a PSMA binding motif (red), linker (blue), and chelator (green) that can be labelled with a number of different radionuclides. (C) The structure of PSMA-I&T, one of the two most common PSMA small molecules, consisting of a urea based PSMA binding motif (red), linker region (blue), and DOTAGA chelator (green).

3.2 Aims

1. To identify murine cell lines that specifically internalise [131]MIBG or [177]PSMA
2. To determine the *in vivo* growth characteristics of these tumour models
3. To determine the biodistribution of [131]MIBG or [177]PSMA

3.3 Results

3.3.1 Murine Neuroblastoma Cell Lines 9464D and 975A2 Demonstrate Significant [131I]MIBG uptake *in vitro,* whilst Murine Prostate Cancer Cell Line PGLS Demonstrates significant [177Lu]PSMA-I&T uptake

The first aim was to identify murine cell lines capable of internalising the clinically relevant radiopharmaceuticals, [131I]MIBG and [177Lu]PSMA-I&T. Given their known uptake mechanisms, these cells were required to express NET and PSMA, respectively.

For [131I]MIBG a majority of the published preclinical work has been conducted in SK-N-SH and SK-N-BE(2)C. As human neuroblastoma cell lines, these are unsuitable for study of the immune response as they would not form tumours in immune competent mice[162–167]. Instead, murine tumour cell lines are required that can form tumours in immune competent, syngeneic hosts. Such cells are also required to express NET, the transporter responsible for selective uptake of [131I]MIBG. As such, NET expression was assessed in two recently developed murine neuroblastoma cell lines, 9464D and 975A2. Whilst neither have yet been used with [131I]-MIBG specifically, the TH-MYCN transgenic mouse model from which both cell lines were isolated has been previously used for such studies. This suggests that these cells are likely to express NET [168]. Conveniently, 9464D allografts have previously been evaluated and shown to have an immune landscape representative of human NBLs and so are likely to reflect the clinical immunological response to [131I]-MIBG [169].

Western blot analysis of these cell lines confirmed expression of NET in both cell lines (Figure 3.2 (B)). Cells were thus assessed for internalisation of [131I]MIBG *in vitro*. Following incubation with pre-labelled [131I]MIBG for various durations, cells were washed and subjected to glycine acid wash to remove any externally bound radiopharmaceutical prior to lysis for quantification of the internalised fraction. Strikingly, the murine cells exhibited almost identical uptake to the human cell line, SK-N-SH (Figure 3.2 (E)). As such, these cells provide an ideal model for the study of [131I]MIBG *in vitro*. It is however worth noting that the retention of [131I]MIBG is relatively poor in all cell lines, as indicated

by a significant loss of internalised activity over time (Figure 3.2 (F)), perhaps due to intracellular deiodination.

Similar to MIBG, a majority of pre-clinical work on PSMA has employed human cell lines, specifically LnCAP. However, unlike [131I]MIBG, there is a small body of work describing assessment of [177Lu]PSMA-I&T in a murine model [170, 171]. These studies employ the murine PCa cell line RM1 transduced to express human PSMA at varying levels (PSMAlow, PSMAmid, and PSMAhigh), along with PGLS (PSMA-positive, Green fluorescent protein–positive, and LuciferaSe-positive) - an RM1 based cell line transduced to express luciferase and GFP alongside PSMA for *in vivo* monitoring of the tumour. The PSMA expression of these cells was thus confirmed in comparison with LnCAP (Figure 3.2 (A)).

In contrast to MIBG, [177Lu]PSMA-I&T is not commercially available in a pre-radiolabelled form and must instead be radiolabelled prior to use. Thus, in order to assess [177Lu]PSMA-I&T internalisation and carry out subsequent *in vitro* and *in vivo* studies, labelling of PSMA with [177Lu] was optimised to achieve labelling efficiency of <95% ensuring limited free [177Lu] and thus maximal uptake (Figure 3.3(A)). This labelling efficiency was confirmed with both HPLC and TLC analysis (Figure 3.3 (A)(B)). Stability of the labelled compound was then assessed in 10% FBS DMEM at 37°C (cell culture conditions), showing formation of a second HPLC peak over time, accounting for 12% [177Lu] within 24 hours, building to 50% of the activity by 120 hrs (Figure 3.4(A)). This suggests that degradation occurs over time, potentially due to radiolysis of the PSMA. As the effect of this degradation is unknown, freshly labelled PSMA was used for every study, though the effect of this degradation *in vivo* may require further consideration.

Following labelling optimisation, uptake of [177Lu]PSMA-I&T was assessed in a similar manner to the neuroblastoma cell lines, demonstrating uptake is dependent on PSMA expression level with uptake 36-fold greater in PSMAhigh compared with RM1, 12-fold greater than PSMAlow, and three-fold greater than PSMAmid following a three hour incubation (Figure 3.2 (C)). Collectively, these findings

support a PSMA dependent mechanism of uptake. Interestingly, this internalisation occurs rapidly, plateauing within 2-4 hours. Collectively, this work confirms that these cells provide a suitable model for study of [177Lu]PSMA-I&T *in vitro*.

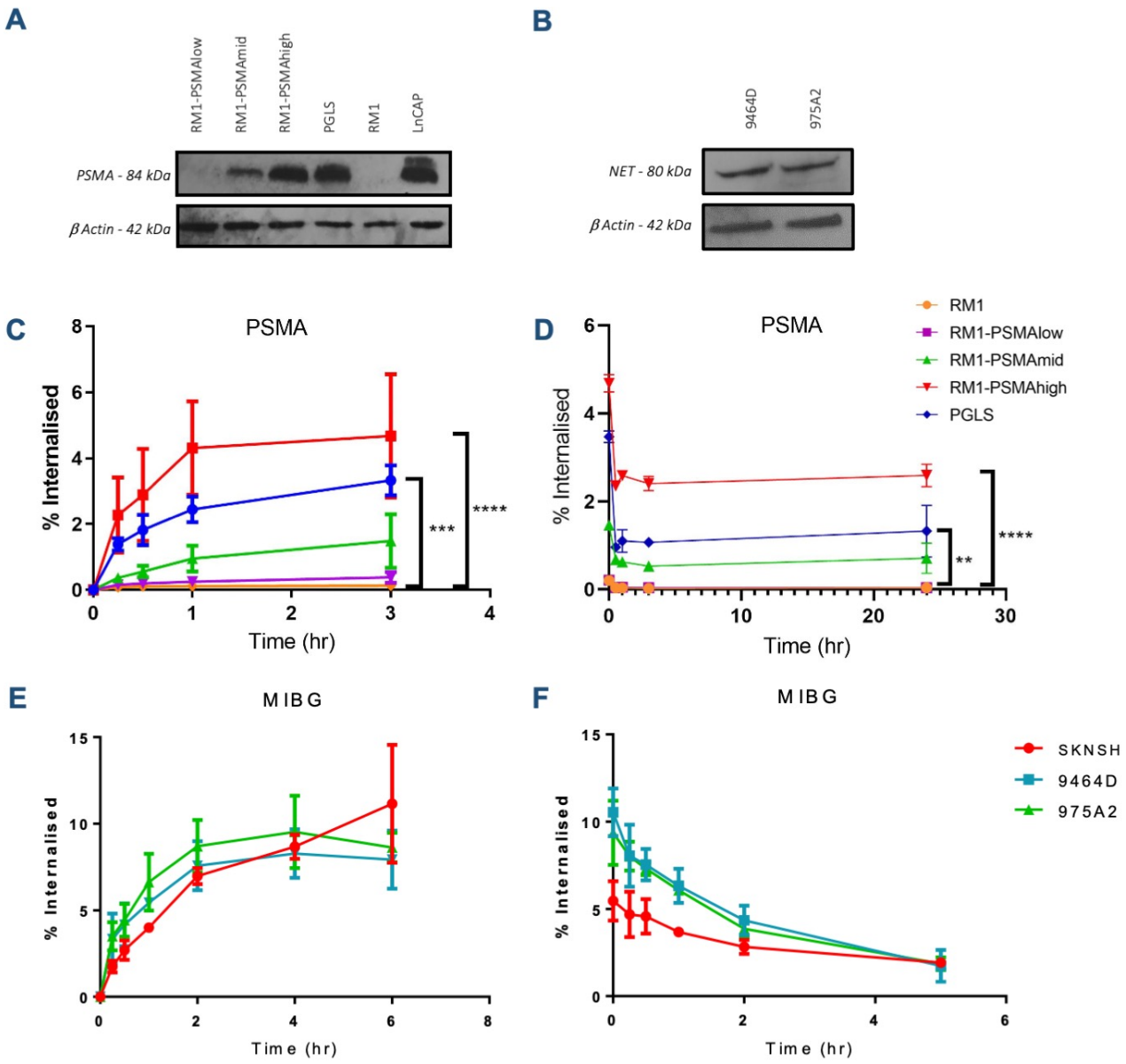

Figure 3.2: Radiopharmaceutical uptake can be achieved in murine cell lines and is dependent on receptor expression

(A) Expression of PSMA in murine prostate cancer cell lines transduced to express human PSMA was compared with human cell line LnCAP as assessed by western blot. **(B)** Expression of NET in murine neuroblastoma cell lines was assessed by western blot. **(C)** Internalisation of 3MBq [177Lu]PSMA-I&T by various murine PCa cell lines over time. Data is shown as mean % internalised ±SEM (n=3). **(D)** Retention of [177Lu]PSMA-I&T following two hour incubation with 3 MBq. Data is shown as mean % internalised ±SEM (n=3). Differences in final timepoint values compared to RM1 were determined by one way ANOVA with Dunnets post hoc adjustment for multiple comparisons *(*p<0.05, **p<0.01, ***p<0.001, ****p<0.0001).* The same process was repeated for [131I]-MIBG internalisation **(E)** and retention **(F)** by neuroblastoma cell lines. Data is shown as mean % internalised ±SEM (n=3).

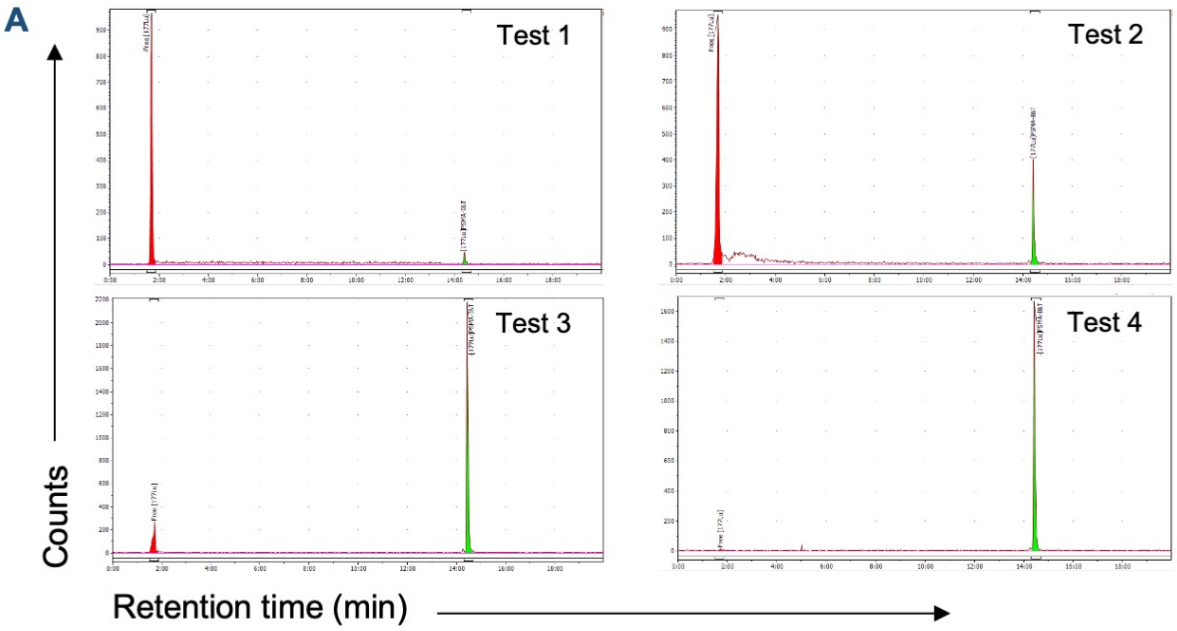

B

Species	KEY	HPLC						TLC
		Start	End	%ROI				%ROI
				Test 1	Test 2	Test 3	Test 4	Text 4
Free ^{177}Lu		1:30	1:51	93.34	79.95	16.9	1.58	98.8
^{177}Lu-PSMA		14:19	14:41	6.66	20.5	83.1	98.42	1.2

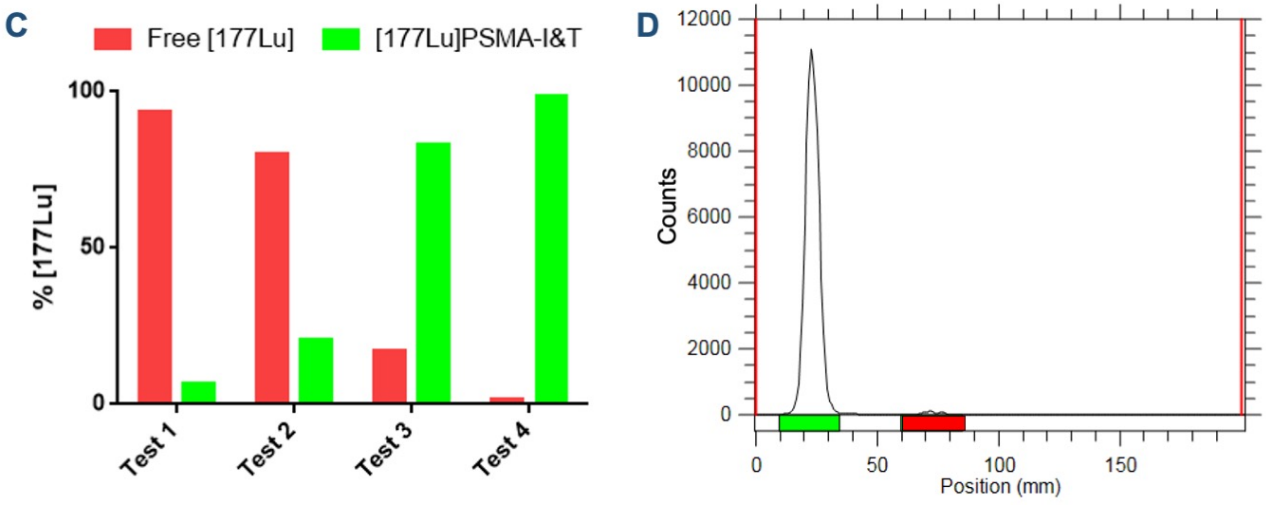

Figure 3.3: PSMA Labelling
(A) [177Lu]PSMA-I&T labelling conditions were optimised by alteration of [177Lu]:PSMA-I&T ratio, along with incubation temperature and time. Labelling efficiency was determined by HPLC. **(B)** Labelling efficiency under four different conditions as determined by HPLC analysis demonstrates that >98% labelling efficiency was achieved following optimisation *(test 4).* **(C)** Improvement in radiolabelling efficiency with optimisation. **(D)** [177Lu]PSMA-I&T labelling under optimised conditions was also confirmed by ITLC.

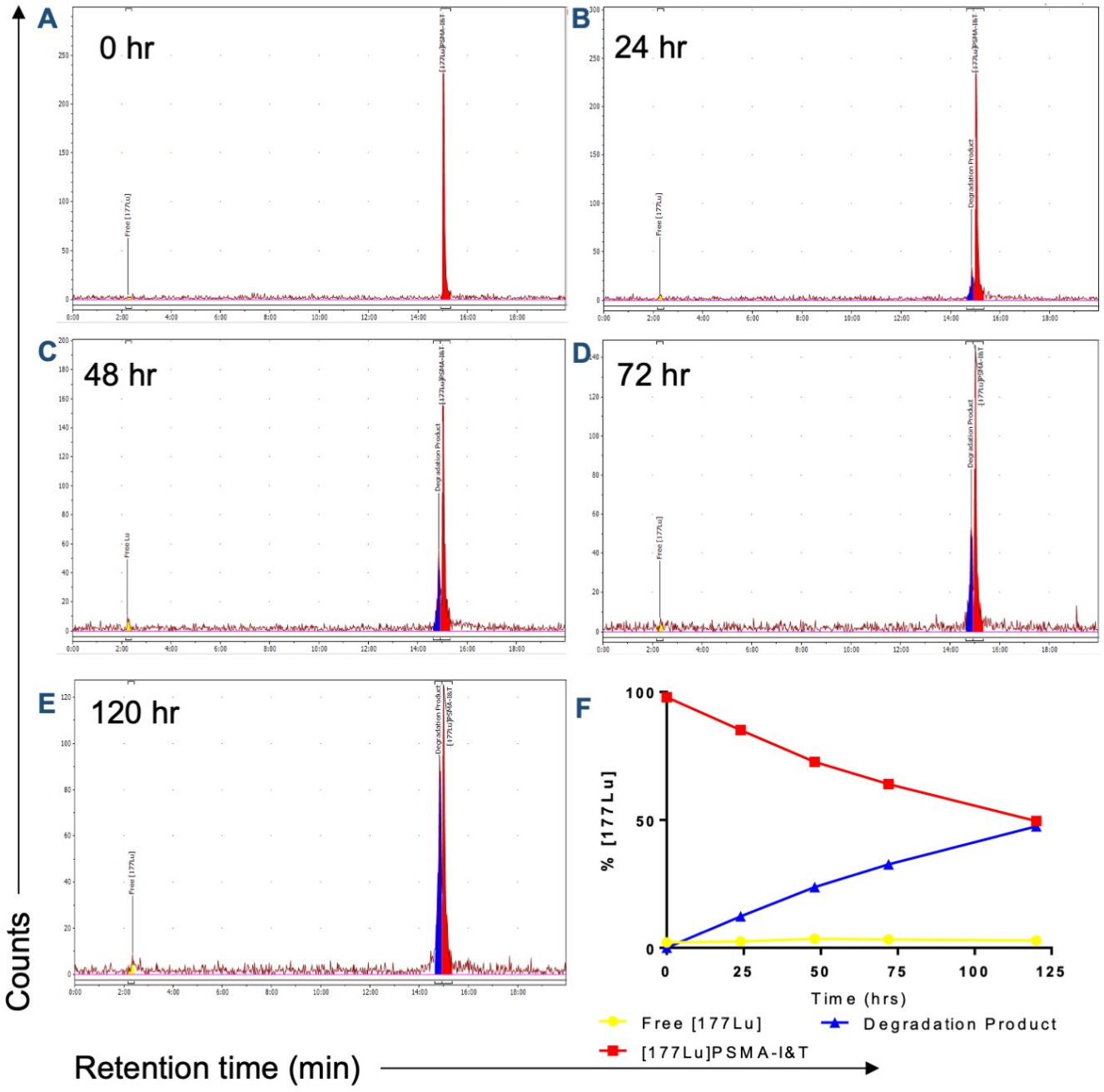

Figure 3.4: [177Lu]PSMA-I&T Stability
Stability of [177Lu]PSMA-I&T in DMEM media containing FBS + PSG over time, as determined by HPLC. The initial peak representing [177Lu]PSMA-I&T (red) at 0 hr (A), steadily degrades to an earlier peak over time (blue). This degradation product is present at low levels by 24 hours (B), accumulating at 48 hours (C), 72 hours (D), and reaching 50% by 120 hours (E). This accumulation over time is illustrated as a line graph (F).

3.3.2 9464D Tumour Uptake of 131I-MIBG is Poor

Given the promising results of the *in vitro* internalisation work, confirming good uptake of [131I]MIBG in both 9464D and 975A2 cells, this work was progressed *in vivo* to assess the ability of MIBG to accumulate within tumour allografts. 9464D cells were selected for this as they have been used previously to generate sub-cutaneous tumours and have been the focus of previous work demonstrating a similar immune microenvironment to human neuroblastoma [169]. 2 x 10^6 9464D cells were inoculated subcutaneously in syngeneic c57BL/6 mice, forming relatively fast-growing tumours (Figure 3.5(A)).

To assess biodistribution of MIBG [123I]MIBG was used for radiation safety reasons as no therapeutic effect was required and the isotope used should not affect biodistribution. Mice bearing 9464D allografts (300 mm^3) received 15 MBq [123I]MIBG via tail vein cannula. Biodistribution was assessed using SPECT analysis at 2 hrs, 24 hrs, 48 hrs and 72 hrs post treatment, indicating little/ no uptake of [123I]MIBG into the tumour (Figure 3.5(D)(E)). Instead, the majority of the activity could be detected in the adrenal glands and excretory organs such as the kidney. At 72 hours post treatment, the mice were euthanised and organs removed to enable quantification of the organ uptake (Figure 3.5(B)(C)). In agreement with the SPECT imaging, this demonstrated very low tumour uptake (Figure 3.5(B)) with no difference in uptake between tumour and muscle (tumour:muscle uptake of 0.9 +/- 0.2)(Figure 3.5(C)), confirming no tumour specific accumulation of the radiopharmaceutical.

The reason for this poor uptake is unclear. One possibility is poor tumour perfusion blocking access for the radiopharmaceutical. This often occurs as a result of a necrotic core forming in the tumour with little/ no perfusion. Given this can be avoided by using less advanced tumours, the biodistribution analysis was repeated on mice bearing less established 9464D tumours at a volume of 80 mm^3. Unfortunately, no improvement was seen, with 1.1% ID/g reaching the tumour and a tumour:muscle ratio of 0.5 72 hours post treatment (Figure 3.6 (A)(B)).

A second possibility is downregulation of NET expression when the tumours are grown in vivo. To test this hypothesis, excised tumours were disaggregated and subject to western blot to assess NET expression compared with cultured cells demonstrating no change in NET expression (Figure 3.6(C)).

Given the lack of tumour uptake, an alternative was to use a different cell line. Observation of the *in vitro* growth suggested 975A2 cells grow at a slower rate, and in less tight colonies compared with 9464D and as such it was anticipated that they may form tumours with differing characteristics that could overcome the problem of low tumour accumulation. Given their similar *in vitro* uptake data (Figure 3.2 (E)), these cells also show promise for an immune competent tumour model. As such, biodistribution of [123I]MIBG in c57BL/6 mice bearing 975A2 tumours was assessed. As previously, 15 MBq [123I]MIBG was administered via tail vein cannula to mice bearing 80 mm^3 975A2 allografts. Unfortunately, similar to 9464D, around 1% ID/g uptake into the tumour was observed, corresponding to a tumour:muscle ratio of 1.4 (Figure 3.6 (D)(E)). Again, no change in NET expression was observed (Figure 3.6(C)). Taken together, this confirms that neither 9464D nor 975A2 allografts are suitable as a preclinical model for study of MIBG as a therapeutic.

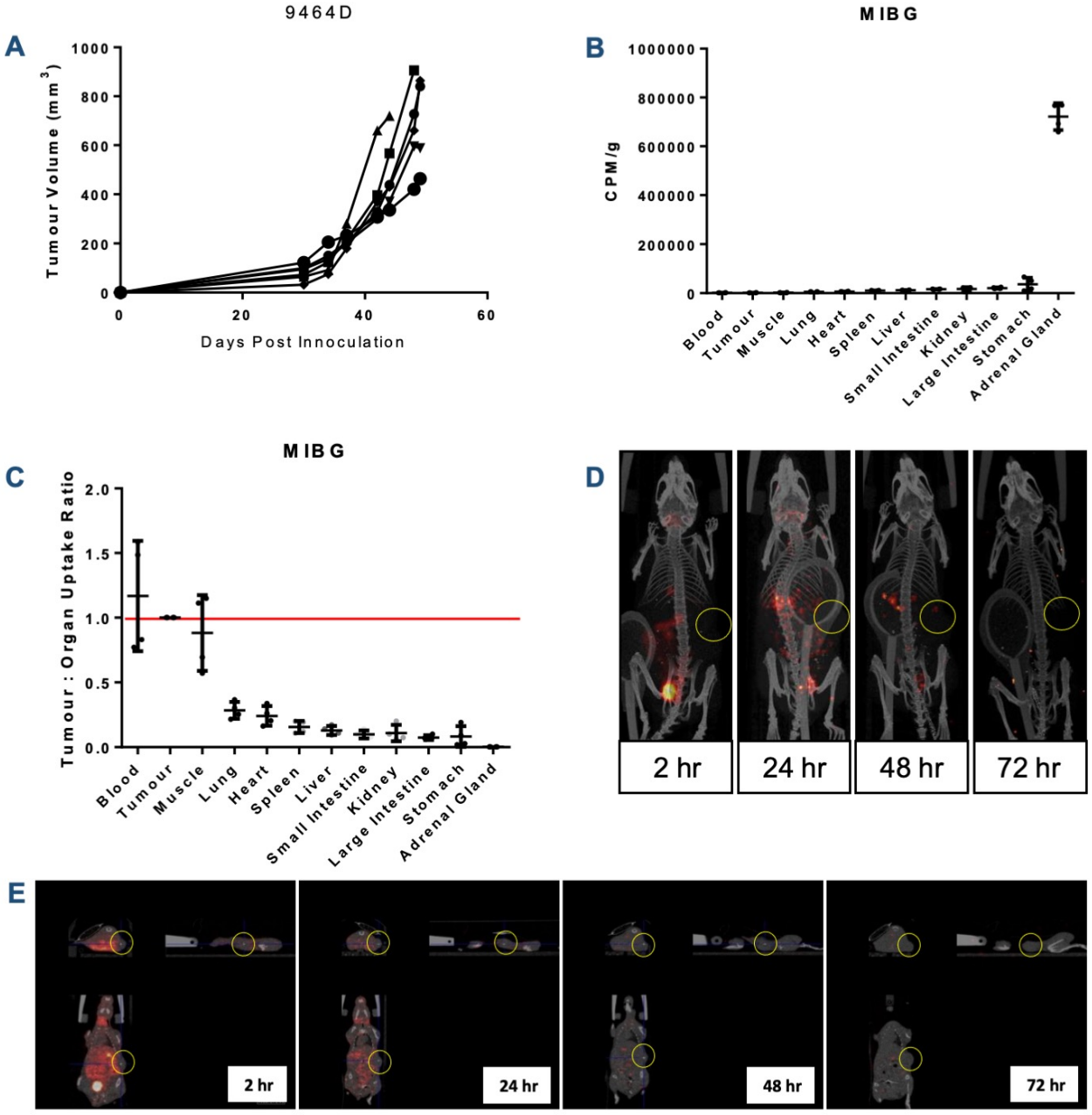

Figure 3.5: 9464D Growth and Biodistribution

(A) Growth of murine neuroblastoma *in vivo.* 2x10^6 9464D cells were inoculated subcutaneously in syngeneic c57BL/6 mice. Tumour growth was monitored twice weekly with callipers. Data is shown for each animal (N=6). **(B)** Biodistribution of [131I]MIBG 72 hours post treatment with 15 MBq [131I]MIBG *iv.* Mice were dissected 72 hours post treatment and organs weighed and activity determined using a gamma counter. Data is shown as mean CPM/g ±SEM (n=4). **(C)** Tumour:Organ uptake ratios determined from the biodistribution data, showing a tumour:muscle ratio of <1. Red line indicates a ratio of one. Data is shown as mean ±SEM (n=4). **(D)** SPECT assessment of biodistribution was also carried out over a 72 hour time course post-treatment. Representative Maximum Intensity Projections **(D)** and cross section views of the tumour **(E)** are shown. Yellow circles indicate the tumour site.

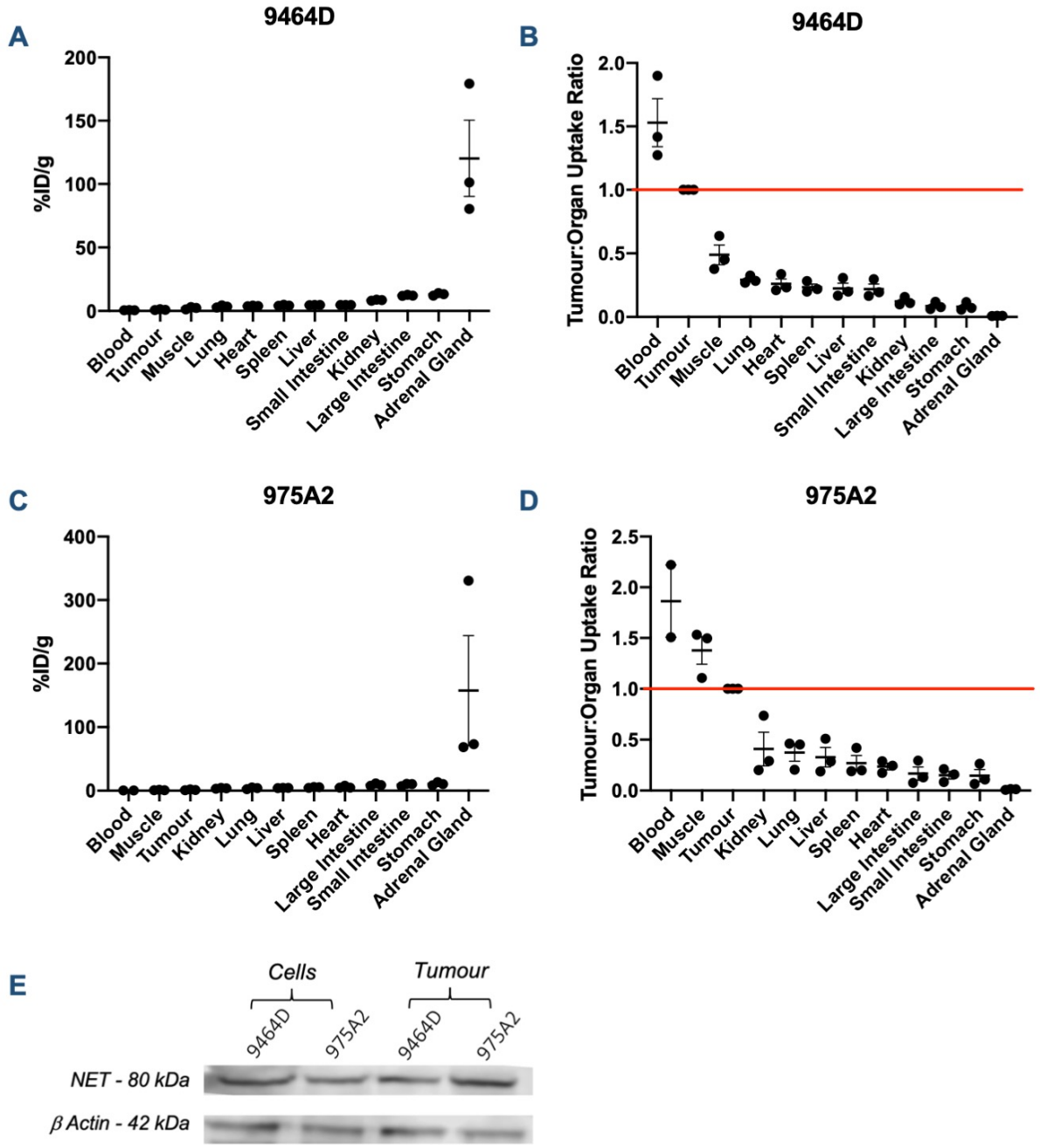

Figure 3.6: [123I]MIBG Biodistribution in Smaller 9464D and 975A2 Tumours
(A) 9464D tumours were grown in c57BL/6 mice and treated with 15 MBq [131I]MIBG iv. When tumours reached a volume of 80mm^3. To determine biodistribution, mice were dissected 72 hours post treatment and organs weighed and activity determined using a gamma counter. Data is shown as mean %ID/g ±SEM (n=4). **(B)** Tumour:Organ uptake ratios determined from the biodistribution data, showing a tumour:muscle ratio of 1.4. Red line indicates a ratio of one. Data is shown as mean ±SEM (n=3). **(C)** 975A2 tumours were grown in c57BL/6 mice and treated with 15 MBq [131I]MIBG iv. when tumours reached a volume of 80mm^3. To determine biodistribution, mice were dissected 72 hours post treatment and organs weighed and activity determined using a gamma counter. Data is shown as mean %ID/g ±SEM (n=4). **(D)** Tumour:Organ uptake ratios determined from the biodistribution data, showing a tumour:muscle ratio of <1. Red line indicates a ratio of one. Data is shown as mean ±SEM (n=3). **(E)** Excised tumours were disaggregated and subject to western blot analysis to assess NET expression compared with cultured cells.

3.3.3 PGLS Cells Form Fast Growing, Well Perfused Tumours in Immunocompetent Mice

In vitro assessment of the murine PCa cell lines demonstrated highest uptake and retention of [177Lu]PSMA-I&T was achieved by the highest PSMA expressing cell lines, PSMAhigh and PGLS. Literature regarding these cell lines has described spontaneous regression of PSMAhigh due to the induction of an immune response against PSMA, however this phenomenon has not been observed for PGLS [171]. As such, PGLS cells were selected for use in *in vivo* work. This cell line has previously only been used for tumour growth using Matrigel, however this can leave small nodules following tumour induction that can potentially obscure the identification of the presence of tumours in subsequent experiments (in particular for the vaccination-rechallenge experiment described in chapter 4). As such, growth of PGLS allografts was first optimised in syngeneic c57BL/6 mice, to facilitate rapid tumour growth without the use of Matrigel (Figure 3.7(A)).

Given the problems experienced with the neuroblastoma tumour models, both ultrasound and contrast MRI were used to assess intratumoural vasculature and perfusion when tumour volume reached 60-90 mm^3 (Figure 3.7). PGLS allografts were first assessed by ultrasound to identify the difference in perfusion between the whole tumour and the tumour core (representative image, Figure 3.7(B)). For the whole tumour, the peak rises from a baseline of ~40 linear a.u to a peak of ~92 linear a.u, giving a fold increase of 2.3. Comparatively, the core has a baseline of ~30 rising to ~75, with a strikingly similar 2.5-fold increase. Together with the short delay in peak rise (~2s) between the periphery and core, this indicates good perfusion throughout the tumour. However, there is possibly some necrosis starting in the centre as it can be seen that the signal at the tumour core starts to plateau over time, rather than continuing to decline.

Following the acquisition of ultrasound images, animals were immediately transferred to the MRI for DCE-MRI analysis (Figure 3.7(C)(D)). The changes in MRI signal over time at various points along a cross section of the tumour indicate there is relatively good perfusion throughout the tumour, with the initial curve showing the perfusion rate and the peak indicating maximum intensity (Figure 3.7(C)). The distribution of the contrast dye throughout the tumour can also be visualised from the initial area

under the curve to 90 seconds (iAUC90). This illustrates the infiltration of the contrast dye throughout the tumour at a given cross-section in the initial 90 seconds following injection and can thus be represented as a cross-sectional image coloured by iAUC90 values (Figure 3.7(D)). These images demonstrate good perfusion throughout the tumours, though the slight decrease in core regions of the tumour may again suggest the onset of necrosis at the tumour core.

Collectively, these data suggest that perfusion throughout the tumour is sufficient up to at least a volume of 60-90 mm^3.

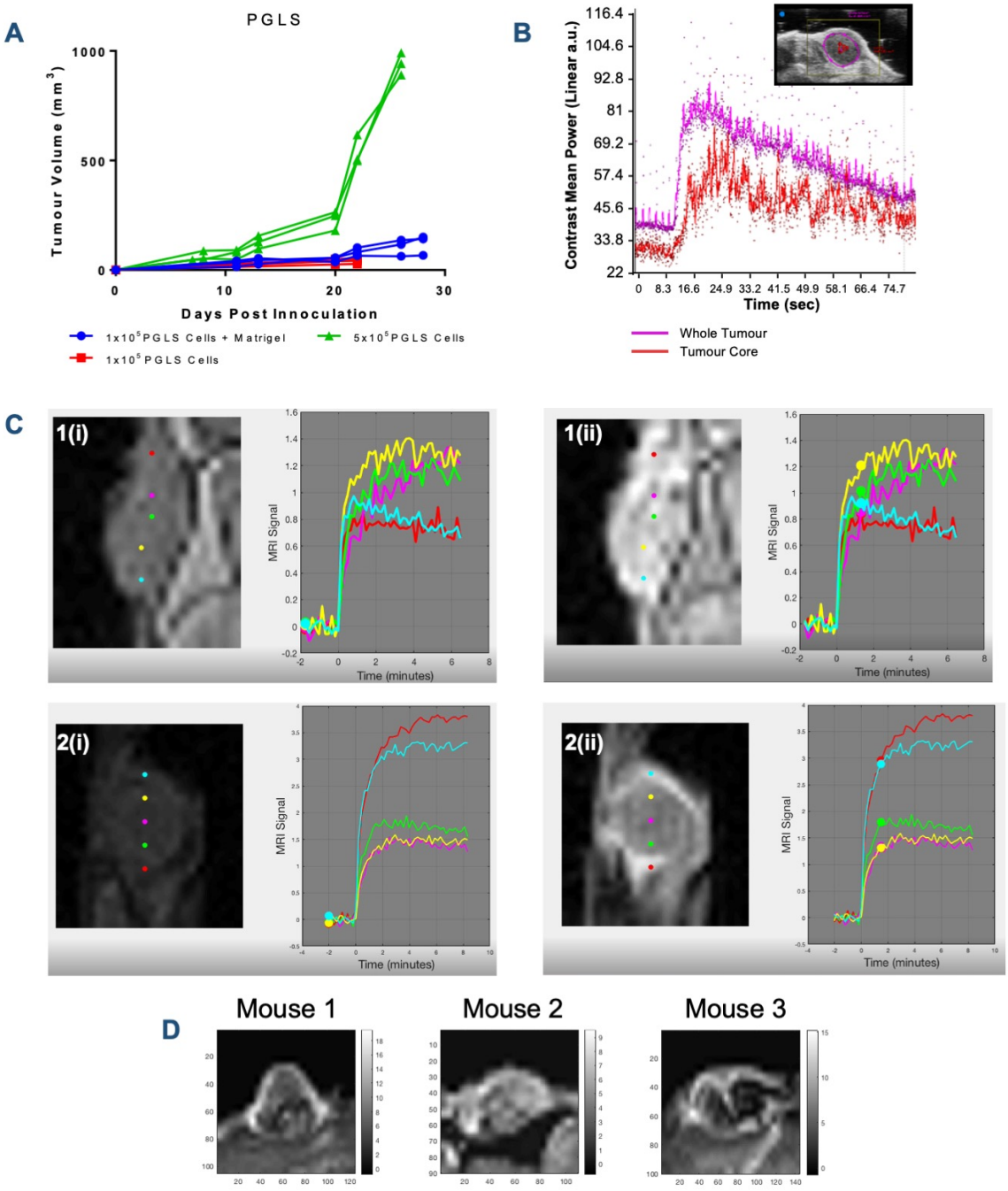

Figure 3.7: PGLS Growth and Vascularisation

(A) Subcutaneous tumour growth optimisation for murine PGLS prostate cancer cells in syngeneic c57BL/6 mice. Data is shown for each animal within each group (n=3). **(B)** Tumour perfusion 7 days post inoculation at tumour volume 60-90 mm^3 as assessed by ultrasound for the outer edge (pink) compared with the tumour core (red). **(C)** Tumour perfusion was assessed at the same time point using contrast MRI. Representative graphs for change in MRI signal over time is shown in various points (blue, yellow, pink, green, red) along a cross section of two tumours (1) (2). Images shown reflect MRI signal at 0 seconds (i) and 90 seconds (ii) **(D)** Representative images for initial area under the curve over 90 seconds is shown. This illustrates the infiltration of the contrast dye throughout the tumour at a given cross-section in the initial 90 seconds following injection, and is represented as a cross-sectional image coloured by iAUC90 values.

Contrast ultrasound was performed with the help of Sheena Wallington. DCE-MRI and tumour contouring were performed by Sheena Wallington. The DCE-MRI parameters were calculated by Danny Allen.

3.3.4 PGLS tumours show high, tumour selective, PSMA dependent uptake of [177Lu]PSMA-I&T

To determine whether good *in vitro* uptake of PSMA corresponded to good tumour uptake, PGLS tumour bearing mice received 30 MBq [177Lu]PSMA-I&T via tail vein cannula 9 days post tumour inoculation when tumours reached a volume of 80 mm^3. 72 hours post injection (p.i.), SPECT/CT images were acquired to visualise biodistribution (Figure 3.8(A)(B)). Clear tumour accumulation can be observed in both maximum intensity projections (Figure 3.8(A)) and single transverse, sagittal and coronoal slices (Figure 3.8(B)), with the majority of the remaining radioactivity in excretory organs. To confirm this uptake, and for quantification of the biodistribution, animals were euthanized, and organs harvested for analysis immediately following SPECT/CT image acquisition. This analysis confirms high tumour accumulation of [177Lu], with 3.9 ±1.1 %ID/g within the tumour, significantly higher than any other organ (Figure 3.8(D)). The normal organ with highest uptake was the kidneys (Figure 3.8(D)). A tumour:muscle uptake ratio of 210 ±59 confirms highly tumour specific accumulation (Figure 3.8(E)). In order to assess the distribution of activity within the tumour, tumour slices were analysed using autoradiography, indicating good distribution throughout the tumour with activity reaching the tumour core (Figure 3.8(C)).

To investigate whether PSMA expression is responsible for this highly tumour specific accumulation, the biodistribution analysis was repeated for parental RM1 allografts that are not transduced to express PSMA. Whilst these allografts demonstrated similar overall biodistribution, very limited tumour uptake was observed at 0.012 ±0.002 %ID/g compared with 3.9 ±1.1 %ID/g for PGLS (Figure 3.8(F)). Moreover, the tumour:muscle uptake ratio was 60-fold lower for RM1 compared with PGLS at 3.5 ±0.4 compared with 210 ±59 (Figure 3.8(G)). Taken together, these data confirm highly specific, PSMA dependent, accumulation of [177Lu]PSMA-I&T, producing a homogenous intratumoural distribution that penetrates to the tumour core.

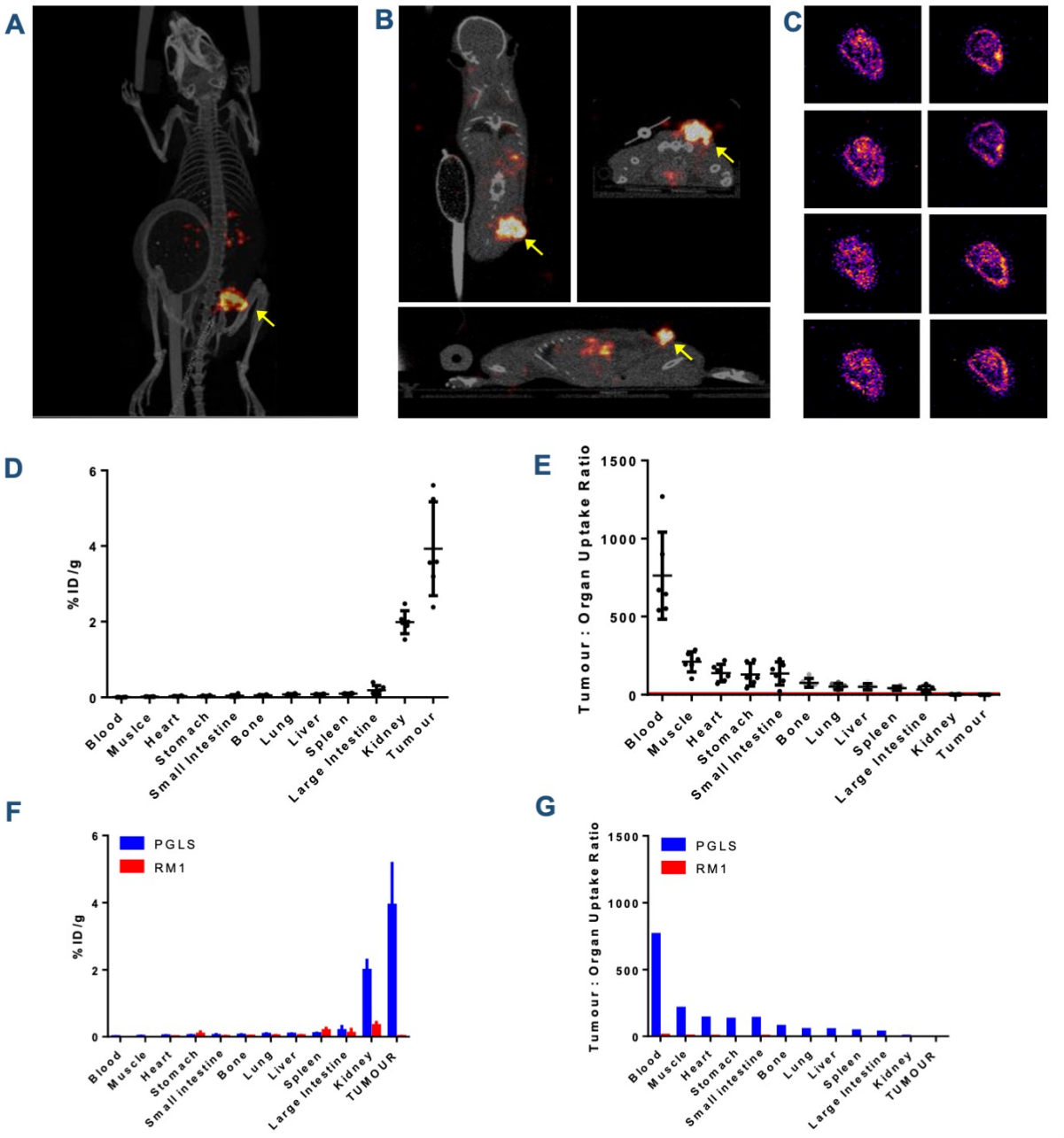

Figure 3.8: PGLS Biodistribution

(A) PGLS tumour bearing mice were treated with 30 MBq [177Lu]PSMA-I&T 7 days post tumour inoculation at a volume of 60-90 mm^3. 72 hours post treatment, mice were subject to SPECT/CT to visualise biodistribution. Representative maximum intensity projections illustrate the whole mouse biodistribution **(A)**, with tumour cross-sections of the animal **(B)**. Yellow arrows indicate the tumour site. **(C)** Following SPECT analysis, mice were sacrificed and organs harvested. Tumour slices underwent autoradiography to show [177Lu] distribution within the tumour. **(D)** All organs were harvested, weighed and assessed for activity. Biodistribution is displayed as injected dose per gram (ID/g). Data is shown as mean %ID/g ±SEM (n=6). **(E)** Tumour to organ uptake ratios were determined from the biodistribution data, showing a tumour:muscle ratio of 207.1. Red line indicates tumour:organ uptake ratio of one. Data is shown as mean ±SEM (n=6). **(F)** Biodistribution in PGLS tumour bearing mice was compared with non-PSMA expressing, RM1, tumour bearing mice treated with the same dose at the same tumour volume (n=3). **(G)** Comparative tumour:organ uptake ratios for PGLS vs. RM1 tumour bearing mice.

3.3.5 Both EBRT and TRT induce growth delay of PGLS tumours

The therapeutic effect of both EBRT and TRT on PGLS allografts was next assessed to determine any growth delay. The therapeutic effect of [177Lu]PSMA-I&T was assessed first. A single dose was used for these studies for initial observations of impact on the immune response, and for radiation safety reasons. However as discussed later future experiments could include assessment of fractionated doses. A dose of 60 MBq was chosen as this dose has been shown to have an effect and no toxicity in literature [172]. c57BL/6 mice bearing PGLS tumours were treated with 60 MBq [177Lu]PSMA-I&T via tail vein cannula when tumours were 60-90 mm^3. By day 20 a significant tumour growth delay could be observed in the treatment group compared with the untreated group (Figure 3.9(A)(B)), leading to a significant improvement in survival (Figure 3.9(C)). No adverse effect on weight was observed following treatment (Figure 3.9(D)).

To assess the therapeutic effect of EBRT, PGLS tumour bearing mice were subjected to a single dose of radiation of 6 Gy delivered using a GulmayRS320 irradiation system at 300 KV, dose rate 2.25 Gy per minute when tumours reached 60-90 mm^3. A single dose was chosen to match the treatment with [177Lu]-PSMA as closely as possible. 6 Gy was chosen based on preliminary data demonstrating that a similar biological effect could be observed with no toxicity at this dose (appendix figure A1). Again, treatment caused a significant tumour growth delay compared with untreated mice (Figure 3.9(E)(F)), with no negative impact on mouse weight (Figure 3.9(G)).

Taken together, these data show that PGLS tumours are sensitive to radiation by either gamma rays, or [177Lu]PSMA-I&T.

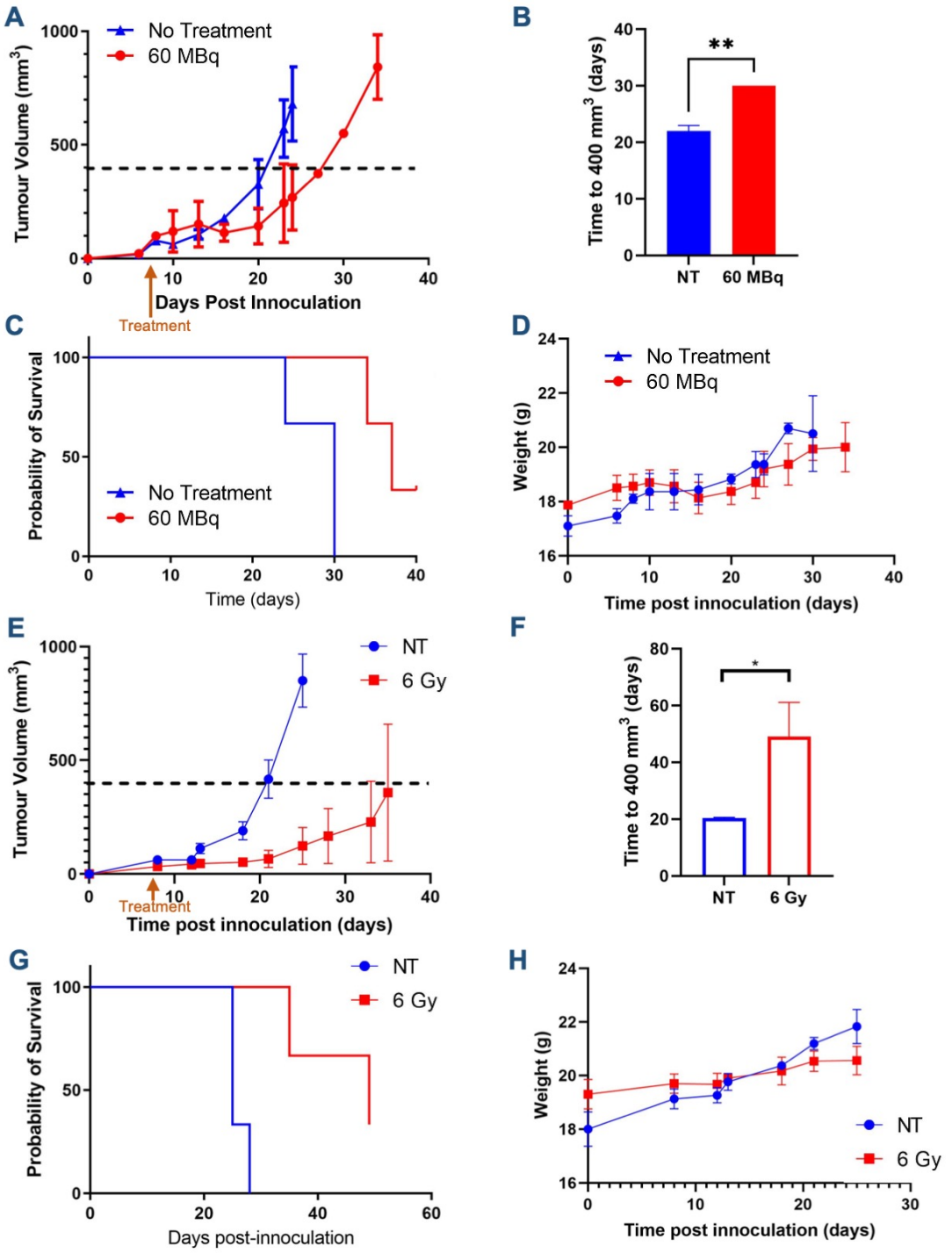

Figure 3.9: PGLS response to radiotherapy
(A) c57BL/6 mice bearing PGLS tumours were treated *iv* with 60 MBq [177Lu]PSMA-I&T at day 7 where tumours were 60-90 mm^3. Data is shown as mean tumour volume ±SEM (n=3). **(B)** Tumour growth delay to ≥400 mm3 analysis of PGLS tumours treated with 60 MBq [177Lu]PSMA-I&T. **(C)** Kaplan-Meier curve for survival. Animals were sacrificed when tumour volume approached 1,000 mm^3. **(D)** Mouse weight throughout the study. **(E)** c57BL/6 mice bearing PGLS tumours were treated with 6 EBRT at day 7 where tumours were 60-90 mm^3. Data is shown as mean tumour volume ±SEM (n=3). **(F)** Tumour growth delay to ≥400 mm3 analysis of PGLS tumours treated with 6 Gy EBRT. **(G)** Kaplan-Meier curve for survival. Animals were sacrificed when tumour volume approached 1,000 mm^3. **(H)** Mouse weight throughout the study. Statistical significance determined by unpaired t-test. n=3 per group *(*p<0.05, **p<0.01, ***p<0.005).*

3.4 Discussion

The importance of the immune response for the therapeutic efficacy of EBRT is well documented, however studies of similar phenomena regarding TRT are limited. Here I assessed models to enable investigation of this response using the clinically relevant radiopharmaceuticals, [177Lu]PSMA-I&T, and [131I]MIBG.

Initial *in vitro* studies confirmed that PSMA expression in the murine cell line PGLS enabled [177Lu]PSMA-I&T uptake comparable to the commonly used human cell line LnCAP. This uptake translated well into allograft models with high tumour specific uptake (3.9 ±1.1 %ID/g) penetrating to the core of PGLS tumours. Comparatively, the non-PSMA expressing parental cell line RM1 demonstrated almost no tumour uptake, with the tumour:muscle uptake ratio 60-fold lower than that of PSMA expressing PGLS tumours. This highlights the dependence of PSMA-I&T uptake on PSMA expression. Initial treatment studies indicated that a dose of 60 MBq [177Lu]PSMA-I&T or 6 Gy EBRT is sufficient to observe a therapeutic response. Together these data suggests that PGLS represents a suitable immune-competent tumour model enabling study of the immune response to [177Lu]PSMA-I&T [173, 174].

Unfortunately, the same success was not met for the neuroblastoma models 9464D and 975A2. These cell lines, isolated from the transgenic neuroblastoma mouse model TH-MYCN, demonstrated good *in vitro* NET expression and uptake of [131I]MIBG, however this did not translate into any observable tumour-specific uptake into either model *in vivo*.

3.4.1 Despite in vitro uptake, no [123I]MIBG tumour accumulation is observed in vivo for 9464D or 975A2 allografts

Uptake of [123I]MIBG by TH-MYCN derived cell lines 9464D and 975A2 was equivalent to that of the human cell line SK-N-SH, which has commonly been used as a pre-clinical model for the study of MIBG. Though retention was modest, dropping significantly within 5 hours, it was again comparable SK-N-

SH. Despite this, no tumour accumulation could be observed *in vivo* for either cell line. In contrast, substantial [131I]MIBG uptake has been previously observed SK-N-SH xenografts in nude mice [166, 175–177]. Follow up studies suggested this lack of uptake was not due to tumour size being too large, or the downregulation of NET *in vivo*. It is interesting to postulate that the poor retention observed *in vitro* could be the cause of the low tumour accumulation of MIBG, however such retention was also observed here for SK-N-SH and is similarly described by Chen *et al* for SK-N-SH cells[178], which have been shown on multiple occasions to have substantial tumour uptake [162, 166]. This suggests that poor *in vitro* retention may not explain the poor tumour accumulation. Instead, it may be poor tumour perfusion or the early formation of a necrotic core causing poor uptake. Clinically, 90% of human tumours have been seen to accumulate MIBG, so these murine cell lines do not reflect the clinical situation [179]. Unfortunately, this means neither cell line provides a suitable model for study of the immune response to [123I]MIBG without significant further analysis and adaptation.

3.4.2 PGLS allografts provide one of the first models suitable for the study of the immune response to TRT

Here, I demonstrate the use of an immune competent murine model with the clinically relevant radiopharmaceutical [177Lu]PSMA-I&T. The lack of such a model thus far has limited study of the immune response to TRT to predominantly *in vitro* work. For example, Chakraborty *et al.* demonstrated the ability of [153Sm]EDTMP to modulate the phenotype of tumour cells and enhance T cell-mediated killing, however the use of a panel of human cell lines precluded further study of this effect *in vivo* [113]. Similarly, the use of human prostate, breast, and lung carcinoma cells by Malamas *et al.* in a study on [223Ra] limited their immune analysis to *in vitro* studies [114]. That said, a small number of murine models have already been used for in vivo assessment of the immune response, though these each faced their own limitations.

In one example, Gorin *et al.* employed the MC38 murine colon carcinoma allograft in C57BL/6 mice to assess the immune response to [213Bi]BSA treatment [127]. However, as this radiopharmaceutical is

not tumour targeting it was not suitable for testing treatment efficacy *in vivo*, and only allowed assessment of the vaccination effect of cells that had been exposed to the radiopharmaceutical *in vitro*.

Similar studies were completed in an EL4 tumour model used by Hernandez *et al.* to assess the response to [90Y]NM600 [120]. Whilst this model is tumour targeting and thus affords the potential for further study of the tumour immune response *in vivo*, the T cell targeting nature of this compound, which is designed to treat T cell Non-Hodgkin lymphoma, may complicate assessment of the immune response. Although the compound is preferentially selective for malignant T-cells, the <4-fold lower uptake of [90Y]NM600 by healthy T cells still results in significant activity in these radiosensitive cells. In this thesis the aim was to simplify the analysis for proof-of-principle work by using a non-immune cell targeting TRT.

This has been done by Wu *et al.* who investigated the immune response to [177Lu]DOTATATE [121]. However, again severe limitations stemmed from the use of human xenografts. As such, nude mice were used that are athymic and thus lack T cells and mature B cells of the adaptive immune response, restricting this study to assessment of the innate compartment including dendritic cells (DCs).

In contrast, the PGLS allograft enables study of the immune response to the clinically relevant, non-immune cell targeting, [177Lu]-PSMA-I&T. This is not limited to *in vitro* studies or growth in immune-compromised mice and can instead form tumours in syngeneic immune-competent C57BL/6 mice.

3.4.3 PSMA dependent uptake and retention is consistent with clathrin mediated endocytosis

Consistent with previous literature the human cell line LnCAP, which has commonly been used for PSMA preclinical studies, was shown to have strong PSMA expression, leading to high [177Lu]PSMA-I&T uptake [180–187] (Figure 3.2). Here, I go on to demonstrate that similar uptake levels are observed in the mouse cell lines transduced to express high levels of human PSMA. Of particular interest, the use of multiple RM1-daughter cell lines with differential expression of human PSMA enabled analysis

of the effect of PSMA expression on [177Lu]PSMA-I&T uptake. This demonstrates a clear dependence, wherein uptake increases with PSMA expression level with almost no uptake by the non-transduced RM1 parental cell line. This ultimately confirms PSMA dependent internalisation of the radiopharmaceutical with little-to-no PSMA-independent uptake. In agreement, the striking [177Lu]PSMA-I&T tumour uptake observed for PGLS allografts is almost entirely absent in allografts using the parental, non-PSMA expressing, cell line RM1.

The ability of PSMA-I&T to specifically enter PSMA+ cells, and equally importantly to remain trapped there and thus accumulate within PSMA+ tumours, is now well supported with both *in vitro* and *in vivo* data of xenograft models of human tumours, as well as clinically [151, 173, 188–191]. Consistently, I show here that internalised activity is almost entirely retained within the cell out to at least 3 days for both LnCAP and the murine cell lines, confirming that once internalised the compound is trapped.

Together, these observations are consistent with the described model for PSMA uptake, wherein the transmembrane protein undergoes a clathrin-dependent endocytic mechanism following ligand binding with the internalised ligand accumulating in endosomes and thus remaining trapped in the cell [192–194].

Interestingly, this internalisation occurs rapidly, plateauing within 2-4 hours. This suggests that any degradation of PSMA (Figure 3.3) is likely to have only a limited effect on cellular uptake of [177Lu]PSMA-I&T. Moreover, the striking retention of PSMA over multiple days implies that the [177Lu] is trapped following internalisation and that subsequent PSMA degradation is of little consequence. Indeed, this is also promising for *in vivo* studies, suggesting good accumulation and retention of radionuclides over time, enabling the absorbed radiation dose to the tumour to accumulate.

Collectively, these data demonstrate that transduced human PSMA functions comparably to endogenous human PSMA, with the high expression level in the PGLS cell line providing a suitable murine alternative to the human cell line LnCAP for *in vitro* studies.

3.4.4 Endogenous PSMA expression varies between mice and humans but biodistribution is comparable

Similar to humans, mice express PSMA in the brain, kidneys, and salivary glands. However, unlike humans, murine PSMA expression is very low in the prostate and jejunum. Perhaps unsurprisingly then, my assessment of the expression of PSMA in various murine PCa cell lines demonstrated little or no expression (appendix figure A2). Accordingly, I chose to use the murine PCa cell line RM1 transduced with human PSMA. Whilst murine PSMA could have been used, human PSMA was chosen as the internalisation of PSMA based pharmaceuticals by murine PSMA is unknown. Indeed, the PSMA protein itself differs between mice and humans, with 85% homology (Figure 3.10). However, whilst the differences in sequence are generally spread across the entire length there is some clustering in the intracellular domain, suggesting ligand binding specificity may be similar in the two species. It is worth noting that the sequence differences likely increase the immunogenicity of the tumours by introducing a novel tumour antigen. This has the benefit of providing a means to assess the induction of a tumour specific (anti-PSMA) immune response. However, it may also alter the immune environment of the untreated tumours.

Despite these differences, the biodistribution of [177Lu]PSMA-I&T in PGLS allografts is comparable to LnCAP xenografts and the biodistribution in human subjects. The PGLS model demonstrates substantial tumour uptake, with significant activity also accumulating in the kidneys (Figure 3.8). Strikingly, this mirrors the distribution described for LnCAP xenografts where uptake has been reported to be between 5-8 % $ID g^{-1}$ in the tumours with the majority of remaining the activity in kidneys [174, 185, 188, 195, 196]. This consistency suggests that PGLS allografts provide a comparable preclinical model to the commonly used LnCAP xenografts whilst affording the assessment of the

immune response in immune-competent animals. However, it is clearly important to also compare this distribution to human biodistribution. Again, the predominant sites of [177Lu] accumulation are the tumour and kidneys, supporting the use of this preclinical model. Indeed, efforts to reduce kidney uptake, for example through linker and chelator modification, are actively ongoing [197].

Also of note is the considerable salivary gland uptake observed clinically, with significant salivary gland toxicity being reported [198]. Consistent with other murine models, my preliminary studies observed very limited salivary gland uptake [173] (appendix figure A3). This is despite PSMA expression in salivary glands being similar across mice and humans, which perhaps relates to the possibility of a non-PSMA-related uptake mechanism that has been proposed to occur in human salivary glands [199, 200]. Whilst this observed difference in biodistribution is both interesting and important to note, particularly for studies relating to toxicity, it does not negate the usefulness of this model for pre-clinical assessment of the immune response to TRT. Indeed, the otherwise strikingly similar biodistribution of [177Lu]PSMA-I&T may prove to be a useful attribute.

A

Sequence ID: Query_47061 Length: 752 Number of Matches: 1

Range 1: 1 to 752 Graphics ▼ Next Match ▲ Previous Match

Score	Expect	Method	Identities	Positives	Gaps
1327 bits(3435)	0.0	Compositional matrix adjust.	638/752(85%)	683/752(90%)	2/752(0%)

```
Query  1    MWNLLHETDSAVATARRPRWLCAGALVLA-GGFFLLGFLFGWFIKSSNEAT-NITPKHNM  58
Sbjct  1    ...A.QDR...EVLGH.Q...RV.T....LT.T..I.........P.....G.VSHSGMK  60

Query  59   KAFLDELKAENIKKFLHNFTQIPHLAGTEQNFQLAKQIQSQWKEFGLDSVELAHYDVLLS  118
Sbjct  61   .E..H...........Y...RT......QN..E.....HD........L...S.......  120

Query  119  YPNKTHPNYISIINEDGNEIFNTSLFEPPPPGYENVSDIVPPFSAFSPQGMPEGDLVYVN  178
Sbjct  121  ......................K...S.Q.......I..V...Y.......T.........  180

Query  179  YARTEDFFKLERDMKINCSGKIVIARYGKVFRGNKVKNAQLAGAKGVILYSDPADYFAPG  238
Sbjct  181  ............E...S..................M...........M..........V.A  240

Query  239  VKSYPDGWNLPGGGVQRGNILNLNGAGDPLTPGYPANEYAYRRGIAEAVGLPSIPVHPIG  298
Sbjct  241  ...................V..................H...HELTN.............  300

Query  299  YYDAQKLLEKMGGSAPPDSSWRGSLKVPYNVGPGFTGNFSTQKVKMHIHSTNEVTRIYNV  358
Sbjct  301  .D.......H...P.......K.G............A..............YTK.......  360

Query  359  IGTLRGAVEPDRYVILGGHRDSWVFGGIDPQSGAAVVHEIVRSFGTLKKEGWRPRRTILF  418
Sbjct  361  ....K..L.............A.............................K.R........  420

Query  419  ASWDAEEFGLLGSTEWAEENSRLLQERGVAYINADSSIEGNYTLRVDCTPLMYSLVHNLT  478
Sbjct  421  ...................H.....................................Y...  480

Query  479  KELKSPDEGFEGKSLYESWTKKSPSPEFSGMPRISKLGSGNDFEVFFQRLGIASGRARYT  538
Sbjct  481  ...Q............D..KE.......I.............................  540

Query  539  KNWETNKFSGYPLYHSVYETYELVEKFYDPMFKYHLTVAQVRGGMVFELANSIVLPFDCR  598
Sbjct  541  ...K...V.S..............V.....T............A..............Q  600

Query  599  DYAVVLRKYADKIYSISMKHPQEMKTYSVSFDSLFSAVKNFTEIASKFSERLQDFDKSNP  658
Sbjct  601  S...A.K....T..N..........A.MI.........N...DV....NQ...EL.....  660

Query  659  IVLRMMNDQLMFLERAFIDPLGLPDRPFYRHVIYAPSSHNKYAGESFPGIYDALFDIESK  718
Sbjct  661  .L..I......Y............G......I.........................S..  720

Query  719  VDPSKAWGEVKRQIYVAAFTVQAAAETLSEVA  750
Sbjct  721  .NA....N......SI.T..........R...  752
```

B

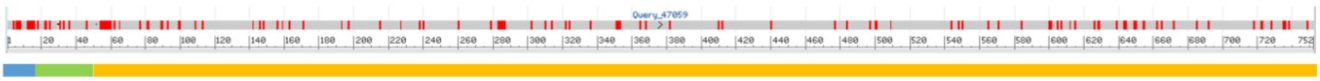

Figure 3.10: Human vs. Mouse PSMA homology
(A) BLASTp of human PSMA (NM_004476.1) vs. Mouse PSMA (AF026380.1) showing homologous sequences. Sequences are shown pairwise with dots representing matches, and differences shown in red. (B) Graphic illustrating the clustering of mismatches (red) along the gene. Coloured bar represents the domain structure with a 19 amino acid N-terminal intracellular domain (blue), a 25 amino acid transmembrane domain (green), and a a 708 amino acid extracellular domain (orange).

3.4.5 60MBq of [177Lu]PSMA-I&T produces an observable effect in PGLS allografts

Another key aspect when considering the clinical relevance of this model is the dose. There are several important factors to consider here, making it difficult to directly compare the applied dose. In my studies, the amount of [177Lu] given to produce an observable delay in tumour growth was a single dose of 80 MBq. When body weight is accounted for (~25g mouse), this equates to ~ 3.2 GBq kg^{-1}. Clinically, doses still vary considerably across clinical trials, however a recent meta-analysis identified 12 studies where doses ranged from 1.1 – 7.4 GBq for one to four cycles [201]. A quick calculation here would suggest that where median patient age is ~70 [202], assuming an average weight of 80 kg [203], each 7.4 GBq dose equates to 92.5 MBq kg^{-1}. This ~35-fold difference suggests that the dosage used here, whilst potentially useful for proof-of-principle work, is not clinically relevant. However, it is also worth noting that clinically these doses are generally given in multiple cycles which may cause differences in the immune response. Moreover, body weight may not provide the best metric for comparison in this case, for example the tumour size for a xenograft model is also important to consider. The tumours treated in my model are typically treated where tumour volume is ~100 mm^3, making the dose 0.8MBq/mm^3. Comparatively, one clinical study measuring tumour from radical prostatectomy states a mean diameter of 1.73 cm, and so assuming l = w = h, the average tumour volume is 2,600 mm^3, making the dose ~1.6 MBq/mm^3 and thus similar to the doses used here.

Ultimately, the only way to truly consider the dose in the case of radiopharmaceuticals is to compare the absorbed dose in each case. The absorbed dose is defined as the energy absorbed per unit mass of tissue, and thus depends on both the activity per unit mass of tissue, and the amount of energy emitted per nuclear transition. Several methodologies exist for the calculation of value, of which the schema developed by the Medical Internal Radiation Dose (MIRD) committee is usually used to calculate doses from TRT[204]. However, this complex modelling analysis which would also need to take into account pharmacokinetic uptake and clearance among other considerations to give an overall absorbed dose that considers both direct dose from internalised [177Lu] and cross-fire from

adjacent cells, is beyond the scope of this thesis. For now, it is simply worth noting where the limitations of this model may lie.

Chapter IV:

Treatment with [177Lu]PSMA-I&T can induce changes to the TIME

4.1 Introduction

Having established a PSMA avid, immune competent tumour model, I next worked to determine whether [177Lu]PSMA-I&T modulates the antitumour immune response. The immune response to EBRT has been extensively characterised (see Chapter 1.4), however the relevance and relative importance of any such mechanisms for TRT remains largely unknown. On a broad scale, this includes changes to immune cell populations such as increased CD8 T cell infiltration [205], changing ratios of immune cell subsets such as increasing M1:M2 macrophages [74], upregulation of pro-immunogenic cytokines and chemokines such as GM-CSF and IL-6 [56–58], and altered expression of proimmunogenic molecules by tumour cells such as MHC class I and Fas [85].

To understand how EBRT interacts with the immune system to provide anti-tumour activity, many researchers have sought to identify changes in the TME following treatment. Typically assessment of changes to immune cell infiltration and immune cell subsets following therapeutic intervention has employed flow cytometric analysis to categorise immune cells [205–207]. Extensive panels have been developed facilitating the classification of changes in immune cell populations, for example enabling the recognition of increasing CD8+ T cell infiltration following EBRT [205]. Unfortunately, such traditional analysis is not possible here due to the radioactive nature of the post-treatment tumour samples and the lack of availability of a multi-colour flow cytometer in a radiation-controlled area. Instead, high throughput transcriptomics can be employed to enable similar exploration of the TME owing to the recent development of computational methods for quantifying cell types from bulk tissue gene expression profiles [136, 208, 209]. Here, I have made use of the NanoString platform to provide broad initial assessment of changes to the TME following TRT. Unlike traditional next generation sequencing platforms, NanoString enables highly multiplexed direct quantification of RNA transcripts using a fluorescent barcode system without a cDNA synthesis step and thus reduces variability

introduced by cDNA errors (Figure 4.1) [210, 211]. The nCounter analysis platform can then be used to delineate immune cell subsets using a cell type profiling algorithm based on high confidence marker genes determined by Danaher *et al.* in 2017[136]. These marker genes were identified though analysis of co-expression patterns in large tumour gene expression datasets, providing cell type scores that are highly concordant with flow cytometry and immunohistochemistry (IHC) readings. Indeed, subsequent analysis by the TRACERx consortium confirmed that these immune signatures provide good estimates of immune infiltrates and also observed strong correlation with pathology TIL estimates [212]. Notably, owing to the applicability of this type of analysis to clinical samples (including FFPE samples), along with other drawbacks of IHC and flow cytometry such as limitations in phenotypic markers and standardisation, use of transcriptomics for immune cell subset enumeration is becoming increasingly widespread [208, 213–216].

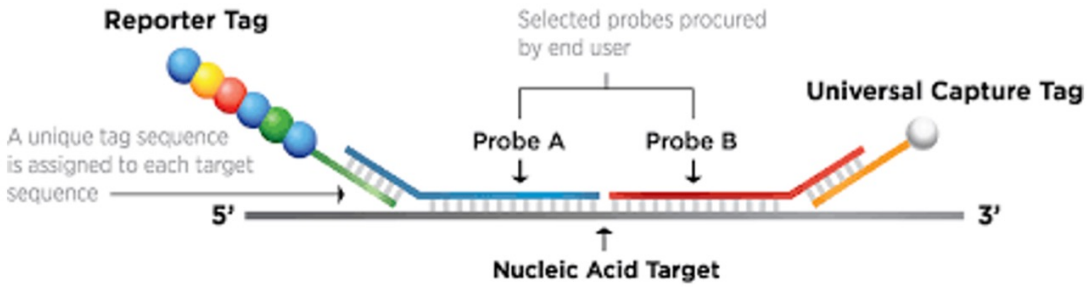

Figure 4.1: NanoString Technology *reproduced from nanostring.com*
NanoString nCounter technology enables direct, multiplexed measurement of gene expression, providing assessment of the relative abundance of hundreds of different mRNA transcripts. This is achieved using gene specific probe pairs that specifically hybridise to their target mRNA. The reporter probe (A) carries a unique fluorescent barcode that can be read by the nCounter machine, whilst the capture probe (B) enables immobalisation so the signals can be read.

In addition to the overall changes to the tumour immune microenvironment (TIME), it is also of interest to ascertain whether TRT is capable of inducing similar immune activating mechanisms as EBRT. One key mechanism is thought to be the induction of immunogenic cell death (ICD). Unlike programmed cell death, this form of regulated cell death is highly immunogenic and can trigger an inflammatory response that can ultimately drive adaptive immunity [42]. The notion that regulated cell death of malignant self-cells can stimulate an immune response has important clinical implications. Specifically, it suggests that the anti-cancer effects of many conventional treatments may not be a result of direct cell killing but are at least in part propagated by the induction of an anti-tumour immune response mediated by this initial cell death.

The immunogenicity of this form of cell death comes not only from the increased uptake of tumour antigens by DCs during/ following cell death (antigenicity), but also from the release of various damage associated molecular patterns (DAMPs) and chemokines that act as immunostimulatory molecules (adjuvanticity)[41]. These molecules act in various ways to facilitate the activation of APCs, and thus the activation and recruitment of T cells. This includes promoting recruitment of APCs, guiding the interaction between APCs and dying cells, promoting phagocytosis of dying cells by APCs, promoting APC activation, and facilitating recruitment of T cells (Figure 4.2(A)). Whilst an ever growing list of such molecules have been identified, three key molecular determinants of ICD have been defined; CRT exposure, HMGB1 release, and ATP release [42] (Figure 4.2(B)).

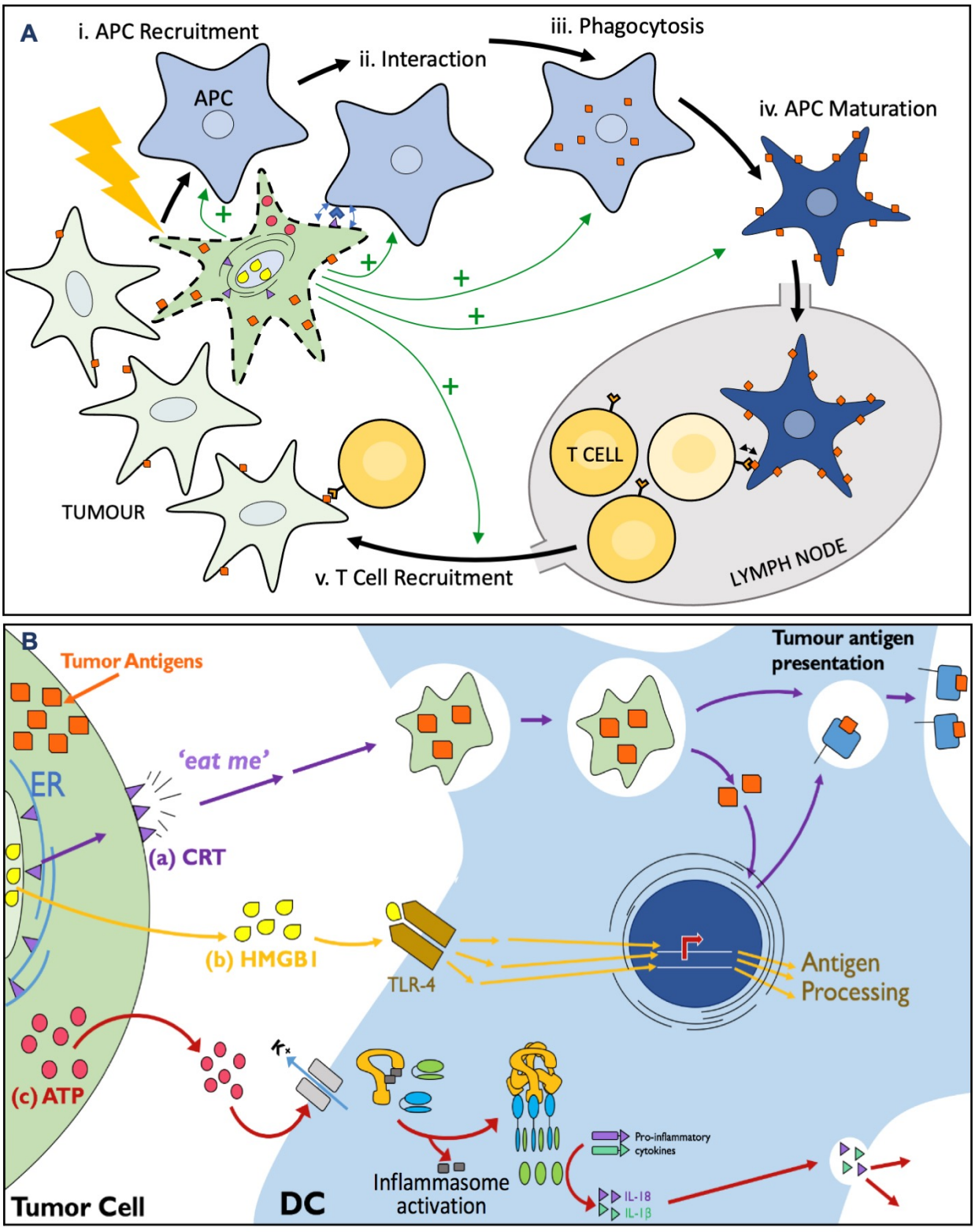

Figure 4.2: Immunogenic Cell Death
(A) ICD associated DAMPs and cytokines act at five main points of the cancer immunity cycle to promote an immune response. ***(i)*** Promote recruitment of APCs to the site of ICD. ***(ii)*** Guide interactions between the dying cell and APCs. ***(iii)*** Act as 'eat-me' signals to stimulate phagocytosis of the dying cell. ***(iv)*** Promote progression of APCs to their mature form to provide cross presentation of antigens. ***(v)*** Promote recruitment of activated T cells to the site of ICD. **(B)** There are three key molecular determinants of ICD ***(a)*** CRT cell surface exposure; ***(b)*** HMGB1 release; ***(c)*** ATP release.

CRT is an endogenous endoplasmic reticulum (ER) protein, however during the process of ICD it undergoes translocation to the cell surface via antegrade ER-Golgi trafficking along with ERp57 [217, 218]. From this location, it is able to interact with APCs, in particular DCs, acting as a potent 'eat-me' signal that promotes uptake of the dying tumour cell by the DC through interaction with receptors such as LDL receptor related protein 1 (LRP1)[44, 219]. It is also thought that CRT may promote IFN1 secretion by APCs to further promote immunogenicity [220, 221]. In 2007 Obeid *et al*. demonstrated that this translocation could be induced by gamma irradiation, and moreover that knockdown of CRT could ablate the immunogenicity of irradiation induced cell death in a manner that was restored by addition of recombinant CRT [43]. This demonstrated that CRT exposure is necessary for the immunogenicity of cell death.

The second key mediator of ICD, HMGB1, is an important regulator of transcription. Upon its release from dying cells, it can signal via a number of receptors including RAGE, TLR2, and TLR4, to induce the transcription of various proinflammatory genes [45, 46, 222, 223]. The importance of this pathway for the immunogenicity of irradiation induced cell death was identified by Apetoh *et al.* through *in vitro* assays showing the accumulation of HMGB1 following irradiation of a panel of tumour cell lines [45]. They went on to demonstrate the importance of this release for the immunogenicity of cell death, showing that immunogenicity was lost upon inhibition of either HMGB1 or the TLR4 receptor. Furthermore, the clinical relevance of this pathway was highlighted as it was noted that breast cancer patients who were carriers of a TLR4 loss-of-function allele relapsed more quickly than those with a normal TLR4 allele following radiotherapy or chemotherapy.

Alongside HMGB1, ATP is also released by cells undergoing ICD and has been identified as a key mediator. Following its release, ATP is able to stimulate the P2XR7 receptor on DCs resulting in potassium efflux that potentiates upregulation and activation of the inflammasome [48, 49]. The inflammasome is a large multi-protein complex which is composed of NLRP3, cardinal, ASC and procaspase-1. Activation of this complex results in cleavage of procaspase-1 proenzyme to produce

the functioning caspase-1 that goes on to cleave and activate pro-IL-1β and pro-IL-18 causing their release. ATP is also thought to act via the purinergic receptor P2RY2, promoting APC recruitment [224]. Again, the induction of ATP release following gamma irradiation has been observed [91, 225], and the propensity of polymorphisms in P2XR7 to influence disease outcome of known ICD inducers has been described [226].

Importantly, whilst emission of ICD-associated DAMPs is necessary for the APC dependent activation of cytotoxic T cells, it is not sufficient to induce ICD. A number of studies have demonstrated stimuli that are capable of inducing these key determinants without promoting an immune response [227]. This may be due to the kinetics and intensity of their release, which is determined by the stimulus, highlighting the importance of the spatiotemporal release. Regardless, it renders the *in vitro* assessment of these factors insufficient to confirm induction of ICD. Instead, the gold standard for ICD is an *in vivo* vaccination assay with immune-competent, syngeneic mice [42]. This assessment involves treatment of tumour cells *in vitro* until a majority are dying/ dead, before thorough washing to remove the stimulus, resuspension in PBS, and subcutaneous inoculation into the flank of an immune-competent, syngeneic host. 7 days later, the host is re-challenged with untreated, live tumour cells in the contralateral flank. Should the dying cells be undergoing an immunogenic form of cell death, the initial challenge will result in the induction of an anti-tumour immune response and thus act as a vaccine against the subsequent challenge. Where the process of cell death is not immunogenic, for example death induced by freeze-thaw cycles which are accompanied my massive antigen release but lacking in adjuvanticity from the induction of DAMPs [228, 229], the rechallenge tumours will grow freely. Thus, tumour free survival, along with growth rate of tumours growing in spite of vaccination, can be used as a measure of the immunogenicity of cell death induced by a given treatment.

4.2 Aims

1. To determine whether [177Lu]PSMA-I&T induces changes to the TIME
2. To explore possible mechanisms responsible for changes to the TIME *in vitro*
3. To explore possible mechanisms responsible for changes to the TIME *in vivo*

4.3 Results

4.3.1 The immune response to [177Lu]PSMA-I&T is characterised by an initial reduction in immune cells, followed by immune stimulation

I first sought to determine whether [177Lu]PSMA-I&T is capable of inducing changes to the TIME. As such, the NanoString high throughput transcriptional analysis platform was employed to assess the TIME in treated vs. untreated tumours. Given the time taken for immune changes to occur, I chose to look at both an early and late time points post treatment. To do this, C57BL/6 mice were first inoculated subcutaneously with $5x10^5$ PGLS tumour cells then 10 days later when tumours reached 70-80 mm^3, animals were treated with 80 MBq [177Lu]PSMA-I&T. 72 hours or 12 days post treatment animals were euthanised, and tumours excised (Figure 4.3(A)). Tumours were flash frozen and immediately ground using a pestle and mortar prior to RNA isolation. Purified RNA was subject to hybridisation and analysis using the NanoString® PanCancer Immune Profiling panel, enabling parallel assessment of 770 immune related genes, followed by analysis with NanoString's nSolver software together with the PanCancer Immune Profiling Advanced Analysis Module to enable delineation of immune cell subsets, along with extended analysis conducted in R.

Quality control (QC) was first carried out to confirm sufficient imaging and binding density, positive control linearity, and a sufficient limit of detection. Representative QC data is shown for the 72 hour timepoint (Figures 4.3 & 4.4), however all 12 day timepoint samples also met the required criteria. Firstly, imaging QC was conducted to ensure good imaging performance. In the NanoString profiling machine each imaging lane is divided into a few hundred fields of view (FOV) which are counted separately and then summed together to give the final raw data count for each lane. Thus, to ensure good imaging performance, FOV successfully counted as a percentage of FOV attempted must be greater than 75% for each lane. Figure 4.3(A) shows representative data for the 72 hour timepoint demonstrating that this value was greater than 95% for all lanes.

Binding density must also be assessed. mRNA molecules are counted by the hybridised fluorescent barcode of the reporter probe, but only codes that are unambiguously distinguishable (i.e. not overlapping) will be counted, thus if too many codes are overlapping then a point of image saturation

is reached where significant data loss can occur. Image saturation, measured as binding density, can be assessed by the number of optical features per square micron for each lane. Within a range of 0.1-1.8 relatively few reporters will overlap, enabling accurate counting. As shown in Figure 4.3(B), all samples fall between 0.7-1.53, and so are well within this range indicating acceptable binding density. In order to ensure linearity of gene expression with counts, five synthetic DNA positive control targets are included in each reaction in a linear concentration range (0.5 fM to 128 fM). In order to determine if linearity is sufficient, the R^2 coefficient from the regression of $\log_2$[known positive controls] vs. $\log_2$[measured positive controls] is calculated and should be greater than 0.95. Figure 4.3(C) shows the R^2 values for the 72 hour timepoint all fall between 0.9938-0.9992 and so the counts data demonstrate very good linearity with concentration.

The lowest concentration positive control (0.5 fM) can also be used to assess the limit of detection. Counts for this control can be compared with the eight synthetic DNA negative control targets also included in the reaction mix. As these probes should not undergo specific hybridization, they approximate general non-specific binding. Thus, if counts for the lowest positive control are more than two times the standard deviation above the mean of the negative control, this indicates successful detection. As shown in Figure 4.3(D) all samples met this requirement. As only ~10,000 copies of this control are present per tube, and the full assay contains only 100ng of total RNA which equates to around 10,000 cells, successful detection of this positive control infers that the assay is able to detect roughly 1 transcript copy per cell for each target.

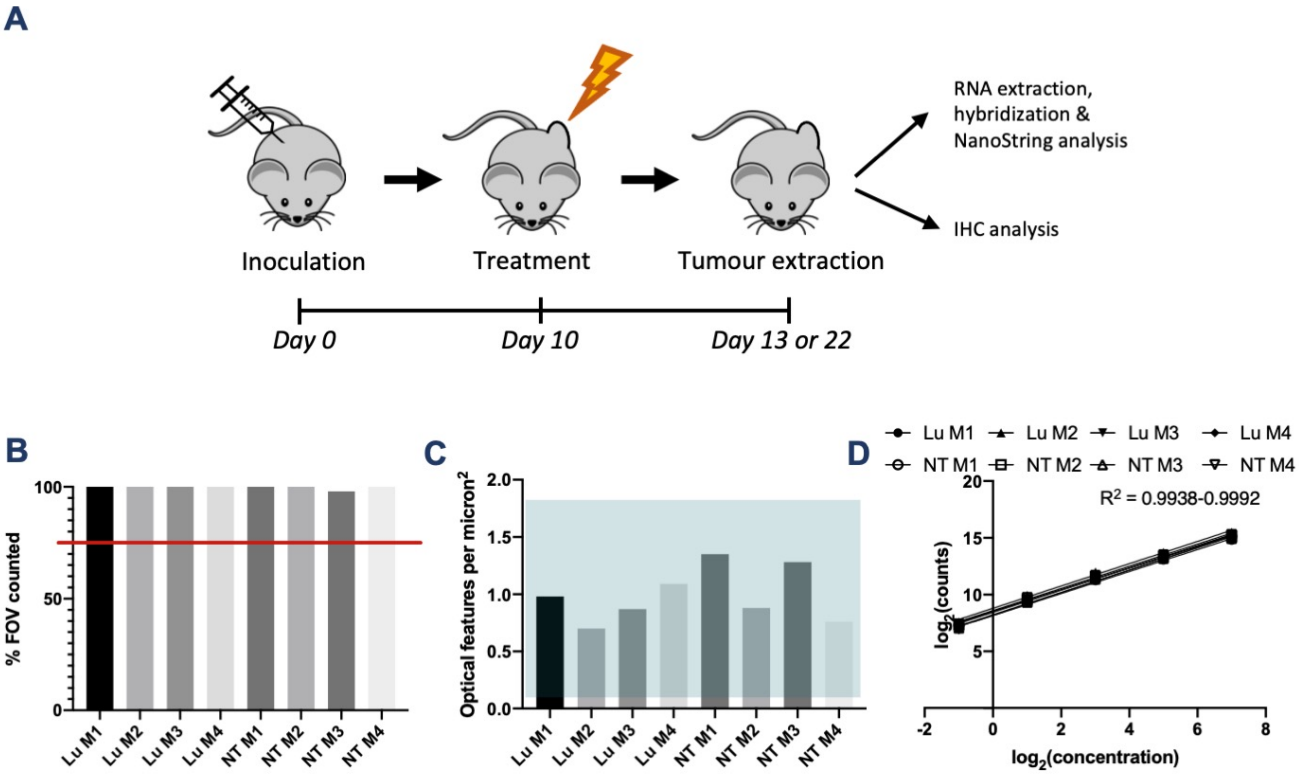

E

Sample.Lane	Lu.M1	Lu.M2	Lu.M3	Lu.M4	NT.M1	NT.M2	NT.M3	NT.M4
Negative Mean	17.50	26.75	18.13	20.00	20.38	18.75	19.38	21.75
Negative SD	3.78	9.44	5.54	4.69	5.45	5.52	7.21	11.80
POS_E	125	192	118	184	158	160	134	172
Above detection limit?	Yes	Yes	Yes	Yes	Yes	Yes	Yes	Yes

Figure 4.3: Nanostring quality control

(A) Treatment schedule; C57BL/6 mice were first inoculated sub-cutaneously with $5x10^5$ PGLS tumour cells then 10 days later when tumours reached 70-80 mm3, animals were treated with 80 MBq [177Lu]PSMA-I&T. 72 hours or 12 days post treatment animals were sacrificed, and tumours excised. Tumours were flash frozen divided in half. Half was immediately ground using a pestle and mortar prior to RNA isolation. The remainder was subject to IHC analysis. **(B)** Imaging QC calculated as (FOV successfully counted/ FOV attempted)*100. The red line indicates the 75% cut off for each lane. **(C)** Binding density shown as the number of optical features per square micron for each lane. The acceptable range of 0.1-1.8 is shown as a blue box. **(D)** Positive control linearity QC assessed on five synthetic DNA positive control. R^2 values shown are calculated from simple linear regression of log2[known positive controls] vs. log2[measured positive controls]. **(E)** Counts for the 0.5fM control were compared with the eight synthetic DNA negative control targets also included in the reaction mix. Where counts for the lowest positive control are more than two times the standard deviation above the mean of the negative control this indicates sufficient detection limits, as shown in the bottom row. Lu M1-M4 = [177Lu]PSMA-I&T treated mice (n=4); NT M1-4 = Untreated control mice (n=4).

Before in depth analysis, samples were first normalized to eliminate run-to-run and sample-to-sample variability. This was done via both positive control normalization to address sources of assay noise from the platform, and CodeSet content normalization using housekeeping genes to address sources of assay noise from the sample. A number of housekeeping genes were included in the assay library for this purpose, however these were first quality checked to ensure they displayed both sufficient expression (i.e. not expressed at or near the background), and low variability. Normalization genes were thus selected to minimize the pairwise variation statistic as shown in the pairwise variance plot (Figure 4.4(A)). Here, pairwise variation is recalculated as successive housekeeping genes are removed and so variation reduces. At the inflection point removing any more genes will begin to increase pairwise variation again, and so this indicates that the most stable reference genes have been selected. The mean and variance scatter plot (Figure 4.4(B)), where selected housekeeping genes are shown in blue and unselected genes in orange, confirms that the selected housekeeping genes are stable (given their low variability and moderate expression levels).

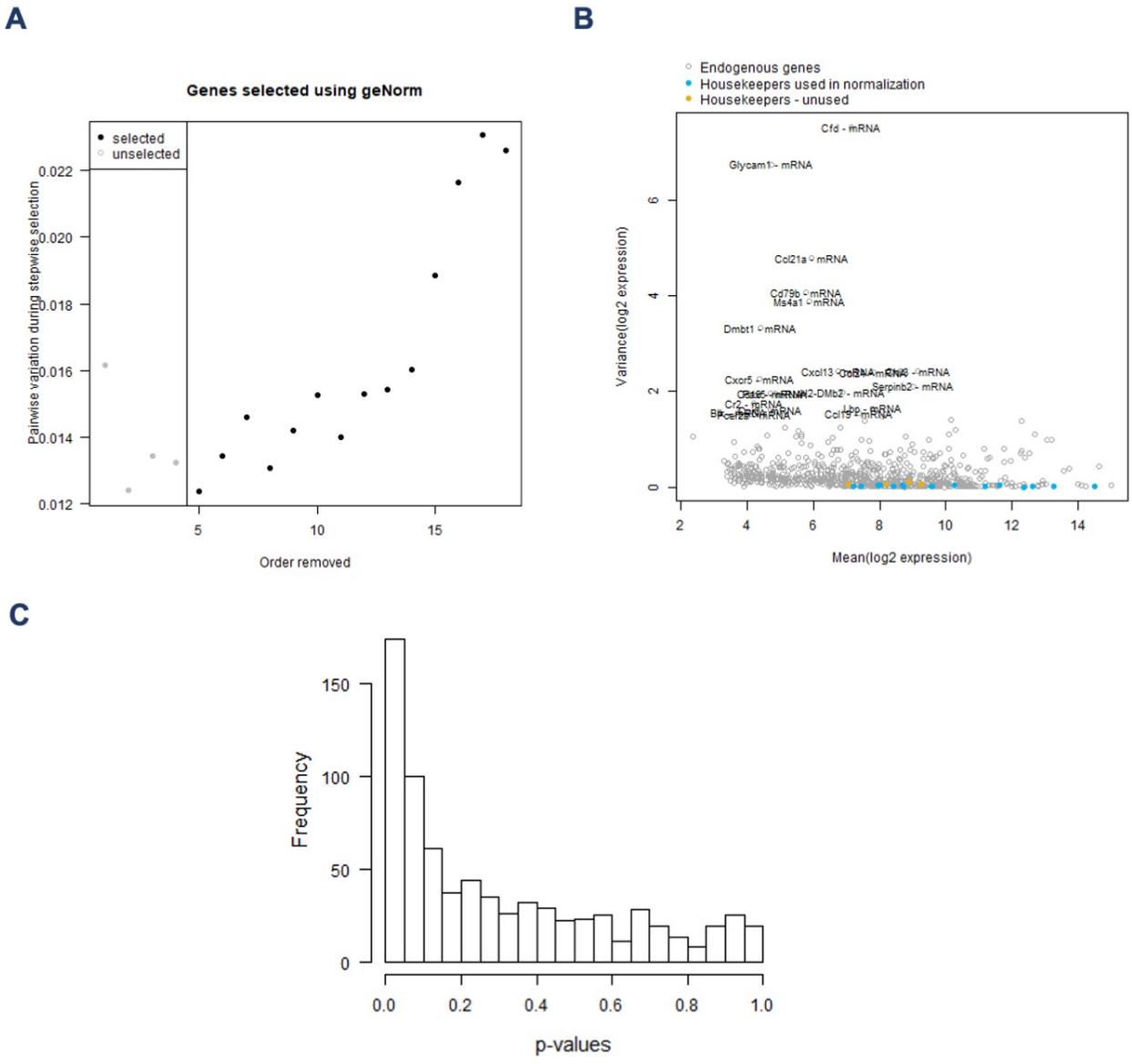

Figure 4.4: Nanostring Normalisation
(A) Housekeeping genes were selected to minimize the pairwise variation statistic. Here, pairwise variation is recalculated as successive housekeeping genes are removed and so variation reduces. At the inflection point (black line) removing any more genes will begin to increase pairwise variation again, and so the indicates that the most stable reference genes have been selected. **(B)** Housekeeping genes were quality checked in ensure they have sufficient expression and low variability. Variance and mean for expression are shown for all measured genes including housekeeping genes selected for normalisation (blue), and those discarded (orange). **(C)** A histogram plot of p-values testing each gene's univariate association with treatment.

Following QC and data normalisation, further analysis could be conducted. A clear indication of differences between the two treatment groups is illustrated by the left weighted P value histogram plot with a peak near zero (Figure 4.4(C)). As such further analysis was carried out to assess both differential gene expression and changes in immune cell subsets.

In order to assess the effect of treatment on the number of different immune cells within the TME, immune cell subset enumeration was required. Such assessment was conducted using the Danaher et al. method [136]. To develop this method, Danaher et al. validated candidate marker genes in actual tumour expression data by testing for two properties that are inherent to good marker genes, (1) That expression is specific to a single cell type, and (2) That expression is stable within that cell type. As these could not be measured directly from the bulk data, they instead identified genes whose expression patterns were consistent with these properties, i.e. if two genes are both ideal markers and expressed with perfect specificity to and stability within a cell type, their expression levels will be perfectly correlated, and the ratio between them will be constant across samples. These qualities were assessed using a pairwise similarity statistic (PSS) (box 1). This same statistic can thus be used to check that the candidate marker genes also exhibit marker gene qualities in the NanoString data presented here. Such analysis demonstrated good correlation for T cell marker genes as shown in Figure 4.5, with PSS values between 0.7-0.97. These data are summarised in a heatmap in Figure 4.6. Good markers were similarly available for T cells, Th1 cells, macrophages and NK CD56dim cells (data not shown).

BOX 1: The Pairwise Similarity Statistic (PSS) - This is an adaptation of Pearson's correlation metric which attempts to draw a line of best fit through the data of two variables where the Pearson correlation coefficient, *r*, indicates how far away all these data points are to this line of best fit but does NOT represent the slope of the line of best fit. The PSS takes the slope in to account as a slope deviating from 1 would indicate that whilst two genes may be regulated by the same biological process, that they do not increase at the same rate and so are not expressed at consistent levels within a single cell type. As such, the PSS equals 1 when the two genes are perfectly correlated with a slope of 1 and decreases for gene pairs with low correlation or with slope diverging from 1.

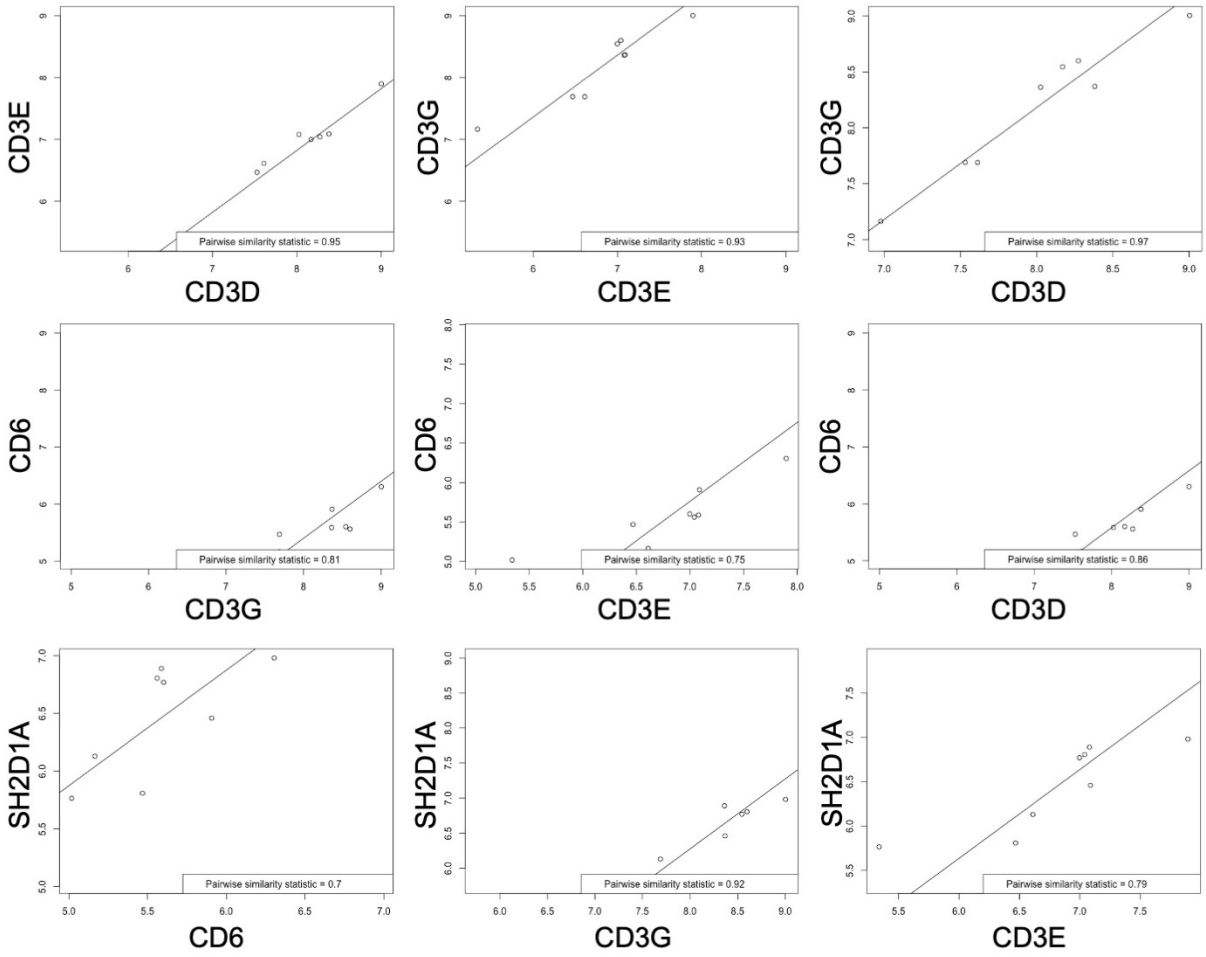

Figure 4.5: Marker gene concordance plots
A pairwise similarity statistic (Danaher et al.,) was calculated between each potential marker gene for each immune cell type to be enumerated. T cell marker genes are shown from the 72 hr timepoint as a representative example (n=8).

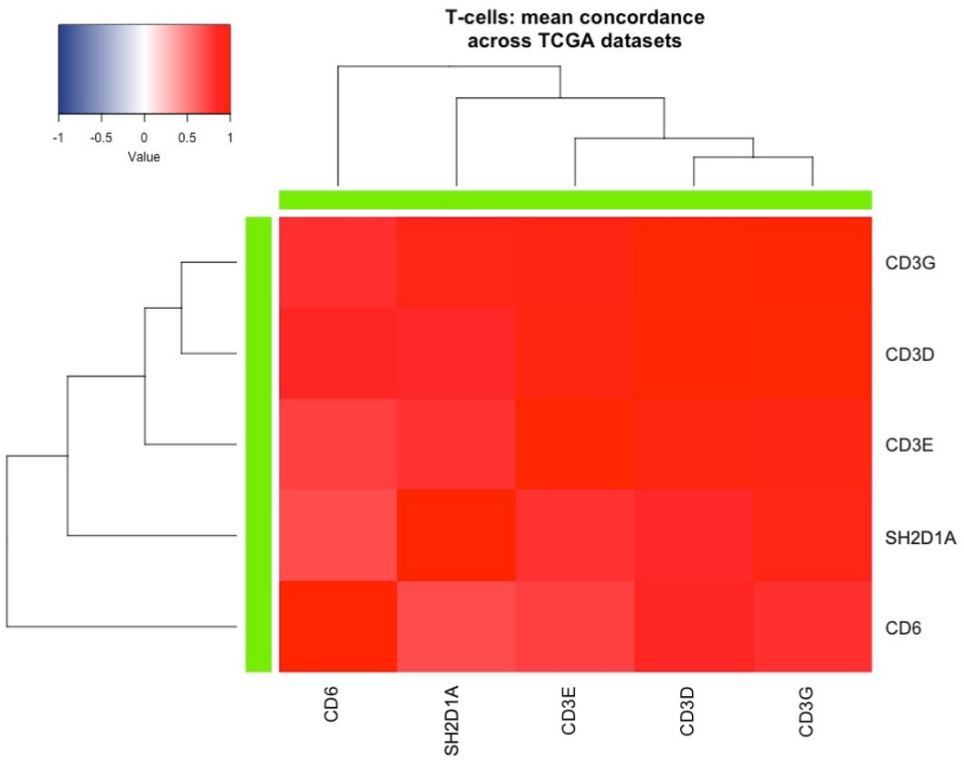

Figure 4.6: Marker gene concordance heatmap
Heatmap showing the pairwise similarity statistic for all T cell marker gene pairs. Data is presented as a heatmap representing the pairwise similarity statistic (Danaher et al.,) for each potential marker gene pair. T cell marker genes are shown from the 72 hr timepoint as a representative example (n=8).

Following immune cell enumeration, comparison of [177Lu]PSMA-I&T treated tumours with untreated controls at the 72 hour post-treatment timepoint demonstrates an initial reduction in immune cells, with low abundance of all measured immune cell types in the TRT treated tumours compared with untreated controls (Figure 4.7(A)(B)). More specifically there is an overall reduction in CD45+ cells (Figure 4.8(A)), with a reduction in total T cells (Figure 4.8(B)). This can also be visualised in a heatmap showing a reduction in all marker genes used for T cell delineation (Figure 4.8(F)). There is also a trend towards a reduction in macrophages, Th1 cells and NK CD56dim cells (Figure 4.8(c-e)), however this does not reach the point of significance, perhaps due to the small number of samples (n=4) in this experiment.

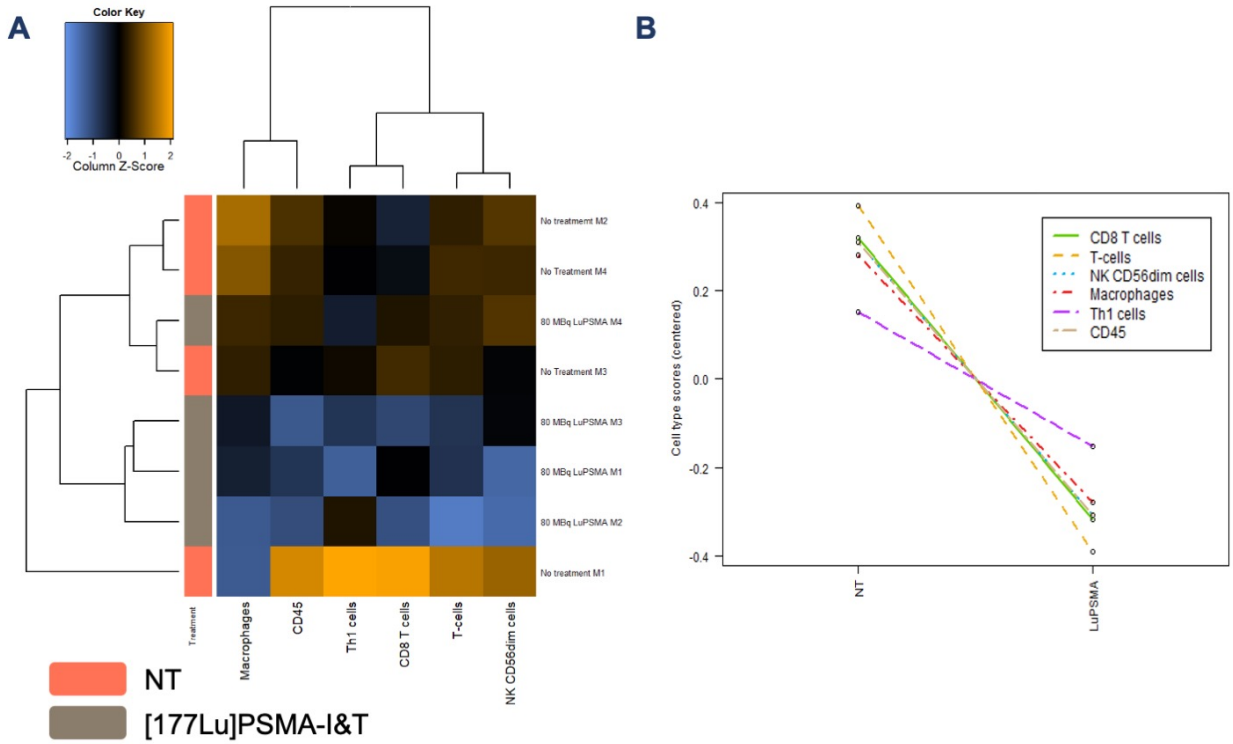

Figure 4.7: Cell type measurements for [177Lu]PSMA-I&T treated vs untreated tumours 72 hours post treatment
(A) Heatmap showing cell type measurements for [177Lu]PSMA-I&T treated vs untreated tumours 72 hours post treatment. Data are presented as a heatmap for each cell type score as determined by the Danaher et al., method for immune cell enumeration. **(B)** Changes in immune cell populations in [177Lu]PSMA-I&T treated tumours vs. untreated controls. n=4 per treatment group.

Despite this initial reduction in immune cells within the TIME, by 12 days post treatment there is a far greater variation in immune cell composition across samples in [177Lu]PSMA-I&T treated tumours when compared with untreated controls, with an overall increase in immune cells (Figure 4.9, 4.10). Importantly, whilst the cell type scores suggest that the overall number of immune cells is reduced in untreated controls at 12 days compared with 72 hours post treatment, significant confounding batch effects arise as the tumour extraction, RNA isolation, codeset hybridisation, analysis cartridge and analysis run were all carried out separately for the later time point, making comparison impossible. As such, I can only consider the impact of treatment compared with untreated controls at each timepoint.

In contrast to the 72 hour timepoint an increase in CD45+ cells in [177Lu]PSMA-I&T treated tumours compared with untreated can be observed, however this does not reach the level of significance ($p=0.13$). In general immune cells can be seen to display a far greater intertumour variation in treated tumour compared with untreated controls, with a trend towards an increase in a number of immune cell types (Figure 4.10(a-e)). In particular, there is evidence of one 'super-responder' demonstrating particularly high CD45+ cell infiltration (Figure 4.10(A)), along with all immune cell subtypes (Figure 4.10(b-e)).

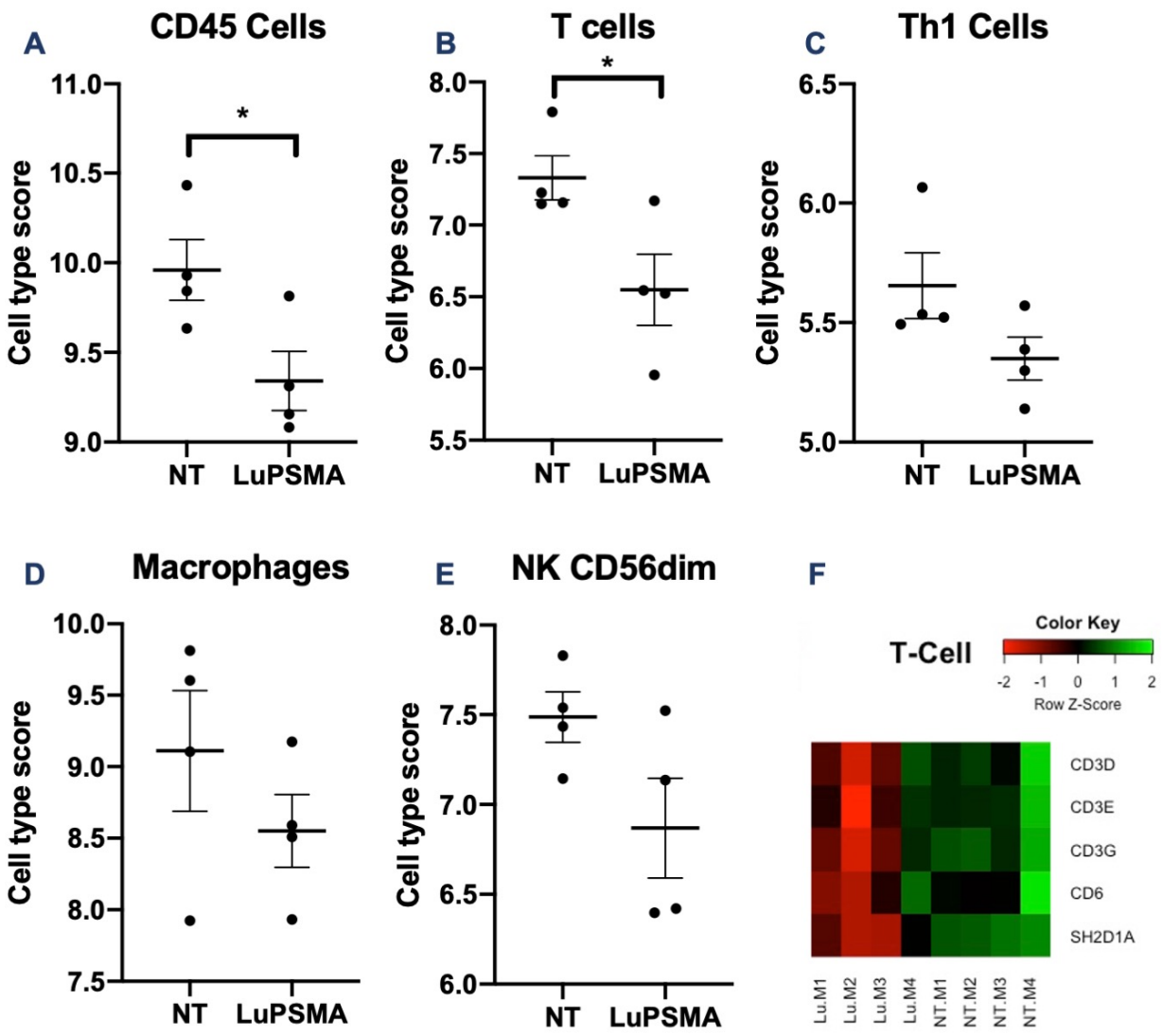

Figure 4.8: Immune cell populations in PGLS tumours 72 hours post [177Lu]PSMA-I&T treatment

(A-E) Relative cell type score as determined using the Danaher et al., method 72 hours post treatment with [177Lu]PSMA-I&T for CD45 cells, T cells, Th1 cells, Macrophages and NK CD56dim cells. Data is presented as mean ± SEM and statistical significance determined by unpaired t-test. n=4 per group; * $p<0.05$; ** $p<0.01$; *** $p<0.001$. **(F)** Heatmap showing changes in gene expression for marker genes for T cells.

Given the relative increase in T cells from the 72 hour time point, I went on to investigate possible mechanisms for the increase. Chew et al. suggested that CCL5/CXCL16 dependent chemotaxis may be responsible for the increased presence of CD8+ T cells following treatment with the related therapeutic Y90 radioembolization, based on strong positive correlation with the chemokines CCL5 and CXCL16. As such, I analysed the impact of [177Lu]PSMA-I&T on both chemokines noting a trend towards a similar increase in both (Figure 4.10(F)). Whilst my analysis does not allow determination of CD8+ T cells due to the poor PSS score of CD8+ marker genes, CCL5 and CXCL16 show a striking correlation with T cell numbers, consistent with a role in T cell chemotaxis (Figure 4.10(G)(H)).

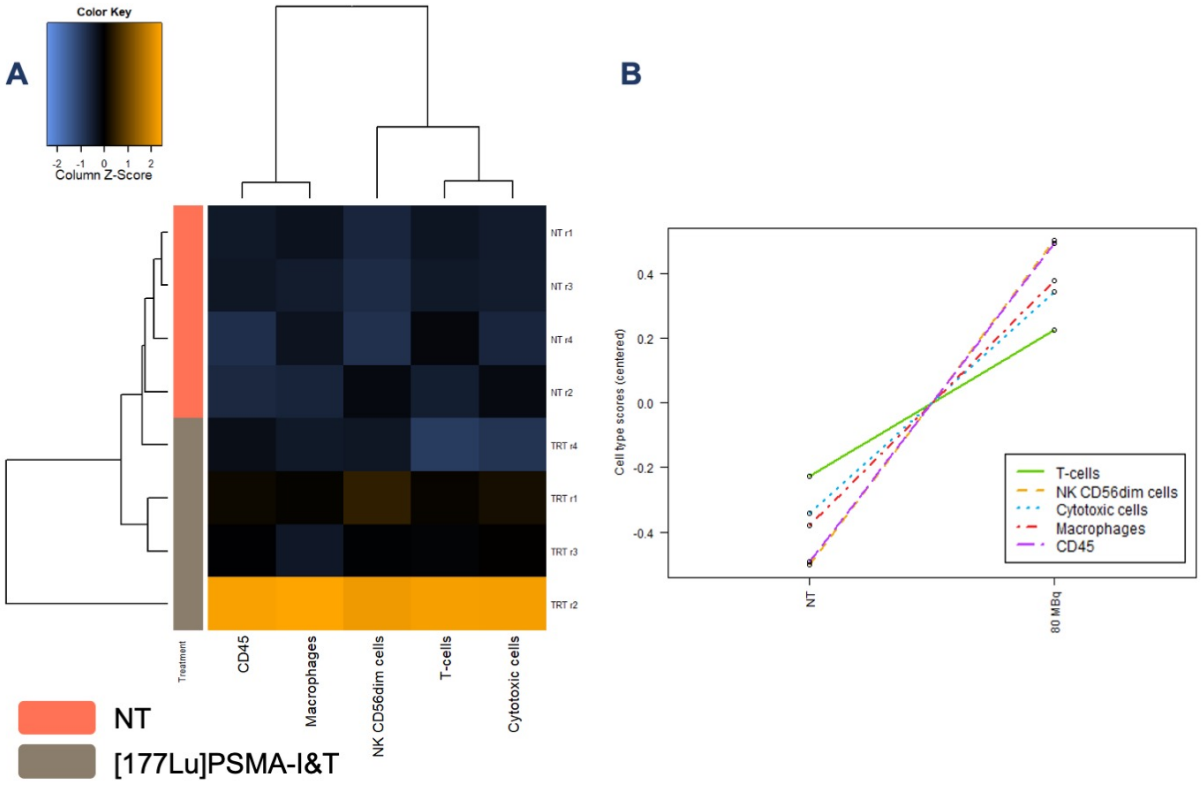

Figure 4.9: Cell type measurements for [177Lu]PSMA-I&T treated vs untreated tumours 12 days post treatment
(A) Heatmap showing cell type measurements for [177Lu]PSMA-I&T treated vs untreated tumours 12 days post treatment. Data is presented as a heatmap for each cell type score as determined by the Danaher et al., method for immune cell enumeration. **(B)** Changes in immune cell populations in [177Lu]PSMA-I&T treated tumours vs. untreated controls. n=4 per treatment group.

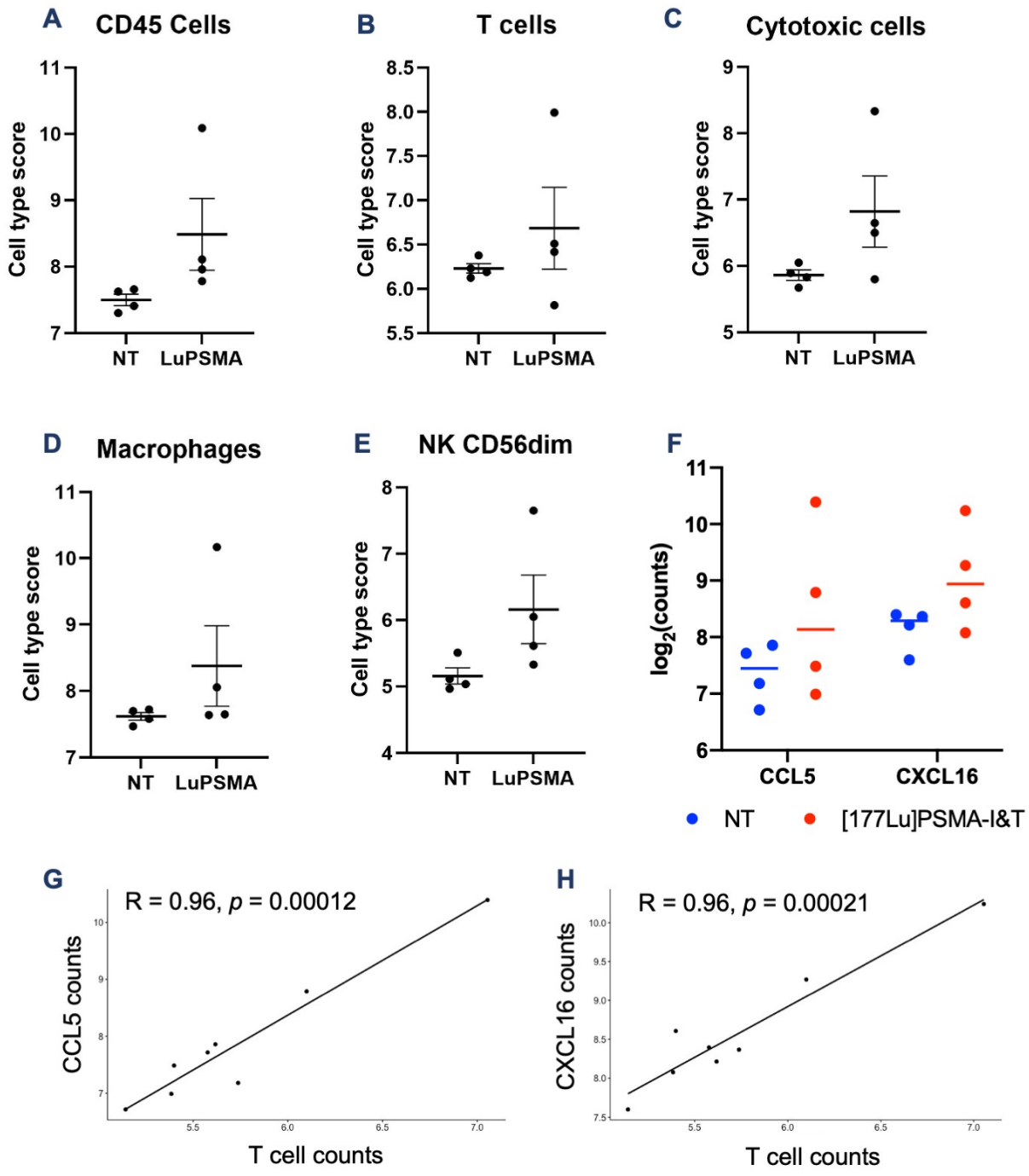

Figure 4.10: Immune cell populations in PGLS tumours 12 days post [177Lu]PSMA-I&T treatment

(A-E) Relative cell type score as determined using the Danaher et al., method 12 days post treatment with [177Lu]PSMA-I&T for CD45 cells, T cells, Cytotoxic cells, Macrophages and NK CD56dim cells. Data is presented as mean ± SEM and statistical significance determined by unpaired t-test. n=4 per group; * p<0.05; ** p<0.01; *** p<0.001 **(F)** Chemokine levels in [177Lu]PMSA-I&T treated vs untreated tumours 12 days post treatment. Mean and individual data points are shown. **(G)** Pearson correlation of CCL5 levels with T cell numbers in both [177Lu]PMSA-I&T treated and untreated tumours 12 days post treatment (n=8). **(H)** Pearson correlation of CXCL16 levels with T cell numbers in both [177Lu]PMSA-I&T treated and untreated tumours 12 days post treatment (n=8).

4.3.2 EBRT treatment of PGLS tumours results in TIME stimulation at both early and late timepoints

In order to compare the changes to the TIME induced by treatment with [177Lu]PSMA-I&T with those induced by EBRT, I similarly conducted high throughput transcription analysis of tumour samples following EBRT treatment at the same timepoints.

As above, RNA was extracted from bulk tumour, followed by expression analysis using the NanoString® PanCancer Immune Profiling panel.

Following QC, normalisation and immune cell enumeration as described above (data not shown), in depth analysis demonstrated that converse to TRT treatment there is no reduction in immune cell infiltration 72 hours post EBRT treatment (Figure 4.11 (A)(B)). Indeed, there is no significant change in immune cell numbers (Figure 4.12(a-f). However, by the 12 day time point, similar to TRT treatment, a trend towards an increase in CD45+ was observed (Figure 4.14(C)), with increased cytotoxic cells and NK CD56dim cells (Figure 4.14(a-e)).

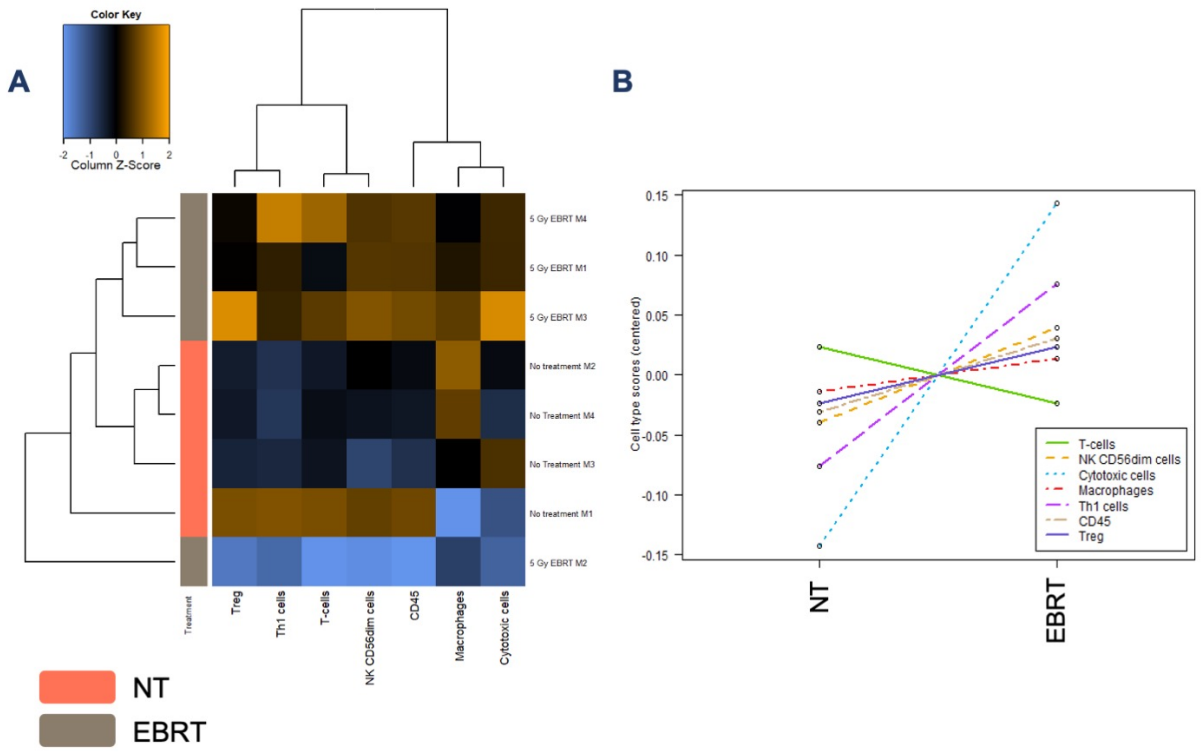

Figure 4.11: Cell type measurements for 6 Gy EBRT treated vs untreated tumours 72 hours post treatment

(A) Heatmap showing cell type measurements for 6 Gy EBRT treated vs untreated tumours 72 hours post treatment. Data is presented as a heatmap for each cell type score as determined by the Danaher et al., method for immune cell enumeration. **(B)** Changes in immune cell populations in EBRT treated tumours vs. untreated controls. n=4 per treatment group.

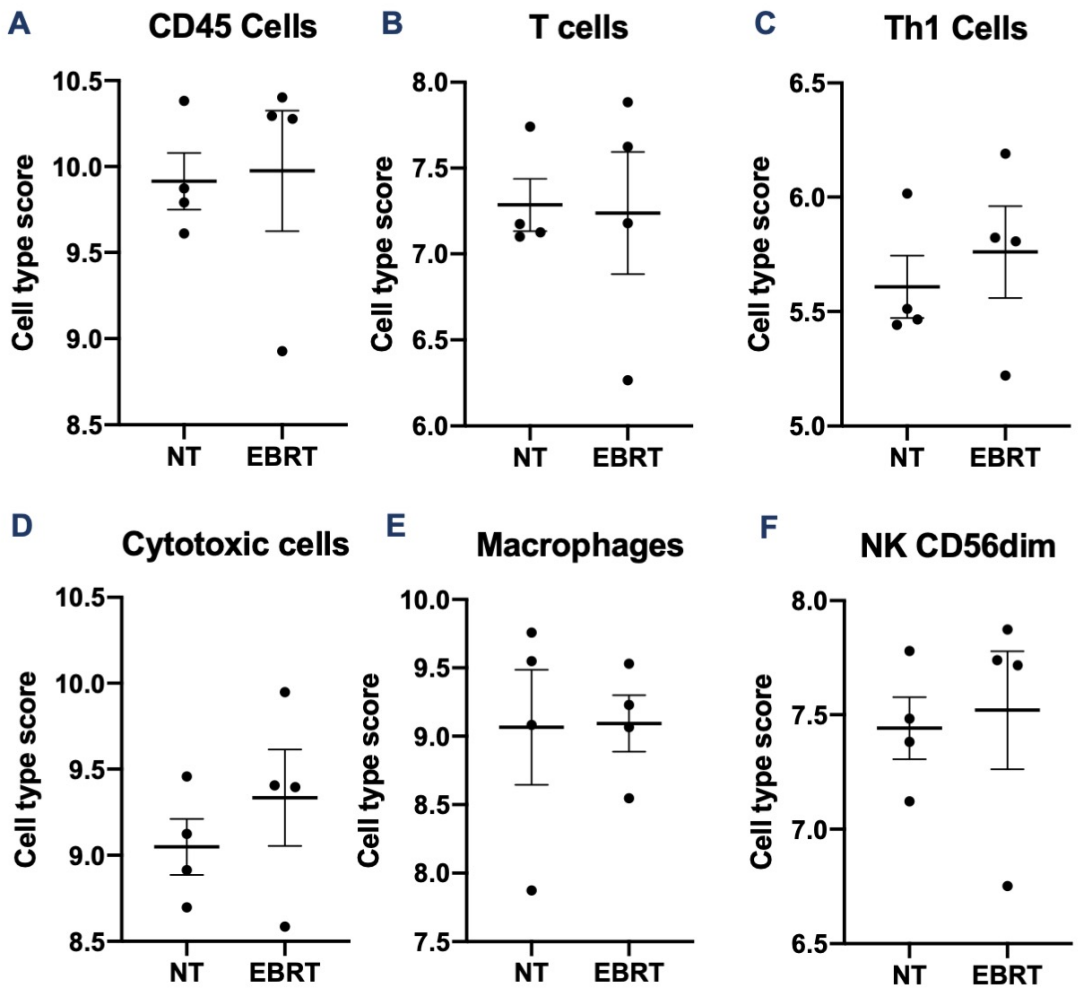

Figure 4.12: Immune cell populations in PGLS tumours 72 hours post EBRT treatment
(A-F) Relative cell type score as determined using the Danaher et al., method 72 hours post treatment with EBRT for CD45 cells, T cells, Th1 cells, Cytotoxic cells, Macrophages and NK CD56dim cells. Data is presented as mean ± SEM and statistical significance determined by unpaired t-test. n=4 per group; * $p<0.05$; ** $p<0.01$; *** $p<0.001$

As this study was conducted in parallel with the TRT treatment assessment, the two treatments could also be compared against each other with respect to gene expression changes. Differential gene expression analysis highlighted a number of genes in common with those elevated 12 days post TRT treatment (Figure 4.15). These include LcK, a non-receptor tyrosine-protein kinase with a key role in T-cell antigen receptor (TCR)-linked signal transduction pathways, highlighting the importance of increased T cell signalling. Another common differentially expressed gene is CCL-11, a chemokine involved in eosinophil recruitment, again suggesting that chemokine activation may be mutually

important for both radiation modalities. TLR1 is also upregulated by both modalities, with a fundamental role in pathogen recognition and activation of innate immunity.

However, there were also a number of genes which were observed to have very different expression between the EBRT and TRT treated groups at 12 days post treatment (Figure 4.15). Strikingly, five of the top eight hits are interferon related genes; Interferon Induced Protein With Tetratricopeptide Repeats 1 (Ifit1), Interferon-induced Protein 44 (Ifi44), Interferon Induced Transmembrane Protein 1 (Ifitm1), interferon regulatory factor 7 (Irf7), and Interferon-stimulated gene 15 (Isg15), with higher mRNA levels of all five genes in the TRT treated group (Figure 4.15). This suggests there may be higher interferon activity in the TRT treated group. As such, I chose to also analyse the effect of TRT vs EBRT treatment on IFN targets known to be of functional importance in modulating the TIME in response to radiotherapy. One such target is CXCL10 and the related chemokine CXCL9, both of which have been shown to be important molecules in affecting CD8+ T cell recruitment and priming downstream of radiation-induced type I IFNs [230]. Consistently, a trend towards increased CXCL10 expression ($p=0.14$), and CXCL9 ($p=0.69$) expression was observed again suggesting greater IFN activity following TRT treatment (Figure 4.15(C)(D)).

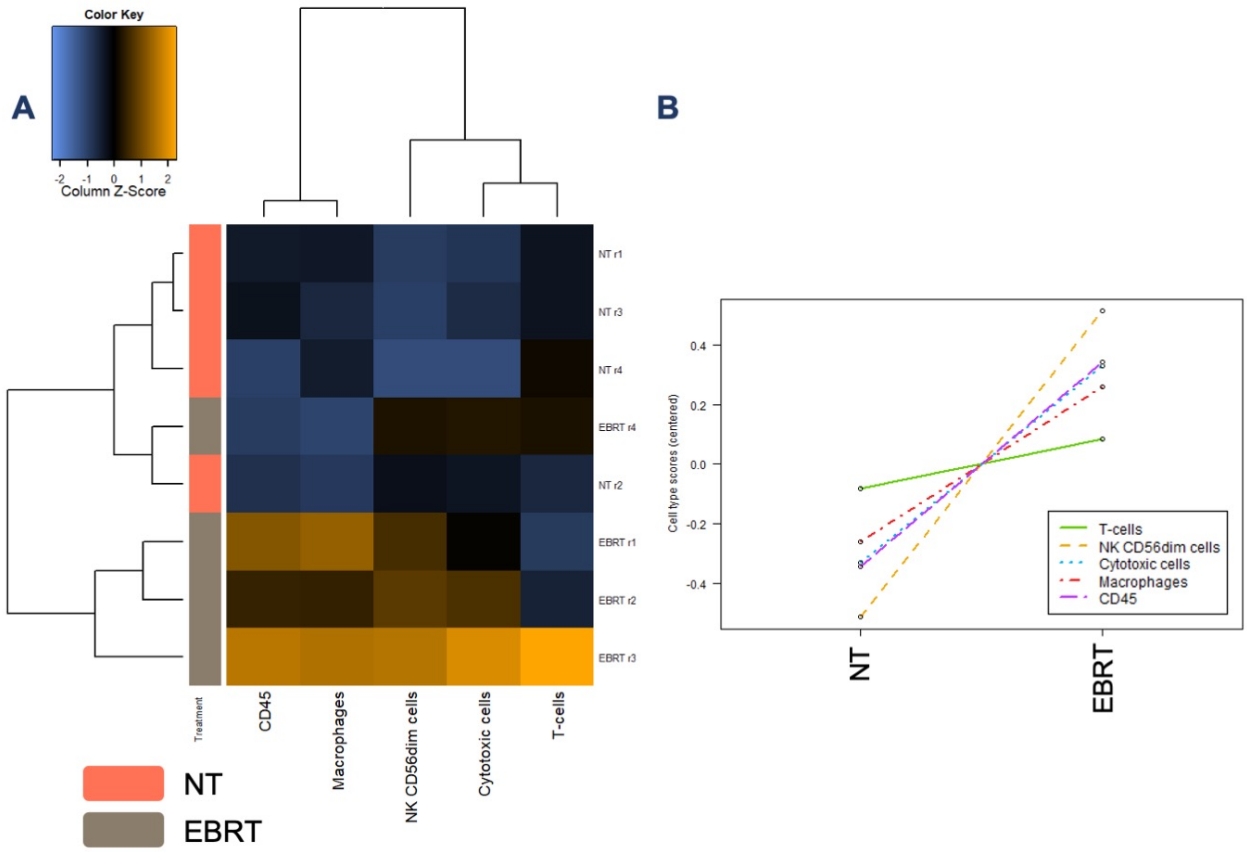

Figure 4.13: Cell type measurements for EBRT treated vs untreated tumours 12 days post treatment

(A) Heatmap showing cell type measurements for EBRT treated vs untreated tumours 12 days post treatment. Data is presented as a heatmap for each cell type score as determined by the Danaher et al., method for immune cell enumeration. **(B)** Changes in immune cell populations in EBRT treated tumours vs. untreated controls. n=4 per treatment group.

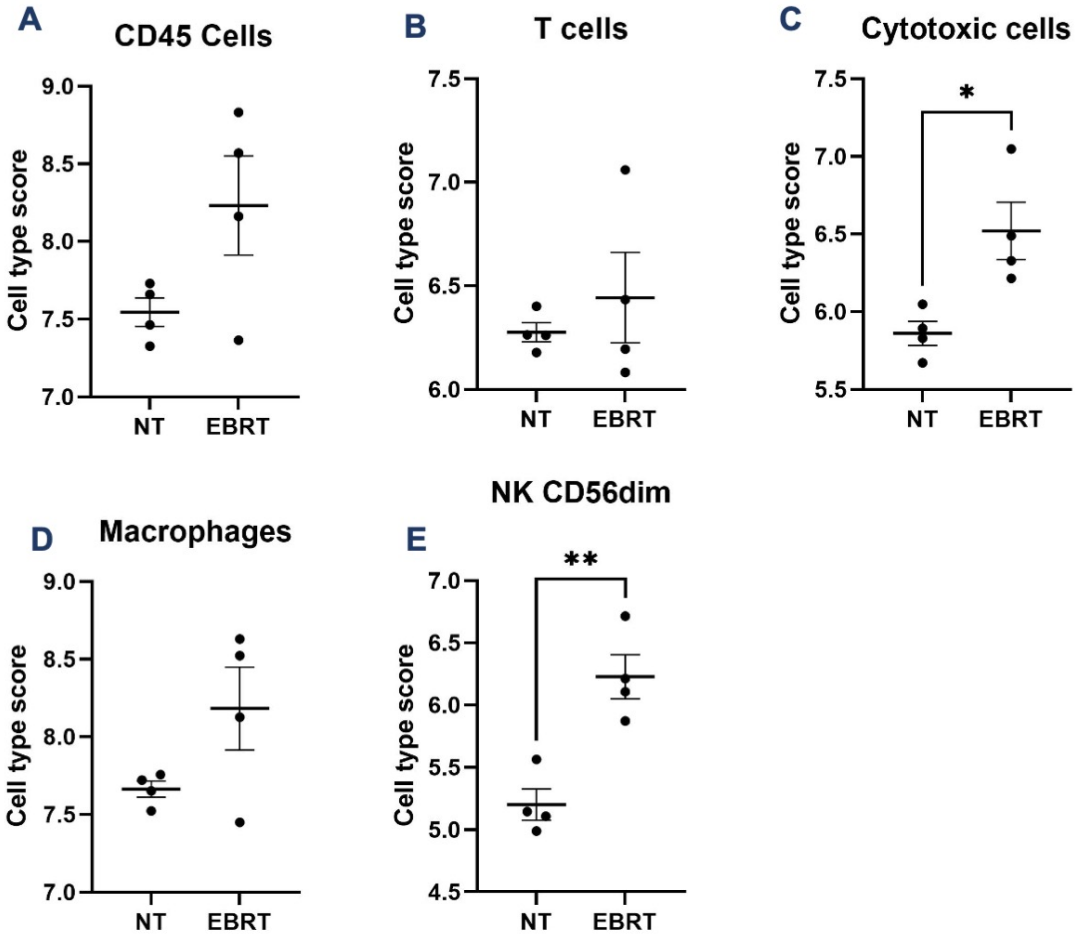

Figure 4.14: Immune cell populations in PGLS tumours 12 days post EBRT treatment (A-E) Relative cell type score as determined using the Danaher et al., method 72 hours post treatment with EBRT for CD45 cells, T cells, Cytotoxic cells, Macrophages and NK CD56dim cells. Data is presented as mean ± SEM and statistical significance determined by unpaired t-test. n=4 per group; * $p<0.05$; ** $p<0.01$; *** $p<0.001$

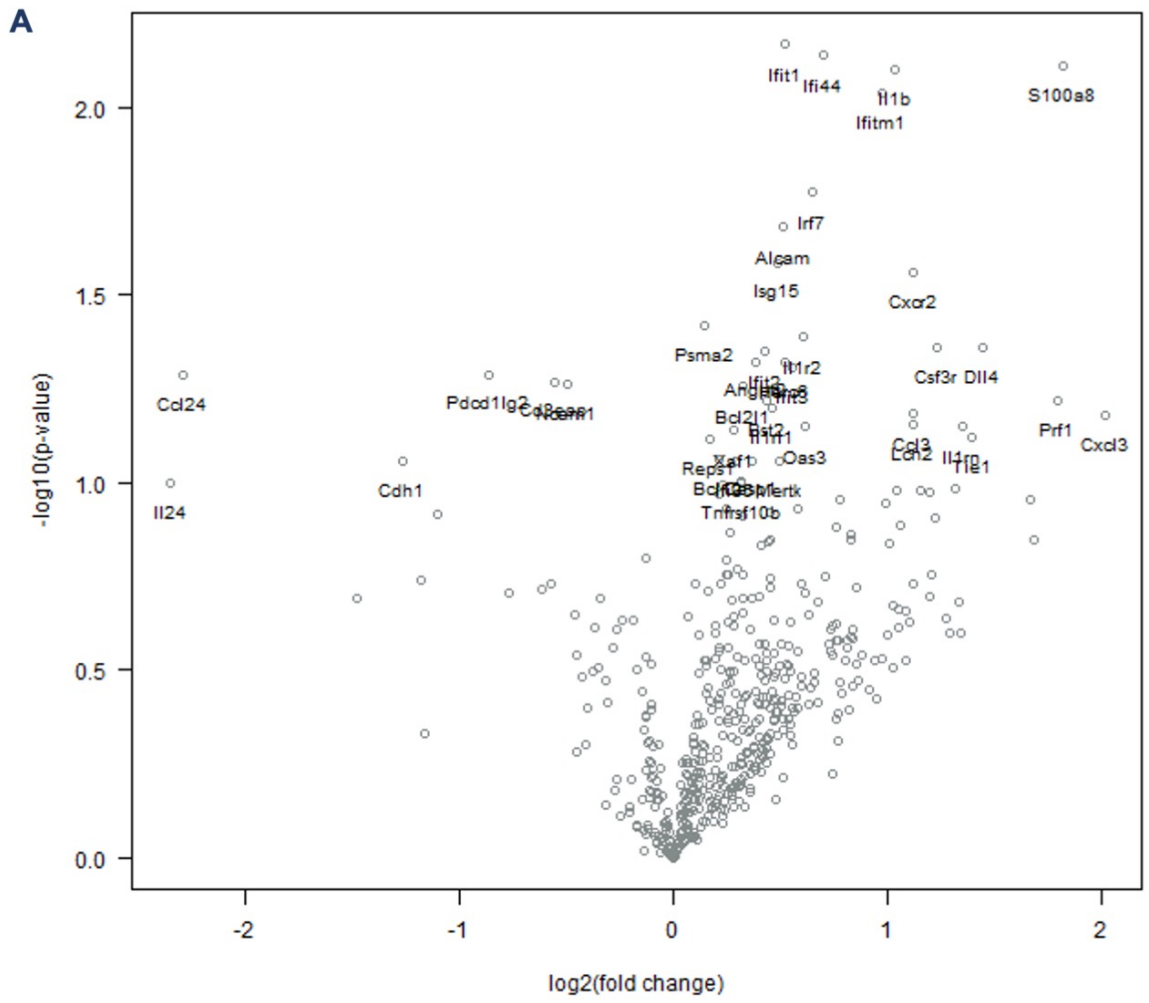

Gene	Log2.fold.change	P-value
Ifit1	0.523	0.00681
Ifi44	0.698	0.00728
S100a8	1.820	0.00775
Il1b	1.030	0.00792
Ifitm1	0.971	0.00917
Irf7	0.650	0.01690
Alcam	0.512	0.02090
Isg15	0.486	0.02600

Figure 4.15: Differential gene expression in PGLS tumours 12 days post EBRT vs TRT treatment

(A) Volcano plot showing genes differentially expressed between TRT and EBRT treated tumours. Genes to the left of 0 are downregulated in TRT compared with EBRT and those to the right are upregulated in TRT compared with EBRT treatment. **(B)** Top 8 DEGs. **(C)** CXCL10 levels and **(D)** CXCL9 in [177Lu]PMSA-I&T treated vs EBRT treated tumours 12 days post treatment. Mean and individual data points are shown. **n**=4 per group.

4.3.3 [177Lu]PSMA-I&T induces the molecular markers of immunogenic cell death *in vitro*

Having demonstrated that [177Lu]PSMA-I&T treatment can induce changes to the TIME, I next sought to identify whether similar mechanisms are responsible as those already described for EBRT. One such mechanism is through induction of ICD. I thus assessed the ability of [177Lu]PSMA-I&T to induce the key molecular determinants of ICD *in vitro*.

To establish whether treatment resulted in translocation of CRT to the cell membrane, a staining protocol was first established that ensured staining of only extracellular CRT, and not the intracellular pool. To do this PGLS cells were treated with a known inducer of ICD, mitoxantrone, and incubated for 24 hours. Following treatment, cells were washed and stained with anti-CRT antibody and DAPI nuclear stain. Incubations were kept short to prevent unwanted entry of the antibody into the cell where it could stain intracellular CRT. Stained cells were then imaged using a fluorescent microscope to assess the staining distribution. Following optimisation of this method, staining of only the cell surface pool of CRT was evident (Figure 4.16(a-c)). This can also be observed in Z stack images, where a vertical stack of images results in a characteristic small dot widening to an open circle as expected for cell surface staining (Figure 4.16(A)(B)).

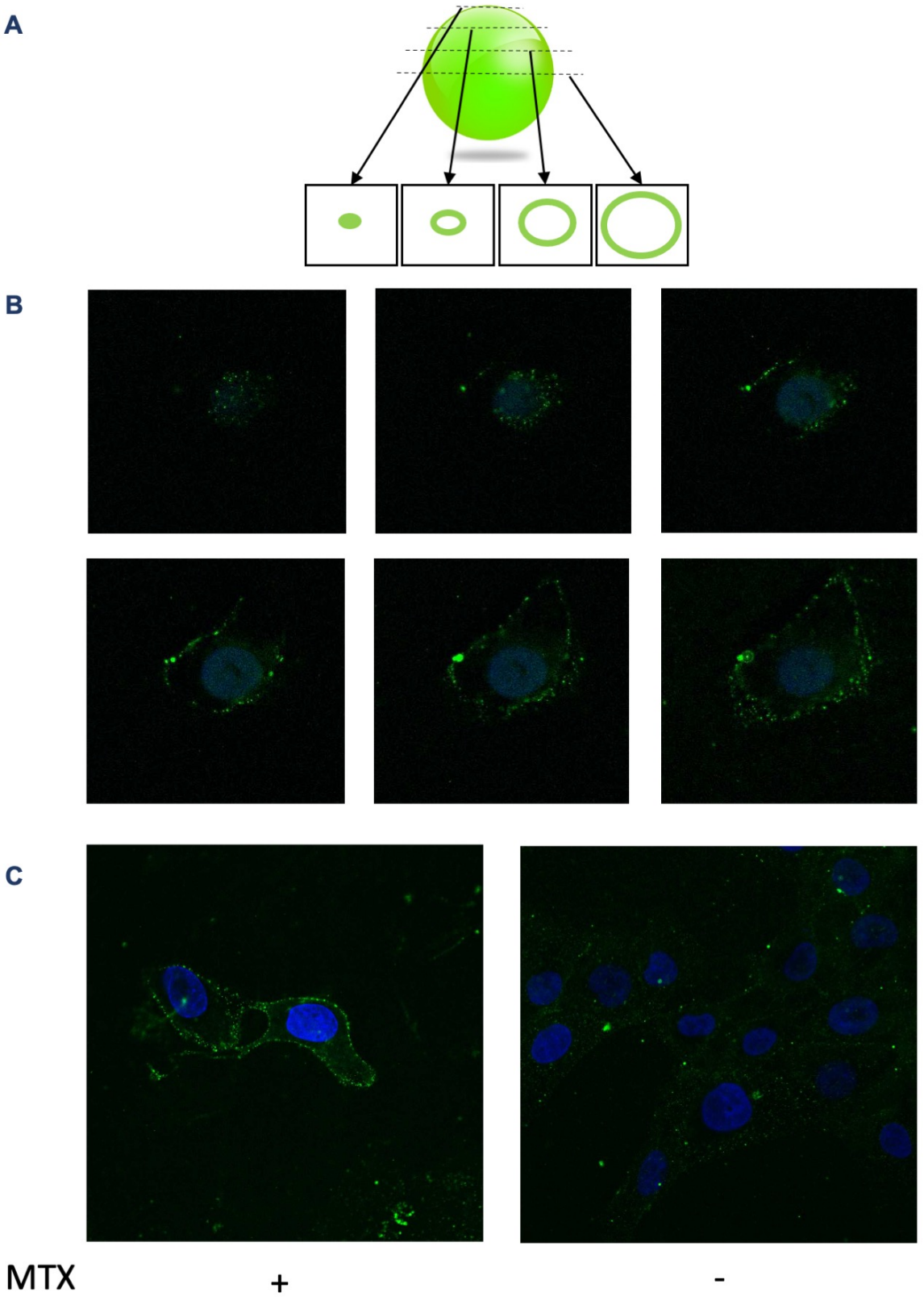

Figure 4.16: Cell surface CRT staining
(A) In order to ensure only cell surface CRT is stained, the staining protocol was optimised. Where cell surface staining is present, a Z stack of images through a cell would be expected to appear first as a small spot that then widens to an open circle. **(B)** Z stack images of mitoxantrone treated PGLS cells showing the expected pattern for cell surface staining. **(C)** Cell surface staining of mitoxantrone treated cells and untreated control cells.

Having optimised this staining protocol and confirmed cell surface staining, PGLS cells were treated with various doses of [177Lu]PSMA-I&T or EBRT and incubated for four to 72 hours. Following treatment, the same staining procedure was conducted followed by propidium iodide (PI) to enable gating of live cells (Figure 4.17(A)). Stained cells were then assessed via flow cytometry to identify live CRT^+ cells (Figure 4.17(B)(C)). Treatment with either radiation modality led to dose-dependent CRT exposure within 24 hours, with the greatest exposure following treatment with 50 MBq at 65.4% CRT^+, or 50 Gy at 54.0%. However, this exposure was significantly reduced by the 72 hour timepoint and back to baseline (no treatment) levels by 144 hours (Figure 4.17(D)(F)).

As confirmation, I also assessed the relocation of a second ER chaperone protein, ERp57, to the cell membrane. As ERp57 has been shown to co-translocate to the cell surface with CRT, and moreover to be necessary for this process to occur, it provides a second marker to confirm the movement of CRT in response to irradiation [231]. Thus, using the same experimental set up cells were subject to treatment with [177Lu]PSMA-I&T followed by staining of non-permeabilised cells and flow cytometric analysis. Consistent with CRT exposure, ERp57 relocation to the cell membrane was observed in a dose-dependent manner 24 hours following treatment with either EBRT or [177Lu]PSMA-I&T, reaching 74.0% CRT^+ after a 50MBq dose, and 67.8% after 50 Gy (Figure 4.17(E)(G)). Again, this was reduced by 72 hours post treatment.

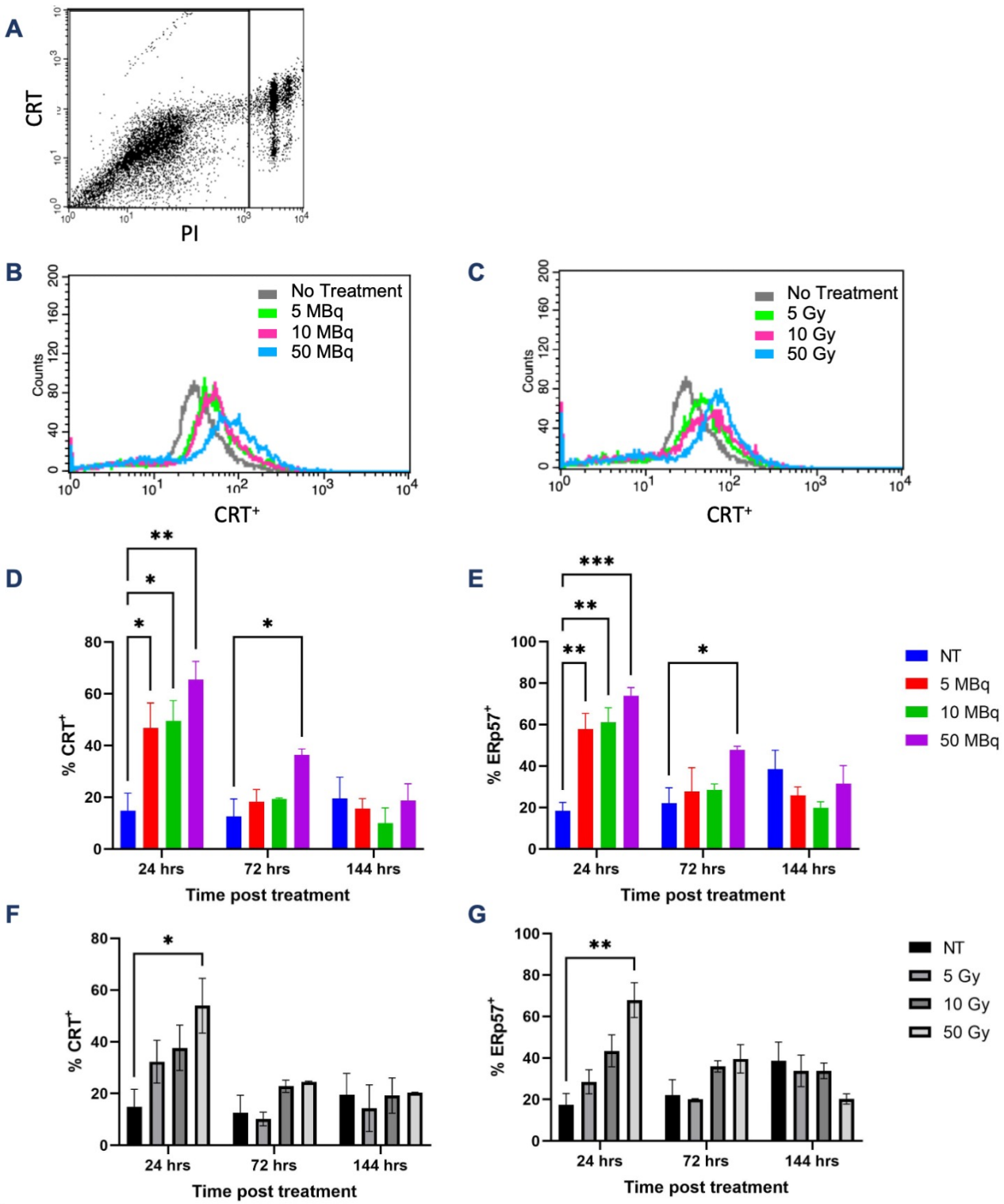

Figure 4.17: [177Lu]PSMA-I&T induces cell surface exposure of ER chaperone proteins CRT and ERp57

PGLS cells were subject to various doses of [177Lu]PSMA or EBRT, and analysed for cell surface exposure of CRT and ERp57 at subsequent time points. **(A)** Cells were gated to select live only (PI^-) cells. **(B)** Representative CRT histogram illustrating the shift in CRT exposure with increasing dose of [177Lu]PSMA-I&T and **(C)** EBRT following 24 hour treatment. Time and dose response of Calreticulin **(D)** and ERp57 **(E)** exposure following [177Lu]PSMA-I&T was determined by flow cytometry. Time and dose response of Calreticulin **(F)** and ERp57 **(G)** exposure following EBRT was determined by flow cytometry. Data are presented as mean ± SEM and statistical significance determined by two way ANOVA with Dunnet's test for multiple comparisons (n=3). * $p<0.05$; ** $p<0.01$; *** $p<0.001$

Having demonstrated the ability of [177Lu]PSMA-I&T to induce cell surface exposure of CRT, I next sought to identify whether the same treatment could promote release of HMGB1. Cells were subject to the same treatment schedule described above, and the supernatant isolated at various timepoints for assessment of HMGB1 release via an ELISA. As with CRT exposure, HMGB1 release was seen to occur following irradiation with either EBRT or [177Lu]PSMA-I&T, however the timing differed perhaps in part due to the time needed for HMGB1 to accumulate in the medium following treatment (Figure 4.18). 24 hour following treatment no increase in HMGB1 release could be detected in any treatment group (Figure 4.18). However, by 96 hours post treatment a statistically significant increase in HMGB1 released was observed for 10 MBq treatment. By 144 hours this elevated release was observed in 50 MBq and 10 Gy treatment groups, with an apparent dose dependent increase in HMGB1 release for both [177Lu]PSMA-I&T and EBRT.

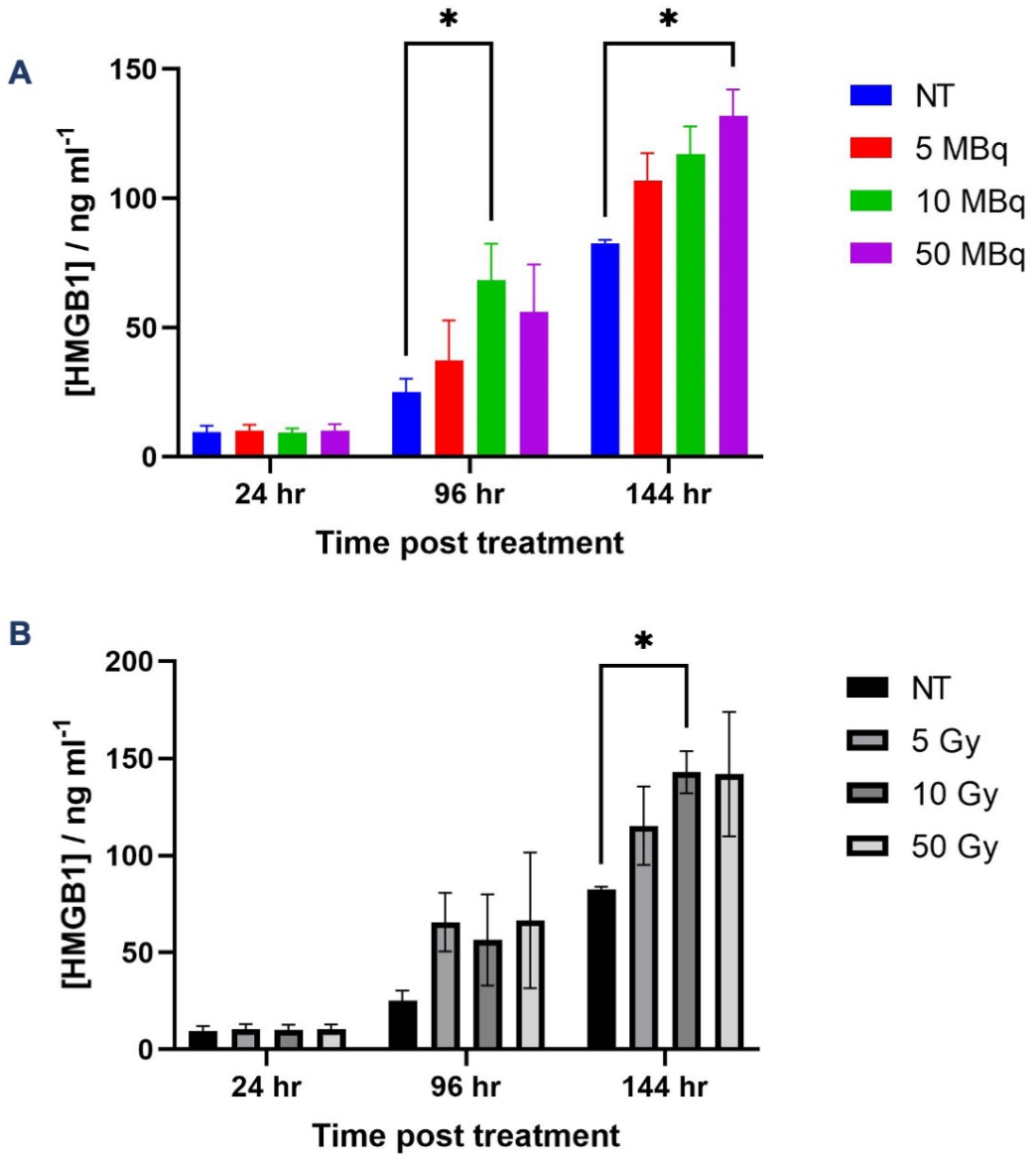

Figure 4.18: [177Lu]PSMA-I&T induces release of HMGB1
PGLS cells were subject to various doses of [177Lu]PSMA or EBRT. The supernatant was harvested at subsequent timepoints, and analysed for HMGB1 released from the cells. Dose response and time dependence of HMGB1 release was determined by ELISA for cells treated with **(A)** [177Lu]PSMA-I&T, **(B)** EBRT. Data are presented as mean ± SEM and statistical significance determined by two way ANOVA with Dunnet's test for multiple comparisons (n=3). * p<0.05; ** p<0.01; *** p<0.001

4.3.4 [177Lu]PSMA-I&T induces immunogenic cell death *in vivo*

Having confirmed the induction of CRT exposure and HMGB1 release, I next sought to identify whether [177Lu]PSMA-I&T is capable of inducing ICD *in vivo* via the gold standard vaccination/ rechallenge assay. This study was carried out as described in Figure 4.19(A). First, PGLS cells were treated *in vitro* with 50 MBq [177Lu]PSMA-I&T or 50 Gy EBRT and incubated for 5 days in T25 flasks followed by washing in PBS to remove the remaining [177Lu]PSMA-I&T. $5x10^6$ washed cells were then inoculated in the right flank of c57BL/6 mice. 7 days later these mice were rechallenged through inoculation of $0.5x10^6$ untreated viable PGLS cells into the contralateral flank. Mice were monitored for tumour growth for 80 days.

Strikingly, vaccination with EBRT or [177Lu]PSMA-I&T treated PGLS cells prevented tumour growth in 100% and 67% of mice vaccinated with EBRT treated cells or TRT treated cells, respectively (Figure 4.19(B)). Of the tumours that did grow in mice vaccinated with TRT treated cells, growth was much delayed compared with controls (Figure 4.19(C)), taking an additional 14-21 days to become visible, and 17-22 days to reach the humane endpoint volume of 1,000 mm^3. This suggests that an anti-tumour immune response was induced by inoculation with the dying cells, confirming they were undergoing immunogenic cell death rather than other non-immunogenic forms of cell death.

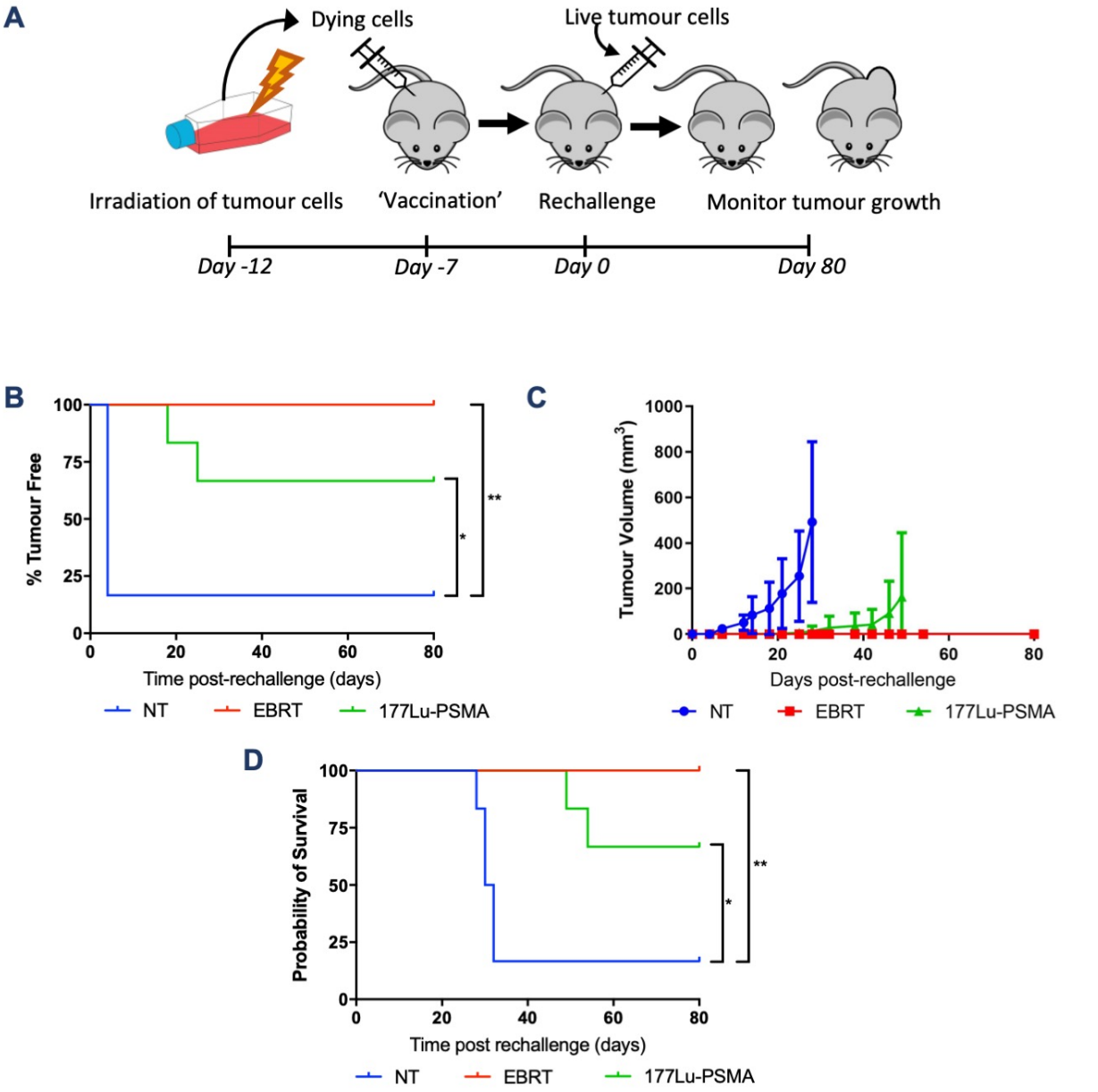

Figure 4.19: [177Lu]PSMA induces immunogenic cell death *in vivo*
(A) Vaccination rechallenge protocol; PGLS cells were first treated *in vitro* with [177Lu]PSMA-I&T or EBRT to induce ~50% cell death. Treated cells were then washed, counted, and inoculated into the right flank of c57BL/6 mice. 7 days later, mice were rechallenged with viable cells in the contralateral flank. Tumour growth was monitored for 80 days post-rechallenge to determine % tumour free **(B),** tumour volume **(C)** and survival **(D)**. Statistical significance determined using log rank test (n=6). * $p<0.05$; ** $p<0.01$; *** $p<0.001$

4.4 Discussion

In this chapter I have shown that [177Lu]PSMA-I&T is capable of inducing changes to the TIME in PGLS tumours with an initial reduction in immune cells 72 hours post treatment, followed by an increase relative to untreated controls by 12 days post treatment (summarised in table 4.1). This contrasts to the observations following EBRT treatment, where no changes in immune cell numbers were detected after 72 hours, but similar increases in immune cells were observable by 12 days (summarised in table 4.1). *In vitro* analysis enabled the identification of ICD as a possible contributor to the immune landscape changes, with induction of CRT exposure and HMGB1 release by [177Lu]PSMA-I&T treatment, and confirmation of ICD induction by the gold standard vaccination-rechallenge assay.

Cell type	Trend relative to no treatment (significance)			
	[177Lu]PSMA-I&T 72 hours	EBRT 72 hours	[177Lu]PSMA-I&T 12 days	EBRT 12 days
CD45+	Reduced (*)	No change	Increased (ns)	Increased (ns)
T cells	Reduced (*)	No change	N/A	No change
Th1 cells	Reduced (ns)	No change	Increased (ns)	Increased (*)
Macrophages	Reduced (ns)	No change	Increased (ns)	Increased (ns)
NK CD56dim	Reduced (ns)	No change	Increased (ns)	Increased (**)
Cytotoxic cells	N/A	No change	Increased (ns)	N/A

Table 4.1: Summary of changes in immune cells in PGLS tumours following irradiation. (ns) $p>0.05$; * $p<0.05$; ** $p<0.01$; *** $p<0.001$.

4.4.1 [177Lu]PSMA-I&T, but not EBRT, triggers an initial reduction of immune cells in the TIME

By employing NanoString high throughput transcriptional analysis I was able to evaluate the immune response to [177Lu]PSMA-I&T treatment in the PGLS tumour model. Unfortunately, as was the case with all NanoString analyses presented in this thesis, the statistical power of this study was limited by the small n number (n=4), restricting the ability to ascertain statistically significant changes leading to most observations being based on an observed trend where $p>0.05$. Further studies will thus be required to confirm the legitimacy of such observations. Despite this, my analysis confirmed that [177Lu]PSMA-I&T is indeed able to modulate the TIME, however as predicted the details of this modulation vary to that of EBRT. Remarkably, 72 hours post treatment with [177Lu]PSMA-I&T I observed a striking initial reduction of immune cells, with a significant reduction in CD45+ cells (overall leukocytes) and specifically in T cells, with a trend towards a reduction in Th1 cells, CD8+ T cells and

NK CD56dim cells. Strikingly, no such change was observed following EBRT treatment. The lack of such a response in EBRT treated animals may be a result of differing timescales of the response wherein a similar reduction in immune cells occurred at an earlier timepoint following EBRT but the cells had already begun to repopulate to pre-treatment levels by 72 hours. Such a decline would have been missed in this experiment. Alternatively, it may be that no such reduction occurs following EBRT and that these immune cells have increased radiosensitivity to the prolonged low dose irradiation delivered by [177Lu]. In support of the later, despite the long standing view that lymphocytes are exceptionally radiosensitive [232, 233] recent work by Arina et al. used an innovative *in vivo* experimental set up to demonstrate that following either fractionated or SBRT-like doses of EBRT a substantial fraction of pre-existing intratumoural T cells survive for at least 9–14 days post-IR, at up to 85% of pre-IR levels [234]. These observations suggest that there is little decline in immune cells following EBRT and thus the difference in immune cell numbers between TRT and EBRT treated groups in my experiments are likely a result of increased sensitivity to TRT rather than differing time scales. Conversely, a transient reduction in immune cells at 24 hours has been described following single high dose treatment with EBRT in a pancreatic cancer model [235]. Further assessment of the relative radiosensitivity of immune cells to the two modalities is therefore necessary both *in vitro* and *in vivo*.

4.4.2 The frequency of immune cells in the TRT treated TME is equal to or greater than untreated tumours by day 12

It is so far unclear whether this initial decline in immune cells numbers is advantageous or detrimental. Ultimately, the immune cells repopulate TRT treated tumours by 12 days, reaching levels similar to EBRT treated tumours and equal to or greater than untreated tumours. Interestingly, as mentioned above, the data suggests that the overall number of immune cells is reduced in untreated controls at 12 days compared with the earlier time point. This is to be expected in the increasingly immune-suppressive TIME of fast growing tumours. Necrosis, poor perfusion and rapid tumour cell proliferation all likely contribute to a relative reduction in immune cells compared with the overall number of cells by 12 days. Making a similar comparison of immune cell scores in TRT treated tumours

at 72 hours and 12 days suggests that there is no overall change in the proportion of immune cells in the microenvironment. Regardless, the change relative to untreated tumours is noteworthy. Whilst at 72 hours post treatment there are significantly fewer immune cells in TRT treated tumours versus untreated tumours, by 12 days there are equal levels, or more, immune cells in TRT treated tumours. Moreover due to significant confounding batch effects between different timepoints, only these intra time-point comparisons can be made. Whether TRT is causing immune activation at this point, or preventing the further development of immune-suppression within the tumour remains unclear.

4.4.3 The ultimate impact of the immune cell depletion will depend on the phenotype and functionality of the depleted cells

What is clear, is that the relative reduction in immune cells following TRT treatment is short lived. This means that the benefit or detriment of the initial reduction is dependent on (1) the phenotype and (2) the functionality of both the depleted cells (as well as the newly infiltrating cells, discussed in 4.4.4) (Figure 4.20).

Phenotype is particularly important given the contrasting tumour-suppressive and tumour-promoting functions of different immune cell subtypes. Thus, understanding which sub-types are depleted and which cells repopulate the tumour is essential. Importantly, existing data for EBRT suggests that different immune cell subtypes have differing radiosensitivity suggesting that depletion may be sub-type specific [236–239]. Specific depletion could shift the balance to be more tumour-suppressive or more tumour-promoting. For example, activated and memory T cells are reported to be more radioresistant to EBRT than naïve T cells [240, 241], but the validity of this for [177Lu] is yet to be assessed. Similarly, the radio-resistance of Tregs [242] has been described as a factor in tumour radio-resistance, so the intrinsic radiosensitivity of these cells to TRT may be of particular interest in future work. Unfortunately, whilst my analysis here demonstrates a significant reduction in CD45+ cells and T cells at the early timepoint, the small study size, bulk tumour data, and lack of flow cytometric analysis limits the ability to further define cell sub-types and the functional phenotype of these cells. As such, further assessment is necessary to better define the phenotype of the depleted cells.

Concurrent assessment of the *in vitro* radiosensitivity of immune cell sub-populations may also help to gain further understanding.

Equally important is the phenotype of the newly populating cells, as discussed below in section 4.4.3. Along with the phenotype of the surviving cells, their functionality is also important. It may be that the surviving cells perform better as the work of Arina et al. demonstrated an improved effector function 9 days post EBRT for surviving T cells compared with pre-treatment [234]. There is also evidence that EBRT treatment can downregulate expression of Foxp3 along with other molecules associated with suppressive activity in Treg cells rendering them less effective at inhibiting CD8+ T cell proliferation [243]. However, surviving cells also display lower proliferation and higher levels of PDL1 and CD19 compared with newly infiltrated immune cells indicating a state of exhaustion [234].

Ultimately, untreated tumours generally contain a high number of immunosuppressive cells, and so if these cells display greater sensitivity to TRT than EBRT and thus decline enabling the influx or proliferation of new, functional immune cell populations to repopulate the TIME this is likely to be beneficial. Conversely, if immune-stimulatory cells are being selectively depleted, or the cells repopulating the TIME are immune-suppressive or have reduced functionality compared with EBRT surviving cells then the effects are likely detrimental. Thus, understanding the TIME changes following treatment will enable the development of rational immunotherapy-radiotherapy combination regimens. For example employing the antagonization of molecules that cause the polarisation of newly infiltrating immune cells to suppressive sub types, using additional therapeutics to increase the infiltration of new immune cells following irradiation, or increasing the radiosensitivity of specific suppressive immune cells.

Determining whether this ability of TRT to modulate the TIME contributes to the therapeutic efficacy will also be an important next step. This will also give some idea about whether the initial immune depletion is good or bad. Similar to previous work in various murine models, this can be done by determining the therapeutic efficacy with and without selective depletion of immune cells to identify whether these immune components are necessary for full therapeutic efficacy [30–32].

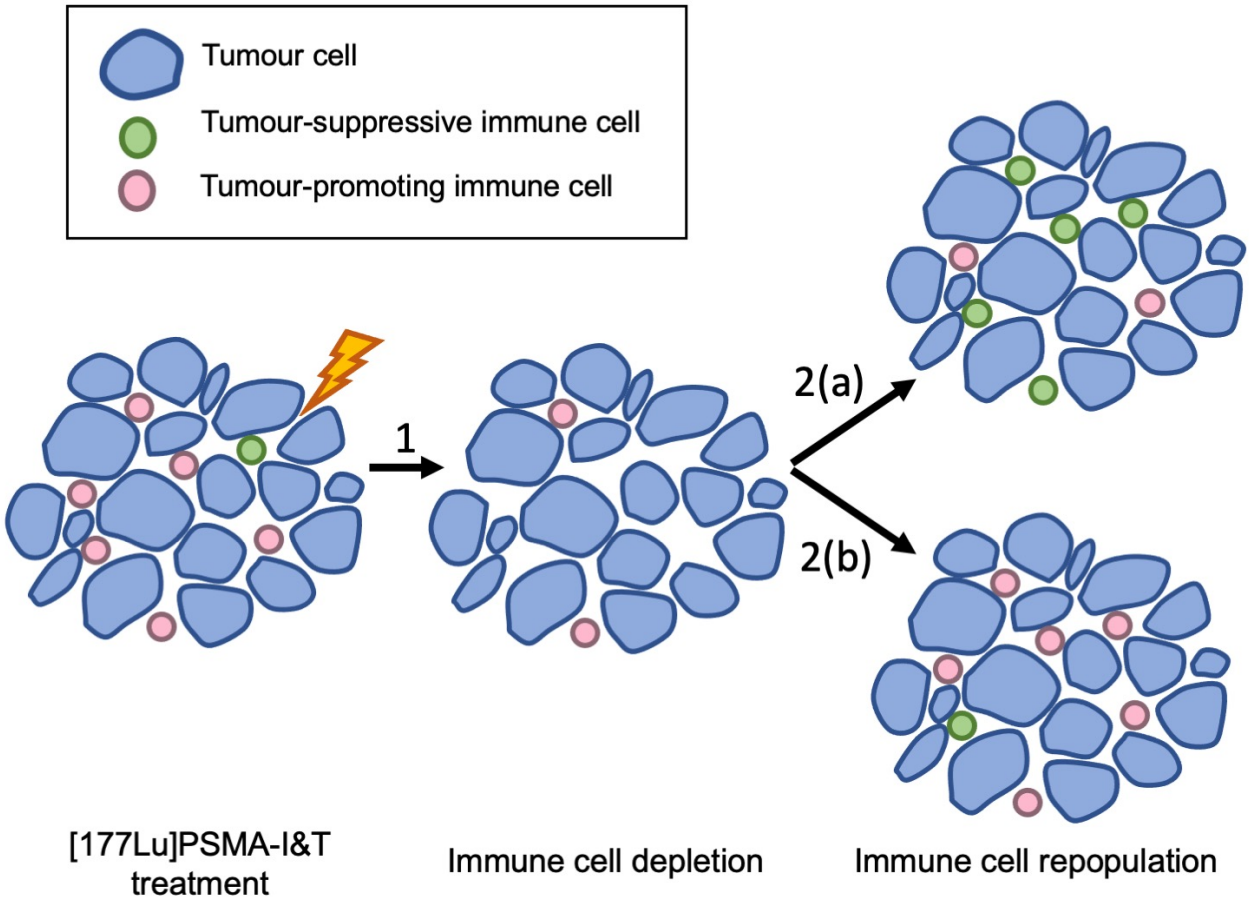

Figure 4.20: [177Lu]PSMA-I&T causes an initial reduction in immune cells, followed by repopulation
(1) [177Lu] treatment causes a reduction in the number of immune cells in the TME. This may be a reduction in tumour-suppressive immune cells (green), or tumour promoting immune cells (red) which generally dominate the TME of untreated tumours, or both. **(2)** Following this initial reduction, the number of immune cells returns to or exceeds pre-treatment levels. This may be due to infiltration or proliferation of tumour-suppressive immune cells (2(a)), or tumour promoting immune cells (2(b)). [177Lu] may also affect the surviving immune cells.

4.4.4 The phenotype and functionality of the immune cells populating the TIME 12 days post treatment is another important factor

As mentioned, the phenotype and functionality of the immune cells populating the TIME 12 days post treatment is also important in determining whether TRT can ultimately induce a functional anti-tumour immune response. Assessment of the immune cell subtypes 12 days post treatment with [177Lu]PSMA-I&T not only suggests that CD45+ and T cells have returned to the same level as untreated controls, but also shows a trend towards increased cytotoxic cells, macrophages and NK CD56dim cells relative to the untreated controls.

A similar increase in macrophages has also been described following treatment with the related therapeutic modality high dose-rate brachytherapy in localized prostate cancer [213]. Notably though, the impact of these cells is dependent on their phenotype. Macrophages can be broadly defined as either M1 (tumour suppressive) or M2 (tumour promoting), and as with other cancers the presence of M1 macrophages has been shown to be associated with favourable outcomes in PCa [244]. However, it has also been shown that macrophages infiltrating PCa are mainly M2 phenotype [245], highlighting potential benefit of therapeutics that can shift the balance in favour of M1 macrophages. It should also be noted that Lundholm *et al.* demonstrated that factors secreted from PCa cells could induce an immunosuppressive macrophage phenotype *in vitro* [245]. This may suggest that even if TRT can induce an influx of potentially tumour suppressive macrophages, the PCa cells may induce an M2 phenotype in these cells. Thus whilst the results presented here suggest a trend towards increased macrophage numbers following treatment, further assessment is necessary to confirm the significance of these changes and to determine the phenotype of these new macrophages, as well as to evaluate the contribution of this change to the therapeutic efficacy of TRT in PCa.

Following the initial decline, the return of T cells to levels equivalent to the untreated tumours is also interesting. An increase in T cell subsets has been described following a number of related treatments. For example, an increase in CD8+ T cells following TRT has also been directly observed using a syngeneic model of T-cell Non-Hodgkins Lymphoma treated with [90Y]NM600 [120]. Similarly Kubo *et al.* - whilst restricted to peripheral blood analysis - demonstrated that activated T cells in peripheral blood of PCa patients increased after iodine-125 low-dose-rate prostate brachytherapy[129]. Chew *et al.* also observed an increase in CD8+ T cells following Y90 RE [118]. Furthermore, the authors described a possible mechanism for this increase due to the observation of a strong positive correlation of CD8+ T cells with the chemokines CCL5 and CXCL16, which bind CCR5 and CXCR6, respectively and have roles in CD8+ chemotaxis and were both also substantially upregulated following Y90 RE. Consequently, the investigators suggest CCL5/CXCL16 dependent chemotaxis may be responsible for the increased presence of CD8+ T cells in the TIME. Indeed, the ability of irradiation

to induce the release of CXCL16 by tumour cells has also been highlighted as an important mechanism by which EBRT promotes CD8+ T cell accumulation [246]. Notably, similar increases in these chemokines were also demonstrated here following [177Lu]PSMA-I&T treatment. Whilst the current analysis does not allow determination of CD8+ T cells, CCL5 and CXCL16 also show a striking correlation with T cell numbers consistent with a role in T cell chemotaxis. Further *in vitro* assessment of the ability of [177Lu]PSMA-I&T to induce CXCL16 release, and the impact of this on CD8+ T cell accumulation would thus be of interest.

It would also be of interest to evaluate whether these newly populated T cells are more tumour suppressive than those present in the untreated tumours. The importance of T cells for therapeutic efficacy of EBRT has been demonstrated in a number of studies where T cell depletion diminished the efficacy of EBRT [30–32]. More generally, the importance of T cells within the TIME has been demonstrated across a variety of cancers, with the presence of cytotoxic and helper T cells conferring a favourable prognosis [247, 248]. A number of clinical trials in a range of solid tumours have demonstrated that a high density of TILs and expression of an IFN-associated gene signature correlate with favourable outcomes [249, 250]. However, the prognostic impact of TILs in PCa is unclear, with contradicting evidence on the role of immune cells, likely due to differing immune contexture and spatial localisation. Whilst a number of studies have reported that low TIL numbers correlated with a high risk of tumour progression and fatal disease [251], others have shown the converse. Leclerc *et al.* observed that a high level of tumour-infiltrating CD8+ T cells was associated with reduced biochemical recurrence (BCR)-free survival in 285 cases of prostate cancer. This prognostic indicator was exacerbated when high CD8+ T cell numbers were accompanied by high CD73+ levels, which the authors suggested is attributable to the conversion of effector CD8+ T cells into immunosuppressive CD8+ T cells [252]. Similarly, based on analysis of 535 patients Ness *et al.* observed that a high density of CD3+ and CD8+ lymphocytes was associated with significantly shorter biochemical failure-free survival [253]. Another recent study by Zhao *et al.* reported that mast cells, natural killer cells, and dendritic cells conferred improved distant metastasis free survival (DMFS), whereas macrophages and

T-cells conferred worse DMFS based on transcriptomic analysis of 678 samples [254]. The negative impact of T cells in these studies is likely due to other factors in the TIME rendering the cells dysfunctional or immunosuppressive, highlighting the importance of further analysis to fully establish the impact of [177Lu]PSMA-I&T on the T cell population.

NK CD56dim cells also trend towards an increase following [177Lu]PSMA-I&T treatment, however again the functionality of these cells requires further assessment. NK cells are phenotypically defined by their CD56 expression, with NK56dim cells being the mature form, whose major roles include perforin release and target cell killing alongside antibody-dependent cellular cytotoxicity (ADCC). Unfortunately, factors in the TIME typically bring about NK cell exhaustion thus restricting NK cell function. However, radiation can have significant effects on NK cells as well. There is evidence that EBRT can induce both NK proliferation and secretion of NK cell effector proteins [255–257]. In fact, the greatest effects have been observed with chronic low dose irradiation, suggesting that the prolonged low dose irradiation provided by TRT has the potential to exert similar effects as seen here [255, 256]. Concordantly, Chew et al. observed a significant infiltration of NK cells alongside more general local immune activation following Yttrium-90 radioembolization in hepatocellular carcinoma, a form of radiotherapy that similarly provides prolonged low dose irradiation [118]. Further analysis will be required to determine whether similar increase in NK cell effector functions occur following [177Lu]PSMA-I&T treatment.

4.4.5 [177Lu]PSMA-I&T induced changes to the TIME differ from EBRT induced changes at day 12

By 12 days post treatment, similar increases in T cells, macrophages and NK CD56dim cells were observed following EBRT treatment. Comparable changes have been described across a broad range of cancers following EBRT (see chapter 1), as well as for PCa specifically. Consistently, Philippou *et al.* demonstrated an increase in the proportion of cells expressing the CD45+ general leukocyte marker 7 days after 3 x 5 Gy EBRT in a TRAMP-C1 PCa model, with an increase in CD4+ T cells and macrophages. Moreover, similar observations have been made in the clinic. For example Tabi *et al.* demonstrated

that antitumor CD4+ and CD8+ T cell responses were detectable after, but not before or during, EBRT of PCa [258]. Similarly, an increase in tumour specific CD8+ T cells was detected in the peripheral blood of some PCa patients following EBRT [259]. The impact of these changes on clinical outcome for PCa is less well studied, however Evans *et al.* demonstrated that an increase in tumour reactive T cells in the peripheral blood following EBRT was protective against the risk of disease progression.

It would also be of interest to see if the elevated immune cell populations persist, as a number of studies have shown that whilst radiotherapy is able to stimulate an increase in TILs such changes are short lived and cell counts ultimately contract back to baseline, though combinations with immunotherapeutics may promote a more sustained response [260–263].

Also of interest are the observed differences in response following EBRT and TRT treatments at the 12 day timepoint. Most strikingly, 5 of the top 8 differentially expressed genes between TRT and EBRT treatment are interferon related; higher levels of Ifit1, Ifi44, Ifitm1, Irf7 and Isg15 in TRT treated tumours suggests a greater activation of interferon pathways. It has long been known that IFNs can exert anti-tumour effects, with IFNα treatment being approved for a range of cancers for more than two decades. It has since been recognised that IFNs may also play a role in the efficacy of EBRT, with evidence that the efficacy of EBRT relies upon induction of type I IFN-dependent innate and adaptive immunity as the antitumor effect can be abolished in type I IFN nonresponsive hosts [264, 265]. There are thought to be a number of mechanisms by which IFN stimulation contributes to EBRT efficacy, including promoting immune cell recruitment, enabling DC cross priming of CD8+ T cells and directly aiding in T cell activation [230, 266]. For example, Lim *et al.* highlighted the importance of radiation-induced type I IFNs causing an increase in CXCL10 chemokine levels within the tumour thus affecting CD8+ T cell recruitment and priming [230]. Consistently, the higher IFN gene expression in TRT treated tumours is accompanied by a trend towards increased CXCL10 expression ($p=0.14$), again suggesting greater IFN activity following TRT treatment. Further assessment is required to determine whether there is a corresponding increase in CD8+ T cell recruitment and priming. It is also important to

recognise that chronic upregulation of IFN-stimulated genes has also been associated with tumour growth and therapy resistance through both PDL1-dependent and PDL1-independent mechanisms, and so understanding where TRT activation sits in this balance is of the upmost importance [71, 267]. Moreover, *in vitro* assessment of IFN activation by TRT vs EBRT would be of interest to confirm whether or not TRT is a more potent stimulator of IFNs. As described in chapter 1, IFN activation by EBRT is thought to be a result of DNA damage which causes the accumulation of DNA fragments in the cytoplasm. This triggers the cGAS/STING pathway which results in IFN expression and secretion. Determining whether TRT can instigate similar changes, and if/how this is more potent than EBRT will thus be of interest.

4.4.6 Induction of immunogenic cell death may contribute to TIME changes

Having observed changes in immune cell numbers following treatment with [177Lu]PSMA-I&T, I wanted to further understand the mechanisms responsible for these changes. One mechanism thought to be key to increased immune cell numbers following EBRT is the induction of immunogenic cell death, and here I show that this mechanism is similarly triggered by [177Lu]PSMA-I&T.

The importance of CRT cell surface exposure in immune activation by EBRT has been known for over a decade. Obeid et al. demonstrated that calreticulin exposure is required for the immunogenicity of gamma-irradiation in 2007 [268], with subsequent clinical evidence showing the upregulation of CRT by EBRT in patients[269]. Here, I have shown for the first time that [177Lu]PSMA-I&T is similarly capable of inducing CRT exposure. Moreover, I have demonstrated that this exposure is dose-dependent with the greatest change following 50 MBq treatment. This closely matched the dose dependence of EBRT induced CRT exposure. Consistently, Golden *et al.* described a very similar trend in murine mammary carcinoma cells 24 hours post treatment [91]. This is not however the first time that any radiopharmaceutical has been shown to induce CRT exposure, with existing evidence that [223Ra] is able to promote calreticulin upregulation and exposure on the cell surface suggesting that this response is not limited to lutetium based radiopharmaceuticals [65]. Importantly, the observation

that this exposure is lost by 144 hours post treatment may have important implications for radiotherapy-immunotherapy combinations.

Alongside CRT exposure, I have also demonstrated a dose dependent release of HMGB1 following [177Lu]PSMA-I&T treatment. Again, this closely matches the release stimulated by EBRT, with continued increases up to at least 144 hours post treatment. This is in line with similar dose dependent HMGB1 release described by Golden *et al*. It seems that this phenomenon is not limited to lutetium-based radiopharmaceuticals, with evidence that [213Bi], is capable of inducing HMGB1 release in a murine model of adenocarcinoma [66]. The clinical relevance of HMGB1 upregulation along with its correlation with antigen-specific T cell responses and overall survival have also been demonstrated [270]. Importantly, extracellular HMGB1 is now known to play multiple roles in the immune response that cover both anti-tumour functions by facilitating the recognition of dying tumour cells, but also immunosuppressive functions [271] and so the impact of TRT induced HMGB1 release may be more nuanced than it first appears.

Interestingly, in both cases the time scale of induction appears similar between TRT and EBRT despite differences in the delivery of radiation. Further comparison based on the dose required to induce such changes is limited as the calculation of absorbed doses is beyond the scope of this thesis, but could form the basis of future experiments.

Confirmation of ICD via the gold standard vaccination-rechallenge assay verifies that this process has the potential to mediate anti-tumour immune responses *in vivo*. Here, TRT was marginally less effective than EBRT at preventing tumour growth, however as the doses were not necessarily equivalent, it is possible that this is an effect of dose differences rather than other differences between the two radiation modalities. To my knowledge, this is the first demonstration of ICD induction by a lutetium-based radiopharmaceutical. Comparably, both [213Bi] and [90Y]NM600 have been previously shown to induce ICD *in vivo* suggesting this may be a widespread phenomenon.

Unfortunately, poor marker gene correlation meant it was impossible to determine DC numbers from the NanoString data, however the increase in cytotoxic cells 12 days post EBRT treatment suggests

that this induction of ICD may be promoting DC activation and subsequent T cell priming within the tumour. Similarly, whilst not statistically significant, the trend towards an increase in cytotoxic cells 12 days post TRT treatment implies the same may be true here. The reduced effectiveness of TRT compared with EBRT in both the vaccination/rechallenge study and in inducing increased cytotoxic cells may suggest a reduced propensity of TRT to induce ICD compared with EBRT. Again, this may be a result of differing doses, and so it would be of interest to determine the absorbed dose in both cases and the clinical relevance of these doses. Moreover, if the doses do appear comparable, it would be interesting to determine why TRT may be less effective at inducing ICD.

Interestingly, another important danger signal thought to be important for ICD is the release of type I IFNs, which have important roles in stimulating the activation of macrophages, DCs and natural killer cells [272, 273]. Accordingly, knocking out IFNAR1 in murine cancer cells abrogates their ability to vaccinate syngeneic hosts following induction of cell death by ICD inducer doxorubicin [274]. Given the differences in IFN signalling observed in the TIME following treatment with either TRT or EBRT this may suggest nuanced differences in ICD induced by either radiation modality, with different DAMPs being major players in either case. Further assessment of interferon release and subsequent TIME changes would be required to assess this further.

4.4.7 Despite preventing tumour growth by vaccination, [177Lu]PSMA-I&T treatment fails to cure established tumours

Strikingly, although vaccination with TRT or EBRT treated cells led to a ≥ 67% prevention of tumour growth, treatment of established tumours led to significantly less pronounced effects. It is therefore interesting to consider why this is. One factor may be the delivered absorbed radiation dose, as the cells used to vaccinate the mice in the rechallenge experiment were exposed to a higher dose *in vitro* than the tumours *in vivo*. The data for CRT exposure and HMGB1 release already highlight a clear dose response, with greater effects at higher doses. Moreover, annexin V/ PI cell death assessment showed a far higher number of dying or dead cells following higher doses and so it may be that the number of cells undergoing ICD influences the magnitude and thus the effectiveness of the anti-tumour immune

response that is induced. Given that there is no observed toxicity at this dose *in vivo*, it would be interesting to see the effect of greater doses on tumour control.

Another extremely important factor is likely the tumour microenvironment within the pre-established tumours. Indeed, the official definition of ICD according to the Nomenclature Committee on Cell Death has recently been adapted to include the importance of the host environment. For example, within the TIME ICD may be limited by immune cell exclusion precluding interactions of dying cells with APCs, or the presence of inhibitory receptors or cytokines blocking immune cell priming. One interesting follow up experiment would therefore be to treat pre-established tumours *in* vivo, followed by rechallenge with healthy tumour cells. If these rechallenge cells grow freely and form tumours, this may suggest that the microenvironment prevented ICD. Alternatively, if the treatment of pre-established tumours resulted in protection from rechallenge, then this would suggest that ICD had occurred and the lack of efficacy in the pre-established tumour is due to TIME processes limiting the effector cells stimulated by ICD. Ultimately, the effect of these negative immune regulators within the TIME highlights the potential for immunotherapeutic combinations with radiotherapeutics.

Chapter V:
Combining Radionuclide Therapy with Immunotherapy

5.1 Introduction

The results thus far demonstrate that [177Lu]PSMA-I&T is capable of inducing a potent immune response in the setting of a vaccination-rechallenge experiment. Unfortunately, translation of this efficacy into an established tumour setting proved less successful. This limited efficacy of [177Lu]PSMA-I&T in a pre-established tumour suggests that the response may be limited by the tumours immune-suppressive microenvironment. This highlights the potential of immunotherapy-radiotherapy combinations that may help to relieve the immune-suppressive TIME, thus 'removing the brakes' from the radiotherapy stimulated induction of an anti-tumour immune response. Indeed, this is particularly important in PCa, where single agents immunotherapies have thus far met with little success. This is perhaps attributable to the immune status of PCa, which is generally thought of as 'immune cold'. This is likely due to a combination of factors including hormonal influence, low tumour mutation burden and low TA expression, DDR defects, and a number of immune exclusion/evasion mechanisms within the TIME [275–278]. Consequently, combining the various immune-activating properties of radiotherapy with agents to remove immune-suppressive effects may be beneficial.

In this vein, I considered a number of potential immunotherapeutics that may synergise with [177Lu]PMSA-I&T based on this new understanding of its interaction with the immune system (Table 5.1).

Target	Functions
CD47	'Don't eat me signal' that inhibits phagocytosis. Also has roles in modulating NK cells, T cells and macrophages.
PDL1	Immune checkpoint. Interacts with PD1 leading to T cell dysfunction, exhaustion, neutralization, and IL-10 production. Also functions to dampen the immune response through B cells, Tregs, NKs and macrophages.
PDL2	Similar to PDL1.
IDO1	Enzyme that degrades tryptophan, contributes to immunosuppression via impaired effector T cell function and the induction of Tregs and tolerogenic DCs.
TGFb	A pleiotropic cytokine which attenuates inflammation and immune responses by suppressing effector T cells and promoting of Tregs, promoting DCs to a tolerogenic phenotype, and inhibiting macrophages and NK cells
CD40	CD40 is a protein expressed on DCs, macrophages and B cells. Interaction with its ligand, CD40L stimulates a number of pro-immunogenic events, enhancing DC activity through enhanced antigen presentation, upregulation of costimulatory ligands, and increased expression of chemokine receptors leading to increased cell trafficking.

Table 5.1: Potential immunological targets for combination with [177Lu]PSMA-I&T in prostate cancer

The first of these is a CD47 antagonist, a growing number of which have recently entered clinical trials [279]. CD47 is a cell surface glycoprotein expressed on the surface of tumour cells that acts as a potent 'do not eat me' signal, enabling tumour cells to evade phagocytosis by macrophages and DCs via interaction with its ligand SIRPα [280, 281]. This directly counteracts the action of the 'eat-me' signal of CRT exposure which, as shown in the last chapter, is induced by [177Lu]PSMA-I&T as cells undergo ICD. It is thus perhaps unsurprising that a range of solid and haematological cancers have been observed to over express CD47 [282–287], employing it's immune-suppressive function to evade detection and destruction by the immune system. Correspondingly, elevated CD47 expression correlates with an aggressive phenotype and poor prognosis in a number of malignancies including acute myeloid leukaemia, oesophageal carcinoma, and ovarian cancer [282, 283, 288–290]. Verifying the importance of this mechanism for tumour growth and development, it has also been shown that inhibition of CD47 signalling can not only promote phagocytosis of tumour cells *in vitro*, but impairs tumour growth and inhibits metastatic spread in a variety of murine tumour models [282–284, 286].

Interestingly, there is also evidence that anti-CD47 blockade can repolarise macrophages towards the anti-tumour M1 subtype *in vivo* [286, 291], suggesting that this therapy may synergise with TRT not just by 'removing the brakes' on its induction of ICD, but also by promoting the M1 phenotype in the increased number of macrophages generated by TRT treatment suggested by the data presented in chapter 3.

Importantly, inhibiting CD47 alone is insufficient to stimulate phagocytosis of tumour cells by DCs. Prophagocytic signals like cell surface exposure of CRT are simultaneously required to produce an effect[292]. This means not only that most normal cells (other than aging red blood cells) are protected from CD47 inhibition due to their lack of prophagocytic signalling, but also suggests that combination with a tumour targeting prophagocytic therapeutic, such as [177Lu]PSMA-I&T could provide a synergistic therapeutic regimen [293].

Whilst much research in the area has focussed on its role as an antiphagocytic signal via interaction with SIRPα, CD47 also functions as a signalling receptor through interactions with matricellular protein thrombospondin-1 (TSP1). This interaction is responsible for inhibiting T cell activation, differentiation and adhesion and thus may more directly modulate adaptive immunity alongside CD47 effects on APCs [294–303]. Consistently, CD47 blockade enhances antigen-dependent T-cell mediated killing of irradiated fibrosarcoma cells in the absence of macrophages *in vitro* [304]. Also of importance here, blocking of CD47 has been shown to provide radioprotection to T cells and endothelial cells via upregulation of prosurvival autophagy [293, 305]. The resulting increased survival of T cells also has the potential to enhance anti-tumour immunity following combinatorial TRT-anti-CD47, particularly given the early reduction in immune cells observed in the previous chapter. Similarly, protection of vascular function has the potential to improve tumour oxygenation increasing oxygen-dependent free radical damage resulting from irradiation as has been suggested for EBRT [293]. Indeed, there is already evidence of effective combination of CD47 antagonists with EBRT [304, 306, 307]. Moreover, CD47 blockade has even been found to confer radioprotection to normal tissues whilst enhancing tumour radiosensitivity through a mechanism involving TSP1 signalling [293].

The second target I have considered is programmed cell death receptor ligand 1 (PD-L1). This protein, along with its binding partner programmed cell death 1 receptor (PD-1), form a key 'immune checkpoint'. Such checkpoints developed evolutionarily as a pathway to control the degree of inflammation to limit normal tissue damage. PD-1 is expressed on T cells, which when activated produce cytokines that promote PD-L1 expression in local tissues which can interact with PD-1 limiting immune activation. Unfortunately, in tumours this mechanism is exploited by overexpression of PD-L1 by tumour cells. This leads to T cell dysfunction, exhaustion, neutralization, and IL-10 production, and thus impedes the induction of an anti-tumour immune response. There is increasing evidence that the PD-1/PD-L1 axis also functions to dampen the immune response through B cells, Tregs, NKs and macrophages. Both PD-1 and PD-L1 inhibitors have thus been developed to pharmacologically disrupt this interaction, thus alleviating this immune-suppression and enabling the immune system to mount a response against the tumour. Indeed, such therapeutics are now one of the most widely used immunotherapies in oncology, with FDA approval for their use in a number of malignancies.

Unfortunately, despite the unprecedented success of these checkpoint inhibitors in certain malignancies, many more show limited or no response [308]. As such, combination with other treatment strategies are being explored to improve response rates. One such strategy is combination with EBRT, which is being assessed in a number of malignancies [98, 262, 309–321]. Data thus far is proving promising, indicating that similar success may be possible in combination with TRT. EBRT combinations are particularly interesting in light of evidence showing that EBRT can upregulate the expression of PD-L1 causing immune-suppression alongside other immune-promoting effects [322, 323]. However the impact of [177Lu]PSMA-I&T on PD-L1 expression, or radiopharmaceuticals in general, remains to be seen. Ultimately, given the ability of [177Lu]PSMA-I&T to induce ICD and thus provide immune-stimulation, employing anti-PDL1 therapeutics to concurrently remove this key barrier of immune suppression provides the opportunity to translate this immune priming signal into a functional immune response with systemic tumour control.

It is also worth considering anti-PDL2 therapeutics, particularly in the context of PCa where recent data has demonstrated that whilst PD-L1 is expressed at low levels in PCa and is not prognostic, PD-L2 is expressed at significantly higher levels and is associated with worse biochemical recurrence free survival [254]. Much like PD-L1, PD-L2 is thought to play an important role in immunosuppression via interaction with PD-1 to suppresses T cell proliferation and cytokine release and so inhibition of PD-L2 poses similar advantages to PD-L1[324].

A fourth potential candidate for combination with TRT is an indoleamine-2,3 dioxygenase 1 (IDO1) inhibitor. IDO1 is an enzyme responsible for the degradation of tryptophan into kynureniene. This local depletion of tryptophan coupled with kynurenine production contributes to immunosuppression via impaired effector T cell function and the induction of Tregs and tolerogenic DCs [325]. It is thus perhaps unsurprising that it is commonly expressed in human tumours, with expression correlating with worse survival [326, 327]. Importantly, the action of IDO1 has been associated with radioresistance following it's induction by irradiation [328–331].

A number of preclinical models demonstrated the effectiveness of IDO1 inhibitors in promoting T cell based immunity, synergising with immune checkpoint inhibitors, vaccines and chemotherapy [328, 332–335]. Unfortunately, despite promising early phase trails a recent randomised phase III study, ECHO-301, in metastatic melanoma in combination with pembrolizumab showed no benefit over pembrolizumab alone, causing a significant set-back in the field with many other trials paused [336–338]. However, this therapeutic approach still shows promise. Indeed, there are several potential reasons for the failure of the ECHO-301 trial including insufficient IDO1 inhibition, poor patient selection or expression of other tryptophan converting enzymes, all of which could be overcome by an optimised trial design [339]. This therapeutic remains particularly attractive in combination with radiotherapy, with existing preclinical evidence of synergy between EBRT and IDO-1 inhibition [329–331, 340]. It may be especially beneficial in combination with [177Lu]PSMA-I&T as there is evidence that radiation can induce IDO1 overexpression via Type II and II IFN signalling [329]. This induction might be enhanced further by [177Lu]PSMA-I&T treatment given the evidence I have presented of

greater IFN activation. However, there is also evidence that IDO-1 inhibitors are only beneficial in combination with both EBRT and PD-L1 inhibitors, so a triple combination may also be necessary for [177Lu]PSMA-I&T [341, 342].

TGFβ antagonists also have the potential to synergise with [177Lu]PSMA-I&T. TGFβ exists as three isoforms; TGF-β1, TGF-β2, TGF-β3, of which TGFβ1 is thought to play a central role in normal tissue injury and tumour radioresistance [343]. TGFβ1 is a pleiotropic cytokine which attenuates inflammation and immune responses by suppressing effector T cells and promoting Tregs, promoting DCs to a tolerogenic phenotype, and inhibiting macrophages and NK cells [344]. Indeed, the powerful role of TGFβ1 as an immunosuppressor is highlighted by studies showing that mice lacking TGFβ1 suffer lethal systemic inflammation and severe autoimmunity [345]. Whilst it can have tumour suppressive effects early on during tumourigenesis by inhibiting cell proliferation and promoting cell differentiation and apoptosis, tumour cells ultimately accumulate mutations and escape this growth inhibition. As such, TGFβ1 becomes pro-tumourigenic driving not just immunosuppression but angiogenesis, invasion and metastasis, and self-renewal of cancer stem cells [344, 346]. Correspondingly, elevated levels of TGFβ1 correlate with poor prognosis in a number of cancers [347–351].

Importantly, the ability of TGFβ1 to drive DCs to a tolerogenic phenotype may limit the benefits of [177Lu]PSMA-I&T induced ICD. Down the line TGFβ1 dependent inhibition of T cell activation and proliferation could further limit the ability of [177Lu] to induce a functional anti-tumour immune response. Moreover, the effector functions of the increased number of NK cells seen post TRT treatment may be reduced by TGFβ1 activity. There is also evidence that radiation can activate TGFβ1 by inducing redox sensitive conformational changes along with direct upregulation, and so may have a key role in radioresistance driving poor clinical outcomes [92, 352–359].

As such, TGFβ inhibition has been assessed in combination with EBRT, demonstrating effectiveness both in pre-clinical models [263, 360–362] and in the clinic[363]. Whilst it remains to be seen if TGFβ1

is also upregulated by TRT, baseline levels in the tumour may be sufficient to exert these immunosuppressive effects. Consequently, TGFβ inhibition may provide a beneficial combinatorial therapeutic alongside [177Lu]PSMA-I&T.

Finally, anti-CD40 agents may be of interest in combination with TRT. CD40 is a protein expressed on DCs, macrophages and B cells. Interaction with its ligand, CD40L stimulates a number of pro-immunogenic events. These include enhancing DC activity through enhanced antigen presentation, upregulation of costimulatory ligands, and increased expression of chemokine receptors leading to increased cell trafficking [364]. This indirectly promotes T cell priming, but CD40L also has direct effects including T cell stimulatory cytokine production. This has led to the development of CD40 agonists, and whilst these have demonstrated limited responses in both mice and humans, complete, durable responses have been observed following their combined treatment with EBRT [235, 360, 365]. Indeed, CD40 agonists in combination with EBRT are now entering clinical trials in combination with a third therapy, FLT3 ligand (NCT04491084). The ability of CD40L to provide additional DC stimulation may boost the action of [177Lu]PSMA-I&T which also stimulates DCs via induction of ICD, making this an interesting avenue to consider.

5.2 Aims

1. To assess the prognostic value of various immunologic targets in PCa
2. To evaluate the efficacy of combined TRT - antiTGFβ
3. To determine the effect of [177Lu]PSMA-I&T on PDL1 expression

5.3 Results

5.3.1 CD47 expression is a positive prognostic marker for PCa, whilst TGFβ1 is a negative prognostic marker

Given the large number of potential immunological targets for combination with [177Lu]PSMA-I&T I first needed to narrow down my choice of molecules before proceeding with further *in vitro* and *in vivo* assessment. The efficacy of immunotherapeutics has been shown to be TME context dependent, with expression levels of therapy targets often predicting worse outcomes [283, 288, 289, 348, 366–369]. As such, a high throughput transcriptomics analysis of a large, open source, PCa dataset was employed to determine which of the selected targets could be most promising for combination with [177Lu]PSMA-I&T in the context of PCa. In order to conduct such analysis, I took advantage of large-scale gene expression profiles of PCa patients from the TCGA database[370]. PCa gene expression data from 497 prostate adenocarcinoma patients (PRAD dataset) was downloaded from the TCGA database and log2 transformed. In order to assess the impact of various immune markers on BCR, patients with a follow up time of less than 36 months were excluded. Patients were then segregated into low and high groups based on expression of each potential target. The cut-off value was determined based on the median value. Kaplan-Meier curves were generated for biochemical recurrence, and statistical significance was determined using the log-rank test. Univariate survival analyses were carried out using the Cox proportional hazards regression model. Due to the relatively long survival of prostate cancer patients, disease free survival data is incomplete, so here I have instead used biochemical recurrence (BCR) as a measure of disease progression to assess the prognostic impact of several potential immunotherapy targets.

As shown in Figure 5.1, PD-L1 (HR = 1.04, 95% CI = 0.55-2.01, p = 0.88), PD-L2 (HR = 1.50, 95% CI = 0.78-2.88, p = 0.22), IDO1 (HR = 0.94, 95% CI = 0.50-1.80, p = 0.86) and CD40 (HR = 1.23, 95% CI = 0.64-2.35, p = 0.54) mRNA expression had no relationship with time to BCR. However, CD47 did display significant prognostic value. Unexpectedly, elevated CD47 mRNA was correlated with better outcomes, i.e. longer time to BCR (HR = 0.41 , 95% CI = 0.20-0.84, p = 0.012). Due to the limitations of dichotomizing continuous variables (whilst still common place in developing prognostic models) [371–

373] I also assessed the impact of CD47 expression on BCR occurrence as a continuous variable, showing that higher CD47 expression also correlated with a better outcome when considered as a continuous variable (p = 0.026). This is contrary to the observed prognostic value of CD47 expression in a range of cancers where elevated CD47 expression predicts worse prognosis [282, 283, 288–290]. The reason for this apparently reversed prognostic value of CD47 may be due to a lesser studied role of the protein in supporting the migration of neutrophils and activated T cells to sites of inflammation [294, 374–376]. I hypothesised that if this correlation with good outcome is due to a need for CD47 to recruit neutrophils and T cells to the tumour then CD47 expression should correlate with both neutrophil and T cell numbers. In order to assess this, cell numbers were determined using the Danaher et al. method described in chapter 4. High PSS values confirmed effective immune cell enumeration for both T cells (Figure 5.2) and neutrophils (Figure 5.3). Having determined T cell and neutrophil numbers for each patient correlation of each immune cell type with CD47 was assessed, with both displaying strong positive correlation ($R=0.44$, $p<2.2x10^{-16}$ and $R=0.5$, $p<2.2x10^{-16}$, respectively) (Figure 5.4), consistent with the hypothesis that CD47 has an important role in recruitment of T cells and neutrophils in PCa. Whilst considerable further investigation would be required to confirm this hypothesis, the seemingly beneficial role of CD47 would suggest that inhibition of this molecule may not be the most therapeutically effective treatment for PCa.

A second potential target that demonstrated a significant prognostic impact in the PRAD dataset is TGFβ1. As expected, high TGFβ1 mRNA expression predicted shorter time to BCR (HR = 2.38, 95% CI = 1.19-4.74, p = 0.01) (Figure 5.1(B)). Similarly, higher TGFβ1 expression also correlated with worse outcomes when considered as a continuous variable (p = 0.009). As described above, TGFβ1 is thought to promote effector T cell dysfunction and accumulation of T regs. I thus also tested correlation of TGFβ1 with FOXP3, a marker of Tregs, and exhausted T cells demonstrating a striking correlation with both ($R=0.52$, $p<2.2x10^{-16}$ and $R=0.6$, $p<2.2x10^{-16}$, respectively). This supports the hypothesis that both may be important for the protumourigenic effects of TGFβ1 in PCa (Figure 5.4).

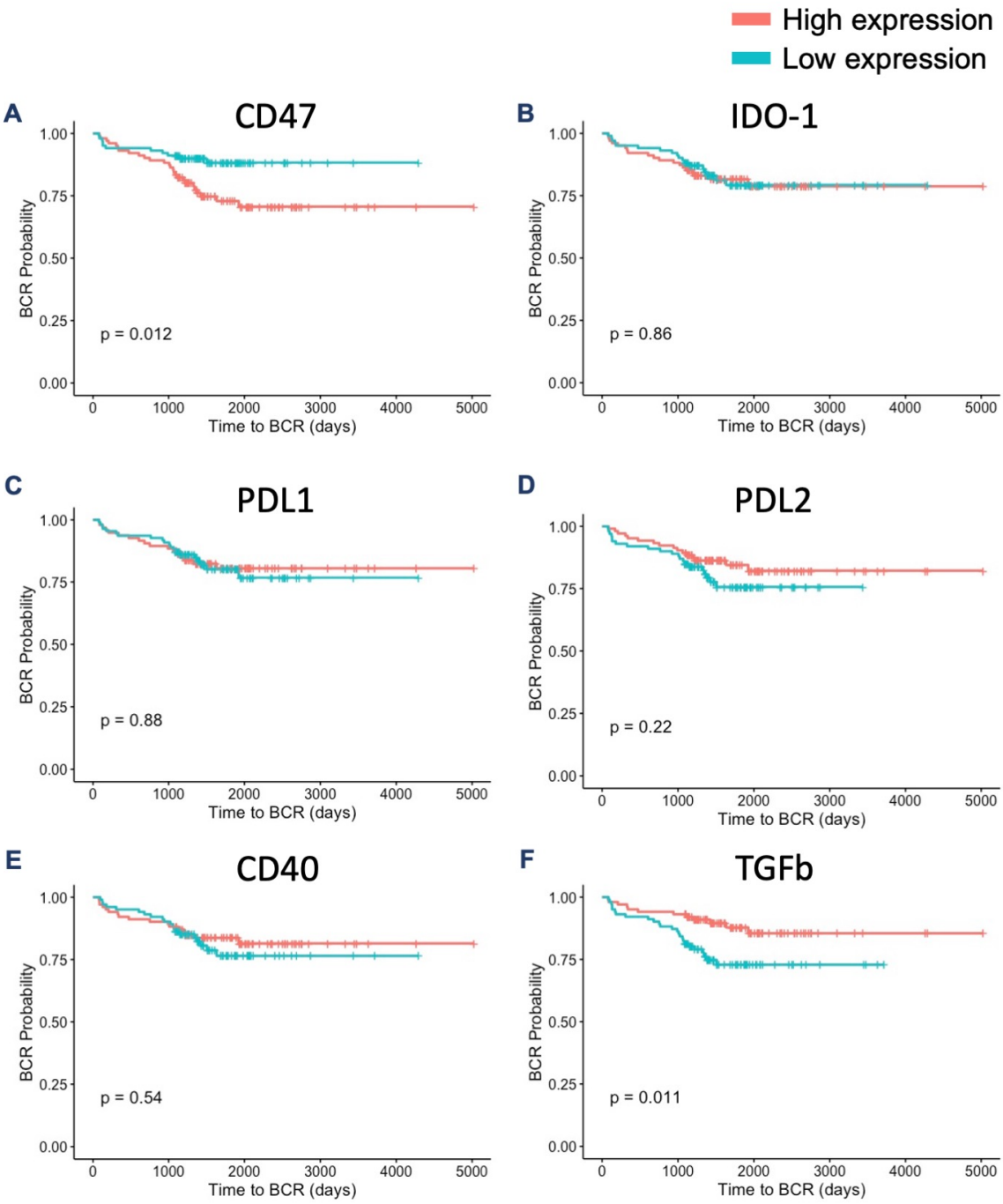

Figure 5.1: Prognostic value of potential immunological targets in prostate cancer PCa gene expression data from the PRAD data set was used to segregate patients into low and high groups based on expression of each potential target. Kaplan-Meier curves were generated for BCR, and statistical significance was determined using the log-rank test. **(A)** CD47, **(B)** IDO1, **(C)** PDL1, **(D)** PDL2, **(E)** CD40, **(F)** TGFB1.

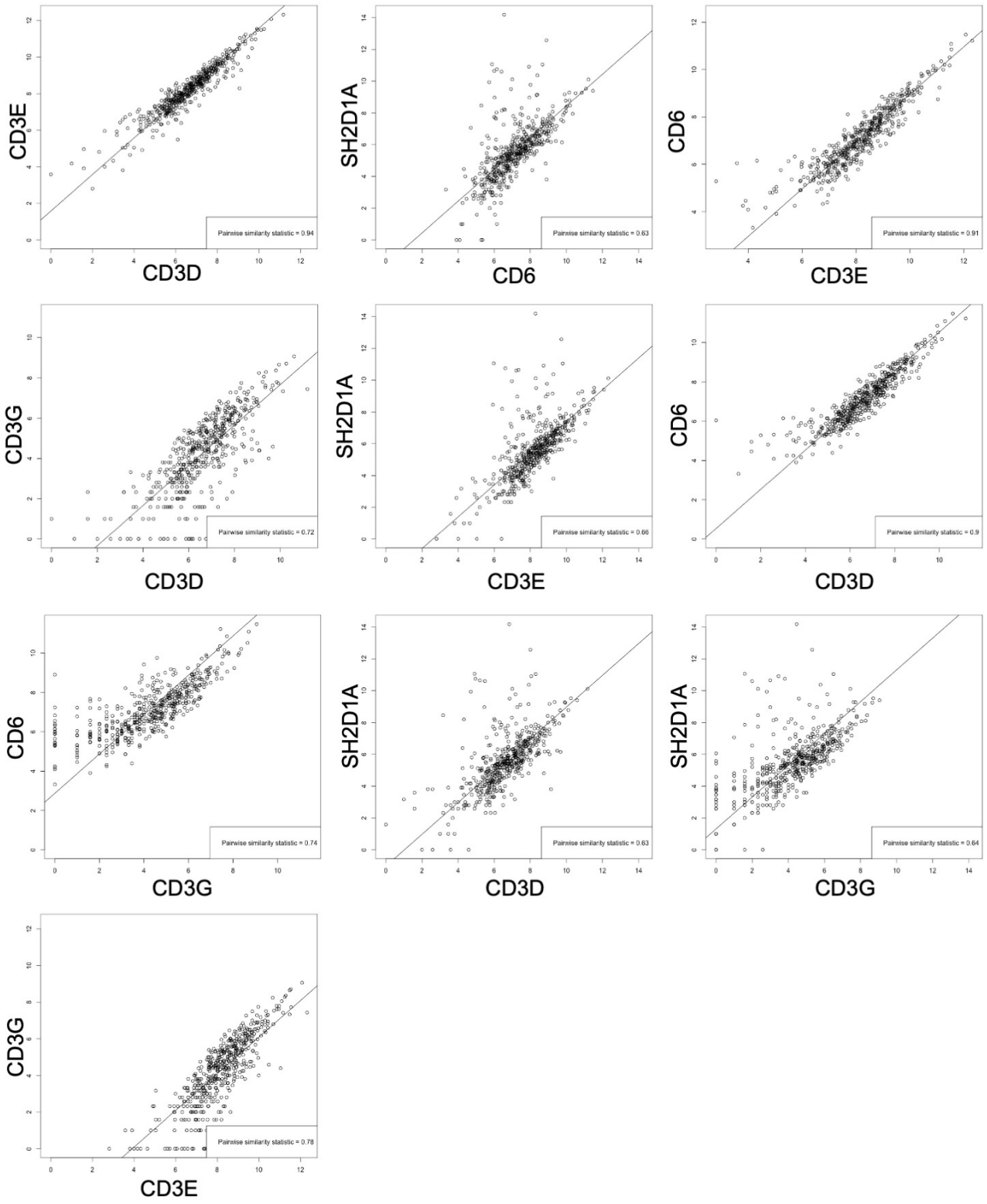

Figure 5.2: Assessment of the validity of T cell marker genes in the PRAD dataset
A pairwise similarity statistic (Danaher et al.,) was calculated between each potential marker gene for T cell enumeration in the PRAD data set.

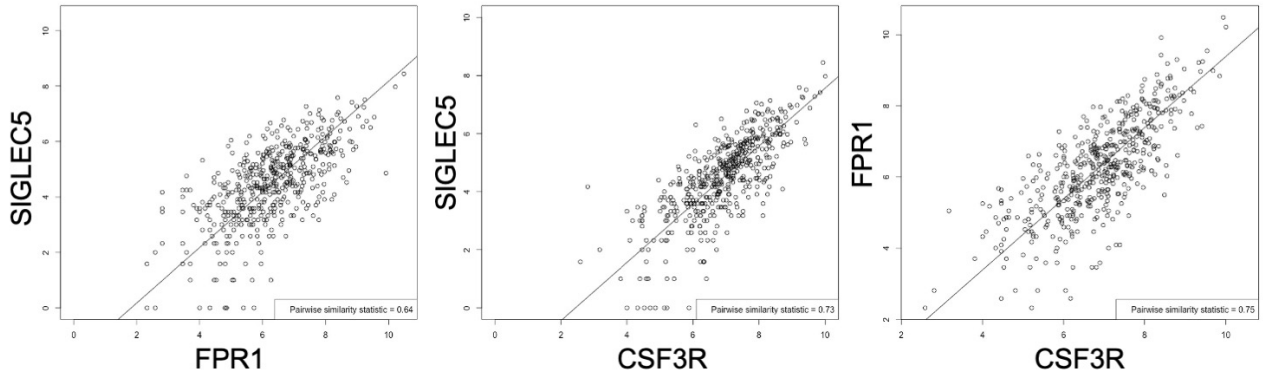

Figure 5.3: Assessment of the validity of neutrophil marker genes in the PRAD dataset

A pairwise similarity statistic (Danaher et al.,) was calculated between each potential marker gene for neutrophil enumeration in the PRAD data set.

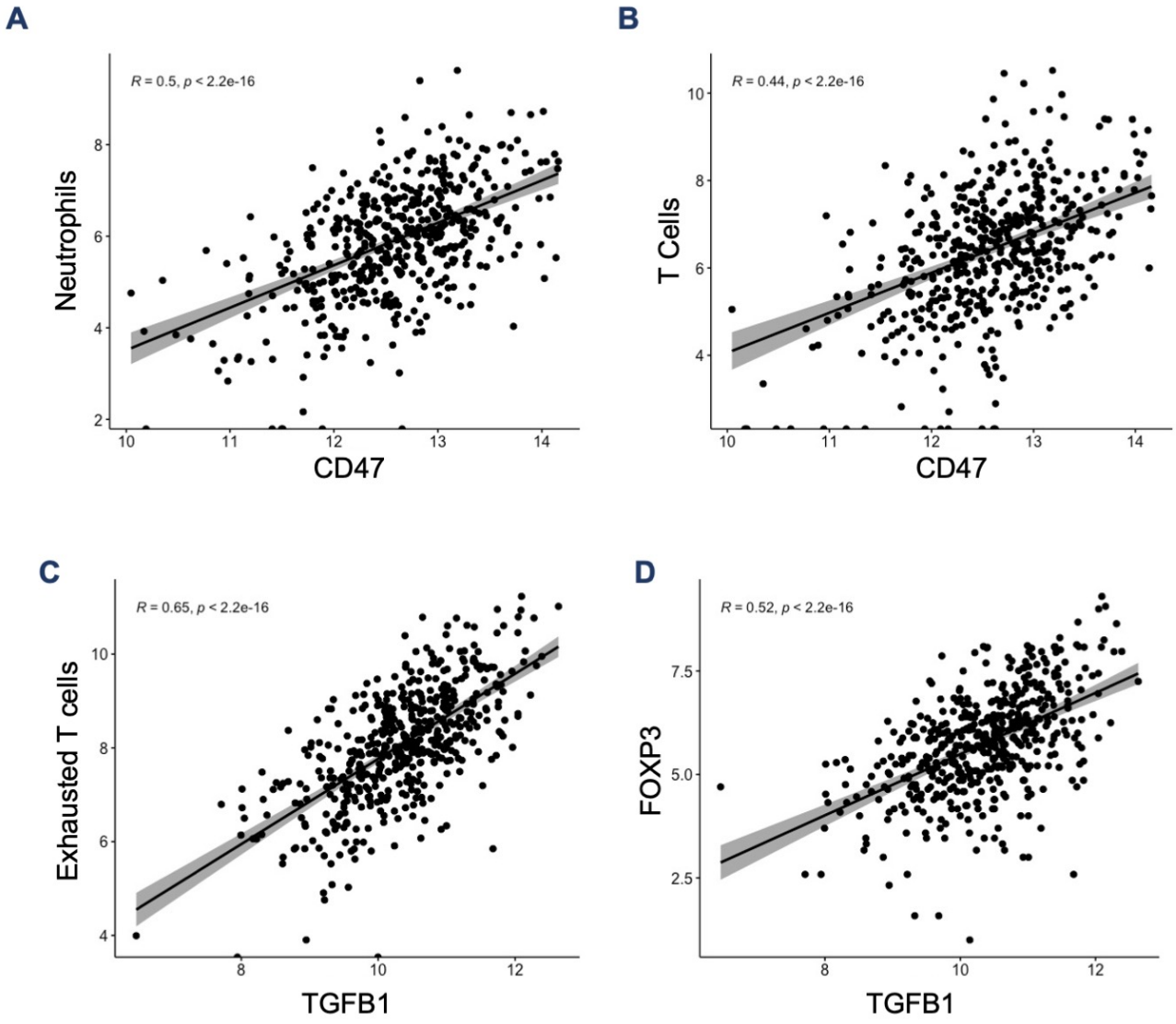

Figure 5.4: CD47 and TGFB1 correlation with immune cell infiltration in prostate cancer

Spearman correlation was used to assess the correlation of **(A)** CD47 expression with neutrophil levels, **(B)** CD47 expression with T cell levels, **(C)** TGFB1 expression with exhausted T cell levels, **(D)** TGFB1 expression with FOXP3 expression in the PRAD data set.

5.3.2 TGFβ1 is not induced by [177Lu]PSMA-I&T and TGFβ inhibition does not work synergistically with a single dose of [177Lu]PSMA-I&T or EBRT in the PGLS model

Having observed a significant negative prognostic influence of TGFβ1 expression in PCa, I chose to move forward with assessment of anti-TGFβ therapeutics to boost the immune response stimulated by [177Lu]PSMA-I&T treatment.

Given previous evidence that EBRT can induce TGFβ1 [352, 377–384], I first assessed the ability of both EBRT and [177Lu]PSMA-I&T to stimulate increased TGFβ1 production. First the bulk tumour gene expression data obtained using NanoString nCounter technology 72 hours and 12 days post treatment was inspected, as described in chapter 4. No change in TGFβ1 was seen following treatment with either EBRT or TRT at either the early or late timepoint (Figure 5.5(A)). As these data shows only gene level changes and may be masked by bulk tumour assessment, I went on to assess TGFβ production following treatment of PGLS cells *in vitro* via an ELISA. Again, this indicated no change in TGFβ produced following irradiation with either modality (Figure 5.5(C)(D)). It has also been shown that EBRT can cause activation of TGFβ, which is released in a latent form in complex with a pro-peptide. As such, the levels of activated TGFβ I also measured in the supernatant of cells exposed to a range of doses of EBRT or [177Lu]PSMA-I&T. Again, no change was observed (Figure 5.5(E)(F)).

Despite this apparent lack of induction of TGFβ by irradiation in PGLS cells, there are still many potential avenues for synergy of anti-TGFβ with [177Lu]PSMA-I&T as described in section 5.1. I thus moved on to assess the effect of the anti-TGFβ antibody clone 1D11 in combination with either [177Lu]PSMA-I&T or EBRT in PGLS allografts. To do this, c57BL/6 mice bearing PGLS tumours were treated with 200 μg anti-TGFβ antibody (clone 1D11.16) via intraperitoneal (i.p.) injection 12 days following tumour inoculation when tumours had reached ~50 mm^3. Treatment was repeated twice weekly for 5 weeks. 24 hours following the initiation of anti-TGFβ treatment, mice received 100 MBq [177Lu]PSMA-I&T via tail vein cannula or 10 Gy EBRT (Figure 5.6(A)). Whilst this treatment resulted in no significant toxicity as shown by stable body weight, there was also no slowing of tumour growth (Figure 5.6(b-e)). Importantly, there were severe limitations to this experiment, due to significantly differing tumour growth rates for the untreated tumours compared to previous observations with this

cell line (Figure 5.6(F)). Moreover, no significant efficacy was observed for the [177Lu]PSMA-I&T or EBRT only treated groups, contrary to previous studies (chapter 3). As such, this study should be repeated before conclusions about the lack of combined efficacy can be drawn.

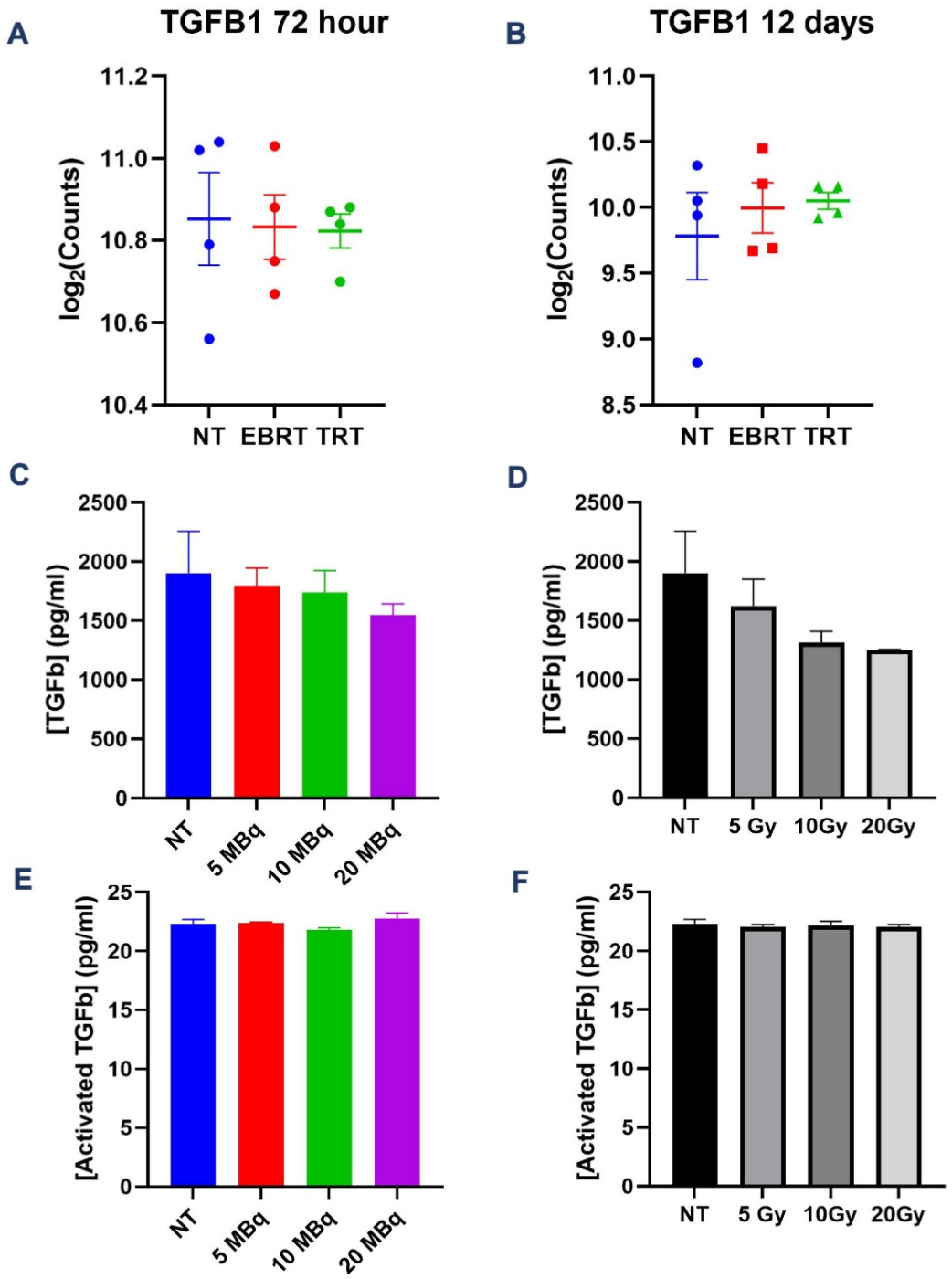

Figure 5.5: Neither EBRT or [177Lu]PSMA-I&T increase TGFb expression in PGLS cells

TGFB1 expression in [177Lu]PMSA-I&T treated, EBRT treated and untreated tumours **(A)** 72 hours and **(B)** 12 days post treatment as determined by NanoString bulk tumour analysis. **(C)** TGFb levels were assessed in the supernatant of cells treated with various doses of [177Lu]PSMA-I&T for 48 hours. **(D)** Total TGFb levels were assessed in the supernatant of cells treated with various doses of EBRT 48 hours post treatment following activation using hydrochloric acid. **(E)** Activated TGFb levels were assessed in the supernatant of cells treated with various doses of EBRT 48 hours post treatment. Data is shown as mean ± SEM and statistical significance determined by one way ANOVA using Dunnet's test for multiple comparisons. n=4 per group.

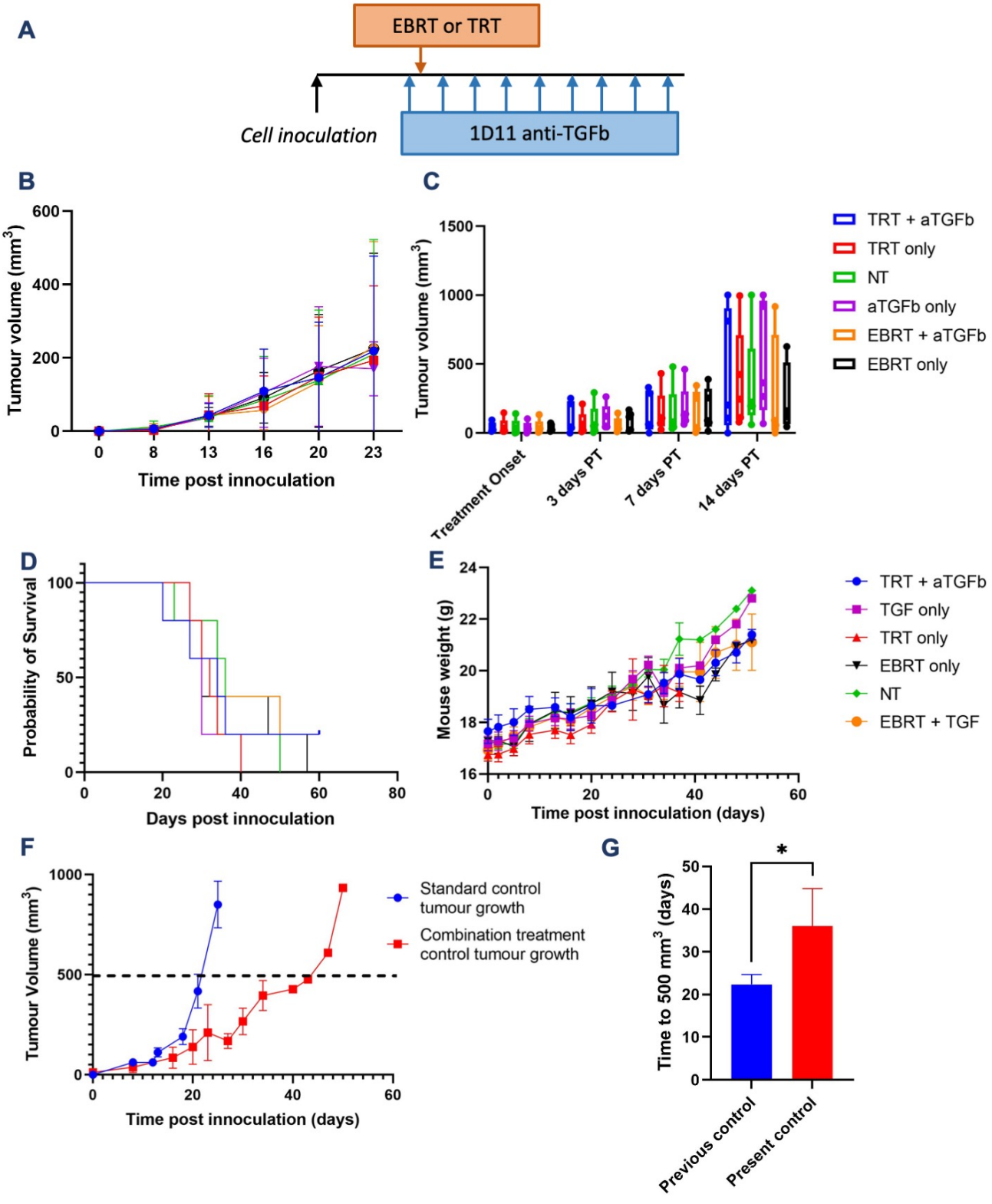

Figure 5.6: Combination of anti-TGFb with radiotherapy
(A) Treatment schedule – mice were inoculated with PGLS cells in the left flank. Anti-TGFb treatment commenced 12 days post-inoculation via i.p. injection. 24 hours post-first i.p. treatment mice were irradiated via EBRT or TRT. **(B)** Tumour growth **(C)** Time taken to reach 400 mm^3 **(D)** Survival **(E)** Mouse weight. **(F)** Tumour growth for the control group in this study was compared to representative data from previous studies using this model. **(G)** Time to 500 mm^3 for the control group in this study was compared to representative data from previous studies using this model. Data is shown as mean ± SEM and statistical significance determined by unpaired t-test. n=6 per group; * $p<0.05$; ** $p<0.01$; *** $p<0.001$

5.3.3 PDL1 is elevated in response to [177Lu]PSMA-I&T and may represent a good target for combination therapy

Given the apparent lack of a response to [177Lu]PSMA-I&T combined with anti-TGFβ, I explored alternative ways to improve immune activation and thus therapeutic efficacy of [177Lu]PSMA-I&T treatment. There is evidence of efficacy of triple combination with anti-PDL1 in situations where EBRT with anti-TGFβ alone had a limited response [263]. I thus hypothesized that PD-L1 may be limiting efficacy and could provide a good target. Given the extensive literature describing elevation of PD-L1 expression by EBRT potentially contributing to radioresistance, I first looked to assess if [177Lu]PSMA-I&T is similarly capable of evoking such a response. As with TGFβ1, I first inspected the bulk tumour gene expression data obtained using NanoString nCounter technology 72 hours and 12 days post treatment. This demonstrated a non-significant increase in PD-L1 expression 12 days post treatment with both modalities (Figure 5.7(A)). I thus went on to confirm this change *in vitro.* Here, PGLS cells were subject to various doses of EBRT or [177Lu]PSMA-I&T, then incubated for 72 hours prior to staining with anti-PDL1 antibody and assessment via flow cytometry. In agreement with the NanoString data, I observed a significant elevation of PD-L1 in PGLS cells following treatment with either EBRT or TRT (Figure 5.7(b-e)). Further analysis will be required to determine whether this elevation contributes to radioresistance, but this data provides initial evidence that anti-PDL1 has the potential to synergise with TRT and may also be worth considering in a triple combination with anti-TGFβ.

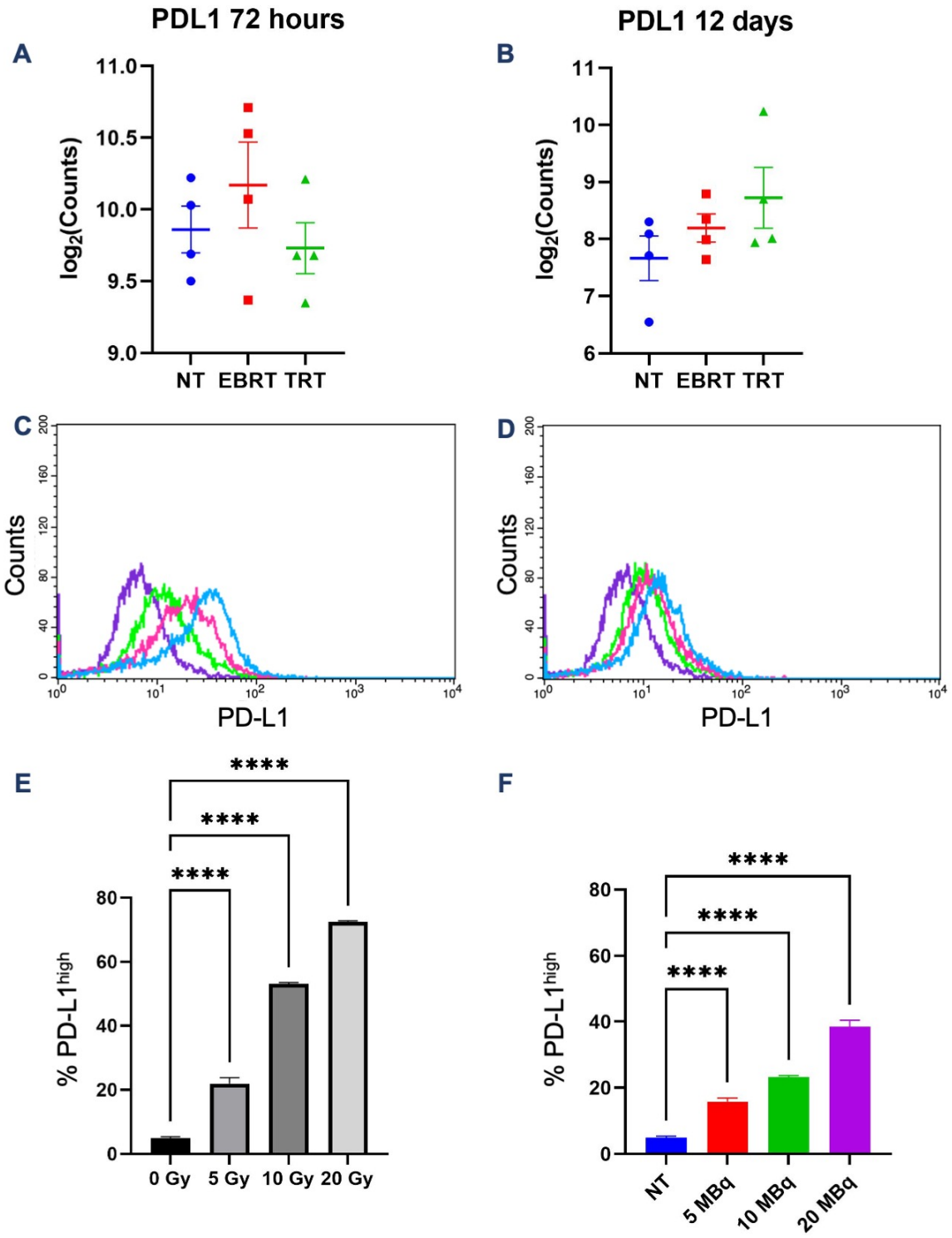

Figure 5.7: Both EBRT and [177Lu]PSMA-I&T induce expression of PDL1 in PGLS cells PDL1 expression in [177Lu]PMSA-I&T treated, EBRT treated and untreated tumours **(A)** 72 hours and **(B)** 12 days post treatment as determined by NanoString bulk tumour analysis. **(C)** PGLS cells were subject to various doses of [177Lu]PSMA or EBRT *in vitro*, and analysed for PDL1 levels 72 hours later. Representative PDL1 histogram illustrating the shift in PDL1 exposure with increasing dose of EBRT. **(D)** Representative PDL1 histogram illustrating the shift in PDL1 exposure with increasing dose of [177Lu]PSMA-I&T **(E)** EBRT dose response of PDL1 as determined by flow cytometry. **(F)** [177Lu]PSMA-I&T dose response of PDL1 as determined by flow cytometry. Data are presented as mean ± SEM (n=3) and statistical significance determined by one way ANOVA with Dunnet's post hoc adjustment for multiple comparisons. * p<0.05; ** p<0.01; *** p<0.001; ****p<0.0001

5.4 Discussion

Here I have shown the prognostic value of a number of potential immunological targets in PCa. Unexpectedly, higher CD47 expression predicted better outcomes. Validation of this in other data sets, and understanding the reason for this requires further exploration. However, correlation with T cell and neutrophil levels may suggest that the benefit is due to the role of CD47 in recruitment of these cells. I also observed the prognostic impact of TGFβ1, with high levels predicting worse outcomes. I thus assessed the potential of combining TRT with anti-TGFβ. I noted no effect of [177Lu]PSMA-I&T on TGFβ production, and no efficacy of combined [177Lu]PSMA-I&T treatment, though there were significant limitations to this study. Existing evidence suggests that the limited response of combined EBRT with anti-TGFβ might be improved by the addition of PD-L1 inhibitors. I thus sought to address the potential of combining PDL1 inhibitors with this treatment. This work highlighted the ability of TRT to induce PD-L1 expression, suggesting this may be a factor in radioresistance and thus combination with PDL1 inhibitors is an interesting avenue to explore in the future.

5.4.1 CD47 levels predict favorable outcomes in PCa

Despite the unprecedented success of immunotherapeutics in a number of cancers such as melanoma, renal cell carcinoma and lung cancer; prostate cancer has yet to see any significant improvements. This is perhaps due to the 'immune cold' microenvironment of PCA, with an abundance of immune-suppressive mechanisms such as loss of MHC expression and high numbers of Tregs and Th17 cells, observed in the tumour microenvironment and limiting the potential for efficacy of a single targeted agent [385–389]. Indeed, single agent studies have thus far showed significant potential in only a very small number of patients, whilst a majority fail to respond suggesting a need for combination treatment approaches to increase response rates. For example, the KEYNOTE-199 study showed 5% of PCa patients were 'super-responders' to the PD-L1 inhibitor pembrolizumab, but a majority failed to respond. Intriguingly, the multi-faceted effects of RT may help to overcome these limitations when used in combination with established immunotherapeutics.

CD47 is a particularly interesting target as it is an antagonist of the pro-immunogenic effects of ICD, which, as demonstrated in chapter 4, can be induced by TRT. The correlation of CD47 expression with poor prognosis was first described for acute myeloid leukemia, leading investigators to assess the potential of anti-CD47 treatment [282]. Similar prognostic value of CD47 has since been shown in a range of solid tumours [282, 283, 288–290]. The impact of CD47 expression in PCa has so far been less well understood. Willingham et al. observed CD47 expression in dissociated patient prostate tumour cells analysed by flow cytometry, but did not go on to assess the prognostic significance of this. The analysis showing that CD47 expression predicts better outcomes is surprising. Whilst similar observations have not yet been described for tumour samples, there is evidence that low expression of CD47 in peripheral blood is associated with progression of gastric cancer [390]. Gao *et al*. also highlighted a potential benefit of CD47, showing that lack of CD47 in tumor stromal cells promotes angiogenesis and enhances vascular integrity and stability leading to accelerated tumor progression [391]. This suggests that the actual cell type that expresses CD47 in the tumour is critical, however this information is lost in bulk transcriptomic data such as the PRAD dataset analyzed here.

It is also possible that other mechanisms are involved. In an attempt to understand the seemingly contradictory prognostic value of CD47 in PCa, I explored an additional role of CD47 as an important factor in the migration of neutrophils and activated T cells to the sites of inflammation. Given the importance of these cells in generating an anti-tumour TIME [294, 374–376], it follows that factors involved in their recruitment are advantageous for tumour control. Concordantly, I observed strong correlation of CD47 with both T cells and neutrophils, however further investigation is warranted to determine whether this effect is causative. Indeed, it is possible that immune cells independently correlate with better outcomes and thus the correlation of CD47 with these cells does not necessarily imply causation. However, should this prove to be the case it would also be interesting to understand why this role is seemingly more important in PCa than other solid cancers, as again this correlation is contrary to observations in human melanomas where an inverse correlation between T-cell infiltration and CD47 expression was observed [392].

Again, it is possible that the differences arise from differences in individual cell expression, or spatial localization, neither of which can be probed from bulk tumour data. Ultimately, further work will be necessary to confirm the beneficial effect of CD47 expression in PCa and to determine the mechanisms underlying this unexpected occurrence. Importantly, the seemingly beneficial effects of CD47 on prognosis does not entirely preclude the possibility that CD47 antagonists could still be beneficial for PCa patients, but significant further study would be required to understand the relative benefits and harm of CD47 in PCa.

5.4.2 Combination of [177Lu]PSMA-I&T with anti-TGFβ

As expected, my analysis demonstrated that TGFβ1 expression correlates with a poor outcome. Consistently, Zhang *et al.* observed a similar effect of TGFβ1 on recurrence free survival in PCa patients using the database of Northwestern University's Prostate SPORE containing microarray data for 243 radical prostatectomy specimens [393]. Similarly, in a much older study Wikstrom *et al.* observed that tumor overproduction of TGF-β1 had shorter median cancer-specific survival [348]. Interestingly, there is also evidence that TGFβ1 signaling can induce androgen receptor activation in PCa, which is essential for tumour growth and survival [394], along with promoting migration and invasion of PCa cells [395]. Ultimately, this suggests that TGFβ1 is particularly important in supporting PCa growth and thus inhibition of TGFβ could be particularly beneficial in this disease. In particular, I predicted that this treatment may synergise with [177Lu]PSMA-I&T based on existing evidence that TGFβ can not only modulate the TIME, but is further upregulated by irradiation, and may also prevent normal tissue toxicity due to fibrosis [377, 378, 396, 397]. Moreover, there is evidence that a modality related to TRT, brachytherapy, can increase TGFβ levels in PCa patients [213].

Despite this, my assessment of the effects of [177Lu]PSMA-I&T on the production of TGFβ suggested no such upregulation of either TGFβ1 mRNA *in vivo*, or of TGFβ protein *in vitro*. Indeed, there was a trend towards a dose dependent reduction in TGFβ production. Similarly no significant change, and indeed a trend towards a dose dependent reduction, was again observed following EBRT, indicating

this may be due to the cell line rather than the ability of the radiation modality to induce any change. Consistently, Satoh *et al.* observed a dose-dependent reduction of TGFβ in the supernatants from malignant glioma cells in response to EBRT [378]. However, when the inhibition of cell growth by irradiation was accounted for, the amount of TGF-β secretion *per cell* was found to be increased after EBRT, highlighting the need to account for cell number here. Although, notably from visual inspection the number of PGLS cells, which are known to be radioresistant, does not significantly decline 48 hours following treatment with the amounts of radioactivity used. Interestingly, TGFβ is secreted in a latent complex, and requires activation to carry out downstream functions. Consequently, changes in activation state are equally important as increased production. Of note, Jobling *et al.* highlighted the ability of EBRT to increase the activation of TGFβ by ROS-induced oxidation of the pro-peptide [377]. Unfortunately, I was again unable to detect such changes following a single dose of either TRT or EBRT. Regardless of the impact of irradiation on TGFβ levels, the existing correlation of TGFβ1 with BCR, together with the immune modulation induced by [177Lu]PSMA-I&T suggests that the two treatments may synergise. Indeed, alongside my work showing that TGFβ1 expression correlates with poor prognosis, there is already evidence of the potential benefits of inhibiting TGFβ signaling in preclinical models of PCa [398]. Moreover, a number of studies have described synergistic responses in combination with EBRT in preclinical studies [263, 361, 399–401], with this success leading to clinical testing [363]. Unfortunately, no such effect was seen in my study on PGLS allografts for either EBRT or TRT. Importantly though, this study was significantly flawed. Unfortunately for unknown reasons, tumour growth was far slower than previously achieved with this model, and moreover the significant growth delay induced by both EBRT and [177Lu]PSMA-I&T in my previous studies was not observed (see chapter 3). For these reasons, repetition of this study is required to determine whether the lack of effect observed is a true reflection of the treatments, or was a result of a confounding error causing altered tumour growth. Should this be a true effect, it would be interesting to understand why, to investigate the changes to the TIME following combination treatment, and to assess the combination in a different murine PCa model to see if the response is model specific. One possible reason for the

failure of the combination treatment is that anti-TGFβ treatment has previously been shown to radiosentitise intratumoural T cells[234]. Given the data I presented in chapter 4 showing the reduction in immune cells at early timepoints following single agent [177Lu]PSMA-I&T, one possible hypothesis is that the dual treatment with repeated anti-TGFβ administration and continued low dose irradiation causes too great a decline of intratumoral T cells and prevents repopulation. Ultimately, further assessment will be required to test this hypothesis and investigate other possibilities to see if this can be overcome.

5.4.3 PD-L1 and other alternatives

Given the apparent lack of efficacy of [177Lu]PSMA-I&T combined with anti-TGFβ, along with its status as one of the most widely used and effective immunotherapeutics in oncology, I was also interested in investigating the possibility of using PD-L1 in combination with TRT. This is particularly attractive in light of evidence for the potential of combining radiotherapy with anti-TGFβ *and* anti-PDL1 treatments [263, 401].

One key reason for considering TRT and anti-PDL1 combination therapy, is the possibility that PD-L1 upregulation may be a mechanism of radioresistance within the tumour, similar to that described for EBRT [318]. The importance of the PD-1/PD-L1 axis in relation to radiosensitivity has even been shown specifically in PCa, where higher PD-1+ TIL scores in the tumour predicted the outcome of patients treated with salvage radiotherapy after BCR [402]. Strikingly, my data demonstrates that treatment with [177Lu]PSMA-I&T *in vitro* does indeed stimulate a significant increase in PD-L1 levels in PGLS cells. Consistently, NanoString analysis suggests a similar increase may occur *in vivo.* Intriguingly, the time scale of this *in vivo* change varies significantly to that observed *in vitro,* with no observable change in *in vivo* PD-L1 expression at the 72 hour timepoint, perhaps indicating a more complex mechanism is occurring within the tumours or that expression is on a different cell type. Understanding this temporal factor may be important in determining optimal treatment regimens. To my knowledge, this is the first evidence that TRT treatment can cause upregulation of PD-L1 in tumour

cells, and suggests that this may be a mechanism of radioresistance. Notably, Chen *et al.* have previously demonstrated that another lutetium based radiopharmaceutical can cause an increase in the percentage of PD-L1+ leukocytes in the TIME. Conversely, Kim et al. described a reduction in the frequency of PD-1 expressing CD8 T cells following treatment with [223Ra], suggesting that these effects may be radioisotope and/or context dependent [403]. Whilst clinical evidence of this phenomena is thus far lacking, there is evidence that related radiotherapeutic modalities can induce similar changes in patients. For example, NanoString immune profiling revealed upregulation of PD-L1 following treatment with high dose-rate brachytherapy in a cohort of 24 patients with localized prostate cancer [213]. Similarly, a number of clinical trials have reported increases in PD-L1 levels following conventional EBRT or chemoradiotherapy across a range of cancers [404–408]. However, other studies have suggested either that expression only increases in a subset of patients, that there is no change, or even that there is a reduction in PD-L1 levels following similar treatments [409–411]. Strikingly, one study in NSCLC reported an increase in only 11% of patients following preoperative chemoradiotherapy, whilst 45% of patients had reduced PDL1 levels [411]. Importantly, those with increased PD-L1 had poor survival compared with the groups in which PD-L1 was reduced or unchanged, consistent with the hypothesis that upregulation of PD-L1 acts as a radioresistance mechanism. Ultimately, this suggests that assessing the impact of [177Lu]PSMA-I&T on PD-L1 levels in patients, and the prognostic value of this on responsiveness, may be an important next step. Moreover, understanding the factors influencing this response and identifying suitable biomarkers to identify patients likely to respond to treatment may be critical.

One interesting consideration is that the increased IFN activity described in chapter 4 is the driver of this PD-L1 induction[71]. This highlights the often paradoxical effects of immunogenic signaling, wherein the same immune pathways can have both immune stimulatory and suppressive effects. Again, this highlights the need to understand TME factors influencing the immune response to enable better patient stratification or identification of possible combination therapies that can shift the balance to immune activation.

Interestingly, my transcriptomic analysis of the PRAD cohort demonstrated no prognostic impact of PD-L1 expression levels. Indeed, the prognostic role of PD-L1 in PCa has been explored in multiple studies, yielding conflicting results with a number showing a similar lack of prognostic impact whilst others show a significant effect [367–369, 412–416]. This is perhaps due to spatial localization of PD-L1, the specific cells expressing PD-L1, or other factors in the immune contexture such as immune cell numbers, or the presence of additional immune checkpoint molecules. Consistently, Tashima *et al*. demonstrated that whilst PD-L1 expression levels were not prognostic, having low lymphocyte to neutrophil ratio ***and*** high PD-L1 levels did predict worse outcomes in squamous cell carcinoma of the lung [417]. It is also possible that these differences in observed prognostic impact arise simply from limitations in the experimental parameters, with differences in IHC protocols, antibody clones, scoring systems and threshold cut offs, given the lack of standardization for PD-L1 scoring. Importantly, a lack of prognostic value for PD-L1 does not preclude the potential effectiveness of anti-PDL1 treatment. Notably, similar conflicting data has been shown for NSCLC [418–420], where a number of successful clinical trials have led to FDA approval of PD-L1 based treatments in this disease. Moreover, studies investigating the impact of PD-L1 levels on responsiveness to anti-PDL1 treatment in NSCLC have similarly reported conflicting results, with some demonstrating greater treatment benefit in patients with higher PD-L1 expression, and others concluding that response is independent of PD-L1 expression level[421–428]. Indeed, there is even evidence that PDL1 treatment can be effective even in tumours with no PDL1 expression [429]. This highlights the need for better understanding of the factors impacting response, and for new biomarkers for selecting patients who should benefit.

Notably, studies investigating the overall level of PD-L1 expression in PCa also show great variability, though again this may be down to a lack of standardization in PD-L1 scoring [368, 414–416, 430, 431]. Interestingly, higher overall levels have been observed in mCRPC, suggesting PD-L1 expression may be employed as a mechanism to avoid immune surveillance in advanced disease [368, 430]. Importantly, there is evidence that even if absolute levels are not critical, some level of PD-L1 expression is an important predictor of response to anti-PDL1 treatment in PCa [432, 433]. For example, in a phase 1

trial assessing the safety and efficacy of an anti-PD1 monoclonal antibody in advanced solid tumour patients (including PCa), 36% of PD-L1 positive tumours responded whilst no objective response was observed in PDL1-negative tumours [432]. In summation, whilst the direct prognostic impact of PD-L1 levels remains unclear, the elevation of PD-L1 in advanced disease together with my findings showing PDL1 upregulation following [177Lu]PSMA-I&T suggest that PD-L1 upregulation may be an important mechanism of immune evasion in PCa, making this a particularly attractive target alongside radiotherapy.

Indeed, a number of clinical trials assessing PD-1/PD-L1 targeting therapies in PCa have already been completed. Single agent clinical trials to date suggest that whilst a small proportion of mCRPC patients do benefit from single-agent PD-1 inhibitor treatment, with an even smaller number experiencing durable responses, a large number do not respond to this treatment alone. In particular, in the phase Ib KEYNOTE-028 trial, the overall response rate (ORR) to pembrolizumab was 17% (4 of 23 PDL1 positive patients), with stable disease in 35% (8 patients). Meanwhile, a large phase II study in 258 mCRPC patients (KEYNOTE-199) pembrolizumab showed equivalent activity in PD-L1-positive and PD-L1-negative soft-tissue disease patients. Objective response rate was only approximately 4%, although strikingly two PD-L1 positive patients achieved a complete response. Again, this shines a light on the potential of immunotherapy in PCa patients, but also the need to develop combination therapies that could sensitize tumours to PD-L1 therapies to increase response rates, unleashing the success observed in other cancer types.

The low number of immune cells present within the 'immune cold' PCa TIME has been suggested as one possible reason for the limited responses observed thus far. Indeed, the importance of immune context has been highlighted by the propensity of TIL scores or immune gene signatures to predict response to checkpoint inhibition [249, 250]. One striking example of this is a small study by Subudhi *et al.* who conducted a clinical trial with ipilimumab in 30 patients with mCRPC [434]. The investigators identified two distinct cohorts based on survival and progression times following treatment, with the favorable cohort having high intratumoral CD8 T cell density and IFN-γ response gene signature and/or

antigen-specific T cell responses. The ability of [177Lu]PSMA-I&T to induce IFN responses and modulate T cells could thus increase the effectiveness of checkpoint inhibitors in non-responders, suggesting that TRT and checkpoint inhibition may be a beneficial combination. Indeed this is already being assessed in both a phase I trial and the phase Ib/II PRINCE trial combining [177Lu]PSMA-I&T with a PD-1 inhibitor pembrolizumab in mCRPC (NCT03805594, NCT03658447). Further evidence that the significant IFN activity induced by TRT may also be beneficial in this instance comes from preclinical evidence demonstrating that IFN activation using an intratumoural STING agonist alongside checkpoint inhibition increased overall survival by 35% compared to checkpoint inhibition alone in a syngeneic mouse model of PCa [435]. Consistently, a recent study investigating another lutetium based radiopharmaceutical in combination with anti-PDL1 treatment demonstrated that this combination stimulated infiltration of CD8+ T cells and improved local tumor control, overall survival and protection against tumor rechallenge [436]. Similarly, there is already both pre-clinical and clinical evidence of the efficacy of combining EBRT with PD-L1 inhibitors [309–311, 314, 315, 317, 318, 437–442]. Although examples where this combination is ineffective highlights the necessity to optimize the dosing schedule, and importance of tumour microenvironment context potentially meaning a third therapeutic is required for optimal effectiveness [323, 443].

Chapter VI:

Concluding Remarks

6.1 Synopsis

The aim of this work was to determine whether TRT is capable of interacting with the immune system and thus causing changes to the TIME. I initially demonstrated that subcutaneous PGLS allografts provide a suitable model in which to address this question using the clinically relevant radiopharmaceutical [177Lu]PSMA-I&T. I confirmed that a high level of radiochemical purity of this radionuclide could be obtained, and went on to demonstrate target protein expression, *in vitro* uptake, *in vivo* tumour growth and perfusion, and satisfactory biodistribution with significant tumour accumulation of [177Lu]PSMA-I&T. I also demonstrated significant therapeutic effect of both TRT and EBRT in this model, although notably this was not observed in the control arms of a subsequent combination therapy study.

Having established a suitable model, I demonstrated that [177Lu]PSMA-I&T was capable of inducing changes to the TIME. Here I observed a notable reduction in immune cells compared with untreated controls 72 hours post treatment, followed by a return to no-treatment levels by day 12 that trended towards an increase. Interestingly the initial decline was not observed for EBRT, though a similar increase in immune cell was seen by day 12. I subsequently initiated investigation into the potential mechanisms involved in this interaction with the immune system, observing that both TRT and EBRT can induce ICD in this model. Interestingly, the ability to eliminate tumour growth by vaccination with TRT-treated cells was lost in the treatment of established tumours. This suggested that other factors in the TIME are limiting the capacity of TRT to induce a functional immune response. I thus looked to investigate potential combinations with immunotherapies to eliminate possible barriers. Here I observed that, contrary to expectations, the phagocytic inhibitory protein CD47 correlated with better

outcomes in the PRAD cohort of PCa patients. The reasons for this remain unclear, but may be due to an additional role in supporting the recruitment of neutrophils and activated T cells.

I also observed a strong correlation of TGFβ1 with worse outcomes, and given there is also significant evidence that TGFβ1 expression may be an important factor limiting immune activation by TRT, I chose to assess the combination of TRT and anti-TGFβ therapy. No effect of the combined therapy was observed, though importantly significant differences in growth were observed compared to previous studies. Strikingly, I observed that [177Lu]PMSA-I&T treatment invokes a remarkable increase in PD-L1 expression in PGLS cells. This suggests that PD-L1 upregulation may be an important mechanism of radioresistance, thus I suggest that combination of TRT with anti-PDL1 and potentially anti-TGFβ could be a valuable avenue to explore.

6.2 Limitations

6.2.1 Limitations of mouse models

This work faces several limitations which must be accounted for when interpreting the results. One of the most significant of these is the use of mouse models. Whilst such models are a cornerstone of biomedical research, they are subject to significant limitations due to genetic, molecular, cellular and physiological differences between mice and humans. One striking example of this is that transcription factor binding sites differ in 41% to 89% of the >4,000 genes in humans and mice [444]. Moreover, other differences between mouse models and human patients including tumour growth rate which also effects stromal and endothelial architecture, shorter lifetime limiting antigenic exposure and cell turnover, and the lack of genetic heterogeneity, as well as the lack of best-practice standards in animal testing all contribute to the limitations of murine models.

More specifically, here I have used sub-cutaneous rather than orthotopic models which introduces further deviation from the clinical scenario. In particular, orthotopic models are thought to better recapitulate some aspects of the TME, cancer progression and metastasis, and are thus thought to be more clinically relevant than subcutaneous models [445]. Interestingly, the TIME also varies between

the two types of model in ways that may be particularly relevant here; for example there is evidence that TGFβ1 is present at higher levels in orthotopic rather than subcutaneous tumours, though importantly heterogeneity in levels seen clinically mean that neither is specifically better at recapitulating human disease [446]. Importantly, to my knowledge there are currently no available immune-competent, PSMA-expressing orthotopic models, precluding their use here. Moreover, subcutaneous models were used in this work to enable assessment of ICD via vaccination-rechallenge, and due to their reproducibility, ease of use, and ability to measure tumours accurately. In the future, the development of an orthotopic models may better mimic the situation in the clinic.

Of particular importance here, where I have been investigating the immune response, the significant differences between human and murine immune systems may limit the extent to which observations reflect human response. For example differences in leukocyte and antibody subset ratios, Toll-like receptors, and transcriptional programmes exist between mice and humans [447–449]. Furthermore, specific pathogen-free mouse husbandry will further deviate the mouse immune system from that of real patients in whom pathogen infections and microbiota affect the basal level of activation and function of the immune system and thus inevitably impact immune responses [450, 451].

Another important factor for the immune analysis in this study is the presence of one dominant tumour antigen, given that human PSMA has been transduced into murine PCa cells. This will inevitably impact the immunogenicity of the tumours and may thus impact the induction of an anti-tumour immune response. Indeed, the difference in PSMA expression in mice versus humans as discussed in chapter 3 may also have an effect.

Together, all of these factors mean that drugs that are successful in preclinical testing all too often fail in clinical trials [452] – although notably it is thought that a significant contributor to this is publication bias leading to an ~ 30% overestimate of the likelihood that a treatment will be effective due to lack of publishing negative results [453]. In spite of these factors, mouse models remain an immensely valuable tool for preclinical research and have of course led to huge gains in our understanding of

disease and treatment. As such, these models are used here to provide early evidence of immune activation by TRT. Ultimately, it is important to consider results in the context of the limitations of murine models, and understand how they differ from human disease.

6.2.2 Human data

The problems associated with mouse models highlights another significant limitation, which is that I have not extended my findings to human data. It would have been useful to assess immune changes in human samples before and after therapy to see if similar changes occur to those observed in mice. Unfortunately, the treatment makes patients and tumour samples radioactive, adding further difficulty to obtaining tumour biopsies. Nonetheless, it is essential to substantiate my findings with reliable clinical data and thus this is an area we are actively exploring for future work. Indeed, even extending my *in vitro* studies of ICD and PD-L1 expression to look at human cell lines such as LnCAP will give an initial indication as to whether my findings are relevant beyond the PGLS model.

6.2.3 Timing and dose considerations

Another consideration is that I conducted my analyses at specified time points, which varied from 24 to 144 hours *in* vitro; and on tumour tissue extracted 72 hours or 12 days *ex vivo*. These time points were selected based on existing literature describing the time taken for similar changes *in vitro*, and the time for induction of adaptive immunity *in vivo*. However, this means I may have missed important changes that take place at other time points. For example, whilst the tumour analysis at 72 hours demonstrates a significant decline in immune cells post treatment with TRT and no such decline following EBRT, it is unclear whether a similar decline occurred following EBRT treatment at an earlier timepoint and was thus missed.

Another significant factor limiting my ability to compare TRT and EBRT treatment is a lack of dose comparison. Whilst it is possible to determine absorbed dose for each treatment in both *in vitro* and *in vivo* scenarios, this analysis is complex and beyond the scope of this thesis. As such, direct dose comparisons were not possible but may provide an interesting basis for future work.

Similarly, the use of single doses of EBRT and TRT does not reflect the clinical situation, where both treatments are typically administered as fractionated doses. As noted in Chapter 3, these single doses were used to provide a simple model for initial analysis of the immune response to TRT, and due to radiation safety considerations for additional treatment of already radioactive animals. Importantly, additional subsequent irradiations are likely to impact the immune response and so will be an important factor to consider in the future.

6.2.4 Immune cell enumeration

Our assessment of the TIME was conducted using NanoString nCounter technology, with immune cells enumerated using the Danaher *et al.* method [136]. Whilst this analysis has demonstrated good concordance with IHC and flow cytometry data in previous studies [212], here this was not possible to check due to limitations regarding use of IHC or flow cytometry with radioactive samples. Conducting western blots, IHC or flow cytometry on the EBRT treated and control tumours may provide further confirmation that NanoString derived immune cell frequency changes are comparable to protein level data. Alternatively, a protein level analysis set up in a radioactive materials laboratory space would enable full western blot, IHC and flow cytometry analysis to be done, and overcome this current limitation.

Another limitation of this analysis is that NanoString analyses involve RNA from bulk tumour samples, precluding assessment of expression changes in individual cell types – for example identifying which cell types may have altered PD-L1 expression – and also losing all spatial information. Importantly, the spatial localisation of immune cells is thought to be key to mounting a successful anti-tumour immune response. Thus, whilst I have observed changes in the number of immune cells following treatment, whether or not these cells penetrate to the tumour core remains unknown. This is particularly relevant for prostate cancer, where spatially guided transcriptomics demonstrated enrichment of immune pathways at the periphery but not the core of prostate adenocarcinoma tissue, highlighting the need for therapeutics to promote immune activation that penetrates the tumour [454]. A future goal is to

use nCounter digital spatial profiling technology, which enables spatially guided transcriptional analysis, to overcome this limitation.

Finally, the NanoString assessment was particularly limited by the low n number for this study, with only 4 animals per group. This severely limited the statistical power of the study, and made it difficult to derive significant results.

6.2.5 Immunotherapy targets and combination therapies

Having shown changes to the TIME following treatment, I went on to assess potential combinations with immunotherapies. Having identified the correlation of TGFβ with poor outcomes in PCa patients, I assessed the combination of anti-TGFβ with TRT. I observed no additive or synergistic effect of combination. However, as noted previously, this experiment was invalid due to significantly slower growth of the control group compared with previous studies. The reason for this slower growth is unclear as all methodology, cell passage number, mouse strain and supplier were identical. Regardless, it appears to have impacted therapeutic effect given the lack of response to TRT or EBRT monotherapies as had been previously observed. Assessment of tumour growth and therapeutic efficacy in further studies is thus required. Importantly, this should also include evaluation of different dosing schedules including repeated dosing, given substantial evidence that this can be key to therapeutic success [30, 112, 455–462].

Another limitation of this work on developing combination therapies is the lack in *in vivo* assessment of combining anti-PDL1 with TRT. Having demonstrated a significant increase in PD-L1 expression induced by TRT, assessment of this combination therapy will be an important next step.

6.3 Future directions

The work presented in this thesis has demonstrated for the first time that [177Lu]PSMA-I&T can interact with the immune system, but it also leads to an understanding of what needs to be done now to advance the field further. This is primarily centered around gaining greater understanding of the

immune changes following TRT, and subsequently using this knowledge to inform radiotherapy-immunotherapy combinations. Ultimately this will need to be compared with human data to ascertain whether similar changes are occurring in human patients with the hope of moving into clinical trials with promising combination therapies.

6.3.1 Immune cell phenotype and mechanistic insights

Firstly, the data presented here illustrates that there are changes in immune cell levels following treatment with TRT. However, this analysis did not enable identification of phenotypic changes, such as tolerogenic vs active DCs, M1 or M2 macrophages, or regulatory, exhausted, or cytotoxic T cells. Given the opposing functions of these cells, and existing evidence that other forms of radiotherapy can modulate the ratio of these cells, this is important avenue for further investigation and ultimately may be valuable in assessing which immunotherapeutics have the greatest potential to synergise with TRT treatment.

In a similar vein, further analysis of both the mechanisms by which TRT interacts with the immune system and the key inhibitory factors limiting TRT responsiveness could also help inform potential therapeutic combinations. For example, given my data showing that TRT induces PD-L1 expression, determining whether this indeed contributes to radioresistance and the relevance of this in human patients is key to understanding the potential value of employing PD-L1 inhibitors alongside TRT. Evaluation of the TIME following combined TRT and anti-PDL1 treatment may also uncover any remaining barriers to the immune response that could be tackled using a third therapeutic. This is particularly important in light of pre-clinical evidence that radiotherapy with anti-PDL1 alone is insufficient to cause a significant response [323].

Similarly, further assessment of ICD may be important. Here, I have demonstrated the induction of ICD both through *in vitro* induction of the key molecular determinants of ICD, and *in vivo* via the gold standard vaccination-rechallenge assay. This work could be advanced by confirming the importance

of HMGB1 or calreticulin in inducing the vaccination response or in treatment of pre-established tumours via knockdown or knockout of these proteins in these treatment settings.

More generally, I have highlighted the ability of TRT to induce changes to the TIME but it would be of interest to identify whether this is important for the efficacy of [177Lu]PSMA-I&T treatment. Such assessment typically involves testing treatment efficacy in WT mice compared with immune depleted mice (for example using antibodies to deplete T cells), and may be an important next step.

6.3.2 Metastatic disease

One particular benefit of TRT over EBRT is the ability to target all tumour sites, meaning all metastatic sites are also treated. Importantly, there is accumulating evidence that treating multiple tumour sites may be key to inducing a systemic and long lasting anti-tumour immune response [25]. Investigating the immune response in a metastatic model is therefore another interesting avenue of future investigation.

6.3.3 Dose and timing

Another key consideration will be the dose and timing of any potential combinations. Given the time dependent changes observed in the TIME, this is likely to be crucial to success. Again, it will be important to follow this up with clinical observations to confirm that, if such changes are occurring, they are on the same time scale in humans. Another consideration for dosing is whether different dose or fractionation schedules would impact on the extent of immune activation. In particular, EBRT is most commonly administered in a fractionated dose schedule (2 Gy, >20 fractions), whilst [177Lu]PSMA-I&T is provided as multiple doses 6 weeks apart. The impact of multiple doses on the TIME changes is therefore unknown. The repeated doses may amplify the changes, or could result in further immune cell killing. Similarly assessing the effect of total dose may be interesting. There is evidence that lower doses may have greater impact at stimulating the immune system, so using the maximum tolerated dose when treating in combination with immunotherapeutics may not prove to be the most successful regimen. Notably, there are somewhat conflicting reports on this for EBRT and so further detailed investigations may be necessary [463].

6.3.4 Immune targets in PCa

In this work I assessed the correlation of various potential targets with outcomes for PCa patients. I conducted this analysis in the largest available dataset of human PCa, but in due course it would be advantageous to confirm my findings in independent cohorts of patients. This work also showed correlation of immune cells with markers they are thought to be modulated by. Importantly, this work shows correlation and does not confirm causation. The work thus identifies a potentially important area to focus on in the future. Further assessment of the contribution of these markers to immune cell accumulation could be conducted via both in vitro and in vivo analysis to advance our understanding of these changes and ascertain whether these correlations are due to direct effects. This may aid in the development of therapeutic combinations and dosing strategies using therapies targeting these immune factors.

6.3.5 Patient stratification

As highlighted in chapter 5, the TME also has a significant impact on the response of a patient to a therapeutic. This may be particularly important for immune-based therapies, given the often paradoxical effects of immune signalling wherein the same immunogenic pathways can have immune-stimulatory or suppressive effects depending on the circumstances. One clear example of this is IFN signalling [267], which we've demonstrated may be important in the immune response to TRT. As such, identifying biomarkers to enable selection of patients likely to respond to [177Lu]PSMA-I&T monotherapy or combination therapies will also be a key factor. My work also suggests that the immune response to TRT and EBRT differs, for example with the initial decline of immune cells following TRT, and the differing levels of IFN activity. It therefore may also be of interest in the future to be able to identify patients more likely to respond to one or the other based on these differences. This will require further evaluation of the differences in response to each radiation modality, as well as identification of biomarkers to enable patient stratification.

6.3.6 Immune cell sensitivity to [177Lu]PSMA-I&T

Our data revealed a significant decline in immune cells soon after TRT treatment, that was not observed following EBRT. As noted above, it is possible that this is due to differing chronology of events after the two treatments – and as such this will be important to investigate. However, it is also interesting to hypothesise that this may be due to differing radiosensitivity to TRT compared with EBRT, or due to the continued low dose irradiation preventing the re-population of the tumour with immune cells at early time points. As such, *in vitro* assessment of immune cell sensitivity to TRT provides another interesting area for future work.

6.3.7 Different radioisotopes, targeting moieties and indications

Finally, whilst I have looked specifically at [177Lu]PSMA-I&T in PCa, it is important to recognise that there are an increasingly large number of different radiopharmaceuticals in use in the clinic in various cancers. It will thus be of importance to determine if different radioisotopes and targeting moieties can exert similar effects. One particularly interesting avenue of investigation would be the effect of PSMA conjugated to an alpha emitter. Such therapeutics are currently undergoing pre-clinical and clinical testing, and are showing promising results [464–467]. Testing the immune effects of a different isotope using the same targeting agent, in the same model, provides an attractive opportunity to assess the impact of different types of radiation. Another interesting consideration is that it may be possible to further stimulate the immune system by using full antibodies as targeting moieties in order to maximise the immune activation by the antibody, or even employing immune activating TRT targets such as radiolabelled PD-L1 antagonists. It could also be of interest to see if the PSMA targeting moiety itself is contributing to changes in the TIME using PSMA-I&T with cold [177Lu], to see if any such effects can be improved or exploited. Finally, development of immune competent models to enable assessment of other radiopharmaceuticals such as [131I]MIBG will enable the application of similar work to a wider range of indications such as neuroblastoma.

6.3 Conclusion

In summary my work highlights the ability of TRT to interact with the immune system, demonstrating both immune cell changes in the TIME following treatment and potential mechanisms contributing to these changes, as well as possible mechanisms of immune-mediated radioresistance. This suggests that combination of immunotherapies with TRT could be an interesting avenue to explore. Ultimately, further work is required to better understand the details of this interaction, including the relative radiosensitivity of immune cells to TRT, the phenotype of different immune cells within the TIME following treatment, the mechanisms responsible for bringing about these changes, and the factors in the TIME limiting this response. However, my work provides valuable evidence that this area is worthy of further investigation and leads to an understanding of what now needs to be done in order to further advance the field.

References:

1. Connell PP, Hellman S (2009) Advances in radiotherapy and implications for the next century: A historical perspective. Cancer Res 69:383–392
2. Lomax ME, Folkes LK, O'Neill P (2013) Biological Consequences of Radiation-induced DNA Damage: Relevance to Radiotherapy. Clin Oncol 25:578–585
3. Boustani J, Grapin M, Laurent PA, Apetoh L, Mirjolet C (2019) The 6th R of radiobiology: Reactivation of anti-tumor immune response. Cancers (Basel) 11:1–16
4. Hanahan D, Weinberg RA, Pan KH, et al (2011) Hallmarks of Cancer: The Next Generation. Cell 144:646–674
5. Sharma RA, Plummer R, Stock JK, et al (2016) Clinical development of new drug-radiotherapy combinations. Nat Rev Clin Oncol 13:627–642
6. Goodfellow DR (1936) Radiation-Induced Lymphopenia. Br J Radiol 9:695–711
7. Campbell AC, Wiernik G, Wood J, Hersey P, Waller CA, Maclennan ICM (1976) Characteristics of the lymphopenia induced by radiotherapy.
8. Knaan-Shanzer S, Houben P, Kinwel-Bohré E, van Bekkum D (1991) Remission induction of adjuvant arthritis in rats by total body irradiation and autologous bone marrow transplantation. Bone Marrow Transplant 8:333–338
9. van Bekkum DW (1999) Effectiveness and risks of total body irradiation for conditioning in the treatment of autoimmune disease with autologous bone marrow transplantation. Rheumatology 38:757–761
10. Walle T, Martinez Monge R, Cerwenka A, Ajona D, Melero I, Lecanda F (2018) Radiation effects on antitumor immune responses: current perspectives and challenges. Ther Adv Med Oncol 10:1758834017742575
11. Goldsmith SJ (2020) Targeted Radionuclide Therapy: A Historical and Personal Review. Semin Nucl Med 50:87–97
12. Ewing J (1917) Radium therapy in cancer. J Am Med Assoc LXVIII:1238–1247
13. Cohen A, Cohen L (1953) Radiobiology of the C3H mouse mammary carcinoma: The effect of body dose on the radiocurability of the tumour treated in situ. Br J Cancer 7:452–455
14. Cohen A, Cohen L (1956) Radiobiology of the c3h mouse mammary carcinoma: Increased radiosensitivity of the tumour induced by inoculation of the host with radiationattenuated isografts. Br J Cancer 10:312–317
15. Slone HB, Peters LJ, Milas L (1979) Effect of host immune capability on radiocurability and subsequent transplantability of a murine fibrosarcoma. J Natl Cancer Inst 63:1229–1235
16. Suit HD, Kastelan A (1970) Immunologic status of host and response of a methylcholanthrene-induced sarcoma to local x-irradiation. Cancer 26:232–238
17. Hewitt HB, Blake ER, Walder AS (1976) A critique of the evidence for active host defence against cancer, based on personal studies of 27 murine tumours of spontaneous origin. Br J Cancer 33:241–259
18. Nobler MP (1969) The abscopal effect in malignant lymphoma and its relationship to lymphocyte circulation. Radiology 93:410–412
19. Ehlers G, Fridman M (1973) Abscopal effect of radiation in papillary adenocarcinoma. Br J Radiol 46:220–222
20. Kingsley DPE (1975) An interesting case of possible abscopal effect in malignant melanoma. Br J Radiol 48:863–866
21. Mole RH (1953) Whole body irradiation; radiobiology or medicine? Br J Radiol 26:234–241
22. Demaria S, Ng B, Devitt ML, Babb JS, Kawashima N, Liebes L, Formenti SC (2004) Ionizing radiation inhibition of distant untreated tumors (abscopal effect) is immune mediated. Int J Radiat Oncol Biol Phys 58:862–870
23. Stamell EF, Wolchok JD, Gnjatic S, Lee NY, Brownell I (2013) The abscopal effect associated with a systemic anti-melanoma immune response. Int J Radiat Oncol Biol Phys 85:293–295
24. Chakravarty PK, Alfieri A, Thomas EK, Beri V, Tanaka KE, Vikram B, Guha C (1999) Flt3-ligand administration after radiation therapy prolongs survival in a murine model of metastatic lung cancer.

Cancer Res 59:6028–32
25. Brooks ED, Chang JY (2019) Time to abandon single-site irradiation for inducing abscopal effects. Nat Rev Clin Oncol 16:123–135
26. Abuodeh Y, Venkat P, Kim S (2016) Systematic review of case reports on the abscopal effect. Curr Probl Cancer 40:25–37
27. Tseng YD, Nguyen MH, Baker K, et al (2018) Effect of patient immune status on the efficacy of radiation therapy and recurrence-free survival among 805 patients with merkel cell carcinoma. Int J Radiat Oncol Biol Phys 102:330–339
28. Postow MA, Callahan MK, Barker CA, et al (2012) Immunologic correlates of the abscopal effect in a patient with melanoma. N Engl J Med 366:925–931
29. Gutkin PM, Hiniker SM, Swetter SM, Reddy SA, Knox SJ (2018) Complete Response of Metastatic Melanoma to Local Radiation and Immunotherapy: 6.5 Year Follow-Up. Cureus 10:e3723
30. Lee Y, Auh SL, Wang YY, et al (2009) Therapeutic effects of ablative radiation on local tumor require CD8 + T cells: Changing strategies for cancer treatment. Blood 114:589–595
31. Takeshima T, Chamoto K, Wakita D, Ohkuri T, Togashi Y, Shirato H, Kitamura H, Nishimura T (2010) Local radiation therapy inhibits tumor growth through the generation of tumor-specific CTL: its potentiation by combination with Th1 cell therapy. Cancer Res 70:2697–706
32. Yoshimoto Y, Suzuki Y, Mimura K, et al (2014) Radiotherapy-induced anti-tumor immunity contributes to the therapeutic efficacy of irradiation and can be augmented by CTLA-4 blockade in a mouse model. PLoS One 9:92572
33. Chen DS, Mellman I (2013) Oncology Meets Immunology: The Cancer-Immunity Cycle. Immunity 39:1–10
34. Kanaseki T, Tokita S, Torigoe T (2019) Proteogenomic discovery of cancer antigens: Neoantigens and beyond. Pathol Int 69:511–518
35. Schumacher TN, Schreiber RD (2015) Neoantigens in cancer immunotherapy. Science 348:69–74
36. Ishak CA, Classon M, De Carvalho DD (2018) Deregulation of Retroelements as an Emerging Therapeutic Opportunity in Cancer. Trends in Cancer 4:583–597
37. Raposo B, Merky P, Lundqvist C, et al (2018) T cells specific for post-translational modifications escape intrathymic tolerance induction. Nat Commun 9:353
38. Coulie PG, Van den Eynde BJ, van der Bruggen P, Boon T (2014) Tumour antigens recognized by T lymphocytes: at the core of cancer immunotherapy. Nat Rev Cancer 14:135–146
39. Kim R, Emi M, Tanabe K (2007) Cancer immunoediting from immune surveillance to immune escape. Immunology 121:1–14
40. Kepp O, Tartour E, Vitale I, et al (2014) Consensus guidelines for the detection of immunogenic cell death. Oncoimmunology 3:11
41. Galluzzi L, Vitale I, Warren S, et al (2020) Consensus guidelines for the definition, detection and interpretation of immunogenic cell death. J Immunother Cancer 8:70
42. Kepp O, Senovilla L, Vitale I, et al (2014) Consensus guidelines for the detection of immunogenic cell death. Oncoimmunology 3:e955691
43. Obeid M, Panaretakis T, Joza N, Tufi R, Tesniere A, van Endert P, Zitvogel L, Kroemer G (2007) Calreticulin exposure is required for the immunogenicity of γ-irradiation and UVC light-induced apoptosis [5]. Cell Death Differ. https://doi.org/10.1038/sj.cdd.4402201
44. Gardai SJ, McPhillips KA, Frasch SC, Janssen WJ, Starefeldt A, Murphy-Ullrich JE, Bratton DL, Oldenborg P-A, Michalak M, Henson PM (2005) Cell-Surface Calreticulin Initiates Clearance of Viable or Apoptotic Cells through trans-Activation of LRP on the Phagocyte. Cell 123:321–334
45. Apetoh L, Ghiringhelli F, Tesniere A, et al (2007) Toll-like receptor 4-dependent contribution of the immune system to anticancer chemotherapy and radiotherapy. Nat Med 13:1050–1059
46. H Y, HS H, K P, et al (2010) A critical cysteine is required for HMGB1 binding to Toll-like receptor 4 and activation of macrophage cytokine release. Proc Natl Acad Sci U S A 107:11942–11947
47. Delamarre L, Couture R, Mellman I, Trombetta ES (2006) Enhancing immunogenicity by limiting susceptibility to lysosomal proteolysis. J Exp Med 203:2049–55
48. Michaud G, Martins I, Sukkurwala A, Adjemian S, Ma Y, Pellegatti P, Shen S, Kepp O, Scoazec O, Mignot G, Rello-Varona S, Tailler M, Menger L, Vacchelli E, Galluzz L KG (2011) Autophagy-Dependent anticancer immune responses induced by chemotherapeutic agents in mice. Science (80-) 334:1573–1577
49. Ghiringhelli F, Apetoh L, Tesniere A, et al (2009) Activation of the NLRP3 inflammasome in dendritic cells induces IL-1β–dependent adaptive immunity against tumors. Nat Med 15:1170–1178

50. Surace L, Lysenko V, Fontana AO, et al (2015) Complement Is a Central Mediator of Radiotherapy-Induced Tumor-Specific Immunity and Clinical Response. Immunity 42:767–777
51. Li K, Sacks SH, Zhou W (2007) The relative importance of local and systemic complement production in ischaemia, transplantation and other pathologies. Mol Immunol 44:3866–3874
52. Peng Q, Li K, Wang N, Li Q, Asgari E, Lu B, Woodruff TM, Sacks SH, Zhou W (2009) Dendritic Cell Function in Allostimulation Is Modulated by C5aR Signaling. J Immunol 183:6058–6068
53. Strainic MG, Liu J, Huang D, An F, Lalli PN, Muqim N, Shapiro VS, Dubyak GR, Heeger PS, Medof ME (2008) Locally Produced Complement Fragments C5a and C3a Provide Both Costimulatory and Survival Signals to Naive CD4+ T Cells. Immunity 28:425
54. Liszewski MK, Kolev M, Le Friec G, et al (2013) Intracellular complement activation sustains T cell homeostasis and mediates effector differentiation. Immunity 39:1143–57
55. Strainic MG, Shevach EM, An F, Lin F, Medof ME (2013) Absence of signaling into $CD4^+$ cells via C3aR and C5aR enables autoinductive TGF-β1 signaling and induction of $Foxp3^+$ regulatory T cells. Nat Immunol 14:162–71
56. Akashi M, Hachiya M, Koeffler HP, Suzuki G (1992) Irradiation increases levels of GM-CSF through RNA stabilization which requires an AU-rich region in cancer cells. Biochem Biophys Res Commun 189:986–93
57. Ao X, Zhao L, Davis MA, Lubman DM, Lawrence TS, Kong F-M (2009) Radiation produces differential changes in cytokine profiles in radiation lung fibrosis sensitive and resistant mice. J Hematol Oncol 2:6
58. Van der Meeren A, Monti P, Vandamme M, Squiban C, Wysocki J, Griffiths N (2005) Abdominal radiation exposure elicits inflammatory responses and abscopal effects in the lungs of mice. Radiat Res 163:144–152
59. Kim J-Y, Son Y-O, Park S-W, Bae J-H, Chung JS, Kim HH, Chung B-S, Kim S-H, Kang C-D (2006) Increase of NKG2D ligands and sensitivity to NK cell-mediated cytotoxicity of tumor cells by heat shock and ionizing radiation. Exp Mol Med 38:474–484
60. Li A, Yi M, Qin S, Song Y, Chu Q, Wu K (2019) Activating cGAS-STING pathway for the optimal effect of cancer immunotherapy. J Hematol Oncol 12:35
61. Ramanjulu JM, Pesiridis GS, Yang J, et al (2018) Design of amidobenzimidazole STING receptor agonists with systemic activity. Nature 564:439–443
62. Deng L, Liang H, Xu M, et al (2014) STING-dependent cytosolic DNA sensing promotes radiation-induced type I interferon-dependent antitumor immunity in immunogenic tumors. Immunity 41:543–852
63. Gekara NO (2017) DNA damage-induced immune response: Micronuclei provide key platform. J Cell Biol 216:2999–3001
64. Härtlova A, Erttmann SF, Raffi FA, et al (2015) DNA damage primes the Type I Interferon system via the cytosolic DNA sensor STING to promote anti-microbial innate immunity. Immunity 42:332–343
65. Mackenzie KJ, Carroll P, Martin C-A, et al (2017) cGAS surveillance of micronuclei links genome instability to innate immunity. Nature 548:461–465
66. Harding SM, Benci JL, Irianto J, Discher DE, Minn AJ, Greenberg RA (2017) Mitotic progression following DNA damage enables pattern recognition within micronuclei. Nature 548:466–470
67. Bartsch K, Knittler K, Borowski C, et al (2017) Absence of RNase H2 triggers generation of immunogenic micronuclei removed by autophagy. Hum Mol Genet 26:3960–3972
68. Lugade AA, Moran JP, Gerber SA, Rose RC, Frelinger JG, Lord EM (2005) Local radiation therapy of B16 melanoma tumors increases the generation of tumor antigen-specific effector cells that traffic to the tumor. J Immunol 174:7516–7523
69. Burnette BC, Liang H, Lee Y, Chlewicki L, Khodarev NN, Weichselbaum RR, Fu YX, Auh SL (2011) The efficacy of radiotherapy relies upon induction of type I interferon-dependent innate and adaptive immunity. Cancer Res 71:2488–2496
70. Vanpouille-Box C, Formenti SC, Demaria S (2017) TREX1 dictates the immune fate of irradiated cancer cells.
71. Benci JL, Xu B, Qiu Y, et al (2016) Tumor Interferon Signaling Regulates a Multigenic Resistance Program to Immune Checkpoint Blockade. Cell 167:1540-1554.e12
72. Liang H, Deng L, Hou Y, et al (2017) Host STING-dependent MDSC mobilization drives extrinsic radiation resistance. Nat Commun 8:1736
73. Post AEM, Smid M, Nagelkerke A, Martens JWM, Bussink J, Sweep FCGJ, Span PN (2018) Interferon-stimulated genes are involved in cross-resistance to radiotherapy in tamoxifen-resistant breast cancer. Clin Cancer Res 24:3397–3408

74. Klug F, Prakash H, Huber PE, et al (2013) Low-Dose irradiation programs macrophage differentiation to an iNOS+/M1 phenotype that orchestrates effective T Cell immunotherapy. Cancer Cell 24:589–602
75. Zhang T, Yu H, Ni C, et al (2017) Hypofractionated stereotactic radiation therapy activates the peripheral immune response in operable stage I non-small-cell lung cancer. Sci Rep 7:4866
76. Matsumura S, Wang B, Kawashima N, et al (2008) Radiation-induced CXCL16 release by breast cancer cells attracts effector T cells. J Immunol 181:3099–107
77. Lim JYH, Gerber S a, Murphy SP, Lord EM (2014) Type I interferons induced by radiation therapy mediate recruitment and effector function of CD8(+) T cells. Cancer Immunol Immunother 63:259–71
78. Hicklin DJ, Marincola FM, Ferrone S (1999) HLA class I antigen downregulation in human cancers: T-cell immunotherapy revives an old story. Mol Med Today 5:178–186
79. Garrido F, Aptsiauri N, Doorduijn EM, Garcia Lora AM, van Hall T (2016) The urgent need to recover MHC class I in cancers for effective immunotherapy. Curr Opin Immunol 39:44–51
80. Johnsen A, Templeton D, Sy M, Harding C (1999) Deficiency of Transporter for Antigen Presentation (TAP) in Tumor Cells Allows Evasion of Immune Surveillance and Increases Tumorigenesis. J Immunol 156:4182–90
81. Rotem-Yehudar R, Groettrup M, Soza A, Kloetzel PM, Ehrlich R (1996) LMP-associated proteolytic activities and TAP-dependent peptide transport for class 1 MHC molecules are suppressed in cell lines transformed by the highly oncogenic adenovirus 12. J Exp Med 183:499–514
82. Pasche B (2001) Role of transforming growth factor beta in cancer. J Cell Physiol 186:153–168
83. Sotomayor EM, Fu YX, Lopez-Cepero M, Herbert L, Jimenez JJ, Albarracin C, Lopez DM (1991) Role of tumor-derived cytokines on the immune system of mice bearing a mammary adenocarcinoma: II. Down-regulation of macrophage-mediated cytotoxicity by tumor-derived granulocyte-macrophage colony-stimulating factor. J Immunol 147:2816–2823
84. Morisada M, Moore EC, Hodge R, Friedman J, Cash HA, Hodge JW, Mitchell JB, Allen CT (2017) Dose-dependent enhancement of T-lymphocyte priming and CTL lysis following ionizing radiation in an engineered model of oral cancer. Oral Oncol 71:87–94
85. Reits EA, Hodge JW, Herberts CA, et al (2006) Radiation modulates the peptide repertoire, enhances MHC class I expression, and induces successful antitumor immunotherapy. J Exp Med 203:1259–1271
86. Lhuillier C, Rudqvist N-P, Elemento O, Formenti SC, Demaria S (2019) Radiation therapy and anti-tumor immunity: exposing immunogenic mutations to the immune system. Genome Med 11:40
87. Tsai CS, Chen FH, Wang CC, Huang HL, Jung SM, Wu CJ, Lee CC, McBride WH, Chiang CS, Hong JH (2007) Macrophages from irradiated tumors E=express higher levels of iNOS, Arginase-I and COX-2, andpromote tumor growth. Int J Radiat Oncol Biol Phys 68:499–507
88. Xu J, Escamilla J, Mok S, David J, Priceman S, West B, Bollag G, McBride W, Wu L (2013) CSFR1 signaling blockade stanches tumor-infiltrating myeloid cells and improves the efficacy of radiotherapy in prostate cancer. Cancer Res 73:2782–2794
89. Kalbasi A, Komar C, Tooker GM, Liu M, Lee JW, Gladney WL, Ben-Josef E, Beatty GL (2017) Tumor-derived CCL2 mediates resistance to radiotherapy in pancreatic ductal adenocarcinoma. Clin Cancer Res 23:137–148
90. Melsens E, Verberckmoes B, Rosseel N, Vanhove C, Descamps B, Pattyn P, Ceelen W (2017) The VEGFR inhibitor cediranib improves the efficacy of fractionated radiotherapy in a colorectal cancer xenograft model. Eur Surg Res 58:95–108
91. Golden EB, Frances D, Pellicciotta I, Demaria S, Helen Barcellos-Hoff M, Formenti SC (2014) Radiation fosters dose-dependent and chemotherapy-induced immunogenic cell death. Oncoimmunology 3:28518
92. Jobling MF, Mott JD, Finnegan MT, et al (2006) Isoform-specific activation of latent transforming growth factor β (LTGF-β) by reactive oxygen species. Radiat Res 166:839–848
93. Fridlender ZG, Sun J, Kim S, Kapoor V, Cheng G, Ling L, Worthen GS, Albelda SM (2009) Polarization of tumor-associated neutrophil phenotype by TGF-β: “N1” versus “N2” TAN. Cancer Cell 16:183–194
94. Tanaka H, Shinto O, Yashiro M, Yamazoe S, Iwauchi T, Muguruma K, Kubo N, Ohira M, Hirakawa K (2010) Transforming growth factor β signaling inhibitor, SB-431542, induces maturation of dendritic cells and enhances anti-tumor activity. Oncol Rep 24:1637–43
95. Kachikwu EL, Iwamoto KS, Liao YP, Demarco JJ, Agazaryan N, Economou JS, McBride WH, Schaue D (2011) Radiation enhances regulatory T cell representation. Int J Radiat Oncol Biol Phys 81:1128–1135
96. Lan J, Li R, Yin L-M, et al (2018) Targeting Myeloid-derived Suppressor Cells and Programmed Death Ligand 1 Confers Therapeutic Advantage of Ablative Hypofractionated Radiation Therapy Compared With Conventional Fractionated Radiation Therapy. Int J Radiat Oncol 101:74–87

97. Tu L, Guan R, Yang H, Zhou Y, Hong W, Ma L, Zhao G, Yu M (2019) Assessment of the expression of the immune checkpoint molecules PD-1, CTLA4, TIM-3 and LAG-3 across different cancers in relation to treatment response, tumor-infiltrating immune cells and survival. Int J Cancer ijc.32785
98. Dovedi SJ, Cheadle EJ, Popple AL, et al (2017) Fractionated radiation therapy stimulates antitumor immunity mediated by both resident and infiltrating polyclonal T-cell populations when combined with PD-1 blockade. Clin Cancer Res 23:5514–5526
99. Derer A, Spiljar M, Bäumler M, Hecht M, Fietkau R, Frey B, Gaipl US (2016) Chemoradiation increases PD-L1 expression in certain melanoma and glioblastoma cells. Front Immunol 7:610
100. Hertz S, Roberts A, Evans RD (1938) Radioactive Iodine as an Indicator in the Study of Thyroid Physiology. Proc Soc Exp Biol Med 38:510–516
101. SEIDLIN SM, OSHRY E, YALOW AA (1948) Spontaneous and experimentally induced uptake of radioactive iodine in metastases from thyroid carcinoma; a preliminary report. J Clin Endocrinol Metab 8:423–432
102. Liepe K, Kropp J, Runge R, Kotzerke J (2003) Therapeutic efficiency of rhenium-188-HEDP in human prostate cancer skeletal metastases. Br J Cancer 89:625–629
103. Furubayashi N, Negishi T, Ura S, Hirai Y, Nakamura M (2015) Palliative effects and adverse events of strontium-89 for prostate cancer patients with bone metastasis. Mol Clin Oncol 3:257–263
104. Li S, Liu J, Zhang H, Tian M, Wang J, Zheng X (2001) Rhenium-188 HEDP to treat painful bone metastases. Clin Nucl Med 26:919–922
105. Tennvall J, Brans B (2007) EANM procedure guideline for 32 P phosphate treatment of myeloproliferative diseases. https://doi.org/10.1007/s00259-007-0407-4
106. Kubo M, Satoh T, Ishiyama H, et al (2018) Enhanced activated T cell subsets in prostate cancer patients receiving iodine-125 low-dose-rate prostate brachytherapy. Oncol Rep 39:417–424
107. Keam SP, Caramia F, Gamell C, Paul PJ, Arnau GM, Neeson PJ, Williams SG, Haupt Y (2018) The transcriptional landscape of radiation-treated human prostate cancer: Analysis of a prospective tissue cohort. Int J Radiat Oncol Biol Phys 100:188–198
108. Hodge JW, Sharp HJ, Gameiro SR (2012) Abscopal regression of antigen disparate tumors by antigen cascade after systemic tumor vaccination in combination with local tumor radiation. Cancer Biother Radiopharm 27:12–22
109. Eric A, Juranic Z, Tisma N, Plesinac V, Borojevic N, Jovanovic D, Milovanovic Z, Gavrilovic D, Ilic B (2009) Radiotherapy-induced changes of peripheral blood lymphocyte subpopulations in cervical cancer patients: Relationship to clinical response. J. Balk. Union Oncol. 14:
110. Morris ZS, Guy EI, Werner LR, et al (2018) Tumor-Specific Inhibition of In Situ Vaccination by Distant Untreated Tumor Sites . Cancer Immunol Res 6:825–834
111. Heylmann D, Rödel F, Kindler T, Kaina B (2014) Radiation sensitivity of human and murine peripheral blood lymphocytes, stem and progenitor cells. Biochim Biophys Acta - Rev Cancer 1846:121–129
112. Garnett CT, Palena C, Chakarborty M, Tsang K-YY, Schlom J, Hodge JW, Hodge JW (2004) Sublethal irradiation of human tumor cells modulates phenotype resulting in enhanced killing by cytotoxic T lymphocytes. Cancer Res 64:7985–7994
113. Chakraborty M, Wansley EK, Carrasquillo JA, Yu S, Paik CH, Camphausen K, Becker MD, Goeckeler WF, Schlom J, Hodge JW (2008) The use of chelated radionuclide (samarium-153-ethylenediaminetetramethylenephosphonate) to modulate phenotype of tumor cells and enhance T cell-mediated killing. Clin Cancer Res 14:4241–9
114. Malamas AS, Gameiro SR, Knudson KM, Hodge JW (2016) Sublethal exposure to alpha radiation (223Ra dichloride) enhances various carcinomas sensitivity to lysis by antigen-specific cytotoxic T lymphocytes through calreticulin-mediated immunogenic modulation. Oncotarget 7:86937–86947
115. Ghodadra A, Bhatt S, Camacho JC, Kim HS (2016) Abscopal effects and Yttrium-90 radioembolization. Cardiovasc Intervent Radiol 39:1076–1080
116. Kwee SA, Lim J, Coel MN (2017) Soft tissue response on 18F-fluorocholine PET/CT in metastatic castrate-resistant prostate cancer treated with 223Ra-dichloride: A possible abscopal effect? Clin Nucl Med 42:868–871
117. Poon DMC, Wong KCW (2018) Lymph node response in a patient with metastatic castration-resistant prostate cancer treated with Radium-223. Clin Genitourin Cancer 16:e397–e401
118. Chew V, Lee YH, Pan L, et al (2018) Immune activation underlies a sustained clinical response to Yttrium-90 radioembolisation in hepatocellular carcinoma. Gut 1–12
119. Gorin J-B, Ménager J, Gouard S, et al (2014) Antitumor Immunity Induced after α Irradiation. Neoplasia 16:319–328

120. Hernandez R, Walker KL, Grudzinski JJ, et al (2019) 90Y-NM600 targeted radionuclide therapy induces immunologic memory in syngeneic models of T-cell Non-Hodgkin's Lymphoma. Commun Biol 2:79
121. Wu Y, Pfeifer A, Myschetzky R, Garbyal R, Rasmussen P, Knigge U, Bzorek M, Kristensen M, Kjaer A (2013) Induction of anti-tumor immune responses by peptide receptor radionuclide therapy with 177Lu-dotatate in a murine model of a human neuroendocrine tumor. Diagnostics 3:344–355
122. Mukai T, Maeda Y, Tamura T, Matsuoka M, Tsukamoto Y, Makino M (2009) Induction of cross-priming of naive CD8 + T lymphocytes by recombinant Bacillus Calmette-Guérin that secretes heat shock protein 70-major membrane protein-II fusion protein. J Immunol 183:6561–6568
123. Oizumi S, Strbo N, Pahwa S, Deyev V, Podack ER (2007) Molecular and cellular requirements for enhanced antigen cross-presentation to CD8 cytotoxic T lymphocytes. J Immunol 179:2310–2317
124. Chao Y, Xu L, Liang C, Feng L, Xu J, Dong Z, Tian L, Yi X, Yang K, Liu Z (2018) Combined local immunostimulatory radioisotope therapy and systemic immune checkpoint blockade imparts potent antitumour responses. Nat Biomed Eng 2:611–621
125. Confino H, Schmidt M, Efrati M, Hochman I, Umansky V, Kelson I, Keisari Y (2016) Inhibition of mouse breast adenocarcinoma growth by ablation with intratumoral alpha-irradiation combined with inhibitors of immunosuppression and CpG. Cancer Immunol Immunother 65:1149–1158
126. Ménager J, Gorin JB, Maurel C, et al (2015) Combining α-radioimmunotherapy and adoptive T cell therapy to potentiate tumor destruction. PLoS One 10:e0130249
127. Gorin JB, Ménager J, Gouard S, et al (2014) Antitumor immunity induced after α irradiation. Neoplasia (United States) 16:319–328
128. Keam SP, Gulati T, Gamell C, Caramia F, Huang C, Schittenhelm RB, Kleifeld O, Neeson PJ, Haupt Y, Williams SG (2018) Exploring the oncoproteomic response of human prostate cancer to therapeutic radiation using data-independent acquisition (DIA) mass spectrometry. Prostate 78:563–575
129. Kubo M, Satoh T, Ishiyama H, et al (2018) Enhanced activated T cell subsets in prostate cancer patients receiving iodine-125 low-dose-rate prostate brachytherapy. Oncol Rep 39:417–424
130. Chao Y, Xu L, Liang C, Feng L, Xu J, Dong Z, Tian L, Yi X, Yang K, Liu Z (2018) Combined local immunostimulatory radioisotope therapy and systemic immune checkpoint blockade imparts potent antitumour responses. Nat Biomed Eng 2:611–621
131. Domankevich V, Cohen A, Efrati M, Schmidt M, Rammensee HG, Nair SS, Tewari A, Kelson I, Keisari Y (2019) Combining alpha radiation-based brachytherapy with immunomodulators promotes complete tumor regression in mice via tumor-specific long-term immune response. Cancer Immunol Immunother 68:1949–1958
132. Domankevich V, Efrati M, Schmidt M, et al (2020) RIG-1-Like Receptor Activation Synergizes With Intratumoral Alpha Radiation to Induce Pancreatic Tumor Rejection, Triple-Negative Breast Metastases Clearance, and Antitumor Immune Memory in Mice. Front Oncol 10:990
133. Choi J, Beaino W, Fecek RJ, Fabian KPL, Laymon CM, Kurland BF, Storkus WJ, Anderson CJ (2018) Combined VLA-4–targeted radionuclide therapy and immunotherapy in a mouse model of melanoma. J Nucl Med 59:1843–1849
134. Chen H, Zhao L, Fu K, et al (2019) Integrin αvβ3-targeted radionuclide therapy combined with immune checkpoint blockade immunotherapy synergistically enhances anti-tumor efficacy. Theranostics 9:7948–7960
135. Kim W, Le TM, Wei L, et al (2016) [18F]CFA as a clinically translatable probe for PET imaging of deoxycytidine kinase activity. Proc Natl Acad Sci U S A 113:4027–4032
136. Danaher P, Warren S, Dennis L, D'Amico L, White A, Disis ML, Geller MA, Odunsi K, Beechem J, Fling SP (2017) Gene expression markers of Tumor Infiltrating Leukocytes. J Immunother Cancer. https://doi.org/10.1186/s40425-017-0215-8
137. Demaria S, Ng B, Devitt ML, Babb JS, Kawashima N, Liebes L, Formenti SC (2004) Ionizing radiation inhibition of distant untreated tumors (abscopal effect) is immune mediated. Int J Radiat Oncol 58:862–870
138. Gutkin PM, Hiniker SM, Swetter SM, Reddy SA, Knox SJ (2018) Complete response of metastatic melanoma to local radiation and immunotherapy: 6.5 year follow-up. Cureus. https://doi.org/10.7759/cureus.3723
139. Golden EB, Chhabra A, Chachoua A, et al (2015) Local radiotherapy and granulocyte-macrophage colony-stimulating factor to generate abscopal responses in patients with metastatic solid tumours: a proof-of-principle trial. Lancet Oncol 16:795–803
140. Dewan MZ, Galloway AE, Kawashima N, Dewyngaert JK, Babb JS, Formenti SC, Demaria S (2009) Fractionated but not single-dose radiotherapy induces an immune-mediated abscopal effect when

combined with anti-CTLA-4 antibody. Clin Cancer Res 15:5379–5388
141. Wieland DM, Wu J, Brown LE, Mangner TJ, Swanson DP (1979) Radiolabeled Adrenergic Neuron-Blocking Agents : AdrenomeduDary Imaging with [1311] Iodobenzylguanidine. 21:349–354
142. Matthay KK, DeSantes K, Hasegawa B, Huberty J, Hattner RS, Ablin A, Reynolds CP, Seeger RC, Weinberg VK, Price D (1998) Phase I dose escalation of 131I-metaiodobenzylguanidine with autologous bone marrow support in refractory neuroblastoma. J Clin Oncol 16:229–236
143. Matthay KK, Yanik G, Messina J, et al (2007) Phase II study on the effect of disease sites, age, and prior therapy on response to iodine-131-metaiodobenzylguanidine therapy in refractory neuroblastoma. J Clin Oncol 25:1054–1060
144. de Kraker J, Hoefnagel KA, Verschuur AC, van Eck B, van Santen HM, Caron HN (2008) Iodine-131-metaiodobenzylguanidine as initial induction therapy in stage 4 neuroblastoma patients over 1 year of age. Eur J Cancer 44:551–556
145. Silver DA, Pellicer I, Fair WR, Heston WD, Cordon-Cardo C (1997) Prostate-specific membrane antigen expression in normal and malignant human tissues. Clin Cancer Res 3:81–5
146. Kawakami M, Nakayama J (1997) Enhanced expression of prostate-specific membrane antigen gene in prostate cancer as revealed by in situ hybridization. Cancer Res 57:2321–4
147. Bostwick DG, Pacelli A, Blute M, Roche P, Murphy GP (1998) Prostate specific membrane antigen expression in prostatic intraepithelial neoplasia and adenocarcinoma: a study of 184 cases. Cancer 82:2256–61
148. Yadav MP, Ballal S, Tripathi M, Damle NA, Sahoo RK, Seth A, Bal C (2017) 177Lu-DKFZ-PSMA-617 therapy in metastatic castration resistant prostate cancer: safety, efficacy, and quality of life assessment. Eur J Nucl Med Mol Imaging 44:81–91
149. Demir M, Abuqbeitah M, Uslu-Beşli L, Yıldırım Ö, Yeyin N, Çavdar İ, Vatankulu B, Gündüz H, Kabasakal L (2016) Evaluation of radiation safety in ^{177} Lu-PSMA therapy and development of outpatient treatment protocol. J Radiol Prot 36:269–278
150. Rahbar K, Ahmadzadehfar H, Kratochwil C, et al (2017) German Multicenter Study Investigating ^{177} Lu-PSMA-617 Radioligand Therapy in Advanced Prostate Cancer Patients. J Nucl Med 58:85–90
151. Hofman MS, Violet J, Hicks RJ, et al (2018) [177Lu]-PSMA-617 radionuclide treatment in patients with metastatic castration-resistant prostate cancer (LuPSMA trial): a single-centre, single-arm, phase 2 study. Lancet Oncol 19:825–833
152. Czerwińska M, Bilewicz A, Kruszewski M, Wegierek-Ciuk A, Lankoff A (2020) Targeted Radionuclide Therapy of Prostate Cancer-From Basic Research to Clinical Perspectives. Molecules. https://doi.org/10.3390/molecules25071743
153. Benesová M, Schäfer M, Bauder-Wüst U, Afshar-Oromieh A, Kratochwil C, Mier W, Haberkorn U, Kopka K, Eder M (2015) Preclinical evaluation of a tailor-made DOTA-conjugated PSMA inhibitor with optimized linker moiety for imaging and endoradiotherapy of prostate cancer. J Nucl Med 56:914–920
154. Harris W, Mostaghel EA, Nelson PS, Montgomery B (2009) Androgen deprivation therapy: progress in understanding mechanisms of resistance and optimizing androgen depletion. Nat Clin Pr Urol 6:76–85
155. Wright GL, Grob BM, Haley C, Grossman K, Newhall K, Petrylak D, Troyer J, Konchuba A, Schellhammer PF, Moriarty R (1996) Upregulation of prostate-specific membrane antigen after androgen- deprivation therapy. Urology 48:326–334
156. Evans MJ, Smith-Jones PM, Wongvipat J, Navarro V, Kim S, Bander NH, Larson SM, Sawyers CL (2011) Noninvasive measurement of androgen receptor signaling with a positron-emitting radiopharmaceutical that targets prostate-specific membrane antigen. Proc Natl Acad Sci U S A 108:9578–9582
157. Vaz S, Hadaschik B, Gabriel M, Herrmann K, Eiber M, Costa D (2020) Influence of androgen deprivation therapy on PSMA expression and PSMA-ligand PET imaging of prostate cancer patients. Eur J Nucl Med Mol Imaging 47:9–15
158. Kantoff PW, Higano CS, Shore ND, et al (2010) Sipuleucel-T immunotherapy for castration-resistant prostate cancer. N Engl J Med 363:411–422
159. Fay EK, Graff JN (2020) Immunotherapy in Prostate Cancer. Cancers (Basel). https://doi.org/10.3390/cancers12071752
160. Strasner A, Karin M (2015) Immune infiltration and prostate cancer. Front Oncol 5:128
161. Sfanos KS, Bruno TC, Maris CH, Xu L, Thoburn CJ, DeMarzo AM, Meeker AK, Isaacs WB, Drake CG (2008) Phenotypic analysis of prostate-infiltrating lymphocytes reveals TH17 and Treg skewing. Clin Cancer Res 14:3254–61
162. Zhang H, Huang R, Cheung N-K V, Guo H, Zanzonico PB, Thaler HT, Lewis JS, Blasberg RG (2014) Imaging

the norepinephrine transporter in neuroblastoma: a comparison of [18F]-MFBG and 123I-MIBG. Clin Cancer Res 20:2182–91
163. Batra V, Makvandi M, Zuppa AF, Patel N, Elias J, Pryma DA, Maris JM (2017) Dexmedetomidine does not interfere with meta-iodobenzylguanidine (MIBG) uptake at clinically relevant concentrations. Pediatr Blood Cancer 64:e26268
164. Pellegrino MJ, Parrish DC, Zigmond RE, Habecker BA (2011) Cytokines inhibit norepinephrine transporter expression by decreasing Hand2. Mol Cell Neurosci 46:671–80
165. McCluskey AG, Boyd M, Ross SC, Cosimo E, Clark AM, Angerson WJ, Gaze MN, Mairs RJ (2005) [131I]meta-iodobenzylguanidine and topotecan combination treatment of tumors expressing the noradrenaline transporter. Clin Cancer Res 11:7929–37
166. Mairs RJ, Russell J, Cunningham S, O'donoghue JA, Gaze MN, Owens J, Vaidyanathan G, Zalutsky MR (1995) Enhanced Tumour Uptake and In Vitro Radiotoxicity of No-carrier-added [1311] Meta-iodobenzylguanidine: Implications for the Targeted Radiotherapy of Neuroblastoma.
167. Accorsi R, Morowitz MJ, Charron M, Maris JM (2003) Pinhole imaging of 131 I-metaiodobenzylguanidine (131 I-MIBG) in an animal model of neuroblastoma. Pediatr Radiol 33:688–692
168. Masic S, Seo Y, Gao D-W, et al (2008) 123I-MIBG SPECT/CT and 18F-FDG PET in vivo imaging of the TH-MYCN neuroblastoma transgenic mouse. Cancer Res. 68:
169. Kroesen M, Nierkens S, Ansems M, Wassink M, Orentas RJ, Boon L, den Brok MH, Hoogerbrugge PM, Adema GJ (2014) A transplantable TH-MYCN transgenic tumor model in C57Bl/6 mice for preclinical immunological studies in neuroblastoma. Int J Cancer 134:1335–1345
170. Lückerath K, Stuparu AD, Wei L, et al (2018) Detection threshold and reproducibility of68Ga-PSMA11 PET/CT in a mouse model of prostate cancer. J Nucl Med jnumed.118.207704
171. Fendler WP, Stuparu AD, Evans-Axelsson S, et al (2017) Establishing 177 Lu-PSMA-617 radioligand therapy in a syngeneic model of murine prostate cancer. J Nucl Med 58:1786–1792
172. Fendler WP, Stuparu AD, Evans-Axelsson S, et al (2017) Establishing 177 Lu-PSMA-617 radioligand therapy in a syngeneic model of murine prostate cancer. J Nucl Med 58:1786–1792
173. Chatalic KLS, Heskamp S, Konijnenberg M, et al (2016) Towards Personalized Treatment of Prostate Cancer: PSMA I&T, a Promising Prostate-Specific Membrane Antigen-Targeted Theranostic Agent. Theranostics 6:849–861
174. Wirtz M, Schmidt A, Schottelius M, Robu S, Günther T, Schwaiger M, Wester HJ (2018) Synthesis and in vitro and in vivo evaluation of urea-based PSMA inhibitors with increased lipophilicity. EJNMMI Res 8:84
175. Vaidyanathan G, Zalutsky MR (2001) The development of meta-iodobenzylguanidine analogues for the therapy of neuroendocrine and other tumours. In: Ther. Appl. Radiopharm. pp 292–300
176. Vaidyanathan G, Friedman HS, Keir ST, Zalutsky MR (1996) Localisation of [131I]MIBG in nude mice bearing SK-N-SH human neuroblastoma xenografts: Effect of specific activity. Br J Cancer 73:1171–1177
177. Rutgers M, Buitenhuis CKM, Hoefnagel CA, Voûte PA, Smets LA (2000) Targeting of meta-iodobenzylguanidine to SK-N-SH human neuroblastoma xenografts: Tissue distribution, metabolism and therapeutic efficacy. Int J Cancer 87:412–422
178. Chen X, Werner RA, Lapa C, Nose N, Hirano M, Javadi MS, Robinson S, Higuchi T (2018) Subcellular storage and release mode of the novel 18F-labeled sympathetic nerve PET tracer LMI1195. EJNMMI Res 8:12
179. Yanik GA, Parisi MT, Shulkin BL, et al (2013) Semiquantitative mIBG scoring as a prognostic indicator in patients with stage 4 neuroblastoma: a report from the Children's oncology group. J Nucl Med 54:541–8
180. Kelly JM, Amor-Coarasa A, Ponnala S, Nikolopoulou A, Williams C, Thiele NA, Schlyer D, Wilson JJ, DiMagno SG, Babich JW (2019) A Single Dose of ^{225} Ac-RPS-074 Induces a Complete Tumor Response in an LNCaP Xenograft Model. J Nucl Med 60:649–655
181. Kelly JM, Amor-Coarasa A, Ponnala S, Nikolopoulou A, Williams C, DiMagno SG, Babich JW (2019) Albumin-Binding PSMA Ligands: Implications for Expanding the Therapeutic Window. J Nucl Med 60:656–663
182. Kelly JM, Amor-Coarasa A, Nikolopoulou A, et al (2017) Dual-Target Binding Ligands with Modulated Pharmacokinetics for Endoradiotherapy of Prostate Cancer. J Nucl Med 58:1442–1449
183. Kuo H-T, Merkens H, Zhang Z, Uribe CF, Lau J, Zhang C, Colpo N, Lin K-S, Bénard F (2018) Enhancing Treatment Efficacy of ^{177} Lu-PSMA-617 with the Conjugation of an Albumin-Binding Motif: Preclinical

Dosimetry and Endoradiotherapy Studies. Mol Pharm 15:5183–5191
184. Benešová M, Schäfer M, Bauder-Wüst U, Afshar-Oromieh A, Kratochwil C, Mier W, Haberkorn U, Kopka K, Eder M (2015) Preclinical evaluation of a tailor-made DOTA-conjugated PSMA inhibitor with optimized linker moiety for imaging and endoradiotherapy of prostate cancer. J Nucl Med 56:914–20
185. Weineisen M, Schottelius M, Simecek J, et al (2015) 68Ga- and 177Lu-Labeled PSMA I&T: Optimization of a PSMA-Targeted Theranostic Concept and First Proof-of-Concept Human Studies. J Nucl Med 56:1169–1176
186. Hillier SM, Maresca KP, Lu G, Merkin RD, Marquis JC, Zimmerman CN, Eckelman WC, Joyal JL, Babich JW (2013) 99mTc-Labeled Small-Molecule Inhibitors of Prostate-Specific Membrane Antigen for Molecular Imaging of Prostate Cancer. J Nucl Med 54:1369–1376
187. Hillier SM, Maresca KP, Femia FJ, et al (2009) Preclinical Evaluation of Novel Glutamate-Urea-Lysine Analogues That Target Prostate-Specific Membrane Antigen as Molecular Imaging Pharmaceuticals for Prostate Cancer. Cancer Res 69:6932–6940
188. Schottelius M, Wirtz M, Eiber M, Maurer T, Wester H-J (2015) [111In]PSMA-I&T: expanding the spectrum of PSMA-I&T applications towards SPECT and radioguided surgery. EJNMMI Res 5:68
189. Zhang J, Kulkarni HR, Singh A, Baum RP (2019) Complete Regression of Lung Metastases in a Patient With Metastatic Castration-Resistant Prostate Cancer Using 177Lu-PSMA Radioligand Therapy. Clin Nucl Med 1
190. Weineisen M, Simecek J, Schottelius M, Schwaiger M, Wester H-J (2014) Synthesis and preclinical evaluation of DOTAGA-conjugated PSMA ligands for functional imaging and endoradiotherapy of prostate cancer. EJNMMI Res 4:63
191. Weineisen M, Schottelius M, Simecek J, et al (2015) 68Ga- and 177Lu-Labeled PSMA I&T: Optimization of a PSMA-Targeted Theranostic Concept and First Proof-of-Concept Human Studies. J Nucl Med 56:1169–76
192. Liu H, Rajasekaran AK, Moy P, Xia Y, Kim S, Navarro V, Rahmati R, Bander NH (1998) Constitutive and antibody-induced internalization of prostate-specific membrane antigen. Cancer Res 58:4055–60
193. Rajasekaran SA, Anilkumar G, Oshima E, Bowie JU, Liu H, Heston W, Bander NH, Rajasekaran AK (2003) A Novel Cytoplasmic Tail MXXXL Motif Mediates the Internalization of Prostate-specific Membrane Antigen. Mol Biol Cell 14:4835–4845
194. Schottelius M, Wurzer A, Wissmiller K, et al (2019) Synthesis and Preclinical Characterization of the PSMA-Targeted Hybrid Tracer PSMA-I&F for Nuclear and Fluorescence Imaging of Prostate Cancer. J Nucl Med 60:71–78
195. Schmidt A, Wirtz M, Fä SF, Osl T, Beck R, Schottelius M, Schwaiger M, Rgen Wester H-J (2018) Effect of Carbohydration on the Theranostic Tracer PSMA I&T. https://doi.org/10.1021/acsomega.8b00790
196. Nonnekens J, Chatalic KLS, Molkenboer-Kuenen JDM, et al (2017) ^{213} Bi-Labeled Prostate-Specific Membrane Antigen-Targeting Agents Induce DNA Double-Strand Breaks in Prostate Cancer Xenografts. Cancer Biother Radiopharm 32:67–73
197. Ruigrok EAM, van Weerden WM, Nonnekens J, de Jong M (2019) The Future of PSMA-Targeted Radionuclide Therapy: An Overview of Recent Preclinical Research. Pharmaceutics. https://doi.org/10.3390/pharmaceutics11110560
198. Langbein T, Chaussé G, Baum RP (2018) Salivary gland toxicity of PSMA radioligand therapy: Relevance and preventive strategies. J Nucl Med 59:1172–1173
199. Tönnesmann R, Meyer P, Eder M, Baranski A-C (2019) [177Lu]Lu-PSMA-617 Salivary Gland Uptake Characterized by Quantitative In Vitro Autoradiography. Pharmaceuticals 12:18
200. Rupp NJ, Umbricht CA, Pizzuto DA, et al (2019) First Clinicopathologic Evidence of a Non–PSMA-Related Uptake Mechanism for ^{68} Ga-PSMA-11 in Salivary Glands. J Nucl Med 60:1270–1276
201. von Eyben FE, Roviello G, Kiljunen T, Uprimny C, Virgolini I, Kairemo K, Joensuu T (2018) Third-line treatment and 177Lu-PSMA radioligand therapy of metastatic castration-resistant prostate cancer: a systematic review. Eur J Nucl Med Mol Imaging 45:496–508
202. Heck MM, Retz M, D'Alessandria C, et al (2016) Systemic Radioligand Therapy with 177Lu Labeled Prostate Specific Membrane Antigen Ligand for Imaging and Therapy in Patients with Metastatic Castration Resistant Prostate Cancer. J Urol 196:382–391
203. Dey DK, Rothenberg E, Sundh V, Bosaeus I, Steen B (2001) Height and Body Weight in Elderly Adults: A 21-Year Population Study on Secular Trends and Related Factors in 70-Year-Olds. Journals Gerontol Ser A Biol Sci Med Sci 56:M780–M784
204. Bolch WE, Eckerman KF, Sgouros G, Thomas SR, Brill AB, Fisher DR, Howell RW, Meredith R, Wessels BW (2009) MIRD pamphlet No. 21: A generalized schema for radiopharmaceutical dosimetry-

standardization of nomenclature. J Nucl Med 50:477–484
205. Gupta A, Probst HC, Vuong V, Landshammer A, Muth S, Yagita H, Schwendener R, Pruschy M, Knuth A, Broek M van den (2012) Radiotherapy Promotes Tumor-Specific Effector CD8+ T Cells via Dendritic Cell Activation. J Immunol 189:558–566
206. Azad A, Yin Lim S, D'Costa Z, et al (2017) PD-L1 blockade enhances response of pancreatic ductal adenocarcinoma to radiotherapy. EMBO Mol Med 9:167–180
207. Jones KI, Tiersma J, Yuzhalin AE, Gordon-Weeks AN, Buzzelli J, Im JH, Muschel RJ (2018) Radiation combined with macrophage depletion promotes adaptive immunity and potentiates checkpoint blockade. EMBO Mol Med 10:e9342
208. Chen B, Khodadoust MS, Liu CL, Newman AM, Alizadeh AA (2018) Profiling tumor infiltrating immune cells with CIBERSORT. Methods Mol Biol 1711:243
209. Chiu Y-J, Hsieh Y-H, Huang Y-H (2019) Improved cell composition deconvolution method of bulk gene expression profiles to quantify subsets of immune cells. BMC Med Genomics 12:169
210. Malkov VA, Serikawa KA, Balantac N, Watters J, Geiss G, Mashadi-Hossein A, Fare T (2009) Multiplexed measurements of gene signatures in different analytes using the Nanostring nCounter™ Assay System. BMC Res Notes 2:80
211. Kulkarni MM (2011) Digital multiplexed gene expression analysis using the NanoString nCounter system. Curr Protoc Mol Biol Chapter 25:Unit25B.10
212. Rosenthal R, Cadieux EL, Salgado R, et al (2019) Neoantigen-directed immune escape in lung cancer evolution. Nature 567:479–485
213. Keam SP, Halse H, Nguyen T, et al (2020) High dose-rate brachytherapy of localized prostate cancer converts tumors from cold to hot. J Immunother cancer. https://doi.org/10.1136/jitc-2020-000792
214. Song SG, Kim S, Koh J, Yim J, Han B, Kim YA, Jeon YK, Chung DH (2021) Comparative analysis of the tumor immune-microenvironment of primary and brain metastases of non-small-cell lung cancer reveals organ-specific and EGFR mutation-dependent unique immune landscape. Cancer Immunol Immunother. https://doi.org/10.1007/s00262-020-02840-0
215. Xiang A, Lin X, Xu L, Chen H, Guo J, Zhou F (2020) PCOLCE Is Potent Prognostic Biomarker and Associates With Immune Infiltration in Gastric Cancer. Front Mol Biosci 7:544895
216. Xu J-L, Guo Y (2020) FCGR1A Serves as a Novel Biomarker and Correlates With Immune Infiltration in Four Cancer Types. Front Mol Biosci 7:581615
217. Panaretakis T, Kepp O, Brockmeier U, et al (2009) Mechanisms of pre-apoptotic calreticulin exposure in immunogenic cell death. EMBO J 28:578–590
218. Sukkurwala AQ, Martins I, Wang Y, et al (2014) Immunogenic calreticulin exposure occurs through a phylogenetically conserved stress pathway involving the chemokine CXCL8. Cell Death Differ 21:59–68
219. Garg AD, Krysko D V, Verfaillie T, et al (2012) A novel pathway combining calreticulin exposure and ATP secretion in immunogenic cancer cell death. EMBO J 31497:1062–1079
220. Chen X, Fosco D, Kline DE, Kline J (2017) Calreticulin promotes immunity and type I interferon-dependent survival in mice with acute myeloid leukemia. Oncoimmunology 6:e1278332
221. Fucikova J, Kasikova L, Truxova I, Laco J, Skapa P, Ryska A, Spisek R (2018) Relevance of the chaperone-like protein calreticulin for the biological behavior and clinical outcome of cancer. Immunol Lett 193:25–34
222. Boone BA, Orlichenko L, Schapiro NE, et al (2015) The receptor for advanced glycation end products (RAGE) enhances autophagy and neutrophil extracellular traps in pancreatic cancer. Cancer Gene Ther 22:326–34
223. Kang R, Tang D, Schapiro N, Loux T, Livesey K, Billiar T, Wang H, Houten B Van, Lotze M, Zeh H (2014) The HMGB1/RAGE inflammatory pathway promotes pancreatic tumor growth by regulating mitochondrial bioenergetics. Oncogene 33:567
224. Elliott MR, Chekeni FB, Trampont PC, et al (2009) Nucleotides released by apoptotic cells act as a find-me signal for phagocytic clearance. Nature 461:282
225. Ohshima Y, Tsukimoto M, Takenouchi T, Harada H, Suzuki A, Sato M, Kitani H, Kojima S (2010) γ-Irradiation induces P2X7 receptor-dependent ATP release from B16 melanoma cells. Biochim Biophys Acta - Gen Subj 1800:40–46
226. Ghiringhelli F, Apetoh L, Tesniere A, et al (2009) Activation of the NLRP3 inflammasome in dendritic cells induces IL-1B-dependent adaptive immunity against tumors. Nat Med. https://doi.org/10.1038/nm.2028
227. Menger L, Vacchelli E, Adjemian S, et al (2012) Cardiac glycosides exert anticancer effects by inducing immunogenic cell death. Sci Transl Med 4:143ra99-143ra99

228. Casares N, Pequignot MO, Tesniere A, et al (2005) Caspase-dependent immunogenicity of doxorubicin-induced tumor cell death. J Exp Med JEM 00:1691–1701
229. Aaes TL, Kaczmarek A, Delvaeye T, et al (2016) Vaccination with Necroptotic Cancer Cells Induces Efficient Anti-tumor Immunity Necroptotic cancer cells release DAMPs and induce dendritic cell maturation in vitro Prophylactic injection of necroptotic cancer cells leads to an anti-tumor vaccination Vacc. Cell Rep 15:274–287
230. Lim JYH, Gerber SA, Murphy SP, Lord EM (2014) Type I interferons induced by radiation therapy mediate recruitment and effector function of CD8(+) T cells. Cancer Immunol Immunother 63:259–71
231. Panaretakis T, Joza N, Modjtahedi N, et al (2008) The co-translocation of ERp57 and calreticulin determines the immunogenicity of cell death. Cell Death Differ 1567:1499–1509
232. Trowell OA (1952) The sensitivity of lymphocytes to ionising radiation. J Pathol Bacteriol 64:687–704
233. Durum SK, Gengozian N (1978) The Comparative Radiosensitivity of T and B Lymphocytes. Int J Radiat Biol Relat Stud Phys 34:1–15
234. Arina A, Beckett M, Fernandez C, et al (2019) Tumor-reprogrammed resident T cells resist radiation to control tumors. Nat Commun 10:3959
235. Rech AJ, Dada H, Kotzin JJ, Henao-Mejia J, Minn AJ, Twyman-Saint Victor C, Vonderheide RH (2018) Radiotherapy and CD40 Activation Separately Augment Immunity to Checkpoint Blockade in Cancer. Cancer Res 78:4282–4291
236. Carvalho H de A, Villar RC (2018) Radiotherapy and immune response: the systemic effects of a local treatment. Clinics (Sao Paulo) 73:e557s
237. Bauer M, Goldstein M, Christmann M, Becker H, Heylmann D, Kaina B (2011) Human monocytes are severely impaired in base and DNA double-strand break repair that renders them vulnerable to oxidative stress. Proc Natl Acad Sci U S A 108:21105–10
238. Wunderlich R, Ernst A, Rödel F, Fietkau R, Ott O, Lauber K, Frey B, Gaipl US (2015) Low and moderate doses of ionizing radiation up to 2 Gy modulate transmigration and chemotaxis of activated macrophages, provoke an anti-inflammatory cytokine milieu, but do not impact upon viability and phagocytic function. Clin Exp Immunol 179:50–61
239. Manda K, Glasow A, Paape D, Hildebrandt G (2012) Effects of ionizing radiation on the immune system with special emphasis on the interaction of dendritic and T cells. Front Oncol 2:102
240. Dunn PL, North RJ (1991) Selective Radiation Resistance of Immunologically Induced T Cells as the Basis for Irradiation-Induced T-Cell-Mediated Regression of Immunogenic Tumor. J Leukoc Biol 49:388–396
241. Grayson JM, Harrington LE, Lanier JG, Wherry EJ, Ahmed R (2002) Differential Sensitivity of Naive and Memory CD8+ T Cells to Apoptosis in Vivo. J Immunol 169:3760–3770
242. Liu S, Sun X, Luo J, Zhu H, Yang X, Guo Q, Song Y, Sun X (2015) Effects of radiation on T regulatory cells in normal states and cancer: mechanisms and clinical implications. Am J Cancer Res 5:3276–85
243. Beauford SS, Kumari A, Garnett-Benson C (2020) Ionizing radiation modulates the phenotype and function of human CD4+ induced regulatory T cells. BMC Immunol 21:18
244. Zhang E, Dai F, Mao Y, He W, Liu F, Ma W, Qiao Y (2020) Differences of the immune cell landscape between normal and tumor tissue in human prostate. Clin Transl Oncol 22:344–350
245. Lundholm M, Hägglöf C, Wikberg ML, Stattin P, Egevad L, Bergh A, Wikström P, Palmqvist R, Edin S (2015) Secreted Factors from Colorectal and Prostate Cancer Cells Skew the Immune Response in Opposite Directions. Sci Rep 5:15651
246. Matsumura S, Wang B, Kawashima N, et al (2008) Radiation-induced CXCL16 release by breast cancer cells attracts effector T cells. J Immunol 181:3099
247. Oudejans JJ, Jiwa NM, Kummer JA, et al (1997) Activated Cytotoxic T Cells as Prognostic Marker in Hodgkin's Disease. Blood 89:1376–1382
248. Vermeij R, de Bock GH, Leffers N, Ten Hoor KA, Schulze U, Hollema H, van der Burg SH, van der Zee AGJ, Daemen T, Nijman HW (2011) Tumor-infiltrating cytotoxic T lymphocytes as independent prognostic factor in epithelial ovarian cancer with wilms tumor protein 1 overexpression. J Immunother 34:516–23
249. Gibney GT, Weiner LM, Atkins MB (2016) Predictive biomarkers for checkpoint inhibitor-based immunotherapy. Lancet Oncol 17:e542–e551
250. Shien K, Papadimitrakopoulou VA, Wistuba II (2016) Predictive biomarkers of response to PD-1/PD-L1 immune checkpoint inhibitors in non–small cell lung cancer. Lung Cancer 99:79–87
251. Vesalainen S, Lipponen P, Talja M, Syrjänen K (1994) Histological grade, perineural infiltration, tumour-infiltrating lymphocytes and apoptosis as determinants of long-term prognosis in prostatic adenocarcinoma. Eur J Cancer 30:1797–1803

252. Leclerc BG, Charlebois R, Chouinard G, Allard B, Pommey S, Saad F, Stagg J (2016) CD73 Expression Is an Independent Prognostic Factor in Prostate Cancer. Clin Cancer Res 22:158–166
253. Ness N, Andersen S, Valkov A, Nordby Y, Donnem T, Al-Saad S, Busund L-T, Bremnes RM, Richardsen E (2014) Infiltration of CD8+ lymphocytes is an independent prognostic factor of biochemical failure-free survival in prostate cancer. Prostate 74:1452–1461
254. Zhao SG, Lehrer J, Chang SL, et al (2019) The Immune Landscape of Prostate Cancer and Nomination of PD-L2 as a Potential Therapeutic Target. JNCI J Natl Cancer Inst 111:301–310
255. Sonn CH, Choi JR, Kim T-J, Yu Y-B, Kim K, Shin SC, Park G-H, Shirakawa T, Kim HS, Lee K-M (2012) Augmentation of natural cytotoxicity by chronic low-dose ionizing radiation in murine natural killer cells primed by IL-2. J Radiat Res 53:823–829
256. Yang G, Kong Q, Wang G, Jin H, Zhou L, Yu D, Niu C, Han W, Li W, Cui J (2014) Low-Dose Ionizing Radiation Induces Direct Activation of Natural Killer Cells and Provides a Novel Approach for Adoptive Cellular Immunotherapy. Cancer Biother Radiopharm 29:428–434
257. Cheda A, Wrembel-Wargocka J, Lisiak E, Nowosielska EM, Marciniak M, Janiak MK (2004) Single Low Doses of X Rays Inhibit the Development of Experimental Tumor Metastases and Trigger the Activities of NK Cells in Mice. Radiat Res 161:335–340
258. Tabi Z, Spary LK, Coleman S, Clayton A, Mason MD, Staffurth J (2010) Resistance of CD45RA- T cells to apoptosis and functional impairment, and activation of tumor-antigen specific T cells during radiation therapy of prostate cancer. J Immunol 185:1330–9
259. Schaue D, Comin-Anduix B, Ribas A, Zhang L, Goodglick L, Sayre JW, Debucquoy A, Haustermans K, McBride WH (2008) T-cell responses to survivin in cancer patients undergoing radiation therapy. Clin Cancer Res 14:4883–90
260. Chow J, Hoffend NC, Abrams SI, Schwaab T, Singh AK, Muhitch JB (2020) Radiation induces dynamic changes to the T cell repertoire in renal cell carcinoma patients. Proc Natl Acad Sci 117:23721–23729
261. Rodríguez-Ruiz ME, Rodríguez I, Mayorga L, et al (2019) TGFβ Blockade Enhances Radiotherapy Abscopal Efficacy Effects in Combination with Anti-PD1 and Anti-CD137 Immunostimulatory Monoclonal Antibodies. Mol Cancer Ther 18:621–631
262. Rodriguez-Ruiz ME, Rodriguez I, Garasa S, et al (2016) Abscopal Effects of Radiotherapy Are Enhanced by Combined Immunostimulatory mAbs and Are Dependent on CD8 T Cells and Crosspriming. Cancer Res 76:5994–6005
263. Vanpouille-Box C, Diamond JM, Pilones KA, Zavadil J, Babb JS, Formenti SC, Barcellos-Hoff MH, Demaria S (2015) TGFβ Is a Master Regulator of Radiation Therapy-Induced Antitumor Immunity. Cancer Res 75:2232–42
264. Burnette BC, Liang H, Lee Y, Chlewicki L, Khodarev NN, Weichselbaum RR, Fu Y-X, Auh SL (2011) The efficacy of radiotherapy relies upon induction of type i interferon-dependent innate and adaptive immunity. Cancer Res 71:2488–96
265. Filatenkov A, Baker J, Mueller AMS, et al (2015) Ablative Tumor Radiation Can Change the Tumor Immune Cell Microenvironment to Induce Durable Complete Remissions. Clin Cancer Res 21:3727–39
266. Lugade AA, Sorensen EW, Gerber SA, Moran JP, Frelinger JG, Lord EM (2008) Radiation-induced IFN-gamma production within the tumor microenvironment influences antitumor immunity. J Immunol 180:3132–9
267. Reading JL, Quezada SA (2016) Too Much of a Good Thing? Chronic IFN Fuels Resistance to Cancer Immunotherapy. Immunity 45:1181–1183
268. Obeid M, Panaretakis T, Joza N, Tufi R, Tesniere A, van Endert P, Zitvogel L, Kroemer G (2007) Calreticulin exposure is required for the immunogenicity of γ-irradiation and UVC light-induced apoptosis [5]. Cell Death Differ 14:1848–1850
269. Singh AK, Winslow TB, Kermany MH, et al (2017) A Pilot Study of Stereotactic Body Radiation Therapy Combined with Cytoreductive Nephrectomy for Metastatic Renal Cell Carcinoma. Clin Cancer Res 23:5055–5065
270. Suzuki Y, Mimura K, Yoshimoto Y, Watanabe M, Ohkubo Y, Izawa S, Murata K, Fujii H, Nakano T, Kono K (2012) Immunogenic tumor cell death induced by chemoradiotherapy in patients with esophageal squamous cell carcinoma. Cancer Res 72:3967–76
271. Liao Y, Liu S, Fu S, Wu J (2020) HMGB1 in Radiotherapy: A Two Headed Signal Regulating Tumor Radiosensitivity and Immunity. Onco Targets Ther 13:6859–6871
272. Galluzzi L, Buqué A, Kepp O, Zitvogel L, Kroemer G (2016) Immunogenic cell death in cancer and infectious disease. https://doi.org/10.1038/nri.2016.107
273. Fucikova J, Kepp O, Kasikova L, Petroni G, Yamazaki T, Liu P, Zhao L, Spisek R, Kroemer G, Galluzzi L

(2020) Detection of immunogenic cell death and its relevance for cancer therapy. Cell Death Dis 11:1013
274. Sistigu A, Yamazaki T, Vacchelli E, et al (2014) Cancer cell-autonomous contribution of type I interferon signaling to the efficacy of chemotherapy. Nat Med 20:1301–9
275. Vitkin N, Nersesian S, Siemens DR, Koti M (2019) The tumor immune contexture of prostate cancer. Front Immunol 10:603
276. Bou-Dargham MJ, Sha L, Sang Q-XA, Zhang J (2020) Immune landscape of human prostate cancer: immune evasion mechanisms and biomarkers for personalized immunotherapy. BMC Cancer 20:572
277. Danaher P, Warren S, Lu R, Samayoa J, Sullivan A, Pekker I, Wallden B, Marincola FM, Cesano A (2018) Pan-cancer adaptive immune resistance as defined by the Tumor Inflammation Signature (TIS): results from The Cancer Genome Atlas (TCGA). J Immunother Cancer 6:63
278. Wang X, Li M (2019) Correlate tumor mutation burden with immune signatures in human cancers. BMC Immunol 20:4
279. Takimoto C, Chao M, Gibbs C, McCamish M, Liu J, Chen J, Majeti R, Weissman I (2019) The Macrophage 'Do not eat me' signal, CD47, is a clinically validated cancer immunotherapy target. https://doi.org/10.1093/annonc/mdz006
280. Barclay AN, van den Berg TK (2014) The Interaction Between Signal Regulatory Protein Alpha (SIRP α) and CD47: Structure, Function, and Therapeutic Target. Annu Rev Immunol 32:25–50
281. van den Berg TK, van der Schoot CE (2008) Innate immune 'self' recognition: a role for CD47–SIRPα interactions in hematopoietic stem cell transplantation. Trends Immunol 29:203–206
282. Majeti R, Chao MP, Alizadeh AA, Pang WW, Jaiswal S, Gibbs KD, van Rooijen N, Weissman IL (2009) CD47 Is an Adverse Prognostic Factor and Therapeutic Antibody Target on Human Acute Myeloid Leukemia Stem Cells. Cell 138:286–299
283. Chao MP, Alizadeh AA, Tang C, Jan M, Weissman-Tsukamoto R, Zhao F, Park CY, Weissman IL, Majeti R (2011) Therapeutic Antibody Targeting of CD47 Eliminates Human Acute Lymphoblastic Leukemia. Cancer Res 71:1374–1384
284. Edris B, Weiskopf K, Volkmer AK, et al (2012) Antibody therapy targeting the CD47 protein is effective in a model of aggressive metastatic leiomyosarcoma. Proc Natl Acad Sci 109:6656–6661
285. Jaiswal S, Jamieson CHM, Pang WW, Park CY, Chao MP, Majeti R, Traver D, van Rooijen N, Weissman IL (2009) CD47 Is Upregulated on Circulating Hematopoietic Stem Cells and Leukemia Cells to Avoid Phagocytosis. Cell 138:271–285
286. Willingham SB, Volkmer J-P, Gentles AJ, et al (2012) The CD47-signal regulatory protein alpha (SIRPa) interaction is a therapeutic target for human solid tumors. Proc Natl Acad Sci 109:6662–6667
287. Chan KS, Espinosa I, Chao M, et al (2009) Identification, molecular characterization, clinical prognosis, and therapeutic targeting of human bladder tumor-initiating cells. Proc Natl Acad Sci U S A 106:14016–14021
288. Wang H, Tan M, Zhang S, Li X, Gao J, Zhang D, Hao Y, Gao S, Liu J, Lin B (2015) Expression and significance of CD44, CD47 and c-met in ovarian clear cell carcinoma. Int J Mol Sci 16:3391–404
289. Suzuki S, Yokobori T, Tanaka N, et al (2012) CD47 expression regulated by the miR-133a tumor suppressor is a novel prognostic marker in esophageal squamous cell carcinoma. Oncol Rep 28:465–72
290. Chao MP, Jaiswal S, Weissman-Tsukamoto R, et al (2010) Calreticulin is the dominant pro-phagocytic signal on multiple human cancers and is counterbalanced by CD47. Sci Transl Med 2:63ra94
291. Zhang M, Hutter G, Kahn SA, et al (2016) Anti-CD47 Treatment Stimulates Phagocytosis of Glioblastoma by M1 and M2 Polarized Macrophages and Promotes M1 Polarized Macrophages In Vivo. PLoS One 11:e0153550
292. Chao MP, Jaiswal S, Weissman-Tsukamoto R, et al (2010) Calreticulin Is the Dominant Pro-Phagocytic Signal on Multiple Human Cancers and Is Counterbalanced by CD47. Sci Transl Med 2:63ra94-63ra94
293. Maxhimer JB, Soto-Pantoja DR, Ridnour LA, Shih HB, DeGraff WG, Tsokos M, Wink DA, Isenberg JS, Roberts DD (2009) Radioprotection in normal tissue and delayed tumor growth by blockade of CD47 signaling. Sci Transl Med 1:3ra7-3ra7
294. Azcutia V, Routledge M, Williams MR, et al (2013) CD47 plays a critical role in T-cell recruitment by regulation of LFA-1 and VLA-4 integrin adhesive functions. Mol Biol Cell 24:3358–3368
295. Li Z, He L, Wilson KE, Roberts DD (2001) Thrombospondin-1 Inhibits TCR-Mediated T Lymphocyte Early Activation. J Immunol 166:2427–2436
296. Li Z, Calzada MJ, Sipes JM, Cashel JA, Krutzsch HC, Annis DS, Mosher DF, Roberts DD (2002) Interactions of thrombospondins with α4β1 integrin and CD47 differentially modulate T cell behavior. J Cell Biol

157:509–519
297. Miller TW, Kaur S, Ivins-O'Keefe K, Roberts DD (2013) Thrombospondin-1 is a CD47-dependent endogenous inhibitor of hydrogen sulfide signaling in T cell activation. Matrix Biol 32:316–324
298. Brooke G, Holbrook JD, Brown MH, Barclay AN (2004) Human Lymphocytes Interact Directly with CD47 through a Novel Member of the Signal Regulatory Protein (SIRP) Family. J Immunol 173:2562–2570
299. Grimbert P, Bouguermouh S, Baba N, Nakajima T, Allakhverdi Z, Braun D, Saito H, Rubio M, Delespesse G, Sarfati M (2006) Thrombospondin/CD47 Interaction: A Pathway to Generate Regulatory T Cells from Human CD4+CD25− T Cells in Response to Inflammation. J Immunol 177:3534–3541
300. Barazi HO, Li Z, Cashel JA, Krutzsch HC, Annis DS, Mosher DF, Roberts DD (2002) Regulation of Integrin Function by CD47 Ligands. J Biol Chem 277:42859–42866
301. Kim MJ, Lee J-C, Lee J-J, Kim S, Lee SG, Park S-W, Sung MW, Heo DS (2008) Association of CD47 with Natural Killer Cell-Mediated Cytotoxicity of Head-and-Neck Squamous Cell Carcinoma Lines. Tumor Biol 29:28–34
302. Bouguermouh S, Van VQ, Martel J, Gautier P, Rubio M, Sarfati M (2008) CD47 Expression on T Cell Is a Self-Control Negative Regulator of Type 1 Immune Response. J Immunol 136:2348–2357
303. Van VQ, Darwiche J, Raymond M, Lesage S, Bouguermouh S, Rubio M, Sarfati M (2008) Cutting Edge: CD47 Controls the In Vivo Proliferation and Homeostasis of Peripheral CD4+CD25+Foxp3+ Regulatory T Cells That Express CD103. J Immunol 181:5204–5208
304. Soto-Pantoja DR, Terabe M, Ghosh A, Ridnour LA, DeGraff WG, Wink DA, Berzofsky JA, Roberts DD (2014) CD47 in the Tumor Microenvironment Limits Cooperation between Antitumor T-cell Immunity and Radiotherapy. Cancer Res 74:6771–6783
305. Soto-Pantoja DR, Miller TW, Pendrak ML, DeGraff WG, Sullivan C, Ridnour LA, Abu-Asab M, Wink DA, Tsokos M, Roberts DD (2012) CD47 deficiency confers cell and tissue radioprotection by activation of autophagy. Autophagy 8:1628–1642
306. Gholamin S, Youssef OA, Rafat M, et al (2020) Irradiation or temozolomide chemotherapy enhances anti-CD47 treatment of glioblastoma. Innate Immun 26:130–137
307. Candas-Green D, Xie B, Huang J, et al (2020) Dual blockade of CD47 and HER2 eliminates radioresistant breast cancer cells. Nat Commun 11:4591
308. Koustas E, Sarantis P, Papavassiliou AG, Karamouzis M V (2020) The Resistance Mechanisms of Checkpoint Inhibitors in Solid Tumors. Biomolecules. https://doi.org/10.3390/biom10050666
309. Luke JJ, Lemons JM, Karrison TG, et al (2018) Safety and Clinical Activity of Pembrolizumab and Multisite Stereotactic Body Radiotherapy in Patients With Advanced Solid Tumors. J Clin Oncol 36:1611–1618
310. Levy A, Massard C, Soria J-C, Deutsch E (2016) Concurrent irradiation with the anti-programmed cell death ligand-1 immune checkpoint blocker durvalumab: Single centre subset analysis from a phase 1/2 trial. Eur J Cancer 68:156–162
311. Liniker E, Menzies AM, Kong BY, et al (2016) Activity and safety of radiotherapy with anti-PD-1 drug therapy in patients with metastatic melanoma. Oncoimmunology 5:e1214788
312. Anderson ES, Postow MA, Wolchok JD, Young RJ, Ballangrud Å, Chan TA, Yamada Y, Beal K (2017) Melanoma brain metastases treated with stereotactic radiosurgery and concurrent pembrolizumab display marked regression; efficacy and safety of combined treatment. J Immunother cancer 5:76
313. Ribeiro Gomes J, Schmerling RA, Haddad CK, Racy DJ, Ferrigno R, Gil E, Zanuncio P, Buzaid AC (2016) Analysis of the Abscopal Effect With Anti-PD1 Therapy in Patients With Metastatic Solid Tumors. J Immunother 39:367–372
314. Antonia SJ, Villegas A, Daniel D, et al (2017) Durvalumab after Chemoradiotherapy in Stage III Non–Small-Cell Lung Cancer. N Engl J Med 377:1919–1929
315. Herter-Sprie GS, Koyama S, Korideck H, et al (2016) Synergy of radiotherapy and PD-1 blockade in Kras-mutant lung cancer. JCI insight 1:e87415
316. Grapin M, Richard C, Limagne E, et al (2019) Optimized fractionated radiotherapy with anti-PD-L1 and anti-TIGIT: a promising new combination. J Immunother Cancer 7:160
317. Deng L, Liang H, Burnette B, Beckett M, Darga T, Weichselbaum RR, Fu Y-X (2014) Irradiation and anti–PD-L1 treatment synergistically promote antitumor immunity in mice. J Clin Invest 124:687–695
318. Dovedi SJ, Adlard AL, Lipowska-Bhalla G, et al (2014) Acquired Resistance to Fractionated Radiotherapy Can Be Overcome by Concurrent PD-L1 Blockade. Cancer Res 74:5458–5468
319. Zeng J, See AP, Phallen J, et al (2013) Anti-PD-1 blockade and stereotactic radiation produce long-term survival in mice with intracranial gliomas. Int J Radiat Oncol Biol Phys 86:343–9
320. Park SS, Dong H, Liu X, Harrington SM, Krco CJ, Grams MP, Mansfield AS, Furutani KM, Olivier KR, Kwon

ED (2015) PD-1 Restrains Radiotherapy-Induced Abscopal Effect. Cancer Immunol Res 3:610–9
321. Gong X, Li X, Jiang T, Xie H, Zhu Z, Zhou F, Zhou C (2017) Combined Radiotherapy and Anti-PD-L1 Antibody Synergistically Enhances Antitumor Effect in Non-Small Cell Lung Cancer. J Thorac Oncol 12:1085–1097
322. Ehlerding E, Ferreira C, Jiang D, KANG L, Engle J, McNeel D, Cai W (2019) Imaging PD-L1 expression in tumors following radiotherapy treatment. J. Nucl. Med. 60:
323. Philippou Y, Sjoberg HT, Murphy E, et al (2020) Impacts of combining anti-PD-L1 immunotherapy and radiotherapy on the tumour immune microenvironment in a murine prostate cancer model. Br J Cancer 123:1089–1100
324. Latchman Y, Wood CR, Chernova T, et al (2001) PD-L2 is a second ligand for PD-1 and inhibits T cell activation. Nat Immunol 2:261–268
325. Munn DH, Mellor AL (2016) IDO in the Tumor Microenvironment: Inflammation, Counter-Regulation, and Tolerance. Trends Immunol 37:193–207
326. Théate I, van Baren N, Pilotte L, et al (2015) Extensive Profiling of the Expression of the Indoleamine 2,3-Dioxygenase 1 Protein in Normal and Tumoral Human Tissues. Cancer Immunol Res 3:161–172
327. Yu C-P, Fu S-F, Chen X, Ye J, Ye Y, Kong L-D, Zhu Z (2018) The Clinicopathological and Prognostic Significance of IDO1 Expression in Human Solid Tumors: Evidence from a Systematic Review and Meta-Analysis. Cell Physiol Biochem 49:134–143
328. Blair AB, Kleponis J, Thomas DL, Muth ST, Murphy AG, Kim V, Zheng L (2019) IDO1 inhibition potentiates vaccine-induced immunity against pancreatic adenocarcinoma. J Clin Invest 129:1742–1755
329. Chen B, Alvarado DM, Iticovici M, Kau NS, Park H, Parikh PJ, Thotala D, Ciorba MA (2020) Interferon-Induced IDO1 Mediates Radiation Resistance and Is a Therapeutic Target in Colorectal Cancer. Cancer Immunol Res 8:451–464
330. Monjazeb AM, Kent MS, Grossenbacher SK, et al (2016) Blocking Indolamine-2,3-Dioxygenase Rebound Immune Suppression Boosts Antitumor Effects of Radio-Immunotherapy in Murine Models and Spontaneous Canine Malignancies. Clin Cancer Res 22:4328–4340
331. Ahlstedt J, Konradsson E, Ceberg C, Redebrandt HN (2020) Increased effect of two-fraction radiotherapy in conjunction with IDO1 inhibition in experimental glioblastoma. PLoS One 15:e0233617
332. Holmgaard RB, Zamarin D, Munn DH, Wolchok JD, Allison JP (2013) Indoleamine 2,3-dioxygenase is a critical resistance mechanism in antitumor T cell immunotherapy targeting CTLA-4. J Exp Med 210:1389–1402
333. Muller AJ, DuHadaway JB, Donover PS, Sutanto-Ward E, Prendergast GC (2005) Inhibition of indoleamine 2,3-dioxygenase, an immunoregulatory target of the cancer suppression gene Bin1, potentiates cancer chemotherapy. Nat Med 11:312–319
334. Spranger S, Koblish HK, Horton B, Scherle PA, Newton R, Gajewski TF (2014) Mechanism of tumor rejection with doublets of CTLA-4, PD-1/PD-L1, or IDO blockade involves restored IL-2 production and proliferation of CD8+ T cells directly within the tumor microenvironment. J Immunother Cancer 2:3
335. Uyttenhove C, Pilotte L, Théate I, Stroobant V, Colau D, Parmentier N, Boon T, Van den Eynde BJ (2003) Evidence for a tumoral immune resistance mechanism based on tryptophan degradation by indoleamine 2,3-dioxygenase. Nat Med 9:1269–1274
336. Mitchell TC, Hamid O, Smith DC, et al (2018) Epacadostat Plus Pembrolizumab in Patients With Advanced Solid Tumors: Phase I Results From a Multicenter, Open-Label Phase I/II Trial (ECHO-202/KEYNOTE-037). J Clin Oncol 36:3223–3230
337. Long G V, Dummer R, Hamid O, et al Epacadostat Plus Pembrolizumab Versus Pembrolizumab Alone in Patients With Unresectable or Metastatic Melanoma: Results of the Phase 3 ECHO-301/KEYNOTE-252 Study Background: Rationale for Combination and Dosing.
338. Platten M, Nollen EAA, Röhrig UF, Fallarino F, Opitz CA (2019) Tryptophan metabolism as a common therapeutic target in cancer, neurodegeneration and beyond. Nat Rev Drug Discov 18:379–401
339. Van den Eynde BJ, van Baren N, Baurain J-F (2020) Is There a Clinical Future for IDO1 Inhibitors After the Failure of Epacadostat in Melanoma? Annu Rev Cancer Biol 4:241–256
340. Liu M, Li Z, Yao W, Zeng X, Wang L, Cheng J, Ma B, Zhang R, Min W, Wang H (2019) IDO inhibitor synergized with radiotherapy to delay tumor growth by reversing T cell exhaustion. Mol Med Rep 21:445–453
341. Fujiwara K, Saung MT, Jing H, et al (2020) Interrogating the immune-modulating roles of radiation therapy for a rational combination with immune-checkpoint inhibitors in treating pancreatic cancer. J

Immunother cancer 8:e000351
342. Ladomersky E, Zhai L, Lenzen A, et al (2018) IDO1 Inhibition Synergizes with Radiation and PD-1 Blockade to Durably Increase Survival Against Advanced Glioblastoma. Clin Cancer Res 24:2559–2573
343. Farhood B, khodamoradi E, Hoseini-Ghahfarokhi M, Motevaseli E, Mirtavoos-Mahyari H, Eleojo Musa A, Najafi M (2020) TGF-β in radiotherapy: Mechanisms of tumor resistance and normal tissues injury. Pharmacol Res 155:104745
344. Seoane J, Gomis RR (2017) TGF-β Family Signaling in Tumor Suppression and Cancer Progression. Cold Spring Harb Perspect Biol 9:a022277
345. Shull MM, Ormsby I, Kier AB, Pawlowski S, Diebold RJ, Yin M, Allen R, Sidman C, Proetzel G, Calvin D (1992) Targeted disruption of the mouse transforming growth factor-beta 1 gene results in multifocal inflammatory disease. Nature 359:693–9
346. Bierie B, Cancer HM-NR, 2006 undefined TGFβ: the molecular Jekyll and Hyde of cancer. nature.com
347. Tsushima H, Kawata S, Tamura S, et al (1996) High levels of transforming growth factor beta 1 in patients with colorectal cancer: Association with disease progression. Gastroenterology 110:375–382
348. Wikström P, Stattin P, Franck-Lissbrant I, Damber J-E, Bergh A (1998) Transforming growth factor β1 is associated with angiogenesis, metastasis, and poor clinical outcome in prostate cancer. Prostate 37:19–29
349. Walker RA, Dearing SJ (1992) Transforming growth factor beta1 in ductal carcinoma in situ and invasive carcinomas of the breast. Eur J Cancer 28:641–644
350. Friedman E, Gold LI, Klimstra D, Zeng ZS, Winawer S, Cohen A (1995) High levels of transforming growth factor beta 1 correlate with disease progression in human colon cancer. Cancer Epidemiol Biomarkers Prev 4:549–54
351. Calon A, Espinet E, Palomo-Ponce S, et al (2012) Dependency of Colorectal Cancer on a TGF-β-Driven Program in Stromal Cells for Metastasis Initiation. Cancer Cell 22:571–584
352. Billiard F, Buard V, Benderitter M, Linard C (2011) Abdominal γ-radiation induces an accumulation of function-impaired regulatory T cells in the small intestine. Int J Radiat Oncol Biol Phys 80:869–76
353. Linard C, Billiard F, Benderitter M (2012) Intestinal Irradiation and Fibrosis in a Th1-Deficient Environment. Int J Radiat Oncol 84:266–273
354. Wang J, Zheng H, Sung CC, Richter KK, Hauer-Jensen M (1998) Cellular sources of transforming growth factor-beta isoforms in early and chronic radiation enteropathy. Am J Pathol 153:1531–40
355. Biswas S, Guix M, Rinehart C, Dugger TC, Chytil A, Moses HL, Freeman ML, Arteaga CL (2007) Inhibition of TGF-beta with neutralizing antibodies prevents radiation-induced acceleration of metastatic cancer progression. J Clin Invest 117:1305–13
356. Bouquet F, Pal A, Pilones KA, et al (2011) TGFβ1 inhibition increases the radiosensitivity of breast cancer cells in vitro and promotes tumor control by radiation in vivo. Clin Cancer Res 17:6754–65
357. Andarawewa KL, Erickson AC, Chou WS, Costes S V, Gascard P, Mott JD, Bissell MJ, Barcellos-Hoff MH (2007) Ionizing radiation predisposes nonmalignant human mammary epithelial cells to undergo transforming growth factor beta induced epithelial to mesenchymal transition. Cancer Res 67:8662–70
358. Saito H, Tsujitani S, Oka S, Kondo A, Ikeguchi M, Maeta M, Kaibara N (2000) An elevated serum level of transforming growth factor-beta 1 (TGF-beta 1) significantly correlated with lymph node metastasis and poor prognosis in patients with gastric carcinoma. undefined
359. Carl C, Flindt A, Hartmann J, Dahlke M, Rades D, Dunst J, Lehnert H, Gieseler F, Ungefroren H (2016) Ionizing radiation induces a motile phenotype in human carcinoma cells in vitro through hyperactivation of the TGF-beta signaling pathway. Cell Mol Life Sci 73:427–43
360. Yasmin-Karim S, Bruck PT, Moreau M, Kunjachan S, Chen GZ, Kumar R, Grabow S, Dougan SK, Ngwa W (2018) Radiation and Local Anti-CD40 Generate an Effective in situ Vaccine in Preclinical Models of Pancreatic Cancer. Front Immunol 9:2030
361. Yang T, Huang T, Zhang D, et al (2019) TGF-β receptor inhibitor LY2109761 enhances the radiosensitivity of gastric cancer by inactivating the TGF-β/SMAD4 signaling pathway. Aging (Albany NY) 11:8892–8910
362. Rodríguez-Ruiz ME, Rodríguez I, Mayorga L, et al (2019) TGFb blockade enhances radiotherapy abscopal efficacy effects in combination with anti-PD1 and anti-CD137 immunostimulatory monoclonal antibodies. Mol Cancer Ther 18:621–631
363. Formenti SC, Lee P, Adams S, et al (2018) Focal irradiation and systemic TGFb blockade in metastatic breast cancer. Clin Cancer Res 24:2493–2504
364. Vonderheide RH (2020) CD40 Agonist Antibodies in Cancer Immunotherapy. Annu Rev Med 71:47–58
365. Sumner W, Kim S, Miyauchi S, Sanders PD, Mell LK, Cohen E, Gutkind JS, Califano JA, Sharabi A (2020)

Radiation Combined With CD40 Agonist And PD-1 Blockade Enhances B-cell Tumor Infiltration And Local Tumor Control. Int J Radiat Oncol 108:e565
366. Majeti R, Chao MP, Alizadeh AA, Pang WW, Jaiswal S, Gibbs KD, van Rooijen N, Weissman IL (2009) CD47 is an adverse prognostic factor and therapeutic antibody target on human acute myeloid leukemia stem cells. Cell 138:286–99
367. Li H, Wang Z, Zhang Y, et al (2019) The Immune Checkpoint Regulator PDL1 is an Independent Prognostic Biomarker for Biochemical Recurrence in Prostate Cancer Patients Following Adjuvant Hormonal Therapy. J Cancer 10:3102–3111
368. Gevensleben H, Dietrich D, Golletz C, et al (2015) The Immune Checkpoint Regulator PD-L1 Is Highly Expressed in Aggressive Primary Prostate Cancer. https://doi.org/10.1158/1078-0432.CCR-15-2042
369. Petitprez F, Fossati N, Vano Y, et al (2019) PD-L1 Expression and CD8+ T-cell Infiltrate are Associated with Clinical Progression in Patients with Node-positive Prostate Cancer. Eur Urol Focus 5:192–196
370. The Cancer Genome Atlas Program - National Cancer Institute. https://www.cancer.gov/about-nci/organization/ccg/research/structural-genomics/tcga. Accessed 4 Feb 2021
371. Altman DG, Royston P (2006) The cost of dichotomising continuous variables. BMJ 332:1080
372. Royston P, Altman DG, Sauerbrei W (2006) Dichotomizing continuous predictors in multiple regression: a bad idea. Stat Med 25:127–141
373. Mallett S, Royston P, Dutton S, Waters R, Altman DG (2010) Reporting methods in studies developing prognostic models in cancer: a review. BMC Med 8:20
374. Liu Y, Bühring H-J, Zen K, Burst SL, Schnell FJ, Williams IR, Parkos CA (2002) Signal regulatory protein (SIRPalpha), a cellular ligand for CD47, regulates neutrophil transmigration. J Biol Chem 277:10028–36
375. Liu Y, Merlin D, Burst SL, Pochet M, Madara JL, Parkos CA (2001) The role of CD47 in neutrophil transmigration. Increased rate of migration correlates with increased cell surface expression of CD47. J Biol Chem 276:40156–66
376. Azcutia V, Stefanidakis M, Tsuboi N, Mayadas T, Croce KJ, Fukuda D, Aikawa M, Newton G, Luscinskas FW (2012) Endothelial CD47 promotes vascular endothelial-cadherin tyrosine phosphorylation and participates in T cell recruitment at sites of inflammation in vivo. J Immunol 189:2553–62
377. Jobling MF, Mott JD, Finnegan MT, et al (2006) Isoform-Specific Activation of Latent Transforming Growth Factor β (LTGF-β) by Reactive Oxygen Species. Radiat Res 166:839–848
378. Satoh E, Naganuma H, Sasaki A, Nagasaka M, Ogata H, Nukui H (1997) Effect of irradiation on transforming growth factor-β secretion by malignant glioma cells. J Neurooncol 33:195–200
379. Martin M, Vozenin MC, Gault N, Crechet F, Pfarr CM, Lefaix JL (1997) Coactivation of AP-1 activity and TGF-beta1 gene expression in the stress response of normal skin cells to ionizing radiation. Oncogene 15:981–9
380. Anscher MS, Kong FM, Murase T, Jirtle RL (1995) Short communication: normal tissue injury after cancer therapy is a local response exacerbated by an endocrine effect of TGF beta. Br J Radiol 68:331–3
381. Rube CE, Uthe D, Schmid KW, Richter KD, Wessel J, Schuck A, Willich N, Rube C (2000) Dose-dependent induction of transforming growth factor beta (TGF-beta) in the lung tissue of fibrosis-prone mice after thoracic irradiation. Int J Radiat Oncol Biol Phys 47:1033–42
382. Canney PA, Dean S (1990) Transforming growth factor beta: a promotor of late connective tissue injury following radiotherapy? Br J Radiol 63:620–3
383. Malley YO, Zhao W, Barcellos-Hoff MH, Robbins MEC (1999) Radiation-Induced Alterations in Rat Mesangial Cell Tgfb1 and Tgfb3 Gene Expression Are Not Associated with Altered Secretion of Active Tgfb Isoforms. Radiat Res 152:622
384. Barcellos-Hoff MH, Derynck R, Tsang ML, Weatherbee JA (1994) Transforming growth factor-beta activation in irradiated murine mammary gland. J Clin Invest 93:892–9
385. Sanda MG, Restifo NP, Walsh JC, Kawakami Y, Nelson WG, Pardoll DM, Simons JW (1995) Molecular Characterization of Defective Antigen Processing in Human Prostate Cancer. JNCI J Natl Cancer Inst 87:280–285
386. Bander NH, Yao D, Liu H, Chen Y-T, Steiner M, Zuccaro W, Moy P (1997) MHC class I and II expression in prostate carcinoma and modulation by interferon-alpha and -gamma. Prostate 33:233–239
387. Heninger E, Krueger TEG, Thiede SM, et al (2016) Inducible expression of cancer-testis antigens in human prostate cancer. Oncotarget 7:84359–84374
388. Kiniwa Y, Miyahara Y, Wang HY, Peng W, Peng G, Wheeler TM, Thompson TC, Old LJ, Wang R-F (2007) CD8 $^{+}$ Foxp3 $^{+}$ Regulatory T Cells Mediate Immunosuppression in Prostate Cancer. Clin Cancer Res 13:6947–6958

389. Kaur HB, Guedes LB, Lu J, et al (2018) Association of tumor-infiltrating T-cell density with molecular subtype, racial ancestry and clinical outcomes in prostate cancer. Mod Pathol 31:1539–1552
390. Sudo T, Takahashi Y, Sawada G, Uchi R, Mimori K, Akagi Y (2017) Significance of CD47 expression in gastric cancer. Oncol Lett 14:801–809
391. Gao L, Chen K, Gao Q, Wang X, Sun J, Yang Y-G (2017) CD47 deficiency in tumor stroma promotes tumor progression by enhancing angiogenesis. Oncotarget 8:22406–22413
392. Soto-Pantoja DR, Terabe M, Ghosh A, Ridnour LA, DeGraff WG, Wink DA, Berzofsky JA, Roberts DD (2014) CD47 in the Tumor Microenvironment Limits Cooperation between Antitumor T-cell Immunity and Radiotherapy. Cancer Res 74:6771–6783
393. Zhang Q, Chen L, Helfand BT, et al (2011) TGF-β regulates DNA methyltransferase expression in prostate cancer, correlates with aggressive capabilities, and predicts disease recurrence. PLoS One 6:e25168
394. Yang F, Chen Y, Shen T, et al (2014) Stromal TGF-β signaling induces AR activation in prostate cancer. Oncotarget 5:10854–10869
395. Vo BT, Morton D, Komaragiri S, Millena AC, Leath C, Khan SA, Khan SA (2013) TGF-β effects on prostate cancer cell migration and invasion are mediated by PGE2 through activation of PI3K/AKT/mTOR pathway. Endocrinology 154:1768–79
396. Linard C, Billiard F, Benderitter M (2012) Intestinal Irradiation and Fibrosis in a Th1-Deficient Environment. Int J Radiat Oncol 84:266–273
397. Liu Y, Kudo K, Abe Y, Hu D-L, Kijima H, Nakane A, Ono K (2009) Inhibition of transforming growth factor-beta, hypoxia-inducible factor-1alpha and vascular endothelial growth factor reduced late rectal injury induced by irradiation. J Radiat Res 50:233–9
398. Paller C, Pu H, Begemann DE, Wade CA, Hensley PJ, Kyprianou N (2019) TGF-β receptor I inhibitor enhances response to enzalutamide in a pre-clinical model of advanced prostate cancer. Prostate 79:31–43
399. Young KH, Newell P, Cottam B, Friedman D, Savage T, Baird JR, Akporiaye E, Gough MJ, Crittenden M (2014) TGFβ inhibition prior to hypofractionated radiation enhances efficacy in preclinical models. Cancer Immunol Res 2:1011–22
400. Bouquet F, Pal A, Pilones KA, et al (2011) TGFβ1 inhibition increases the radiosensitivity of breast cancer cells in vitro and promotes tumor control by radiation in vivo. Clin Cancer Res 17:6754–65
401. Rodríguez-Ruiz ME, Rodríguez I, Mayorga L, et al (2019) TGFβ Blockade Enhances Radiotherapy Abscopal Efficacy Effects in Combination with Anti-PD1 and Anti-CD137 Immunostimulatory Monoclonal Antibodies. Mol Cancer Ther 18:621–631
402. Nardone V, Botta C, Caraglia M, et al (2016) Tumor infiltrating T lymphocytes expressing FoxP3, CCR7 or PD-1 predict the outcome of prostate cancer patients subjected to salvage radiotherapy after biochemical relapse. Cancer Biol Ther 17:1213–1220
403. Kim JW, Shin MS, Kang Y, Kang I, Petrylak DP (2018) Immune Analysis of Radium-223 in Patients With Metastatic Prostate Cancer. Clin Genitourin Cancer 16:e469–e476
404. Lim SH, Hong M, Ahn S, et al (2016) Changes in tumour expression of programmed death-ligand 1 after neoadjuvant concurrent chemoradiotherapy in patients with squamous oesophageal cancer. Eur J Cancer 52:1–9
405. Hecht M, Büttner-Herold M, Erlenbach-Wünsch K, Haderlein M, Croner R, Grützmann R, Hartmann A, Fietkau R, Distel L V. (2016) PD-L1 is upregulated by radiochemotherapy in rectal adenocarcinoma patients and associated with a favourable prognosis. Eur J Cancer 65:52–60
406. Chiang S-F, Huang C-Y, Ke T-W, Chen T-W, Lan Y-C, You Y-S, Chen WT-L, Chao KSC (2019) Upregulation of tumor PD-L1 by neoadjuvant chemoradiotherapy (neoCRT) confers improved survival in patients with lymph node metastasis of locally advanced rectal cancers. Cancer Immunol Immunother 68:283–296
407. Chen T-W, Huang KC-Y, Chiang S-F, Chen WT-L, Ke T-W, Chao KSC (2019) Prognostic relevance of programmed cell death-ligand 1 expression and CD8+ TILs in rectal cancer patients before and after neoadjuvant chemoradiotherapy. J Cancer Res Clin Oncol 145:1043–1053
408. Patel KR, Martinez A, Stahl JM, et al (2018) Increase in PD-L1 expression after pre-operative radiotherapy for soft tissue sarcoma. Oncoimmunology 7:e1442168
409. Jomrich G, Silberhumer GR, Marian B, Beer A, Müllauer L (2016) Programmed death-ligand 1 expression in rectal cancer. Eur Surg 48:352–356
410. Ogura A, Akiyoshi T, Yamamoto N, Kawachi H, Ishikawa Y, Mori S, Oba K, Nagino M, Fukunaga Y, Ueno M (2018) Pattern of programmed cell death-ligand 1 expression and CD8-positive T-cell infiltration

before and after chemoradiotherapy in rectal cancer. Eur J Cancer 91:11–20
411. Fujimoto D, Uehara K, Sato Y, et al (2017) Alteration of PD-L1 expression and its prognostic impact after concurrent chemoradiation therapy in non-small cell lung cancer patients. Sci Rep 7:11373
412. Li Y, Huang Q, Zhou Y, He M, Chen J, Gao Y, Wang X (2019) The Clinicopathologic and Prognostic Significance of Programmed Cell Death Ligand 1 (PD-L1) Expression in Patients With Prostate Cancer: A Systematic Review and Meta-Analysis. Front Pharmacol 9:1494
413. Sharma M, Yang Z, Miyamoto H (2019) Immunohistochemistry of immune checkpoint markers PD-1 and PD-L1 in prostate cancer. Medicine (Baltimore) 98:e17257
414. Baas W, Gershburg S, Dynda D, Delfino K, Robinson K, Nie D, Yearley JH, Alanee S (2017) Immune Characterization of the Programmed Death Receptor Pathway in High Risk Prostate Cancer. Clin Genitourin Cancer 15:577–581
415. Ness N, Andersen S, Khanehkenari MR, et al (2017) The prognostic role of immune checkpoint markers programmed cell death protein 1 (PD-1) and programmed death ligand 1 (PD-L1) in a large, multicenter prostate cancer cohort. Oncotarget 8:26789–26801
416. Massari F, Ciccarese C, Caliò A, et al (2016) Magnitude of PD-1, PD-L1 and T Lymphocyte Expression on Tissue from Castration-Resistant Prostate Adenocarcinoma: An Exploratory Analysis. Target Oncol 11:345–351
417. Tashima Y, Kuwata T, Yoneda K, Hirai A, Mori M, Kanayama M, Imanishi N, Kuroda K, Ichiki Y, Tanaka F (2020) Prognostic impact of PD-L1 expression in correlation with neutrophil-to-lymphocyte ratio in squamous cell carcinoma of the lung. Sci Rep 10:1243
418. Tsao M-S, Le Teuff G, Shepherd FA, et al (2017) PD-L1 protein expression assessed by immunohistochemistry is neither prognostic nor predictive of benefit from adjuvant chemotherapy in resected non-small cell lung cancer. Ann Oncol 28:882–889
419. Schmidt LH, Kümmel A, Görlich D, et al (2015) The prognostic impact of PD1 and PDL1 expression in non-small cell lung cancer. In: 11.1 Lung Cancer. European Respiratory Society, p PA4244
420. Brody R, Zhang Y, Ballas M, Siddiqui MK, Gupta P, Barker C, Midha A, Walker J (2017) PD-L1 expression in advanced NSCLC: Insights into risk stratification and treatment selection from a systematic literature review. https://doi.org/10.1016/j.lungcan.2017.08.005
421. Rizvi NA, Mazières J, Planchard D, et al (2015) Activity and safety of nivolumab, an anti-PD-1 immune checkpoint inhibitor, for patients with advanced, refractory squamous non-small-cell lung cancer (CheckMate 063): a phase 2, single-arm trial. Lancet Oncol 16:257–265
422. Gettinger SN, Horn L, Gandhi L, et al (2015) Overall Survival and Long-Term Safety of Nivolumab (Anti-Programmed Death 1 Antibody, BMS-936558, ONO-4538) in Patients With Previously Treated Advanced Non-Small-Cell Lung Cancer. J Clin Oncol 33:2004–12
423. Segal NH, Ou S-HI, Balmanoukian AS, et al (2016) Updated safety and efficacy of durvalumab (MEDI4736), an anti-PD-L 1 antibody, in patients from a squamous cell carcinoma of the head and neck (SCCHN) expansion cohort. Ann Oncol 27:vi328
424. Spigel DR, Chaft JE, Gettinger SN, et al (2015) Clinical activity and safety from a phase II study (FIR) of MPDL3280A (anti-PDL1) in PD-L1–selected patients with non-small cell lung cancer (NSCLC). J Clin Oncol 33:8028–8028
425. Spira AI, Park K, Mazières J, Vansteenkiste JF, Rittmeyer A, Ballinger M, Waterkamp D, Kowanetz M, Mokatrin A, Fehrenbacher L (2015) Efficacy, safety and predictive biomarker results from a randomized phase II study comparing MPDL3280A vs docetaxel in 2L/3L NSCLC (POPLAR). J Clin Oncol 33:8010–8010
426. Liu S V., Powderly JD, Camidge DR, et al (2015) Safety and efficacy of MPDL3280A (anti-PDL1) in combination with platinum-based doublet chemotherapy in patients with advanced non-small cell lung cancer (NSCLC). J Clin Oncol 33:8030–8030
427. Herbst RS, Soria J-C, Kowanetz M, et al (2014) Predictive correlates of response to the anti-PD-L1 antibody MPDL3280A in cancer patients. Nature 515:563–567
428. Gulley JL, Rajan A, Spigel DR, et al (2015) 3090 Avelumab (MSB0010718C), an anti-PD-L1 antibody, in patients with metastatic or recurrent non-small-cell lung cancer progressing after platinum-based chemotherapy: A phase Ib trial. Eur J Cancer 51:S629
429. Aguiar PN, Santoro IL, Tadokoro H, de Lima Lopes G, Filardi BA, Oliveira P, Mountzios G, de Mello RA (2016) The role of PD-L1 expression as a predictive biomarker in advanced non-small-cell lung cancer: a network meta-analysis. Immunotherapy 8:479–88
430. Haffner MC, Guner G, Taheri D, et al (2018) Comprehensive Evaluation of Programmed Death-Ligand 1 Expression in Primary and Metastatic Prostate Cancer. Am J Pathol 188:1478–1485

431. Fankhauser CD, Schüffler PJ, Gillessen S, et al (2018) Comprehensive immunohistochemical analysis of PD-L1 shows scarce expression in castration-resistant prostate cancer. Oncotarget 9:10284–10293
432. Topalian SL, Hodi FS, Brahmer JR, et al (2012) Safety, Activity, and Immune Correlates of Anti–PD-1 Antibody in Cancer. N Engl J Med 366:2443–2454
433. Taube JM, Klein A, Brahmer JR, Xu H, Pan X, Kim JH, Chen L, Pardoll DM, Topalian SL, Anders RA (2014) Association of PD-1, PD-1 ligands, and other features of the tumor immune microenvironment with response to anti-PD-1 therapy. Clin Cancer Res 20:5064–74
434. Subudhi SK, Vence L, Zhao H, et al (2020) Neoantigen responses, immune correlates, and favorable outcomes after ipilimumab treatment of patients with prostate cancer. Sci Transl Med. https://doi.org/10.1126/scitranslmed.aaz3577
435. Ager CR, Reilley MJ, Nicholas C, Bartkowiak T, Jaiswal AR, Curran MA (2017) Intratumoral STING Activation with T-cell Checkpoint Modulation Generates Systemic Antitumor Immunity. Cancer Immunol Res 5:676–684
436. Chen H, Zhao L, Fu K, et al (2019) Integrin αvβ3-targeted radionuclide therapy combined with immune checkpoint blockade immunotherapy synergistically enhances anti-tumor efficacy. Theranostics 9:7948–7960
437. Mauclet C, Duplaquet F, Pirard L, et al (2019) Complete tumor response of a locally advanced lung large-cell neuroendocrine carcinoma after palliative thoracic radiotherapy and immunotherapy with nivolumab. Lung Cancer 128:53–56
438. Anderson ES, Postow MA, Wolchok JD, Young RJ, Ballangrud Å, Chan TA, Yamada Y, Beal K (2017) Melanoma brain metastases treated with stereotactic radiosurgery and concurrent pembrolizumab display marked regression; efficacy and safety of combined treatment. J Immunother cancer 5:76
439. Gong J, Le TQ, Massarelli E, Hendifar AE, Tuli R (2018) Radiation therapy and PD-1/PD-L1 blockade: the clinical development of an evolving anticancer combination. J Immunother cancer 6:46
440. Kwon ED, Drake CG, Scher HI, et al (2014) Ipilimumab versus placebo after radiotherapy in patients with metastatic castration-resistant prostate cancer that had progressed after docetaxel chemotherapy (CA184-043): a multicentre, randomised, double-blind, phase 3 trial. Lancet Oncol 15:700–712
441. Dovedi SJ, Cheadle EJ, Popple AL, et al (2017) Fractionated Radiation Therapy Stimulates Antitumor Immunity Mediated by Both Resident and Infiltrating Polyclonal T-cell Populations when Combined with PD-1 Blockade. Clin Cancer Res 23:5514–5526
442. N S, AE L, K B, D V, JW G, SC F, EB G, P L (2017) Previous radiotherapy and the clinical activity and toxicity of pembrolizumab in the treatment of non-small-cell lung cancer: a secondary analysis of the KEYNOTE-001 phase 1 trial. Lancet Oncol. https://doi.org/10.1016/S1470-2045(17)30380-7
443. Newton JM, Hanoteau A, Liu HC, et al (2019) Immune microenvironment modulation unmasks therapeutic benefit of radiotherapy and checkpoint inhibition. J Immunother Cancer 7:216
444. Johnson LSM (2020) The Trouble with Animal Models in Brain Research. Springer, Cham, pp 271–286
445. Nakano K, Nishizawa T, Komura D, Fujii E, Monnai M, Kato A, Funahashi S-I, Ishikawa S, Suzuki M (2018) Difference in morphology and interactome profiles between orthotopic and subcutaneous gastric cancer xenograft models. J Toxicol Pathol 31:293–300
446. Choudhury A, Moniaux N, Ulrich AB, Schmied BM, Standop J, Pour PM, Gendler SJ, Hollingsworth MA, Aubert J-P, Batra SK (2004) MUC4 mucin expression in human pancreatic tumours is affected by organ environment: the possible role of TGFβ2. Br J Cancer 90:657–664
447. Mestas J, Hughes CCW (2004) Of mice and not men: differences between mouse and human immunology. J Immunol 172:2731–8
448. Shay T, Jojic V, Zuk O, et al (2013) Conservation and divergence in the transcriptional programs of the human and mouse immune systems. Proc Natl Acad Sci U S A 110:2946–51
449. Seok J, Warren HS, Cuenca AG, et al (2013) Genomic responses in mouse models poorly mimic human inflammatory diseases. Proc Natl Acad Sci U S A 110:3507–12
450. Reese TA, Bi K, Kambal A, et al (2016) Sequential Infection with Common Pathogens Promotes Human-like Immune Gene Expression and Altered Vaccine Response. Cell Host Microbe 19:713–719
451. Beura LK, Hamilton SE, Bi K, et al (2016) Normalizing the environment recapitulates adult human immune traits in laboratory mice. Nature 532:512–516
452. Mak IW, Evaniew N, Ghert M (2014) Lost in translation: animal models and clinical trials in cancer treatment. Am J Transl Res 6:114–8
453. Sena ES, van der Worp HB, Bath PMW, Howells DW, Macleod MR (2010) Publication Bias in Reports of Animal Stroke Studies Leads to Major Overstatement of Efficacy. PLoS Biol 8:e1000344

454. Berglund E, Maaskola J, Schultz N, et al (2018) Spatial maps of prostate cancer transcriptomes reveal an unexplored landscape of heterogeneity. Nat Commun 9:2419
455. Liu X, Pu Y, Cron K, Deng L, Kline J, Frazier WA, Xu H, Peng H, Fu Y-X, Xu MM (2015) CD47 blockade triggers T cell–mediated destruction of immunogenic tumors. Nat Med 21:1209–1215
456. Spary LK, Al-Taei S, Salimu J, Cook AD, Ager A, Watson HA, Clayton A, Staffurth J, Mason MD, Tabi Z (2014) Enhancement of T cell responses as a result of synergy between lower doses of radiation and T cell stimulation. J Immunol 192:3101–10
457. Serre R, Barlesi F, Muracciole X, Barbolosi D (2018) Immunologically effective dose: a practical model for immunoradiotherapy. Oncotarget 9:31812–31819
458. Diegeler S, Hellweg CE (2017) Intercellular Communication of Tumor Cells and Immune Cells after Exposure to Different Ionizing Radiation Qualities. Front Immunol 8:664
459. Poleszczuk J, Enderling H (2018) The Optimal Radiation Dose to Induce Robust Systemic Anti-Tumor Immunity. Int J Mol Sci. https://doi.org/10.3390/ijms19113377
460. Dutt S, Atallah MB, Minamida Y, Filatenkov A, Jensen KP, Iliopoulou BP, Tamosiuniene R, Waters J, Engleman EG, Strober S (2018) Accelerated, but not conventional, radiotherapy of murine B-cell lymphoma induces potent T cell-mediated remissions. Blood Adv 2:2568–2580
461. Vanpouille-Box C, Alard A, Aryankalayil MJ, Sarfraz Y, Diamond JM, Schneider RJ, Inghirami G, Coleman CN, Formenti SC, Demaria S (2017) DNA exonuclease Trex1 regulates radiotherapy-induced tumour immunogenicity. Nat Commun 8:15618
462. Punnanitinont A, Kannisto ED, Matsuzaki J, Odunsi K, Yendamuri S, Singh AK, Patnaik SK (2020) Sublethal Radiation Affects Antigen Processing and Presentation Genes to Enhance Immunogenicity of Cancer Cells. Int J Mol Sci. https://doi.org/10.3390/ijms21072573
463. Arnold KM, Flynn NJ, Raben A, Romak L, Yu Y, Dicker AP, Mourtada F, Sims-Mourtada J (2018) The Impact of Radiation on the Tumor Microenvironment: Effect of Dose and Fractionation Schedules. Cancer Growth Metastasis 11:1179064418761639
464. Tagawa ST, Osborne J, Fernandez E, et al (2020) Phase I dose-escalation study of PSMA-targeted alpha emitter ^{225} Ac-J591 in men with metastatic castration-resistant prostate cancer (mCRPC). J Clin Oncol 38:5560–5560
465. Stenberg V, Juzeniene A, Ma L-W, Bruland OS, Larsen RH (2020) Targeting of metastatic prostate cancer with alpha particle generating 212Pb-labeled PSMA seeking ligands. J. Nucl. Med. 61:
466. De Vincentis G, Gerritsen W, Gschwend JE, et al (2019) Advances in targeted alpha therapy for prostate cancer. Ann Oncol Off J Eur Soc Med Oncol 30:1728–1739
467. Hammer S, Hagemann UB, Zitzmann-Kolbe S, et al (2020) Preclinical Efficacy of a PSMA-Targeted Thorium-227 Conjugate (PSMA-TTC), a Targeted Alpha Therapy for Prostate Cancer. Clin Cancer Res 26:1985–1996

Appendix:

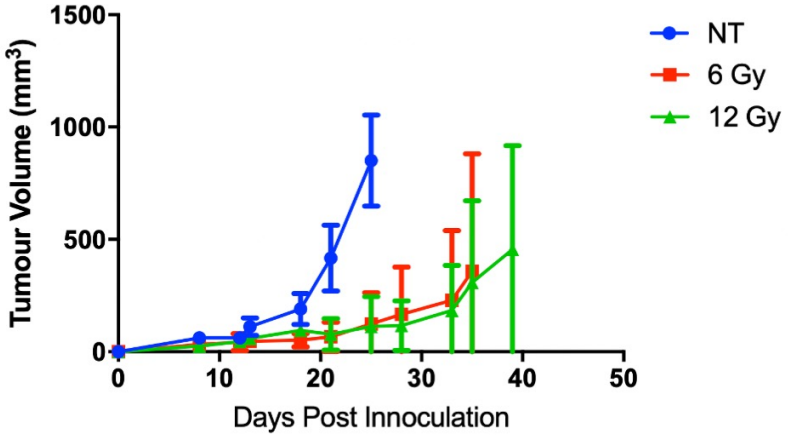

Appendix Figure A1: Pilot study to assess the efficacy of EBRT in PGLS tumours. c57BL/6 mice bearing PGLS tumours were treated with 6 Gy or 12 Gy EBRT at day 7 where tumours were 60-90 mm^3. Data is shown as mean tumour volume ±SEM (n = 2 to 3).

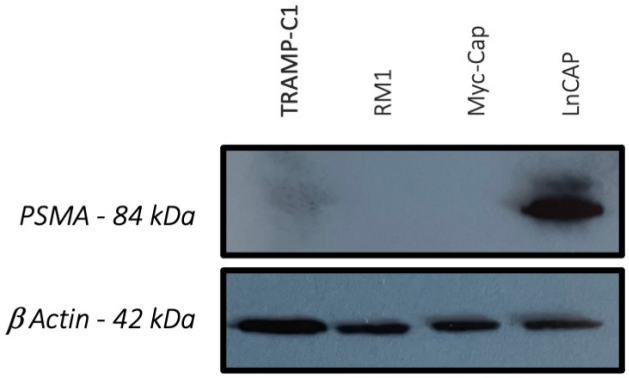

Appendix Figure A2: Expression of PSMA in murine prostate cancer cell lines
Expression of PSMA in murine prostate cancer cell lines was compared with human cell line LnCAP as assessed by western blot.

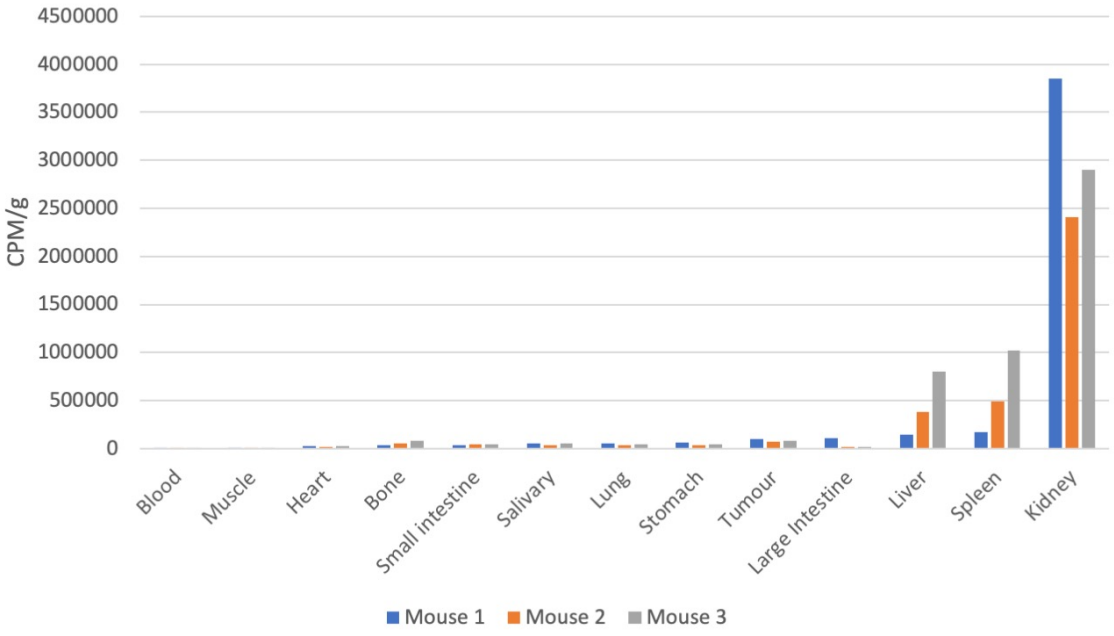

Appendix Figure A3: Pilot biodistribution study to assess biodistribution of [177Lu]PSMA-I&T in PGLS allografts

PGLS tumour bearing mice were treated with 30 MBq [177Lu]PSMA-I&T 7 days post tumour inoculation at a volume of 60-90 mm^3. 72 hours post treatment, mice were sacrificed and organs harvested, weighed and assessed for activity. Biodistribution is displayed as cpm per gram (cpm/g). Data is shown for each mouse (n=3).